Functional Analysis of Cancer-Causing *FBXW7* Mutations



Hayley Louise Davis

Linacre College

University of Oxford

A thesis submitted for the degree of

Doctor of Philosophy

Hilary Term 2012

Functional Analysis of Cancer-Causing *FBXW7* Mutations

Hayley Louise Davis
Linacre College, University of Oxford, D.Phil, Hilary 2012

Abstract

FBXW7 encodes the substrate recognition component of an SCF E3 ubiquitin ligase complex. This complex regulates the degradation of multiple targets, such as Notch1, c-Jun, c-Myc and cyclin E, that function in critical developmental and cancer pathways. *FBXW7* mutations are found in cancers of diverse tissue origins, with one of the highest mutation rates in the colorectrum. *FBXW7* mutations are typically missense mutations that disrupt the substrate recognition domain at critical arginine propellor-tips. Mutations are often mono-allelic suggesting that *FBXW7* is not a typical tumour supressor gene. Despite this, most of the evidence on FBXW7 function to date comes from null systems.

Several *Fbxw7*-null mouse models have been generated and suffer homozygous embryonic lethality due to disrupted vascular development. Conditional *Fbxw7*-null mice have been created but do not in general reflect the mutation spectrum found in human tumours. In order to analyse the functional effects of *Fbxw7* propellor-tip missense mutations, mice carrying a commonly-occurring *Fbxw7* R482Q mutation were generated.

This propellor-tip mutation was knocked-in constitutively and whilst heterozygous mice developed normally *in utero*, they died perinatally due to defective lung development. Cleft palate and eyelid fusion defects were also observed with incomplete penetrance. Fbxw7 substrates were screened in embryonic lungs and significantly elevated protein levels of Klf5 and Tgif1 were observed.

The *Fbxw7* R482Q mutation was also conditionally knocked-in in the gut. In the heterozygous state, large adenomas in the small intestine were observed at a low multiplicity, in approximately 30% of mice at an age greater than 300 days. Upregulation of Wnt signalling and *Ctnnb1* mutations have been identified in a selection of these tumours. Breeding the $Fbxw7^{R482Q}$ allele onto *Apc*-mutant backgrounds led to accelerated morbidity, in which compound R482Q/*Apc*-mutant mice exhibited polyps of increased number and size. Elevated protein levels of Fbxw7 substrates Klf5 and Tgif1 were observed in adenoma and normal intestinal tissue from these mice.

In vitro work using epitope-tagged murine wildtype and propellor-tip mutant Fbxw7 proteins showed that they were capable of dimerising, opening the prospect of investigating a dominant negative mechanism of action.

To conclude, an *Fbxw7* propellor-tip mutation studied *in vivo* resulted in both disrupted embryonic development and intestinal tumorigenesis and was distinct from *Fbxw7*-null alleles.

Acknowledgements

Firstly I would like to thank Professor Ian Tomlinson for me giving the opportunity to undertake work in your laboratory and enjoy the experience at Oxford University. Thank you for your stimulating discussions, support and guidance. I also appreciate your patience and constant positivity towards my work.

Next I would like to give a massive thank you to Dr Annabelle Lewis, who without your help, this would not have been possible. I am really grateful for you teaching me so many techniques in the lab, especially helping with endless hours of dissections! Your constant motivation and reassurance has definitely kept me sane at times. Also I am grateful for your constructive criticism on many versions of this thesis.

I would like to thank other members of the Molecular Population and Genetics lab especially Angela for moral support, Chiara for helping with the lentiviral work, Simon for many valuable suggestions and David, Claire and Stefi for useful input on the final edits of this thesis.

I am extremely grateful to Bradley Spencer-Dene, Hilda Tateossian and Professor Marco Novelli for helping identify mice phenotypes. I am also grateful to all the animal technicians who have looked after my mice.

I would like to thank my Mum, Dad and Susannah for their interest in my work and for believing in me throughout. Finally I would like to say a huge thank you to Jon, for sharing all the ups and down as well as for invaluable help with formatting this thesis.

Preface

This thesis is a collection of the research work carried out by the author in the Molecular and Population Genetics Laboratory, Wellcome Trust Centre for Human Genetics, Department of Clinical Medicine, University of Oxford, between October 2008 and March 2012, under the supervision of Professor Ian Tomlinson.

I state that the research described herein is original, though the work of others is cited with appropriate references within the text. No part of this research has previously been submitted for a degree at this or any other University.

Some of the work described in this thesis has been published in the following papers:

1. **Davis H** , Lewis A, Spencer-Dene B, Tateossian H, Stamp G, Behrens A, Tomlinson I (2011) Fbxw7 mutations typically found in human cancers are distinct from null alleles and disrupt lung development, *Journal of Pathology*, 224(2):180-9.

2. **Davis H**, Tomlinson I (2012) CDC4/FBXW7 and the 'just enough' model of tumourigenesis, *Journal of Pathology*, 227(2):131-5.

3. Babaei-Jadidi R, Li N, Saadeddin A, Spencer-Dene B, Jandke A, Muhammad B, Ibrahim EE, Muraleedharan R, Abuzinadah M, **Davis H**, Lewis A, Watson S, Behrens A, Tomlinson I, Nateri AS (2011) FBXW7 influences murine intestinal homeostasis and cancer, targeting Notch, Jun, and DEK for degradation. *The Journal of Experimental Medicine*, 208(2):295-312.

4. Sancho R, Jandke A, **Davis H**, Diefenbacher ME, Tomlinson I, Behrens A (2010) F-box and WD repeat domain-containing 7 regulates intestinal cell lineage commitment and is a haploinsufficient tumor suppressor. *Gastroenterology*, 139(3):929-41.

In papers 3 and 4 I was involved in sequencing human colorectal tumours to identify *FBXW7* mutations. I was not involved in the generation or analysis of *Fbxw7*-null mice.

I have additionally contributed to the following publications that are not covered in this thesis:

1. Leedham SJ, Rodenas-Cuadrado P, Howarth K, Lewis A, Mallappa S, Segditsas S, **Davis H**, Jeffery R, Rodriguez-Justo M, Keshav S, Travis SP, Graham TA, East J, Clark S, Tomlinson IP. (2012) A basal gradient of Wnt and stem-cell number influences regional tumour distribution in human and mouse intestinal tracts. *Gut*, Accepted manuscript, in press.

2. Lewis A, **Davis H**, Deheragoda M, Pollard P, Nye E, Jeffery R, Segditsas S, East P, Poulsom R, Stamp G, Wright N, Tomlinson I (2012) The C-terminus of Apc does not influence intestinal adenoma development or progression. *Journal of Pathology*, 226(1):73-83.

3. Lewis A, Segditsas S, Deheragoda M, Pollard P, Jeffery R, Nye E, Lockstone H, **Davis H**, Clark S, Stamp G, Poulsom R, Wright N, Tomlinson I (2010) Severe polyposis in Apc(1322T) mice is associated with submaximal Wnt signalling and increased expression of the stem cell marker Lgr5. *Gut*, 59(12):1680-6.

Contents

Abstract **i**

Acknowledgements **ii**

List of Figures **xiv**

List of Tables **xix**

List of Abbreviations **xxi**

1 Introduction **1**

1.1 Colorectal cancer 1

1.1.1 Anatomy and normal intestinal biology 2

1.1.2 Life cycle of intestinal epithelial cells 3

1.1.3 Colorectal cancer: Cell biology 4

1.1.4 Mutations of critical signalling pathway components 5

1.1.4.1 *Adenomatous Polyposis Coli (APC)* 5

1.1.4.2 *KRAS* 8

1.1.4.3 *SMAD4* 8

1.1.4.4 *TP53* 9

1.2 Ubiquitin proteasome system 9

1.2.1 E3 ubiquitin ligases 10

1.3 *FBXW7* 12

1.3.1 Introduction to function 12

1.3.2 Isoforms 13

1.3.3 Protein domains 15

1.3.3.1 F-box domain . . . 15
1.3.3.2 WD40 domain . . . 15
1.3.3.3 Dimerisation domain . . . 16
1.3.4 CDC4 Phosphodegron (CPD) . . . 16
1.3.5 FBXW7 and cancer . . . 17
1.3.5.1 Cancer types . . . 17
1.3.5.2 Incidence of *FBXW7* mutations in colorectal lesions 19
1.3.6 Mutation spectrum . . . 20
1.3.6.1 Structural basis of arginine propellor-tip mutations . 22
1.3.7 Deregulation of FBXW7 in tumours without mutations in *FBXW7* 24
1.3.8 Mechanism of action of *FBXW7* mutations . . . 24
1.3.9 Substrates . . . 25
1.3.9.1 Cyclin E . . . 25
1.3.9.2 c-Myc . . . 27
1.3.9.3 c-Jun . . . 28
1.3.9.4 Notch1 . . . 29
1.3.9.5 Aurora A . . . 30
1.3.9.6 KLF5 . . . 30
1.3.9.7 TGIF1 . . . 31
1.3.10 Tissue-specificity of substrates . . . 31
1.3.11 Regulation of FBXW7 . . . 34
1.3.11.1 Transcriptional regulation . . . 34
1.3.11.2 Post-translational modifications . . . 35
1.3.12 Targeted therapeutics . . . 36
1.3.13 Mouse models to study Fbxw7 function . . . 37
1.4 Outline of thesis . . . 38

2 Materials and Methods **39**
2.1 Mouse procedures . . . 39
2.1.1 Generation of $Fbxw7^{R482Q}$ mice . . . 39
2.1.2 Ear snips . . . 40
2.1.3 Breeding . . . 40
2.1.4 Embryo collections . . . 40

2.1.5 Gut preparations . . . 41
2.1.6 Individual crypt isolation . . . 41
2.2 Histology . . . 42
2.2.1 Adenoma scoring . . . 42
2.2.2 Processing . . . 42
2.2.3 Embedding . . . 42
2.2.4 Sectioning and staining . . . 43
2.2.4.1 Haematoxylin and Eosin (H and E) staining . . . 43
2.2.4.2 Alcian-blue stain for goblet cells . . . 44
2.3 DNA . . . 44
2.3.1 DNA extraction . . . 44
2.3.1.1 DNA extraction from ES cells . . . 44
2.3.1.2 Isolation of DNA from mouse ears for genotyping purposes . . . 44
2.3.1.3 Isolation of DNA from embryonic tails and other adult mouse tissues . . . 45
2.3.1.4 DNA extraction from laser capture microdissected samples . . . 45
2.3.2 DNA purification . . . 46
2.3.2.1 DNA purification from agarose gels . . . 46
2.3.2.2 Phenol-chloroform purification of nucleic acids . . . 46
2.3.3 Determination of nucleic acid concentration and quality . . . 46
2.3.4 Polymerase Chain Reaction (PCR) . . . 47
2.3.5 Long-range PCR screening . . . 48
2.3.6 Sequencing . . . 49
2.3.7 Southern blotting . . . 50
2.3.8 Array comparative genomic hybridisation . . . 50
2.4 RNA / cDNA . . . 51
2.4.1 RNA extraction . . . 51
2.4.2 RNA extraction from individual crypts . . . 51
2.4.3 Reverse transcription of RNA into cDNA . . . 51
2.4.4 *In situ* hybridisation . . . 52

2.4.5 Quantitative real time-PCR (qRT-PCR): TaqMan (ABI) . . . 52
2.4.5.1 Pre-amplification of cDNA . . . 53
2.4.6 SYBR-Green RT-PCR . . . 55
2.5 Protein . . . 56
2.5.1 Immunohistochemistry . . . 56
2.5.1.1 Immunohistochemistry quantification . . . 57
2.5.2 Immunofluorescence . . . 58
2.5.3 Western blotting . . . 58
2.5.3.1 Quantification of protein lysates . . . 59
2.5.3.2 Running western gel and transfer . . . 59
2.5.3.3 Epithelial isolation of cells from intestinal tissue . . . 61
2.5.3.4 Cell fractionation for western analysis . . . 61
2.5.4 Co-immunoprecipitation . . . 61
2.5.4.1 Myc Co-IP . . . 62
2.5.4.2 FLAG co-IP . . . 62
2.6 Cell culture . . . 63
2.6.1 Maintenance of cell lines . . . 63
2.6.2 Counting cells . . . 63
2.6.3 Transient transfections . . . 64
2.6.4 Measurement of cell viability . . . 64
2.6.5 Derivation of mouse embryonic fibroblasts (MEFs) . . . 64
2.6.6 Synchronising cells by serum starvation . . . 65
2.7 *In vitro* shRNA knockdown of *FBXW7* . . . 65
2.7.1 Production of lentiviral particles . . . 67
2.7.2 Titration of lentiviral stocks . . . 67
2.7.3 Transduction of cell lines . . . 68
2.8 Cloning . . . 69
2.8.1 Standard cloning . . . 69
2.8.1.1 Ligation . . . 69
2.8.1.2 Blunt-ended ligation . . . 69
2.8.1.3 Transformation . . . 69
2.8.1.4 Amplification of DNA products from bacteria . . . 70

2.8.2 Site-directed mutagenesis 70
2.9 Statistical Analysis 71

3 Investigation of a constitutive *Fbxw7* propellor-tip mutation 72
3.1 Introduction 72
3.1.1 Existing *Fbxw7* mutant mice 73
3.1.2 Possible mechanisms behind characteristic mutation spectrum 74
3.1.3 Conservation of FBXW7 protein sequence between human and mouse 75
3.2 Aims of chapter 76
3.3 Results 77
3.3.1 Generation of *Fbxw7* R482Q construct 77
3.3.2 Generation of constitutive R482Q model 79
3.3.3 Confirmation that observed phenotype was specific to targeted *Fbxw7* R482Q mutation 82
3.3.4 Defect in lung development in R482Q/+ mice 85
3.3.4.1 Molecular characterisation of lung developmental defect in R482Q/+ mice 88
3.3.4.2 Assessment on FBXW7 substrate protein abundance in R482Q/+ lungs 91
3.3.5 Assessing potential tissue-specificity of R482Q/+ mutation . . 95
3.3.6 Additional developmental abnormalities in R482Q/+ E18.5 embryos 96
3.3.7 Analysis of specific signalling pathways 99
3.3.7.1 Tgf-β pathway 99
3.3.7.2 Notch pathway 100
3.3.7.3 Retinoic acid pathway 102
3.3.8 Comparison to *Fbxw7*-null mouse model 102
3.4 Discussion 103
3.4.1 Generation of informative *Fbxw7*-mutant mice 103
3.4.2 Constitutive *Fbxw7* R482Q model 104
3.4.3 Lung development 105
3.4.4 Additional developmental abnormalities 105

3.4.5 Comparable mouse models / Critical signalling pathways . . . 106
3.4.6 Fbxw7 substrates . . . 110
3.4.6.1 Tgif1 . . . 110
3.4.6.2 Klf5 . . . 111
3.4.7 Heterozygous propellor-tip mutation . . . 112

4 Investigation of an intestinal-specific *Fbxw7* propellor-tip mutation 114
4.1 Introduction . . . 114
4.1.1 Role of *FBXW7* in cancers of diverse tissue type . . . 114
4.1.2 Role of Fbxw7 in intestinal tissue . . . 115
4.1.3 Aims of chapter . . . 117
4.2 Results . . . 117
4.2.1 Generation of conditional R482Q knock-in mice . . . 117
4.2.2 Characterisation of tissue-specific recombination mediated by *Vil1*-Cre crosses . . . 119
4.2.3 Tissue-specific recombination of *Fbxw7*-null allele mediated by *Vil1*-Cre crosses . . . 121
4.2.4 Gross morphological analysis of R482Q mice . . . 123
4.2.4.1 Intestinal polyp analysis on *Fbxw7*-null mice . . . 125
4.2.5 Molecular analysis of *Fbxw7* mutant mice . . . 126
4.2.5.1 Intestinal cell lineage analysis in morphologically normal *Fbxw7* mutant mice . . . 126
4.2.5.2 Proliferation and apoptosis in morphologically normal tissue in *Fbxw7* mutant mice . . . 128
4.2.6 Molecular analysis of R482Q/+ tumours . . . 130
4.2.6.1 Assessment of Wnt signalling pathway . . . 131
4.2.7 Protein abundance of Fbxw7 substrates in morphologically normal R482Q mice . . . 135
4.3 Discussion . . . 137
4.3.1 R482Q/+ mutation causes intestinal tumorigenesis . . . 137
4.3.2 R482Q/+ invasive adenocarcinoma . . . 138
4.3.3 R482Q/+ mutation in morphologically normal intestinal tissue 139

4.3.4 Possible role of elevated Klf5 and Tgif proteins in intestinal tumorigenesis . . . 140

5 Investigation of an *Fbxw7* propellor-tip mutation in an *Apc*-mutant background 143

5.1 Introduction . . . 143
5.1.1 *Apc* mutant mouse models . . . 143
5.1.2 Aims of chapter . . . 145
5.2 Results . . . 145
5.2.1 Crosses with *Apc*-mutant mice and subsequent evaluation of phenotype modification . . . 145
5.2.1.1 R482Q/+ Apc^{Min} compound mice . . . 146
5.2.1.2 R482Q/+ Apc^{1322T} compound mice . . . 149
5.2.1.3 Molecular analysis: R482Q/+ Apc^{1322T} compound tumour proliferation . . . 151
5.2.1.4 Fbxw7 protein substrate analysis in R482Q/+ Apc^{1322T} compound tumours . . . 154
5.3 Discussion . . . 157
5.3.1 R482Q/+ mutation enhances intestinal tumorigenesis in *Apc*-mutant mice . . . 157
5.3.2 Elevated levels of Klf5 and Tgif1; implications for tumorigenesis 158
5.3.3 Retinoic acid pathway in intestinal tumorigenesis . . . 159
5.3.4 Comparison to *Fbxw7*-null tumorigenesis in an *Apc*-mutant background . . . 160

6 Investigating consequences of *FBXW7* propellor-tip mutations in cell-based systems 162

6.1 Introduction . . . 162
6.1.1 FBXW7 dimerisation and potential dominant negative effect . 163
6.1.2 Distinguishing *FBXW7* propellor-tip mutations from *FBXW7*-null setting . . . 164
6.2 Aims of chapter . . . 166
6.3 Results . . . 167

6.3.1 Cell-based system to test Fbxw7 wildtype and R482Q dimerisation and potential dominant negative effect 167
6.3.1.1 Generation of tagged Fbxw7 wildtype and R482Q mutant mammalian expression vectors 167
6.3.1.2 Fbxw7 R482Q and wildtype interaction 173
6.3.1.3 Assessment of dominant negative effect of propellor-tip mutant Fbxw7 175
6.3.2 Targeted *FBXW7* shRNA knockdown in colorectal cancer cell lines 177
6.3.2.1 Colorectal cancer cell lines with *FBXW7* mutations . 178
6.3.2.2 Testing *FBXW7* shRNA efficiency by transient transfection 179
6.3.2.3 Comparison of *FBXW7* shRNA knocked-down and *FBXW7* propellor-tip mutant cells 180
6.3.3 Overexpression of wildtype FBXW7 in propellor-tip mutant cell lines 184
6.3.3.1 Method of overexpressing FBXW7 in colorectal cancer cell lines: Plasmid details 184
6.3.3.2 Assessment of wildtype FBXW7 overexpression on selected FBXW7 substrates in unsynchronised propellor-tip mutant cells 185
6.3.3.3 Assessment of cyclin E levels in synchronised FBXW7 propellor-tip mutant cells with wildtype FBXW7 overexpression 185
6.3.3.4 Assessment of p-c-Myc levels in synchronised FBXW7 propellor-tip mutant cells with wildtype FBXW7 overexpressed 189
6.3.3.5 Assessment of TGIF protein levels in the nuclear fraction of propellor-tip mutant cells 191
6.4 Discussion 194
6.4.1 Interaction between Fbxw7 wildtype and R482Q proteins . . . 194

6.4.2 shRNA *FBXW7* knockdown has no effect on FBXW7 substrates in FBXW7 propellor-tip mutant cell lines 194
6.4.3 Overexpression of wildtype FBXW7 in propellor-tip mutant cells can overcome potential dominant negative effect 195
6.4.4 Further work 197

7 Discussion and further work **198**
7.1 Summary of results 198
7.2 Discussion 200
7.2.1 Just-Enough hypothesis 200
7.2.2 *FBXW7* mutations within the adenoma-carcinoma progression sequence 203
7.2.3 Therapeutic targets 204
7.3 Further work 205

Appendices **207**

A Nomenclature of *Fbxw7*-mutant mice **207**

B Primers **208**

C FBXW7 protein alignment **211**

D Aged *Fbxw7*-mutant mice **215**

E R482Q/*Vil1*-Cre/*Apc*-mutant breeding **217**

F Raw intestinal polyp data from R482Q/+ *Apc*-mutant compound mice **220**

References **223**

List of Figures

1.1 Morphology of small intestinal and colonic mucosa of an adult mouse 3
1.2 Genetic model of colorectal carcinogenesis 5
1.3 Summary of the Wnt signalling pathway 7
1.4 Overview of ubiquitin-proteasome pathway 11
1.5 Schematic representation of an E3 SCF ubiquitin ligase complex . . . 12
1.6 FBXW7 isoforms 14
1.7 Functional protein domains of FBXW7 15
1.8 Alignment of phosphodegron (CPD) sequences of FBXW7 substrates 17
1.9 Spectrum of mutations found in *FBXW7* 21
1.10 Structural model of FBXW7 23
1.11 Schematic diagram of the functions of FBXW7 substrates in connection with cancer progression 33
1.12 Schematic diagram of post-translational modifications that alter FBXW7 activity 36

2.1 Confirming amplification efficiency of TaqMan probes 54
2.2 SYBR-Green RT-PCR: Dissociation curve 56
2.3 Schematic representation of the HIV-1 Virion and p24 ELISA 68

3.1 Alignment of FBXW7 protein sequence surrounding a common mutation site in the WD40 domain in human and mouse 75
3.2 Interaction of FBXW7 WD40 propellor domain with FBXW7 substrates 76
3.3 *Fbxw7* targeting construct and recombined alleles 77
3.4 Homologous recombination of targeting construct in electroporated ES cells 79

3.5 PCR genotype screening for *Fbxw7* R482Q mice 80
3.6 Confirmation of heterozygous *Fbxw7* R482Q mutation in R482Q/+ mice 83
3.7 No difference in *Fbxw7* mRNA expression in R482Q/+ mice 83
3.8 Genes surrounding *Fbxw7* 83
3.9 No biologically significant changes in mRNA expression in genes surrounding *Fbxw7* 84
3.10 High expression of *Fbxw7* mRNA in the brain and lung at E18.5 . . . 84
3.11 *Fbxw7α* is the most abundant isoform in the lung at E18.5 85
3.12 No difference observed in the weight of R482Q/+ and wildtype E18.5 whole embryos 86
3.13 Normal gross external appearance of E18.5 R482Q/+ embryos 86
3.14 Alveolar septal thickening in R482Q/+ E18.5 embryos 87
3.15 Increased proliferation in E18.5 R482Q/+ lungs 89
3.16 Analysis of lung cell-lineage markers in R482Q/+ E18.5 lungs 90
3.17 No difference in lung architecture in E16.5 R482Q/+ lungs 92
3.18 No difference in protein levels of several Fbxw7 substrates in E18.5 R482Q/+ lungs 93
3.19 Elevation of Klf5 and Tgif protein levels in E18.5 R482Q/+ lungs . . 94
3.20 No increase in mRNA expression of *Klf5* and *Tgif1* in E18.5 R482Q/+ lungs 94
3.21 Elevation of protein level of Tgif in R482Q/+ MEFs 95
3.22 Identification of cleft palate phenotype in E18.5 R482Q/+ embryos . 97
3.23 Eyes-open-at-birth phenotype found in R482Q/+ E18.5 embryos . . . 98
3.24 Occurrence of other developmental abnormalities in R482Q/+ embryos 98
3.25 No difference in location or intensity of phospho-Smad2 in R482Q/+ E18.5 lungs 99
3.26 No change in mRNA expression of selected downstream targets of the Tgf-β pathway in E18.5 wildtype and R482Q lungs 100
3.27 No difference in Smad4 protein levels in the nuclear fraction of E18.5 R482Q/+ lungs 101
3.28 No difference in *Hes1* mRNA expression in E18.5 R482Q/+ lungs . . 101

3.29 No change in mRNA expression of selected retinoic acid pathway targets in R482Q/+ E18.5 lungs 102
3.30 Schematic representation of murine palatogenesis 106
3.31 Retinoic acid signalling in lung development 109

4.1 *Fbxw7* targeting construct showing Cre-mediated neomycin cassette deletion and recombined alleles 118
4.2 Removal of neomycin cassette in an ES clone 119
4.3 Tissue-specific knock-in of R482Q mutation 121
4.4 Intestinal recombination in $Fbxw7^{\Delta/+}$ and $Fbxw7^{\Delta/\Delta}$ mice 122
4.5 Invasive adenocarcinoma in the small intestine of a R482Q/+ mouse . 124
4.6 Non-invasive polyps in small intestine of a R482Q/+ mice 125
4.7 Differentiated cell types in the intestines of *Fbxw7* mutant and wildtype 6-weeks old mice 127
4.8 Quantification of goblet and enteroendocrine cells in the small intestine of *Fbxw7* mutant and wildtype 6-weeks old mice 128
4.9 Proliferation and apoptosis analysis in *Fbxw7* mutant and wildtype 6-weeks old intestines 129
4.10 No loss of heterozygosity was observed in R482Q/+ tumours 130
4.11 Ki67 and β-catenin immunohistochemistry staining on R482Q/+ polyp 132
4.12 *Ctnnb1* mutation in R482Q/+ tumours 133
4.13 No significant change in mRNA expression of stem cell lineage markers in *Fbxw7*-mutant small intestinal crypts 134
4.14 Protein expression of Fbxw7 target proteins in intestines from *Fbxw7* mutant 6-weeks old mice, Klf5 and Tgif show elevated protein levels in *Fbxw7*-mutant mice compared to wildtype mice 136

5.1 Protein domains of APC 144
5.2 R482Q mutation enhanced tumorigenesis in R482Q/+ Apc^{Min} compound mice 148
5.3 R482Q mutation enhanced tumorigenesis in R482Q/+ Apc^{1322T} compound mice 150
5.4 Proliferation in R482Q/+ Apc^{1322T} compound tumours 152

5.5 β-catenin immunohistochemistry on R482Q/+ Apc^{1322T} compound and Apc^{1322T} tumours 153
5.6 No significant difference in *Lgr5* mRNA expression between R482Q/Apc^{1322T} and Apc^{1322T} tumours 154
5.7 Elevated protein levels of Klf5 and Tgif1 in R482Q/Apc^{1322T} tumours, levels of other Fbxw7 substrates were not elevated 155
5.8 Fold change in mRNA expression of selected downstream targets of the Tgf-β signalling pathway and retinoic acid pathway in R482Q/+ Apc^{1322T} and Apc^{1322T} tumours. 156

6.1 Restriction site map of pCMV-HA and pCMV-Myc plasmids 168
6.2 Amplification of *Fbxw7* R482Q and wildtype cDNA 169
6.3 *Fbxw7* R482Q mutation in pCMV-HA Fbxw7 R482Q plasmid 170
6.4 Efficient transfection of RKO but not NIH3T3 cells 171
6.5 Elevated *Fbxw7* mRNA expression in RKO cells following transient transfection of pCMV-HA and pCMV-Myc Fbxw7 plasmids 172
6.6 Forward primer for amplification of Fbxw7 R482Q cDNA with an N-terminal FLAG tag 173
6.7 FLAG and Myc-tagged Fbxw7 detected in RKO cells 174
6.8 Interaction of wildtype and R482Q Fbxw7 protein 174
6.9 No significant changes in NICD1, cyclin E and TGIF protein levels were seen in RKO cells overexpressing Fbxw7 R482Q and wildtype plasmids 176
6.10 Variable TGIF protein levels in a panel of CRC cell lines 178
6.11 *FBXW7* mutations in LOVO and SW1463 cells 179
6.12 shRNA-mediated knockdown of *FBXW7* mRNA expression in transiently transfected LOVO cells 180
6.13 shRNA-mediated knockdown of *FBXW7* mRNA expression in LOVO and SW1463 cells 181
6.14 Unaltered cell proliferation in *FBXW7* shRNA knocked-down LOVO and SW1463 cells 182

6.15 No significant differences in protein levels of FBXW7 substrates were seen between *FBXW7* shRNA knocked-down and propellor-tip mutant parental LOVO and SW1463 cells 183
6.16 Cyclin E and TGIF protein levels in FBXW7-overexpressing LOVO and SW1463 cells 186
6.17 Periodicity of cyclin E mRNA and protein expression relative to cell cycle stage 186
6.18 Protein levels of cyclin E in a panel of synchronised cells overexpressing wildtype FBXW7 188
6.19 p-c-Myc protein levels remain unchanged in synchronised LOVO cells overexpressing wildtype FBXW7 190
6.20 TGIF protein levels were decreased in the nuclear fraction of LOVO cells overexpressing wildtype FBXW7 191
6.21 TGIF western blot on the nuclear fraction of a panel of cell lines overexpressing wildtype FBXW7 192

7.1 Schematic representation of various models of tumour suppression . . 202

C.1 Alignment of FBXW7α isoform protein sequence of human and mouse 212
C.2 Alignment of FBXW7β isoform protein sequence of human and mouse 213
C.3 Alignment of FBXW7γ isoform protein sequence of human and mouse 214

E.1 Examples of breeding crosses used to generate R482Q/+ Apc^{Min} compound mice 218
E.2 Examples of breeding crosses used to generate R482Q/+ Apc^{1322T} compound mice 219

List of Tables

1.1 *FBXW7* mutation frequency according to tumour site 18
1.2 Additional substrates that FBXW7 regulates and their functions . . . 32
1.3 Tissue-specificity of critical Fbxw7 substrates 33

2.1 Genotyping primers 48
2.2 ES cell screening primers 48
2.3 Sequencing primers 49
2.4 TaqMan probes 53
2.5 Antibodies used for immunohistochemistry 57
2.6 Antibodies used for western blotting 60
2.7 Sequences of pLKO.1 shRNA *FBXW7* Clones 66

3.1 Nomenclature of R482Q mice used in this study 80
3.2 No R482Q/+ offspring resulted from R482Qfl/+ x *PGK*-Cre crosses . 81
3.3 Expected Mendelian ratios of R482Q/+ embryos found at all embryonic stages of development 81
3.4 Increased alveolar septal thickness in E18.5 R482Q/+ lungs 88
3.5 Stages of murine lung development 105
3.6 Mouse models with developmental phenotypes similar in those observed in the R482Q/+ model 107

4.1 Summary table of R482Q/+ mice with intestinal polyps 124
4.2 Mouse models that exhibit invasive small intestinal adenocarcinomas 139

5.1 Number of polyps at each intestinal location in R482Q/+ Apc^{Min} compound and Apc^{Min} mice 147

6.1 Effect of FBXW7 overexpression on the abundance of FBXW7 protein substrates in a panel of CRC cell lines 193

A.1 Nomenclature of *Fbxw7*-mutant mice used in this study 207

B.1 SYBR-Green primer sequences 209
B.2 Sequencing primers 210

D.1 Ages of *Fbxw7*-mutant mice which did not display any intestinal phenotypes 216

F.1 Raw intestinal polyp data from R482Q/+ Apc^{Min} compound and Apc^{Min} mice 221
F.2 Raw intestinal polyp data from R482Q/+ Apc^{1322T} compound and Apc^{1322T} mice 222

List of Abbreviations

AAR	amino acid repeat
ACF	aberrant crypt foci
APC	adenomatous polyposis coli
ATP	adenosine triphosphate
BCA	bicinchoninic acid
BLAST	Basic Local Alignment Search Tool
bp	base pair
BrdU	bromodeoxyuridine
BSA	bovine serum albumin
cDNA	complementary DNA
CDK	cyclin dependent kinase
C/EBPα	CCAAT/enhancer-binding protein transcription factor
CIN	chromosome instability
CMV	cytomegalovirus
co-IP	co-immunoprecipitation
COSMIC	Catalogue of Somatic Mutations in Cancer database
CPD	Cdc4 phosphodegron
cPML	cytoplasmic promyelocytic leukaemia
CRC	colorectal carcinoma
Cre	cyclization recombination enzyme
CSL	CBF1/Su(H)/LAG-1
CT	cycle threshold
Cul1	Cullin1
DAB	3,3'-diaminobenzidine
DAPI	4',6-diamidino-2-phenylindole dihydrochloride
dH20	distilled water
DMSO	dimethyl sulfoxide
DMEM	Dulbecco's Modified Eagles Medium
DNA	deoxyribonucleic acid
DPX	di-N-butyl phthalate in xylene (histology mounting media)
DTA	diptheria toxin
DTT	dithiothreitol
E	embryonic age in days

EDTA	ethylenediamine tetra-acetic acid
ELISA	enzyme-linked immunosorbent assay
ENU	N-ethyl-N-nitrosourea
ES	embryonic stem
EV	empty vector
FAP	familial adenomatous polyposis
FBS	foetal bovine serum
FBXW7	F-box WD40-repeat domain containing 7
FITC	fluorescein isothiocyanate
GAPDH	glyceraldehyde 3-phosphate dehydrogenase
GBP	guanylate binding protein
GFP	green fluorescent protein
GTP	guanosine triphosphate
H and E	Haematoxylin and Eosin stain
HA	haemagglutinin
HECT	homologous to the E6-AP carboxyl terminus
HEPES	N-2-hydroxyethylpiperazine-N'-2-ethanesulfonic acid
HNPCC	hereditary non-polyposis colorectal cancer
HOTSHOT	hot sodium hydroxide and tris
HRP	horseradish peroxidase
IMDM	Iscove's Modified Dulbecco's Medium
IPTG	isopropylthio-β-D-galactoside
ISH	*in situ* hybridisation
JNK	c-Jun N-terminal kinases
kb	kilo base pairs
kDA	kilo Dalton
LB	Luria-Bertani Media
LOH	loss of heterozygosity
LoxP	locus of chromosomal crossover in the bacteriophage P1
MAPK	mitogen activated protein kinase
MCR	mutation cluster region
MCS	multiple cloning site
MEFs	mouse embryonic fibroblasts
Mega9	Nonanoyl-N-methylglucamide (detergent)
MOPS	3-(N-morpholino)propanesulfonic acid
Min	multiple intestinal neoplasia
mRNA	messenger RNA
MSI	microsatellite instability
MTT	3-(4,5-Dimethylthiazol-2-yl)-2,5-diphenyltetrazolium bromide
neo	neomycin resistance cassette
NICD	Notch intracellular domain
NP40	nonyl phenoxypolyethoxylethanol (detergent)
ORF	Open Reading Frame

PBS	phosphate buffered saline
PBST	phosphate buffered saline supplemented with tween
PCR	polymerase chain reaction
PDVF	polyvinylidene difluoride
PEI	polyethylenimine
PGK	3-phosphoglycerate kinase
PKC	Protein kinase C
Q	glutamine residue
qRT-PCR	quantitative reverse transcription PCR
R	arginine residue
RING	Really Interesting New Gene domain
RNA	ribonucleic acid
RPMI	Rosewell Park Memorial Institute (where medium was developed)
rpm	revolutions per minute
SB	small bowel
SCF	Skp1/Cul1/F-box
scr	scrambled shRNA control
SDS PAGE	sodium dodecyl sulphate polyacrylamide gel electrophoresis
SEM	standard error of the mean
Ser	Serine
siRNA	short interfering RNA
shRNA	short hairpin RNA
Skp1	S-phase kinase-associated protein 1
SREBP1	sterol regulatory element-binding protein 1
T-ALL	T-cell acute lymphoblastic leukaemia
TE	tris-EDTA
TBE	tris-borate-EDTA
TBS	tris buffered saline
TCF	ternary complex factors
TGF-β	transforming growth factor beta
Thr	threonine
TSG	tumour suppressor gene
UTR	untranslated region
UV	ultraviolet
Vil1	Villin gene
VSV-G	vesicular stomatitis virus protein G
WD40	tryptophan-aspartic acid residues in protein domain
WT	wildtype
X-gal	5-bromo-4-chloro-3-indolyl-β-D-galactopyranoside

Chapter 1

Introduction

FBXW7 (F-box and WD40 repeat domain-containing 7, also known as *FBW7*, *hCDC4*), a gene that has been classified as a tumour suppressor due to its ability to negatively regulate multiple oncoproteins, is mutated in a diverse range of cancer types, including approximately 10% of colorectal cancer cases [1]. Intriguingly, the most commonly-occurring mutations in this gene are mono-allelic missense mutations. *FBXW7* is therefore not typical of a conventional tumour suppressor gene. Chapter 1 outlines current understanding of colorectal cancer genetics and summarises the role of FBXW7 in ubiquitin-mediated degradation of proteins in critical cancer pathways, mutations of *FBXW7* found in cancers and functional studies of *FBXW7* to date.

1.1 Colorectal cancer

Carcinogenesis is a multi-step process in which accumulated mutations and epigenetic changes alter the behaviour of cells, providing a growth advantage, for example, by activation of proto-oncogenes, inactivation of tumour suppressor genes or disruption of caretaker genes such as DNA repair genes. As cells progress from a normal to neoplastic state, the mutations they acquire allow them to exhibit characteristics which have been described as the 'Hallmarks of Cancer' [2; 3]. These include: sustain-

ing proliferative capacity; evading growth suppression; resisting apoptosis; enabling replicative immortality; inducing angiogenesis; activating invasion and metastasis; reprogramming energy metabolism; and evading immune destruction.

Colorectal carcinoma (CRC) is a leading cause of cancer-related death in the Western world, with approximately 1.2 million new cases diagnosed per year worldwide [4]. The aetiology of CRC is a complex interplay of multiple contributory factors including both environmental and genetic components.

1.1.1 Anatomy and normal intestinal biology

The anatomy and physiology of the human small and large intestine will be briefly described here. The intestinal tract is essentially a tube consisting of three layers. The outer protective layer is called the serosa and is composed of connective tissue. The middle layer is a muscle layer that is able to produce rhythmical contractions to force digested food along through a process called peristalsis. The inner surface of the intestinal tract constitutes a sheet of cuboidal epithelial cells called the mucosa, which process and absorb nutrients from food.

The small intestine is the site where most chemical digestion of food and absorption of nutrients occurs. The first part of the small intestine, the duodenum, is where the acidic gastric content is neutralised. The remainder of the small intestine, the jejunum and ileum, together typically measure 4-6 metres in humans. In the large intestine, remaining water is removed and the semi-solid faeces are passed onto the rectum before expulsion from the body.

The normal biology of the intestinal epithelium is similar in humans and mice. To increase the absorptive surface area, the small intestine is composed of luminal protrusions called villi and invaginations within the mucosa called the crypts of Lieberkühn (Figure 1.1). The colorectrum does not contain villi, so has a flat surface epithelium, but it also contains crypts.

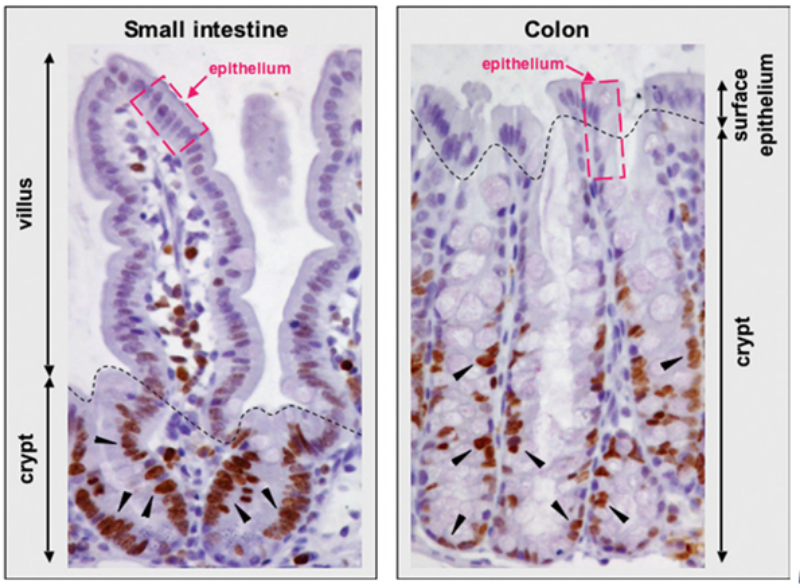


Figure 1.1: Morphology of small intestinal and colonic mucosa of an adult mouse. Figure adapted from ref [5], with permission of John Wiley & Sons, Inc.. The small intestine epithelium is organised into crypts and villi (delimited by dashed lines). In the colon, the crypts are larger and there are no villi but a flat surface epithelium. Proliferative units are shown by expression of the cell cycle marker Ki67 (arrowheads).

1.1.2 Life cycle of intestinal epithelial cells

Intestinal homeostasis involves complex interactions between stem cells, their progeny and the microenvironment. There is rapid renewal of the intestinal epithelial layer, with almost the whole epithelium renewed every three days in mice and five days in humans [6]. Intestinal stem cells are located at the bottom of the crypt and give rise to transit-amplifying cells. Epithelial cells are in a constant upward movement and as cells migrate up the crypt they differentiate into absorptive enterocytes, goblet cells (secreting mucous) or enteroendocrine cells (secreting gut hormones). Cells undergo apoptosis and are shed into the lumen as they reach the top of the villus. Another cell type found in the small intestine, called Paneth cells (secreting anti-bacterial proteins), escape the upward cell migration and reside at the bottom of the crypt alongside stem cells.

1.1.3 Colorectal cancer: Cell biology

Disruption of intestinal epithelial homeostasis can lead to the formation of neoplastic lesions. Colorectal cancers originate from the epithelial lining of the colon. CRC initiation and progression has been well described by the adenoma-carcinoma sequence. In humans the smallest identifiable lesions are aberrant crypt foci (ACF) which can be hyperplastic or dysplastic. Dysplastic ACF are possibly precursor lesions to adenomatous polyps (adenomas), where 'polyp' is a general term to describe localised lesions that project above the surrounding mucosa. ACF have been identified in some mouse models of colorectal cancer for example in Apc^{1638N} mice [7], however, they have only been identified at a low frequency in Apc^{Min} mice [8]. Adenomas arise from glandular epithelium and are characterised by dysplastic morphology and altered differentiation of epithelial cells within the lesion. Adenomas are considered the main precursors to carcinomas. As tumour cells become invasive they penetrate the muscularis mucosae into the submucosa. Tumour cells can ultimately metastasise to the lymph nodes, liver, lung or other tissues. Cancers progress from benign to malignant tumours by the accumulation of genetic events (section 1.1.4).

Aberrant stem cell behaviour has been studied extensively as an underlying cause of cancer. Recently a number of papers have identified putative stem cell markers in the gastrointestinal tract including: a polycomb ring finger protein (*Bmi1*) [9]; neural RNA-binding protein Musashi (*Msh1*) [10; 11] and the leucine-rich-repeat-containing G-protein coupled receptor 5 (*Lgr5*) [12]. Lineage-tracing experiments by Barker *et al* [12] provided compelling evidence that identified *Lgr5*, a Wnt target gene, as a reliable stem cell marker. These discoveries allow assessment of the stem-cell compartment in mouse intestinal tumorigenesis models.

1.1.4 Mutations of critical signalling pathway components

In 1990, Fearon and Vogelstein formalised a model of colorectal tumorigenesis in which successive accumulation of mutations in tumour suppressor genes and oncogenes was required for tumour progression [13]. Since then, extensive sequencing efforts have elucidated that over 80 somatic mutations may be present in a primary CRC, however, only a limited number of these genes are mutated in a large proportion of tumours [14]. The most frequently occurring mutations in CRC are found in *APC* followed by *KRAS*, *TP53*, *PIK3CA*, *BRAF*, *FBXW7* then *SMAD4* [15; 16; 17]. Typically, *APC* mutations initiate the tumour-development pathway but are then followed sequentially by mutations in other genes. As *FBXW7* mutations have been detected in adenomas, these mutations may occur as an early event in colorectal tumorigenesis [18; 19; 20]. Figure 1.2 shows schematic representation of the accumulation of genetic mutations in the adenoma-carcinoma sequence of CRC.

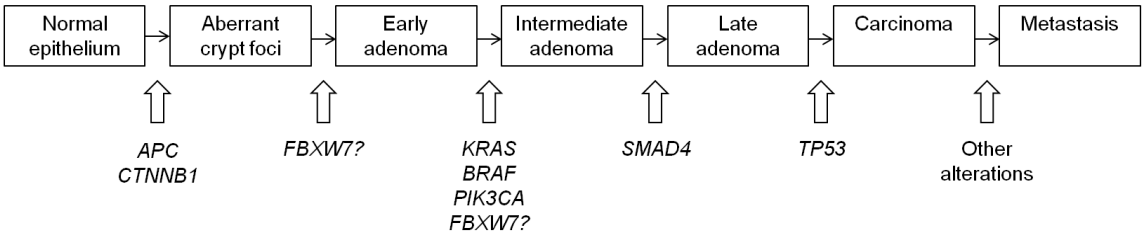


Figure 1.2: Genetic model of colorectal carcinogenesis. Mutations of *APC* or *CTNNB1* are required for tumour initiation. Subsequent progression towards malignancy is accompanied by sequential mutations in *FBXW7*, *KRAS*, *BRAF*, *PIK3CA*, *SMAD4* and *TP53*.

In the next section I will briefly describe mutations in *APC*, *KRAS*, *TP53* and *SMAD4*. The main focus of this thesis however, will concentrate on mutations found in *FBXW7* (section 1.3).

1.1.4.1 *Adenomatous Polyposis Coli (APC)*

Several Mendelian syndromes predispose to CRC. However, these syndromes account for the minority of CRC cases, with 95% occurring sporadically [21]. Despite this,

studies of hereditary colorectal cancer syndromes greatly improved knowledge of the molecular genetics of cancer development and proved highly relevant to understanding the biology of sporadic CRC. Familial adenomatous polyposis (FAP) is an autosomal dominant inherited disease characterised by the presence of numerous (hundreds to thousands) adenomatous polyps in the colon and rectum. These polyps develop in patients in their late teens/early twenties and often progress to adenocarcinomas. Germline 5q21 deletions and genetic linkage analysis of FAP kindreds identified *APC* as the gene mutated in FAP [22; 23]. In sporadic cases of CRC, spontaneous mutations in *APC* are acquired somatically in colonic epithelial cells, usually early in tumour development.

APC encodes a 312 kDa protein which exhibits a broad range of functions in cell adhesion, migration, apoptosis and chromosomal segregation in mitosis [24]. Importantly, APC also plays a critical role in the Wnt signalling transduction pathway, by its ability to interact with β-catenin via specific β-catenin-binding protein domains. This role of APC is crucial in regulating intestinal epithelial cell proliferation. The Wnt signalling pathway is summarised schematically in Figure 1.3. In brief, in the absence of a WNT signal, APC as part of the 'destruction complex' with AXIN and GSK3-β phosphorylates β-catenin. This phosphorylation event targets β-catenin for ubiquitination by the β-transducin repeat-containing protein (β-TrCP) ubiquitin ligase complex, subsequently marking it for degradation by the proteasome. Conversely, in the presence of a WNT signal, the 'destruction complex' is inhibited and fails to phosphorylate β-catenin which thus accumulates in the cytoplasm prior to translocation to the nucleus where it activates the transcription of TCF-responsive genes, for example *MYC* and *CCND1* [25; 26].

Notably, when APC is inactivated, phosphorylation and degradation of β-catenin is disrupted mimicking constitutive activation of WNT ligand-mediated signalling. Bi-allelic inactivating mutations, often found in the last exon of *APC*, result in trun-

cated APC proteins in 70-80% of sporadic CRCs. Bi-allelic null *APC* mutations are rarely found in human tumours. Instead, the two-hits are co-selected dependent on their remaining β-catenin binding domains, to leave a critical, yet partial, ability to downregulate β-catenin. The combination of mutations from both alleles produces an optimal level of Wnt signalling; this concept has been coined the 'Just-Right' hypothesis [27; 28]. This activation of the canonical Wnt signalling pathway in the colonic epithelium is a major event in polyp initiation.

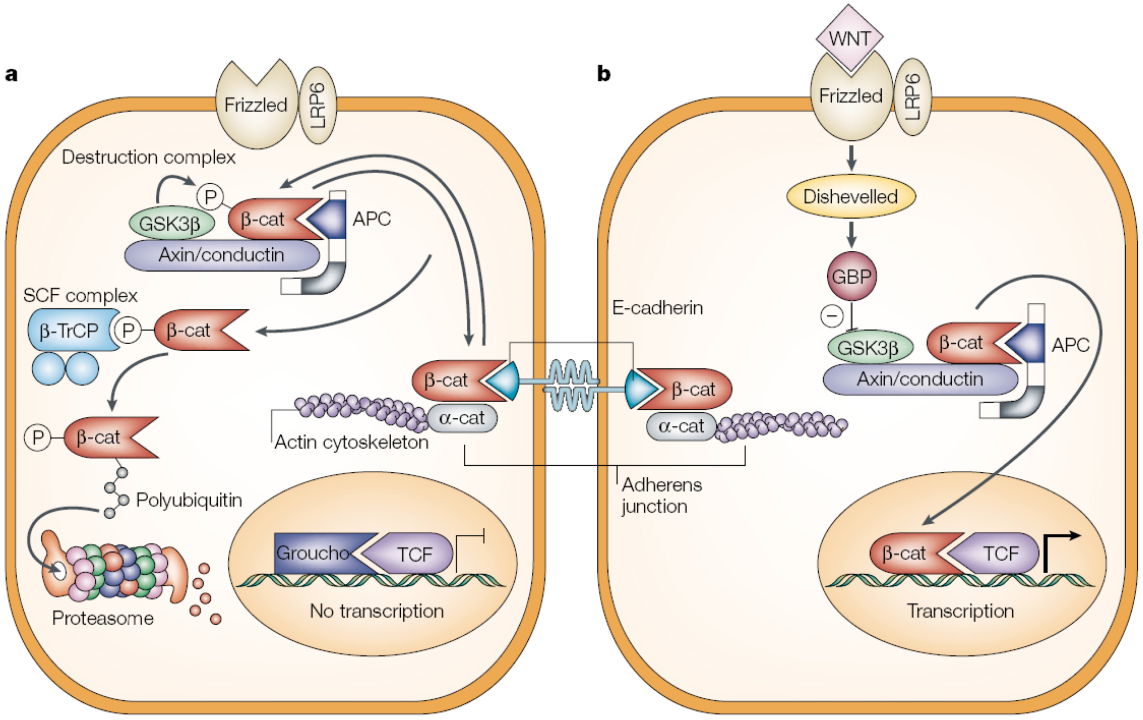


Figure 1.3: Summary of the Wnt signalling pathway (Reprinted by permission from Macmillan Publishers Ltd: [Nat Rev Cancer] (ref [29]), copyright (2002)).
a) In the absence of a WNT signal, free cytoplasmic β-catenin is recruited to a 'destruction complex' containing APC, axin/conductin and GSK3-β. CK1α (casein kinase 1α) and GSK3-β phosphorylate β-catenin allowing it to be ubiquitinated by β-TrCP and thus degraded in the proteasome. Groucho, a co-repressor, prevents the activation of TCF-responsive genes in the absence of β-catenin. b) In the presence of WNT, its receptor Frizzled is activated in a complex with LRP6. This leads to a signalling cascade in which Dishevelled activates GBP, an inhibitor of GSK3-β. Consequently β-catenin cannot be targeted for destruction and is free to diffuse to the nucleus where it acts as a co-activator for TCF-responsive genes.

1.1.4.2 *KRAS*

There are three isoforms of the *RAS* gene - *KRAS*, *HRAS* and *NRAS*, although, of these three genes, *KRAS* is the most frequently mutated in human tumours of epithelial origin.

RAS genes encode 21 kDa membrane-bound proteins, with intrinsic GTPase activity and signal transduction capacity [30]. Upon activation by growth factors, RAS becomes attached to GTP and commences a signalling cascade that induces cell proliferation. The mutated RAS product is less sensitive to the hydrolysing action of GTPase activating proteins and therefore maintains constitutive activation.

In human colorectal tumours, missense mutations of codon 12 or 13 of *KRAS* are present in 40-45% of sporadic adenomas and carcinomas [31]. *KRAS* mutations are often relatively early events in colorectal tumorigenesis.

1.1.4.3 *SMAD4*

SMAD4 is a component of the TGF-β signalling pathway. In brief, TGF-β ligands (TGF-β, BMP and activins) bind to receptor molecules (type I and type II serine-threonine kinase receptors) which results in the cross-phosphorylation of the type I receptor by the type II receptor. Intracellular messengers of the TGF-β signalling pathway are classified into three groups of SMAD proteins: receptor-regulated SMADs (R-SMADs: SMAD1/2/3/5/8), common SMAD (SMAD4) and inhibitory SMADs (SMAD6/7). R-SMADs become phosphorylated by activated type I receptors, associate with SMAD4 and translocate to the nucleus where this SMAD4 complex regulates transcription of target genes. TGF-β plays an important role in inhibiting proliferation of normal epithelial cells [32], for example by transcriptionally regulating *CDKN1A*, which encodes a cyclin-dependent kinase inhibitor. Paradoxically, TGF-β signalling may induce tumour progression by promoting angiogenesis, epithelial-to-mescenchymal transformation and immunosuppressive activities [33]. TGF-β ligands

signal through R-SMADs SMAD2 and SMAD3, whereas BMP signalling is mediated through SMAD1/5/8. In human CRC, 34% of sporadic tumours show loss of SMAD4 protein but less than 10% have *SMAD4* mutations [34; 35].

1.1.4.4 *TP53*

TP53 is a tumour suppressor gene encoding a transcription factor that has critical roles in cell cycle inhibition, apoptosis, maintenance of genomic stability and inhibition of angiogenesis [36]. In response to DNA damage or cellular stress, p53 activity increases, initiating a cascade of events that block cell division and may result in apoptosis. The p53 protein does not function correctly in most human cancers; in about half of these tumours, p53 is inactivated directly as a result of mutations in the *TP53* gene [37].

TP53 mutations are found in 50-60% of human colorectal carcinomas but such mutations are only seen in less than 10% of colorectal adenomas [31], indicating that they occur as a relatively late event in tumorigenesis.

1.2 Ubiquitin proteasome system

FBXW7 is a key component of an SCF E3 ubiquitin ligase complex. The ubiquitin proteasome system plays a critical role in regulating both normal and cancer-related cellular processes by tagging proteins for degradation in cellular compartments called proteasomes. Protein degradation is a routine process which disposes of damaged, misfolded or mutant proteins that could be harmful to cells, as well as removing regulatory proteins that control signal transduction, transcription, cell cycle and antigen processing. The proteasome was first described in 1988 and is a large multi-subunit organelle composed of proteases and enzymes which hydrolyse ATP [38]. Ubiquitin is a 76 amino-acid, highly evolutionary conserved protein, containing seven lysine

residues that function as receptor sites for ubiquitin molecules to form chains of different linkages. Proteins that require degradation through this system are marked by the covalent addition of polyubiquitins, which are attached to lysine residues in the target protein. Attachment of four or more ubiquitin molecules through K48 lineages typically targets a protein for degradation, whereas polyubiquitin chains linked through other lysines have non-proteolytic functions. Ubiquitin-mediated degradation is a complex, energy dependent process. Ciechanover and co-workers described the enzymes involved: ubiquitin-activating enzymes (E1s), ubiquitin-conjugating enzymes (E2s) and ubiquitin ligases (E3s) [39]. Figure 1.4 shows an overview of the enzymatic cascade of the ubiquitin proteasome system. In brief, ubiquitin moieties are added to substrates via a series of enzymatic reactions to target them for degradation in the 26S proteasome. In humans, there is one E1 enzyme, but a large number of E2 and E3 enzymes conferring substrate specificity.

1.2.1 E3 ubiquitin ligases

E3 ubiquitin ligases are a group of enzymes that play a fundamental role in the enzymatic cascade that ubiquitinates proteins for degradation in the proteasome. They can be classified into three groups: single-subunit RING finger type, multi-subunit RING finger type and HECT domain type. Throughout this thesis I will focus on a specific multi-subunit RING finger type called the SKP1-CUL1-F-box protein (SCF) E3 ubiquitin ligase. Figure 1.5 shows the components of this complex.

The F-box protein is the component that confers substrate specificity through its protein interaction domain, which is either a WD40 domain or a leucine-rich repeat domain. The F-box domain, first discovered in cyclin F, is a 40 amino-acid domain that permits interaction with S-phase kinase-associated protein 1 (SKP1), the linker protein between the F-box protein and the rest of the SCF complex [41]. Cullin1 (CUL1) is a scaffold protein, which associates with SKP1 at one end and RBX1

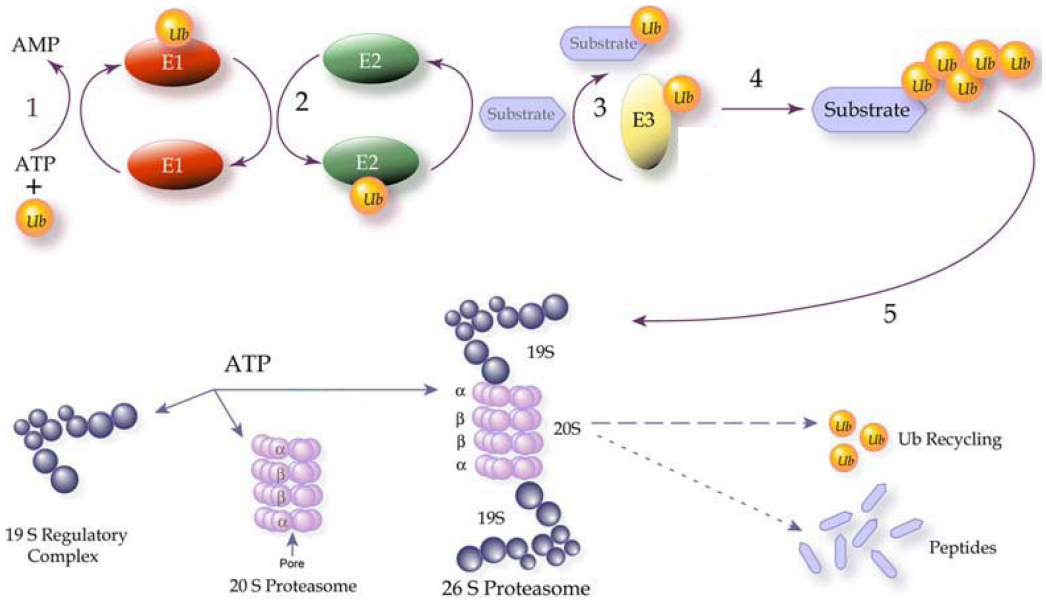


Figure 1.4: Overview of ubiquitin-proteasome pathway, figure modified from ref [40] reprinted with permission from Elsevier. Step 1: Ubiquitin activation, step 2: Ubiquitin-activating enzyme (E1) mediates an ATP-dependent transfer of ubiquitin to a ubiquitin-conjugating enzyme (E2) via a thioester linkage, step 3: Ubiquitin-ligase (E3) facilitates the transfer of ubiquitin from the ubiquitin-conjugating enzyme (E2) directly to the substrate, step 4: Ubiquitin chain elongation by conjugation of ubiquitin to lysine residues of ubiquitin at position 48 by ubiquitin-ligase enzyme (E3), step 5: transfer of ubiquitin tagged proteins for ATP-dependent substrate degradation by 26S proteasome (assembles from a 20S and two 19S regulatory subunits). The tagged protein is broken up into short pepetides and ubiquitin is released and recycled by activity of deubiquitinating enzymes.

(RING box 1) at the opposite end. RBX1 associates with the ubiquitin-conjugating enzyme (E2). To summarise, all the components of the SCF machinery function to bring substrates into close proximity to the core ubiquitination machinery to facilitate ubiquitination.

There are approximately 70 F-box domain-containing proteins in the human genome, each likely to target a unique set of substrates for degradation, although the majority of these F-box proteins still remain uncharacterised [42]. Several F-box proteins have been directly linked to tumorigenesis, these include Skp2, an oncoprotein that catalyses the ubiquitination of cell-dependent kinase inhibitors that negatively regulate cell cycle progression [43] and FBXW7 which will be the focus of this thesis.

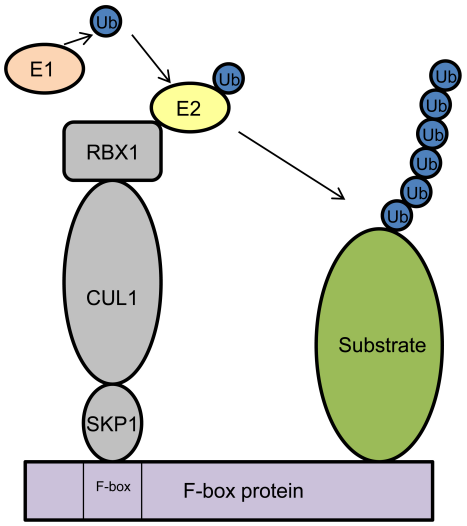


Figure 1.5: Schematic representation of an E3 SCF ubiquitin ligase complex. Components include: SKP1 (S-phase kinase-associated protein 1), CUL1 (cullin1), RBX1 (RING box1) and an F-box domain protein which binds the ubiquitin machinery via its F-box domain. RBX1 recruits the E2 (ubiquitin-conjugating enzyme) that was previously charged with ubiquitin by the E1 (ubiquitin-activating enzyme). Polyubiquinated substrates are then targeted for destruction by the proteasome.

1.3 *FBXW7*

1.3.1 Introduction to function

It is now recognised that *FBXW7* is a tumour suppressor gene, as it is a negative regulator of multiple proteins with established roles in the control of cell division and growth and is perturbed in many human malignancies [1].

The *FBXW7* (F-box and WD40 repeat domain-containing 7, also known as *FBW7*, *hCDC4*) gene spans over 200 kb on human chromosome 4q and encodes the substrate recognition component of an SCF-E3 ubiquitin ligase complex. *FBXW7* has been highly conserved throughout evolution; it is called *Cdc4* in *Saccharomyces cerevisiae*, *Sel-10* in *Caenorhabditis elegans* and *Ago* in *Drosophila melanogaster*. Furthermore, the protein sequence of FBXW7 is 96% identical between human and mouse (Appendices C.1, C.2, C.3).

Cdc4 was first identified as a regulator of cell-cycle related proteins in *Saccha-*

romyces cerevisiae by Hartwell and colleagues in 1973 [44]. It was later discovered to be important for the regulation of cyclin-dependent kinase inhibitors including Sic1 [45] and Far1 [46]. In *Caenorhabditis elegans*, Sel-10 was first discovered as a negative regulator of Lin-12 (Notch) signalling by genetic screening [47]. FBXW7 negatively regulates the abundance of an expanding list of key oncoproteins including cyclin E, c-Jun, c-Myc and Notch (section 1.3.9). There are several excellent reviews of the growing knowledge of FBXW7 [48; 49; 50; 51].

1.3.2 Isoforms

There are three transcripts of FBXW7 (α, β and γ) produced by alternative splicing [52; 53; 54; 55]. Each isoform has a unique first exon, while exons 2 to 11 are common to all isoforms. Each isoform also possesses its own promoter and therefore may be subjected to isoform-specific transcriptional control (section 1.3.11.1). The N-terminal ends of FBXW7 protein isoforms are different and *in vitro* work using fluorescently tagged proteins by Welcker and colleagues [56] elucidated that each isoform occupies a different subcellular location (Figure 1.6). The α isoform is localised to the nucleus, the β isoform to the endoplasmic reticulum of the cytoplasm [57] and the γ isoform to the nucleolus [56]. A nuclear localisation signal and trans-membrane domain has been identified in the isoform specific exons of α and β isoforms respectively, thus mediating their cellular localisation. Furthermore, it has recently been recognised that localisation of FBXW7γ to the nucleolus is dependent upon binding to regulatory proteins including nucleophosmin [58] and EBNA1-binding protein 2 (EBP2) [59].

Importantly, Matsumoto *et al* [60] explored the tissue-specific expression of mRNA levels of *Fbxw7* isoforms in adult mouse tissues, highlighting that whilst *Fbxw7*α was expressed ubiquitously, *Fbxw7*β and *Fbxw7*γ were only detected at high levels in the brain and muscles respectively.

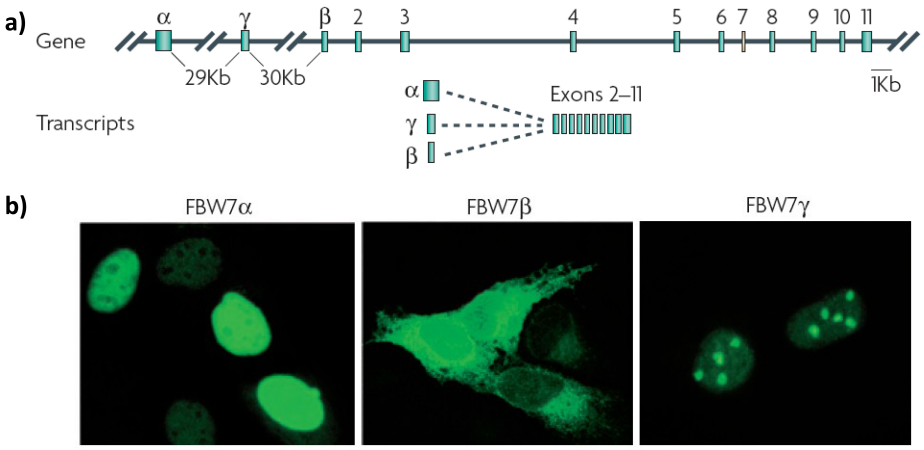


Figure 1.6: FBXW7 isoforms, figure modified by permission from Macmillan Publishers Ltd: [Nat Rev Cancer] (ref [50]), copyright (2007). a) Schematic of alternative splicing that generates three distinct transcripts and proteins of FBXW7 (α, β and γ). Each isoform has a unique first exon and common exons 2-11. b) Distinct subcellular localisations of FBXW7 isofoms in U2OS cells using fluorescently tagged proteins have localised FBXW7α to the nucleus, FBXW7β to the cytoplasm and FBXW7γ to the nucleolus.

Akhoondi *et al* [1] identified a mutation in a prostate carcinoma, whereby a proline insertion at amino acid 16 of the FBXW7α isoform led to mislocalisation of FBXW7α to the cytoplasm and thus prevented its interaction with cyclin E. Isoform-specific studies in cell-culture systems have also revealed that FBXW7 isoforms have non-redundant functions [61]. Additionally, it has been reported that in certain cell lines both FBXW7α and FBXW7γ are cooperatively involved in the ubiquitination of cyclin E [62; 63].

In order to address isoform-specific functions *in vivo*, mice lacking FBXW7β were generated and did not display any developmental abnormalities, appearing normal at least up to 1 year of age [57]. However, primary cultures of cells derived from the brains of these mice were sensitive to oxidative stress; thus it was hypothesised that the β isoform may degrade a currently unknown substrate that is necessary for sensitivity to reactive oxygen.

1.3.3 Protein domains

FBXW7 has several important protein domains depicted in Figure 1.7.

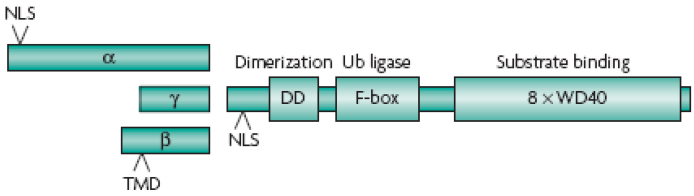


Figure 1.7: Functional protein domains of FBXW7, figure modified by permission from Macmillan Publishers Ltd: [Nat Rev Cancer] (ref [50]), copyright (2007). The three isoforms of FBXW7 are shown. The isoforms differ in their N-termini, which contain dominant signals to localise FBXW7α to the nucleoplasm and FBXW7β to cytoplasmic membranes (Golgi and ER). FBXW7γ localises to the nucleolus. DD: dimerisation domain, NLS: nuclear localisation signal and TMD: trans-membrane domain.

1.3.3.1 F-box domain

As discussed in section 1.2.1, in SCF-E3 ligases the F-box domain allows the association with the rest of the E3 SCF complex through direct interaction with SKP1 [41].

1.3.3.2 WD40 domain

The WD40 domain is a protein-interacting domain which contains repeats of 40-60 amino acids that terminate with tryptophan-aspartic acid (WD) residues [64]. Crystallographic studies have revealed that the WD40 domain forms an eight-bladed barrel-shaped β-propellor structure, with the propellors providing a binding pocket for substrates in both yeast Cdc4 [65] and human FBXW7 [66]. Critical arginine residues at the apex of the propellors (R465, R479 and R505) directly interact with the phosphodegron sequences (section 1.3.4) in substrates [65; 66].

It has been reported that most F-box proteins mediate their own degradation via an autocatalytic mechanism when their substrates are unavailable [67]. However,

Pashkova and colleagues [68] have recently identified residues within the WD40 domain that are involved in ubiquitin binding and hence in autoregulation of FBXW7 protein levels.

1.3.3.3 Dimerisation domain

In addition to the important F-box and WD40 domains, another protein-interacting domain called the dimerisation domain has been identified just upstream of the F-box [69; 70; 71]. This domain was identified by immunoprecipitation experiments using tagged FBXW7α constructs transiently expressed in 293A cells. Although not all substrates require FBXW7 dimerisation to regulate their degradation, this may allow for more efficient degradation of substrates with lower affinity phosphodegrons (section 1.3.4). For example, the protein cyclin E can be regulated by either FBXW7 dimerisation or hyper-phosphorylation of the C-terminus CPD at T380/S384, providing an additional level of regulation [69; 70] (section 1.3.9.1).

1.3.4 CDC4 Phosphodegron (CPD)

Substrates which interact with FBXW7 have a motif containing the CDC4 phosphodegron (CPD) consequence sequence. This optimal motif was identified by Nash and colleagues [72] through structural studies in *S.cerevisiae*. Several characteristics of the CPD were determined and it was found that a phosphorylated threonine at the central position, a proline in the 1+ position, as well as a negatively charged residue at the 4+ position were strongly required. Figure 1.8 shows the CPD motifs in some FBXW7 substrates. Structural and mutational studies have highlighted that the points of contact between substrates and FBXW7 occur by hydrogen bonds between the central phosphorylated threonine/serine in the CPD of the substrate and arginine residues in the β-propellor repeats in the WD40 domain [53; 65]. Some substrates have several CPDs with different affinities for FBXW7, phosphorylation of multiple

phosphodegrons may also require FBXW7 dimerisation for substrate degradation as exemplified by degradation of the yeast Cdc4 substrate Sic1 [66].

CPD: I/L–I/L/P–pT–P–<K/R>4
(where K and R are unfavourable residues in positions 2 to 5).

CYCLIN E	L	L	**T**	P	P	Q	**S**	G	K	
CYCLIN E	I	P	**T**	P	D	K	**E**	D	D	
C-MYB	L	M	**T**	P	V	S	**E**	D		
MYC	L	P	**T**	P	P	L	**S**	P	S	
JUN	G	E	**T**	P	P	L	**S**	P	I	
SBERBP1	T	L	**T**	P	P	P	**S**	D	A	
NOTCH1	F	L	**T**	P	S	P	**E**	S	P	
PRESENILIN1	I	Y	**T**	P	F	T	**E**	D	T	
TGIF1	F	N	**T**	P	P	P	**T**	P		
KLF5 1	L	N	**T**	P	D	L	D	M		
KLF5 2	P	P	**S**	P	P	S	**S**	E		
KLF5 3	N	L	**T**	P	P	P	**S**	Y		
SV40 large T antigen	P	P	**T**	P	P	P	**E**	P	E	
MCL1 1	G	S	A	G	A	S	P	P	S	T
MCL1 2	A	D	A	I	M	S	P	E	E	E
C/EBPα	H	P	**T**	P	P	P	**T**	P		
mTOR	L	L	**T**	S	I	H	**L**			
SRC			**S**	P	M	A	**S**			
PGC1 1	P	L	**T**	P	E	S	**P**	N		
PGC1 2	G	L	**T**	P	P	T	**T**	P		
P63	L	P	**S**	V	S	Q	L	I	N	P

Figure 1.8: Alignment of phosphodegron (CPD) sequences of FBXW7 substrates. Note the central phosphorylated threonine residue, the proline at the 1+ position and the negative charge at the 4+ position. Several substrates contain more than one CPD sequence.

1.3.5 FBXW7 and cancer

1.3.5.1 Cancer types

Since it became apparent that FBXW7 regulates many oncoproteins, it was hypothesised that mutations in *FBXW7* may cause tumorigenesis. *FBXW7* mutations were initally identified by Spruck and colleagues in ovarian and breast cancer cell lines

[52; 55]. Since then many studies have assessed *FBXW7* mutation status in a range of cancer types and Table 1.1 summarises the frequency of *FBXW7* mutations, categorised by tissue type according to the Sanger Institute catalogue of somatic mutations in cancer (COSMIC) database [73]. A study by Akhoondi *et al* [1] significantly contributed to this collection, as extensive genetic screening of over 500 primary tumours of diverse tissue origins was carried out, identifying mutations in *FBXW7* in 6% of tumours. *FBXW7* mutations were observed in many different types of malignancies, including both solid tumours and haematological neoplasms. Variations in mutation frequencies amongst these tissues were seen, with highest frequencies found in the bile duct, endometrium, blood and colorectrum. Individual studies analysed various tumour types including acute myeloid leukaemia, oesteosarcoma, melanoma, liver and lung tumours and showed absence or infrequent mutations in *FBXW7* [74; 75; 76; 77]. The tissue-specificity of *FBXW7* mutations is discussed further in section 1.3.10.

Tissue	**Mutation rate %**	**No of samples**
Biliary tract	29.6	27 (8)
Endometrium	10.9	119 (13)
Large intestine	9.3	1009 (94)
Haematopoietic + Lymphoid	7.5	1529 (115)
Stomach	6.4	249 (16)
Cervix	5.9	17 (1)
Ovary	3.3	269 (9)
Pancreas	3.0	99 (3)
Skin	2.7	73 (2)
Lung	2.2	639 (14)
Kidney	1.3	237 (3)
Prostate	1.0	202 (2)
Bone	0.5	188 (1)
CNS	0.5	627 (3)
Breast	0.4	466 (2)

Table 1.1: *FBXW7* mutation frequency according to tumour site. Data obtained from COSMIC database on 18/02/12 [73]. The percentage of lesions with *FBXW7* mutations are shown with the number of samples analysed indicated. The figure in brackets shows the number of cases wherein *FBXW7* mutations were found.

Notably, substrates can also evade degradation via FBXW7-mediated destruction, if they themselves harbour mutations in the CPD motif necessary for recognition by FBXW7. For example, mutations in *NOTCH1* (section 1.3.9.4) have been identified in over 50% of cases of T-cell acute lympoblastic leukaemia (T-ALL) [78]. The majority of these mutations truncate the C-terminus of the protein in the PEST domain, which contains the CPD sequence necessary for FBXW7-mediated degradation. A selection of *NOTCH1* mutations are missense changes that occur within the CPD sequence which is centred around T2512 in the PEST domain [78; 79]. Sequencing analysis of both paediatric and adult T-ALL cases has identified *FBXW7* mutations in approximately 15-30% of cases, as an alternative mechanism to result in elevated NOTCH1 protein levels [80; 81].

1.3.5.2 Incidence of *FBXW7* mutations in colorectal lesions

The incidence of mutations in colorectal lesions has been assessed in several studies [18; 19; 20]. Rajagopalan *et al* [18] reported a 12% FBXW7 mutation rate in a cohort of 190 colorectal carcinomas. A large porportion of the mutations identified were mono-allelic mutations in the WD40 domain. Work by our group [19] analysed a cohort of 202 colorectal carcinomas, 10 metastases, 32 adenomas and 40 CRC cell lines and reported a 6% mutation rate. The majority of mutations observed were also mono-allelic missense mutations located in critical arginine residues in propellor-tips within the WD40 domain, involved in substrate binding. Loss of heterozygosity was observed infrequently, suggesting that *FBXW7* does not function as a standard tumour suppressor gene through the two-hit mechanism of inactivation described by Knudson *et al* [82]. Additionally, no colorectal tumour was found to carry two *FBXW7* mutations predicted to abolish protein function and therefore only partial loss of FBXW7 function may cause tumorigenesis [19]. Variation in the mutation frequency reported between groups was possibly due to selection biases in sample

collections.

Rajagopalan *et al* [18] also reported an *in vitro* experiment, whereby a colorectal cancer cell line (HCT116) was modified by homologous recombination using a bipartite vector system to delete exon 5 (critical F-box domain) in both alleles of *FBXW7*. This tool was used to assess aberrant cell properties mediated by deregulation of FBXW7 substrates. Analysis on this *FBXW7*-null line, identified an increased abundance of cyclin E protein levels and microscopic analysis revealed cytological abnormalities including micronuclei and formation of multipolar mitotic spindles. Based on these findings the authors hypothesised that inactivation of *FBXW7* may be a chief cause of chromosomal instability in cancer. However, work by our group [19], did not confirm an association between *FBXW7* mutation and chromosomal instabilty in a cohort of colorectal lesions. Further analysis of colorectal lesions (>800 cases) from a different cohort by our group has also failed to find an association between *FBXW7* mutation status and chromosome instability (Domingo, pers comm).

Finally, Miyaki *et al* [20] assessed the frequency of *FBXW7* mutations in colorectal tumours obtained from patients with inherited colorectal predisposition syndromes (FAP and HNPCC) and noted a similar occurence (10%) to that seen in sporadic carcinomas. The authors also assessed loss of heterozygosity, by PCR-based analysis of five microsatellite markers on chromosome 4 and reported its occurrence in 8% of tumours. All three of these studies detected *FBXW7* mutations in early colorectal lesions (adenomas) indicating they may occur as an early event in colorectal tumorigenesis.

1.3.6 Mutation spectrum

Analysis of the COSMIC data on *FBXW7* highlights that these mutations tend to be of several types, in decreasing order of frequency: i) missense changes that affect critical arginine residues, especially those at positions 465, 479 and 505 (approxi-

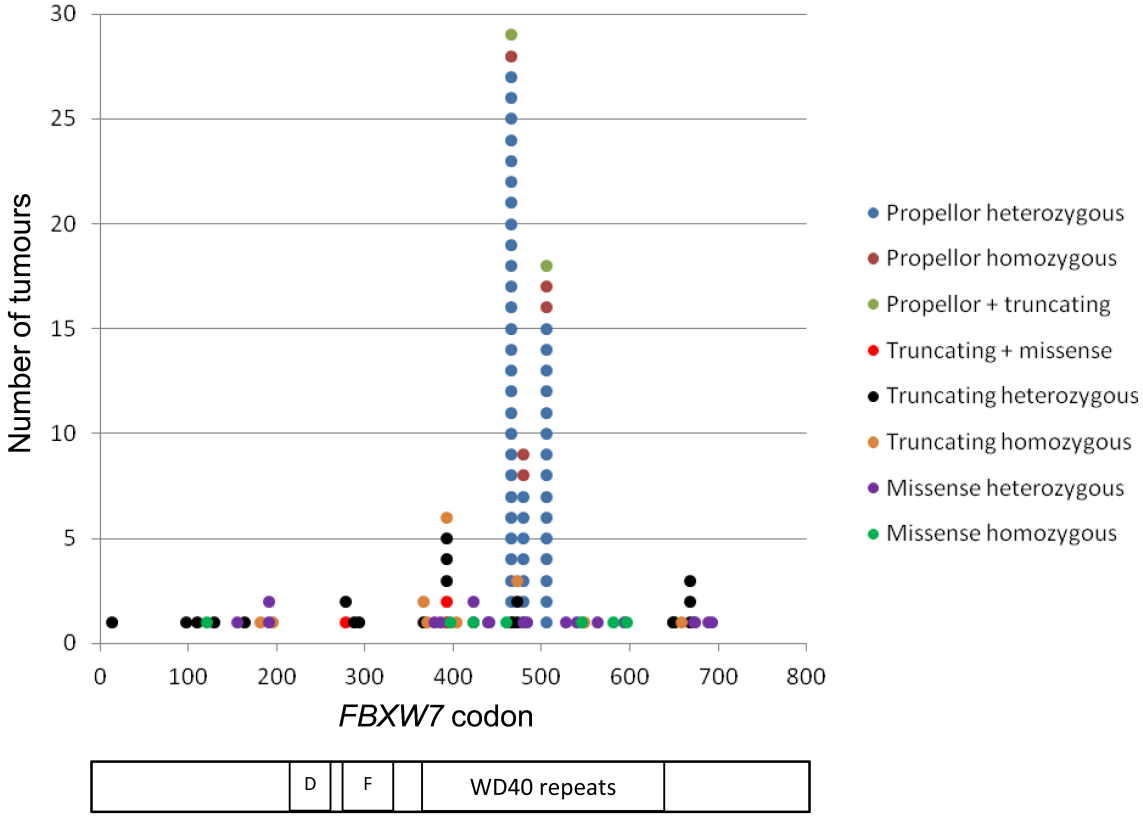


Figure 1.9: Spectrum of mutations found in *FBXW7*. Graph generated with data obtained from the COSMIC database (access Oct 2011), across all tissue types. Only cases reporting zygosity data have been included. Propellor homozygous indicates tumours that had propellor-tip mutation and loss of heterozygosity. Functional domains of FBXW7 are depicted below the graph. D = dimerisation domain, F = F-box protein domain.

mately 66% of all *FBXW7* mutations); ii) missense changes elsewhere in the gene; iii) nonsense changes throughout the gene; iv) frameshift mutations throughout the gene; v) loss of heterozygosity, generally of unknown type and copy number. Less than 4% of mutations were identified in the isoform specific exons, 6% in the F-box domain while 88% of mutations were identified in the WD40 domain.

FBXW7 is located at chromosome position 4q32 and this chromosomal region is deleted in approximately 30% of cancers across a broad spectrum [83], including oesophageal adenocarcinomas [84]. Translocations are an extremely rare mechanism of disrupting *FBXW7* in human malignancies, with only one case reported in a renal cell carcinoma [85].

Figure 1.9 visually represents the mutation spectrum of FBXW7 relative to the protein domains. Inspection of these data allow some simple observations: i) no tumours have two protein-truncating mutations, but some have one protein-truncating mutation and LOH; ii) the majority of propellor-tip mutations occurs in the heterozygous state, with loss of heterozygosity or additional truncating mutations identified rarely; and iii) tumours with mutations outside of the WD40 domain have a greater frequency of second hits.

1.3.6.1 Structural basis of arginine propellor-tip mutations

As discussed in section 1.3.6, missense mutations at arginine residues 465, 479 and 505 are the most commonly occurring *FBXW7* mutations. These residues fall within the WD40 protein-interacting domain (section 1.3.3.2). Figure 1.10 shows a structural representation of FBXW7 protein and highlights that these residues are found at the apex of β-propellor sheets which are involved in the interaction with the CPD sequence of substrates. These so called 'propellor-tip' mutations thus potentially disrupt or abolish substrate binding. Two *in silico* prediction programs, SIFT (http://sift.jcvi.org) and Polyphen (http://genetics.bwh.harvard.edu/pph) predicted

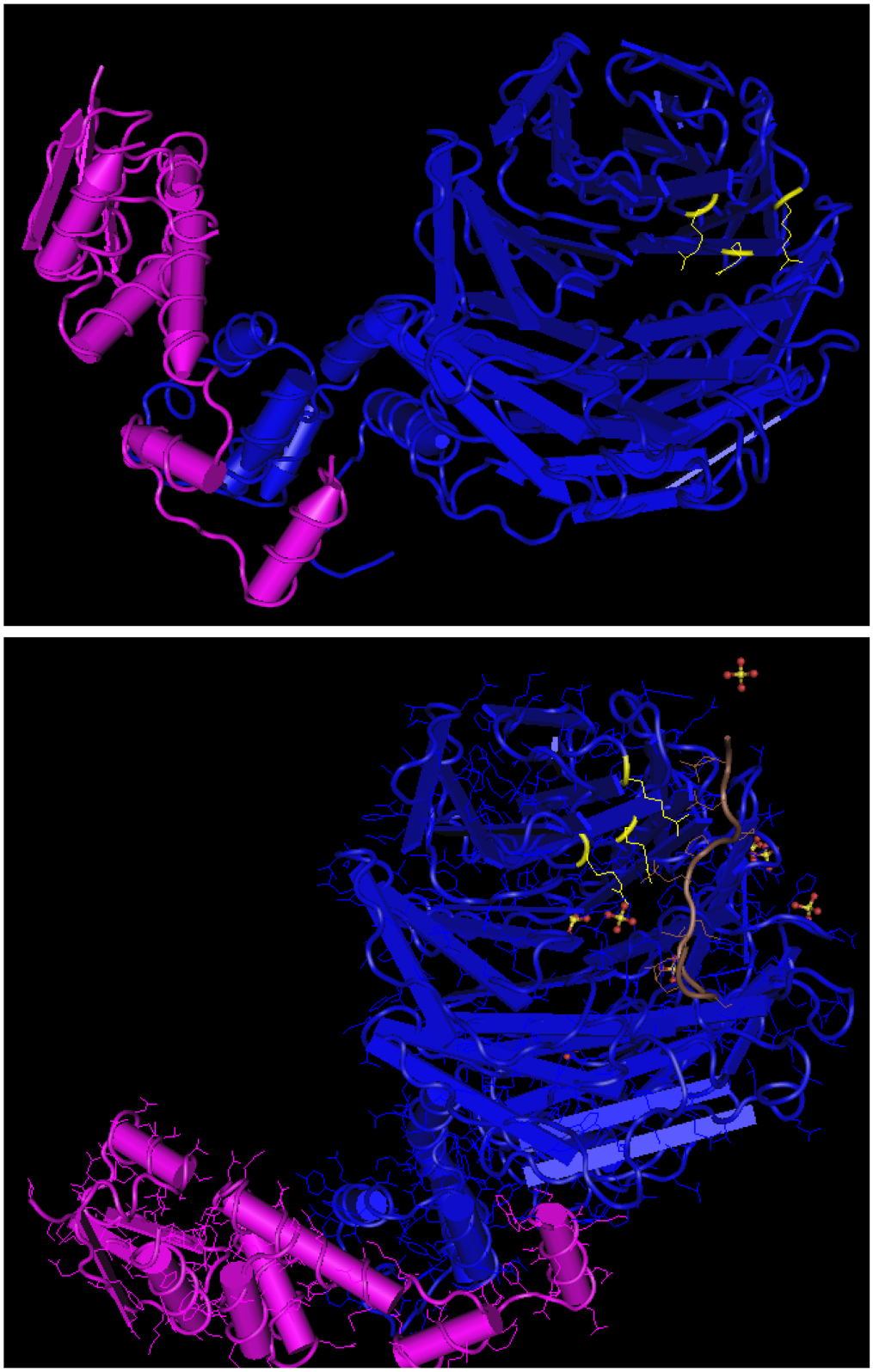


Figure 1.10: Structural model of FBXW7. The pink domain is the F-box domain, the blue domain is the WD40 domain. The yellow residues are arginines 465, 479 and 505. In the lower image the brown structure represents the CPD sequence of cyclin E. Images generated using Cn3D software (NCBI).

that R479Q substitution, from a basic to an uncharged polar amino acid, affects protein function and may be damaging.

1.3.7 Deregulation of FBXW7 in tumours without mutations in *FBXW7*

Several more recent studies have also shown that *FBXW7* expression is downregulated in several cancer types. A study in which mRNA expression of *FBXW7* was assessed by qRT-PCR analysis in glioblastoma samples, identified loss of *FBXW7* expression (independent from allelic loss) as an important step in disease progression; the mechanism for this remains unexplained [86]. Yokobori *et al* [87] also reported that loss of expression of *FBXW7* in gastric cancer has been associated with poor prognosis. CpG island promoter hypermethylation is now established as a mechanism of inactivation of tumour suppressor genes, with examples including *RB1*, *VHL* and *CDKN2A* [88]. As *FBXW7* mutations were infrequently observed in breast cancer, Akhoondi *et al* [89] assessed *FBXW7β* promoter hypermethylation by bisulphite sequencing in breast cancer samples and discovered this is a mechanism of inactivation in over 50% of specimens analysed. Promoter hypermethylation of *FBXW7β* has also been observed in thymomas [90]. MicroRNAs that target FBXW7 have recently been identified (section 1.3.11.1), potentially explaining some of these findings.

1.3.8 Mechanism of action of *FBXW7* mutations

As *FBXW7* mutations are mostly mono-allelic with a wildtype allele remaining, it was proposed that *FBXW7* was a haploinsufficient tumour suppressor gene, with loss of a single allele sufficient to promote tumorigenesis. Evidence from Mao *et al* [91] showing that heterozygous *Fbxw7*-null mutant mice had greater susceptibility to radiation-induced tumorigenesis supported this hypothesis. However, genetic data

showing few cases in which *in-trans* truncating and missense mutations occur, along with the relative low incidence of truncating mutations outside the WD40 domain, suggest that simple haploinsufficiency cannot fully explain the mutation spectrum.

It has been proposed that arginine propellor-tip mutations may abolish protein function by acting as dominant negatives [1]. A dominant negative protein can be defined as a defective protein that retains its interaction capabilities and distorts or competes with normal proteins. Mutant FBXW7 may therefore bind wildtype FBXW7 through its dimerisation domain and reduce functional protein levels by 50%. *In vitro* assays whereby overexpression of propellor-tip mutant FBXW7 reduced degradation of overexpressed cyclin E, give some credence to this hypothesis [1]. However, further evidence, especially from *in vivo* systems, is necessary to validate this hypothesis. These concepts are discussed in more detail in Chapter 3.

1.3.9 Substrates

Over 20 substrates of FBXW7 have now been reported and this list is continually expanding. The following section highlights some key details of the known substrates of FBXW7 which I have evaluated in both *in vivo* and *in vitro* work in this thesis. Table 1.2 summarises additional FBXW7 substrates that have not been studied in detail in this thesis.

1.3.9.1 Cyclin E

Many studies focus on cyclin E as one of the major substrates regulated by FBXW7. In 2001, three independent groups reported that FBXW7 was responsible for cyclin E degradation across species [52; 53; 54]. Subsequently, the critical phosphorylation site in the phosphodegron of cyclin E was identified at T380 [65; 92].

Cyclin E binds to and activates cyclin-dependent kinase 2 (CDK2) and this complex catalyses the transition from G1 to S-phase in the cell cycle. The cyclin E-CDK2

complex phosphorylates and activates proteins necessary for cell cycle progression, for example those involved in histone biosynthesis and centrosome duplication, as well as inactivating inhibitors of cyclin-dependent kinases.

In normal dividing cells, cyclin E accumulates at the G1/S-phase boundary and is degraded as cells progress through S phase thus allowing DNA replication [93]. Cyclin E periodicity is regulated by a number of factors including E2F dependent transcription, cyclin E abundance, presence of cyclin-dependent kinase inhibitors (p21 and p27) and CDK2 phosphorylation. Cyclin E unbound to CDK2 is also ubiquitinated by Cullin-3 ubiquitin ligase [94].

Elevated protein levels of cyclin E have been identified in many tumours and cancer cell lines and have been associated with poor prognostic outcome in breast cancer patients [95]. Constitutive overexpression of *CCNE1* in human breast epithelial cells was shown to result in chromosomal instability and it has been speculated that loss or mutation of *FBXW7* could also result in CIN [96; 97]. In order to explore cyclin E deregulation at more physiologically relevant expression levels, a knock-in mouse model was generated in which the T380 phosphorylation site was ablated [98]. Although these mice displayed tissue-specific elevation of cyclin E protein levels, no phenotypic abnormalities were observed up to 2 years of age. This highlighted the potential redundancy of cyclin E/CDK2 amongst other cyclin/CDK complexes. These mice showed an enhanced rate of tumorigenesis on a *Tp53*-null background [98], reiterating the importance of functional p53-p21 pathway in CDK inhibition.

Two CPD sequences were identified in cyclin E although the C-terminal one was widely considered to be the dominant phosphorylation site, a further CPD sequence was found at the N-terminus with the central phosphorylation site at residue T62 [92]. In a study in which both degrons were mutated by threonine to alanine subsitutions in a knock-in mouse model, accumulation of cyclin E principally led to proliferative abnormalities particularly in the expansion of progenitors of the haematopoietic sys-

tem, with results reminiscent of human myelodysplastic syndrome [99]. This study therefore highlighted that the N-terminal degron also has critical roles in cyclin E regulation.

There are two phosphorylation sites within the C-terminus CPD: T380, which is phosphorylated both by GSK-3β and CDK2 itself and S384, a phosphorylation site exclusive to CDK2. Phosphorylation at S384 increases the strength of the C-terminal phosphodegron by providing a negative charge at the 4+ position and allows cyclin E to be regulated by monomeric FBXW7, whereas cyclin E phosphorylated only at T380 requires FBXW7 dimerisation for degradation [66].

1.3.9.2 c-Myc

Myc proteins are basic helix-loop-helix/leucine zipper transcription factors that regulate growth, proliferation, apoptosis and differentiation. Myc dimerises with Max and binds to the DNA element CACGTG (E-box) in order to activate transcription. c-Myc protein is transiently expressed and has a short half-life of approximately 30 min [100]. c-Myc is virtually undetectable in quiescent cells, but its abundance rapidly increases as cells enter G1 in response to serum or mitogenic stimulation, decreasing to a low steady rate whilst the cells are still proliferating.

c-Myc directly regulates the expression of hundreds of target genes, including *CCND2* and *CDK4* [101; 102].

Accumulation of c-Myc is found in many tumours including lymphomas, often due to mutations, amplifications or chromosomal translocations of *MYC* [103].

Yada *et al* [104] used cell-based systems to investigate the interaction of FBXW7 and c-Myc principally in HEK293T cells. They identified the CPD of c-Myc to be centred around T58, in Myc Box 1 in the transactivation domain, which requires prior phosphorylation by GSK-3β [104]. This group also noted accumulation of c-Myc in embryonic stem cells derived from an *Fbxw7*-null mice.

It has been shown that phosphorylation at T58 requires prior phosphorylation of S62 via the MAPK pathway [105]. The γ isoform of FBXW7 was found to regulate c-Myc and it was shown that shRNA-mediated knockdown of FBXW7γ resulted in c-Myc protein overexpression and an increase in cell size [56].

Myc is also degraded by other ubiquitin ligases including SKP2 and β-TrCP [106; 107].

1.3.9.3 c-Jun

c-Jun is a transcription factor component that heterodimerises with c-Fos to constitute the AP-1 transcription factor. AP-1 activity is induced by growth factors and mediated through the extracellular signal regulated kinase (ERK) subgroup of MAPKs, which translocate to the nucleus and phosphorylate and thus promote transcriptional activity of ternary complex factors (TCF) that bind to *Fos* promoters. Additionally, induction of AP-1 by cytokines and genotoxic stress is mostly mediated by the c-Jun N-terminal kinase (JNK) and p38 MAPK cascades [108], by translocation of activated JNK to the nucleus, with consequent phosphorylation of c-Jun and enhanced transcriptional activity.

The AP-1 transcription factor controls apoptosis, proliferation and transformation by regulating the transcription of *CCND1*, *TP53* and *CNKN1A* amongst other genes [109]. It has been shown that deficiency in c-Jun can lead to apoptosis in neuronal cells [110]. This study also showed that c-Jun stability is regulated by Jun N-terminal kinase (JNK) phosphorylation in the transactivation N-terminal domain. It was later reported that c-Jun ubiquitination is mediated by FBXW7 and is dependent on phosphorylation of T239 by GSK3-β as well as priming phosphorylation of S243 in the C-terminal domain [111]. Protein levels of c-Jun are also regulated by other ubiquitin ligases including Itch [112].

1.3.9.4 Notch1

NOTCH proteins are involved in a signalling pathway important for development, differentiation, cell proliferation and apoptosis. Notch signalling plays a role in cell fate determination in many different tissues, including the nervous, vascular and haematopoietic systems and has been referred to as the 'gatekeeper against differentiation' [113]. This signalling pathway is mediated by cell-to-cell contact through interactions of Notch proteins (NOTCH 1-4), which are large transmembrane receptors and their membrane-bound ligands (Jagged1, Jagged2, Delta-like 1 (Dll1), Dll3, Dll4). Ligand binding initiates several cleavage reactions, one involving the γ secretase complex, that results in the formation of the Notch Intracellular Domain (NICD). The NICD then translocates to the nucleus where it acts in a transcriptional activation complex with the transcription factor CSL. Transcription factors of the *Hairy/enhancer of split* (*Hes*) and *Hes*-related (*HRT/HRP/Hey*) families are direct target genes of the CSL transcription factor [114].

Point mutations and chromosomal translocations involving *NOTCH1* that lead to constitutive signalling have been identified in T-cell acute lymphoblastic leukaemias [78]. Deregulated Notch signalling promotes this tumour type due to defective T-cell differentiation. Accumulating evidence implicates deregulated Notch signalling in tumorigenesis of other human malignancies [115].

Initial work in *Caenorhabditis elegans* provided genetic evidence for Sel-10 (homolog of FBXW7) to be a negative regulator of Lin-12 (homolog of NOTCH1) [47]. This interaction was subsequently identified in the mouse and human counterparts [116; 117]. A study investigating disrupted NOTCH regulation by *FBXW7* mutations in T-ALL cell lines highlighted the CPD of NOTCH1 in the PEST domain, with the central phosphorylation site at T2512 [79]. Notch1 is also regulated by other E3 ubiquitin ligases including Itch [118].

1.3.9.5 Aurora A

Aurora A kinase, a serine/threonine kinase encoded by *AURKA* is an important regulator of mitotic progression from G2 to M phase. This protein is frequently overexpressed in cancer, leading to malfunctioning G2 and spindle checkpoints, cytokinesis failure and chromosome instability [119]. Two studies observed elevated protein levels of Aurora A as a consequence of *Fbxw7* inactivation *in vitro* [91; 120]. In a study investigating the effect of *FBXW7* inactivation on chemotherapeutic agents, *FBXW7* inactivated cells subjected to spindle toxins showed elevated levels of Aurora A-induced polyploidy [121].

1.3.9.6 KLF5

Kruppel-like factor 5 (KLF5) is a zinc finger domain containing transcription factor that contributes to the TGF-β, retinoic acid and Protein Kinase C (PKC) signalling pathways [122; 123]. Hundreds of genes regulated by KLF5 have been identified by microarray analysis and are associated with cell cycle regulation, apoptosis, migration, differentiation, angiogenesis and lipid metabolism [124; 125]. Chen *et al* [124] overexpressed *KLF5* in a bladder cancer cell line and injected these cells into immunodeficient mice in order to assess the effect of *KLF5* overexpression in tumorigenesis. KLF5 was shown to promote cell proliferation and tumorigenesis primarily by upregulating *CCND1* and *PDGFA* [124]. siRNA mediated knockdown of *Klf5 in vivo* also inhibited angiogenesis in a xenograft model [126]. Two independent studies showed that KLF5 protein degradation was mediated by FBXW7, with the central CPD phosphorylation site at S303, requiring prior phosphorylation by GSK3-β [127; 128]. KLF5 has a short half-life (2 h) and is additionally regulated by the WWP1 E3 ligase and in a ubiquitin-independent manner [129; 130].

1.3.9.7 TGIF1

TGF-β-induced factor 1 (TGIF1), a member of the three-amino-acid loop extension (TALE) superfamily of homeodomain proteins, is a transcriptional repressor that negatively regulates the TGF-β pathway and retinoid acid signalling pathway [131]. The TGF-β signalling pathway regulates many cellular processes involving differentiation, proliferation and apoptosis. Section 1.1.4.3 provided a brief overview of TGF-β signalling, where a TGF-β signal binds to the heterodimeric receptor complexes and subsequent auto-phosphorylation mediates a cascade of events involving SMAD proteins that ultimately regulates transcription of specific genes. Mutations in components of the TGF-β pathway, for example *SMAD4* has been implicated in human malignancies.

TGIF1 represses TGF-β signalling by several mechanisms: it targets repressor complexes containing histone deacetylases to Smad2 [132; 133]; it recruits Tiul1-WWP1 (TGIF-interacting ubiquitin ligase 1-WW-containing protein 1), a ubiquitin ligase complex to facilitate the degradation of Smad2; and it sequesters cPML (cytoplasmic promyelocytic leukaemia), an auxiliary protein involved in Smad2 phosphorylation in the nucleus thus preventing Smad2 phosphorylation [134].

TGIF1 was found to be ubiquitinated and degraded by Fbxw7α and Fbxw7γ in a phosphorylation-dependent manner [135]. Mutation of *FBXW7* therefore could lead to an accumulation of phosphorylated TGIF1 protein and repression of TGF-β signalling.

1.3.10 Tissue-specificity of substrates

Figure 1.11 summarises how upregulation of multiple FBXW7 substrates could alter multiple cellular processes and thus contribute to tumorigenesis.

With so many substrates regulated by FBXW7, the focus of ongoing research is to pinpoint which are the most critical for specific cancer types. There is accumulating

Substrate	Function	Ref
PGC-1α	Transcriptional cofactor, regulates energy metabolism. 2 CPDs, regulated by GSK3-β and priming phosphorylation.	[136]
Presenilin	Component of γ secretase complex, mediates intracellular cleavage of Notch receptor.	[137; 138]
mTOR (mammalian target of rapamycin)	Regulates cell growth, metabolism and proliferation. Breast cancer cells with Fbxw7 mutations were responsive to rapamycin (mTOR inhibitor).	[139]
c-Myb	Proto-oncogene, regulates differentiation and proliferation in haematopoietic cells. In humans c-Myb may be regulated in a CPD independent fashion.	[140; 141]
SRC-3/AIB	Growth co-activator, the excessive activation of which results in oncogenesis. Plays an important role in the initiation and progression of mammary gland tumorigenesis. Multi (mono)-ubiquitination has been shown to enhance transcriptional activity of SRC-3.	[142]
SREBP1	Transcription factor that regulates lipid metabolism.	[143; 144]
C/EBPα	CCAAT/enhancer-binding protein transcription factor involved in adipocyte differentiation.	[145]
MCL1	Pro-survival BCL2 family member, regulates apoptosis in T-cells. The CPD is phosphorylated by GSK3-β, all Fbxw7 isoforms can target MCL1.	[146; 147]
NRF1	Nuclear factor erythoid-derived-related factor 1 transcription factor important in cellular stress response.	[148]

Table 1.2: Additional substrates that FBXW7 regulates and their functions.

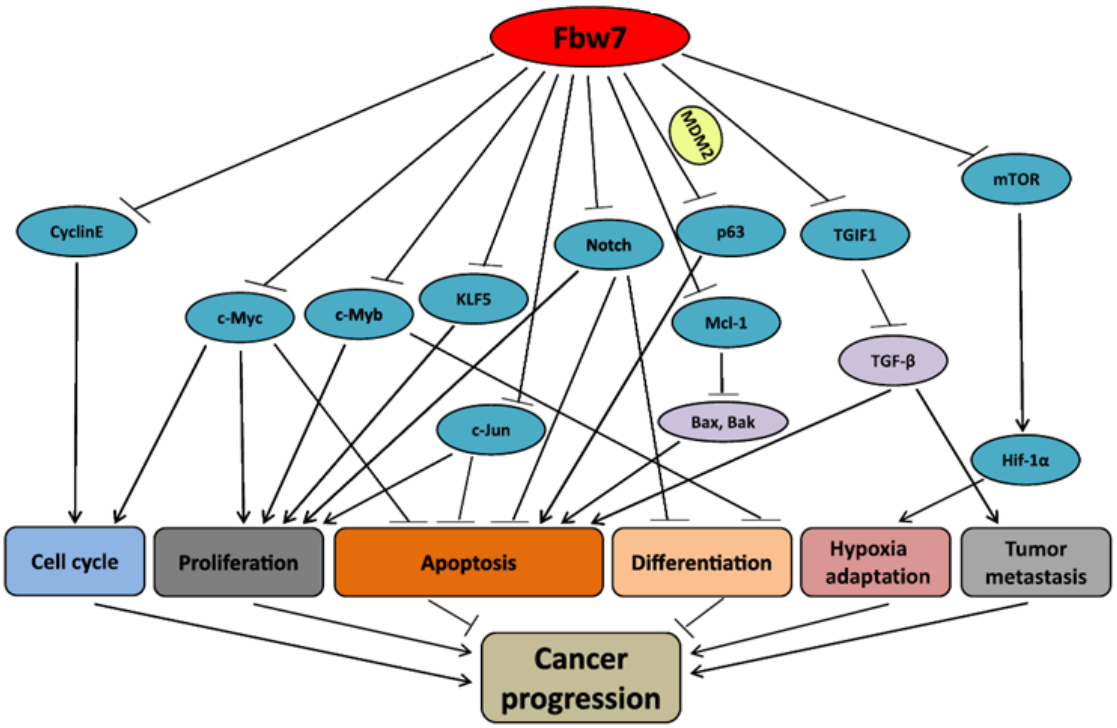


Figure 1.11: Schematic diagram of the functions of FBXW7 substrates in connection with cancer progression, adapted from ref [51] with kind permission from Springer Science and Business Media.

evidence that FBXW7 substrates are differentially regulated in a tissue-specific manner. Table 1.3 summarises the critical substrates in different tissues as identified by *in vivo* work using conditional *Fbxw7*-null systems. Many factors may contribute to this tissue-specficity, including: substrate expression, expression of kinases that are required for priming phosphorylation in CPD sequences, FBXW7 isoform abundance and expression of other ubiquitin ligases that can mediate degradation of substrates.

Tissue	Substrates	Ref
Brain	c-Jun, Notch	[149; 150]
Gut	c-Jun, Notch	[151]
Liver	Srebp1, Notch	[152]
Thymus	c-Myc, Notch	[153]
Mouse embryonic fibroblasts	c-Jun, Notch	[91; 154]
Haematopoietic stem cells	c-Jun	[155]

Table 1.3: Tissue-specificity of critical Fbxw7 substrates.

1.3.11 Regulation of FBXW7

Recent work has uncovered aspects of both transcriptional and post-translational mechanisms of *FBXW7* regulation.

1.3.11.1 Transcriptional regulation

Recent evidence showed that the transcription factor C/EBPδ binds to a sequence in the *FBXW7*α promoter directly inhibiting its transcription [156]. This results in an accumulation of the FBXW7 substrate mTOR and subsequent increased translation of HIF1-α, which allows tumour progression and metastasis by promoting adaptation to hypoxic conditions.

Additionally a cDNA microarray-based system, which re-expressed wildtype p53 in a *Tp53*-deficient glioblastoma cell line, identified *FBXW7*β as a transcriptional target of p53 [157]. A p53 binding site was subsequently revealed in exon 1β of *FBXW7*. Mao *et al* also reported that *FBXW7*β has p53 DNA-response elements in its promoter [91].

MicroRNAs, small non-coding RNAs, can post-transcriptionally control gene expression by binding specifically to mRNA targets and causing mRNA cleavage or translational repression. It has been reported that microRNA-223 (miR-223) regulates *FBXW7* by targeting the 3'-UTR [158]. Xu *et al* [158] demonstrated that overexpression of miR-223 led to reduced expression of *FBXW7* mRNA, along with increased cyclin E protein levels and genomic instability. This has been found to be clinically significant in oesophageal squamous cell carcinoma where elevated expression levels of miR-223 correlate with poor prognosis [159]. miRNA-27a has also been identified as a major suppressor of *FBXW7*, although only in the G1-S phase of the cell cycle [160].

1.3.11.2 Post-translational modifications

The most common mechanism for regulating substrate degradation by FBXW7 is phosphorylation of CPD motifs within substrates. Glycogen synthase kinase 3-β (GSK3-β) is the kinase responsible for phosphorylating most of FBXW7 substrates with the exception of Notch and Presenilin. The phosphorylation reaction generates the optimal CPD sequence in substrates, with a central phosphorylated threonine residue. Insulin and phosphatidylinositol 3 kinase (PIK-3)/Akt signalling pathways can inhibit GSK3-β activity through phosphorylation of an N-terminal serine residue that renders GSK3-β inactive [161]. This therefore inhibits phosphorylation of many substrates and blocks their subsequent ubiquitination and degradation. Several recent studies have identified additional post-translational modifications of FBXW7 which control its activity, some of which are summarised in a schematic in Figure 1.12.

Durgan *et al* [162] identified two residues (S10 and S18) in the Fbxw7α N-terminus that were phosphorylated by Protein Kinase C (a serine/threonine kinase). As these residues are close to the nuclear localisation signal, phosphorylation at these sites inhibited this signal and led to FBXW7 re-localisation.

Residues within propellor blades, distinct from those at the propellor-tips, have been identified as important for ubiquitin binding allowing autoregulation of Fbxw7 [68].

Mo *et al* [163] described Serum and glucocorticoid inducible proten kinase (SGK1) as responsible for the phosphorylation of FBXW7 at S227. This event facilitated the interaction between FBXW7 and NICD1 by generation of a heterotrimeric complex and enhanced its degradation [163]. An independent study also identified phosphorylation of S227 in a PIK-3 dependent manner, which enhanced the ability of FBXW7 to ubiquitinate c-Myc and cyclin E [164].

Deubiquitinating enzymes remove ubiquitin tags from substrates rescuing them from degradation. USP28, a deubiquitinating enzyme, has been reported to antag-

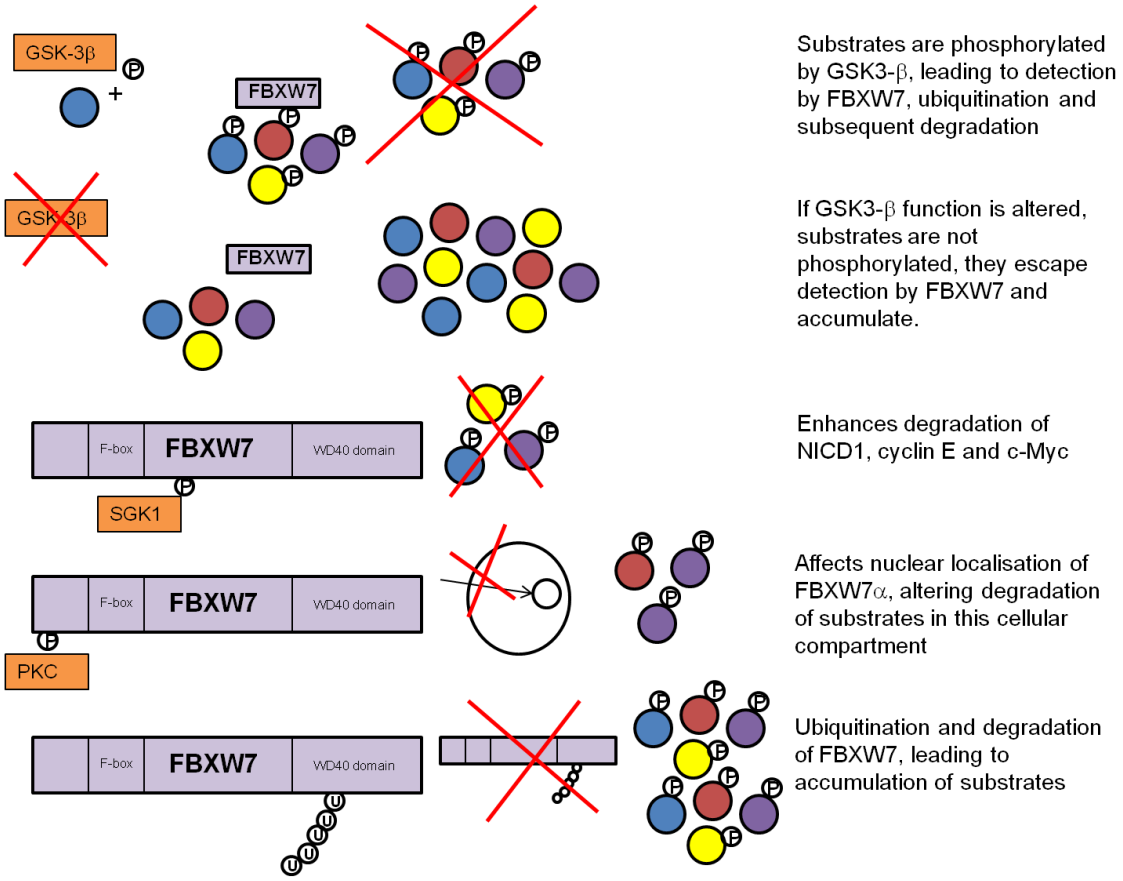


Figure 1.12: Schematic diagram of post-translational modifications that alter FBXW7 activity.

onise FBXW7-mediated ubiquitination of Myc and cyclin E in human tumour cells [107]. A study by Popov *et al* [165] identified *USP28* overexpression in breast and colon carcinomas [165]. USP9X, a deubiqitinating enzyme of MCL1 (another FBXW7 substrate) has also been reported. Increased *USP9X* expression in human follicular and diffuse large B-cell lymphomas resulted in elevated MCL1 protein levels, consistent with the removal of polyubiquitination chains that would normally mark MCL1 for proteasomal degradation [166].

1.3.12 Targeted therapeutics

Better understanding of the mechanisms of action of *FBXW7* mutations as well as the most critical oncogenic protein substrates deregulated in specific tumours types

could ultimately enable the development of targeted therapeutics, to more effectively treat the subset of cancer patients which have acquired *FBXW7* mutations. As most *FBXW7* mutant cancers retain expression of FBXW7 mutant protein, one approach would be to develop pharmacological agents that targets FBXW7 in these tumours. It has recently been reported by Orlicky *et al* [167] that a small molecular compound has been identified that inhibits wildtype Cdc4 in yeast, by distorting the substrate binding pocket allosterically by targeting the β-strands. If a similar compound that acts specifically in the propellor-tip mutant FBXW7 was developed, there may be a future in exploring *FBXW7* status as a means of targeted therapeutics. A more direct and perhaps easier approach would be to inhibit the activity of oncogenic targets of FBXW7 that are found to be most critical in specific tumour types. Compounds that target several of FBXW7 substrates (e.g c-Myc, Notch, mTOR, KLF5) have recently been developed [139; 168; 169; 170].

1.3.13 Mouse models to study Fbxw7 function

In order to study the function of FBXW7 *in vivo*, two independent groups generated simple *Fbxw7* knockout mice [171; 172]. The exons encoding the critical F-box domain were targeted in order to generate *Fbxw7*-null alleles. In the ubiquitous heterozygous mutant state, these mice appeared normal with no tumour formation up to 1 year of age. However, in a homozygous state, *Fbxw7*-null resulted in embryonic lethality at E10.5-11.5 due to a combination of compromised vascular development and cardiovascular abnormalities attributed to elevated Notch1 protein expression [171; 172].

To circumvent the problem of embryonic lethality, conditional *Fbxw7*-null mice have been generated and used to study Fbxw7 function in T-cell [153], haematopoietic stem cell [155; 173] and gut lineages [151]. These conditional mouse models are discussed in more detail in section 4.1.1.

1.4 Outline of thesis

Since it has become apparent that there is a predominance of mono-allelic missense propellor-tip mutation over other mutations in *FBXW7*, I hypothesised that these mutations provide a sufficient selective advantage for tumorigenesis. To date, all *in vivo* work has utilised *Fbxw7*-null mouse models and thus these studies do not faithfully recapitulate the most common human mutations. Surprisingly, no *in vivo* and only a few *in vitro* studies investigating specific missense arginine propellor-tip mutations have been reported to date. In order to test this hypothesis, I wished to construct a suitable *Fbxw7*-mutant mouse to search for phenotypic and functional differences from null alleles. I aimed to generate a mouse model which 'knocks-in' one of the most commonly-occurring propellor-tip missense mutations in *FBXW7* and to analyse the effects of this mutation constitutively (Chapter 3).

Work by our laboratory and others previously reported that *FBXW7* mutations occur at a moderate frequency in colorectal lesions. I therefore additionally wished to conditionally knock-in the propellor-tip mutation in the gut and study its ability to cause intestinal tumorigenesis (Chapter 4). The propellor-tip mutation was assessed in conjunction with Apc-mutant proteins, as is the case for most human colorectal tumours (Chapter 5). Throughout this thesis the novel propellor-tip mutant model was compared to an existing *Fbxw7*-null model in order to ascertain whether propellor-tip mutations provide a selective advantage over *Fbxw7*-null mutations.

An *in vitro* approach was also taken to explore the mechanism of action of *FBXW7* propellor-tip mutations using colorectal cancer cell lines (Chapter 6). Specific aims are presented at the beginning of each of the results chapters.

Chapter 2

Materials and Methods

2.1 Mouse procedures

All procedures were carried out in accordance to Home Office UK regulations and the Animals (Scientific Procedures) Act 1986. All mice were housed in individual ventilated cages initially at the animal unit at Clare Hall laboratories, Cancer Research UK, London Reseach Institute and subsequently at the Functional Genetics Facility, Wellcome Trust Centre for Human Genetics, University of Oxford.

2.1.1 Generation of $Fbxw7^{R482Q}$ mice

Design of the targeting construct was carried out by Dr Annabelle Lewis and a commercial company (Taconic) cloned the targeting construct. I took over the project from this point onwards.

Mice were derived using standard methods, in brief the target construct was linearised and electroporated into 129Sv/J embryonic stem (ES) cells and selected with G418, this was carried out by transgenic services at Cancer Research UK, Clare Hall Institute. The neomycin cassette was removed by transiently transfecting ES clones with pCM1-Cre plasmid. Homologous recombinants were identified initially by

long-range PCR analysis and subsequently by Southern blot analysis (section 2.3.7). Selected targeted ES cells were injected into C57Bl/6J blastocysts. The resultant chimeras containing tissues derived from both the transplanted ES cells and the host cells were bred with C57Bl/6J mice and genotyped to assess whether the mutation had incorporated into the germline. Mice were crossed onto the C57Bl/6J genetic background for more than six generations. All mouse colonies used for this thesis were maintained on the C57Bl/6J genetic background.

2.1.2 Ear snips

At three weeks of age, post-weaning, ear punches were taken from mice both for identification purposes and to provide material for genotyping. An identification system whereby different numbers of ear punches on either or both ears was carried out, to ensure each mouse per cage had a different identification mark. DNA was extracted from these ear snips (section 2.3.1.2) and used for genotyping.

2.1.3 Breeding

Breeding pairs were put together from the age of sexual maturity (6-weeks) onwards. Trios with two females to one stud male were also used to enhance the number of offspring per generation of breeding as required.

2.1.4 Embryo collections

In order to collect embryos at specific stages of development, timed matings were set up. Gestation was dated by detection of a vaginal plug (as embryonic day E0.5). Embryos were dissected out of the womb and killed by decapitation. The yolk sac or embryo tail were collected for genotyping. Various tissues were dissected out of the embryos and either snap frozen in liquid nitrogen or fixed in 10% neutral buffered

formalin (NBF).

2.1.5 Gut preparations

The mice were sacrificed at a pre-determined age or when showing symptoms of intestinal polyps (anaemia - white feet, hunching) by carbon dioxide asphyxiation and/or cervical dislocation and gut preparations were carried out.

The intestinal tract was removed immediately after euthanasia and divided into four segments, consisting of three equal lengths of the small intestine (proximal SB1, middle SB2 and distal SB3) and the whole of the large intestine. The intestines were opened longitudinally, using a gut preparation apparatus described by Rudling *et al* [174], washed in PBS, fixed overnight in 10% neutral buffered formalin (NBF) and then transferred to 70% ethanol for temporary storage prior to polyp counting (section 2.2.1) or processing for embedding (section 2.2.2).

2.1.6 Individual crypt isolation

After longitudinally opening the gut and washing with PBS, several 2 mm sections were sliced from the distal end of SB3 and the distal end of colon and incubated in 5 ml media (30 mM EDTA in DMEM without Ca^{2+} and Mg^{2+}, 0.5 mM DTT, 2% RNAlater (Life Technologies)) for 15 min at 37^{o}C. The digested tissue was then transferred to a small bijoux of RNase-free PBS using RNase-free forceps. This bijoux was then shaken vigorously for 30 s to release crypts. The contents of the bijoux were poured onto a small petri dish and observed under a dissection microscope. Individual crypts were selected and transferred to eppendorfs containing RLT buffer using a drawn out glass pipette, ready for subsequent RNA extraction (section 2.4.2).

2.2 Histology

2.2.1 Adenoma scoring

After fixation but before processing, gut preparations were stained with 0.2% methylene blue for 10 s and washed in PBS for 20 min. Tumours were counted with a dissecting microscope at 3x magnification and categorised according to size. It was important not to mistake Peyer's patches (aggregate lymphoid follicles) as tumours.

2.2.2 Processing

Prior to processing, fixed gut sections were rolled into Swiss Rolls, pinned together and placed in a histology cassette. Specimens were processed using a Histomaster machine (Bavimed).

Gut rolls were processed with the following protocol: 70% ethanol for 45 min, 95% ethanol for 30 min, 95% ethanol for 45 min, 100% ethanol for 30 min, 100% ethanol for 45 min, 100% ethanol for 45 min, Histoclear for 30 min, Histoclear for 30 min, Histoclear for 30 min, wax for 30 min, wax for 45 min, wax for 45 min.

Embryo heads used to analyse cleft palate and EOB phenotype were decalcified in DFB (Pioneering Research Chemicals) solution for 48 h prior to processing. These samples were processed with the following modified protocol: 70% ethanol for 1 h, 95% ethanol for 1 h, 95% ethanol for 1 h, 100% ethanol for 2 h, 100% ethanol for 2 h, 100% ethanol for 2 h, Histoclear for 3 h 45 min, Histoclear for 3 h, Histoclear for 2 h, wax for 3 h, wax for 2 h, wax for 1 h.

2.2.3 Embedding

Processed samples were embedded in paraffin wax using a paraffin embedding station (EG1150H, Leica).

2.2.4 Sectioning and staining

Tissues embedded in paraffin blocks were sectioned at 4 μm slices using a microtome (RM2255, Leica).

For laser capture microdissection, MembraneSlide 1.0 PEN slides (Zeiss) required prior exposure to UV light for 30 min. 10 μm tissue slices were cut using a microtome and put on these activated slides. The slides were baked at 37^{o}C for 30 min, then dewaxed for 5 min and rehydrated through graded alcohols to water for 3-5 min each. The slides were then briefly dipped in methyl green, washed in water and dried at 37^{o}C for 1 hr. The PALM system was used to dissect out tumours/normals and DNA extracted (section 2.3.1.4).

2.2.4.1 Haematoxylin and Eosin (H and E) staining

Paraffin sections were stained with Haematoxylin and Eosin for histological examination using the following protocol: Sections were dewaxed in xylene for 5 min, then rehydrated through graded ethanols (100%, 90%, 70%) for 5 min each followed by 2 min in tap H_20. Sections were then stained in Harris Haematoxylin for 30 sec and washed in running H_20 until the H_20 ran clear. The slides were then briefly dipped into acid alcohol and left in H_20 for 5 min. Sections were then stained in Eosin for 3 min, followed by a quick dip in H_20 and then dehydrated through degraded alcohols for 2-5 min each, before mounting a coverslip with DPX.

In order to quantify thickening of alveolar septa in E18.5 lungs (Figure 3.14), microscope images of H and E stained sections at 20x magnification were captured and the field of view divided into quadrants. One quadrant was selected at random and the thickness of all alveolar septae measured.

2.2.4.2 Alcian-blue stain for goblet cells

Sections were dewaxed in xylene for 5 min, then rehydrated through graded ethanols (100%, 90%, 70%) for 5 min each followed by 2 min in tap H_20. Slides were then stained in alcian-blue solution (Sigma) for 30 min, then washed in running tap H_20 for 2 min, before being rinsed in dH_20. Slides were then stained in nuclear fast red solution (Sigma) for 5 min and washed in running tap H_20 for 1 min. Slides were then dehydrated through degraded alcohols for 2-5 min each, before mounting a coverslip with DPX. The average number of goblets cells per villus (Figure 4.7) was quantified by counting 100 villi from SB3 in at least three mice of each genotype.

2.3 DNA

2.3.1 DNA extraction

2.3.1.1 DNA extraction from ES cells

Cells from an ES colony were transferred to a well of a 96-well plate and grown to confluence. The medium was removed from each well and the cells were lysed after two washes in PBS by the transgenic service at Cancer Research UK, Clare Hall Institute. The lysates were transferred to eppendorfs and DNA precipitated by adding 50 μl isopropanol and centrifuging at maximum speed for 30 min in a bench top centrifuge. The DNA pellets were then washed in 70% ethanol and left to air dry before resuspending in TE buffer.

2.3.1.2 Isolation of DNA from mouse ears for genotyping purposes

The hot sodium hydroxide and tris (HotSHOT) method was used to extract DNA for genotyping purposes following protocols described by Truett *et al* [175]. In brief, 50 μl of HotSHOT reagent (25 mM NaOH, 0.2 mM disodium EDTA, pH 12) were

added to the ear snips in an eppendorf and incubated at 95^{o}C for 30 min. 50 μl of neutralisation buffer (40 mM Tris-HCL, pH 5) were then added and the mix was cooled to 4^{o}C. 1 μl or 2 μl of this mix was then used subsequently for PCR analysis.

2.3.1.3 Isolation of DNA from embryonic tails and other adult mouse tissues

Samples were incubated overnight at 55^{o}C in 400 μl of digestion buffer (95% buffer (100 mM EDTA pH 8, 50 mM TRIS-HCL pH 8, 100 mM NaCl, 1% SDS) + 5% proteinase K solution (20 μg/ml in dH_20)). Upon complete digestion of the tissue, the samples were centrifuged at maximum speed for 20 min in a table top centrifuge to precipitate debris. The supernatant was transferred into a clean eppendorf tube and 430 μl isopropanol and 25 μl of 5M sterile-filtered NaCl solution were added to the sample to precipitate DNA. 1 μl of glycogen was added to facilitate DNA identification. The DNA was pelleted by centrifugation at maximum speed for 20 min, after which the supernatant was discarded. The pelleted DNA was washed by adding 500 μl of 70% ethanol and centrifuging at maximum speed for 5 min. The ethanol was removed and the samples left to air dry. Finally the samples were resuspended in 50 μl of TE.

2.3.1.4 DNA extraction from laser capture microdissected samples

Some tumours/normal tissue required laser capture microdissection (section 2.2.4), followed by DNA extraction using the PicoPure DNA extraction kit (Arcturus) following manufacturer's instructions.

2.3.2 DNA purification

2.3.2.1 DNA purification from agarose gels

DNA was extracted from agarose gels using the QIAquick Gel Extraction kit (Qiagen) following manufacturer's protocols. In brief, the desired bands were excised from agarose gels under UV light and solubilised in QG buffer at 50^{o}C, this mix was then added to a column in which DNA adsorbs to a silica membrane. Impurities were washed away and the pure DNA eluted in water.

2.3.2.2 Phenol-chloroform purification of nucleic acids

Phenol-chloroform purification of nucleic acids was carried in out for generation of ISH probes and preparation of DNA for aCGH analyis. Eppendorf phase-lock gel tubes were used. First they were centrifuged at 13000 rpm for 1 min. 350 μl of PK digested tissue or restriction enzyme digested DNA was added to 350 μl of phenol-chloroform and added to the phase-lock tubes. The tubes were mixed to emulsify and then spun for 5 min at 13000 rpm. A further 350 μl of phenol-chloroform were added to the tubes, mixed and spun for a further 5 min. The upper (aqueous) phase was then transferred to a fresh eppendorf and 300 μl of chloroform were added, shaken gently to emulsify then centrifuged at 13000 rpm for 5 min. The upper (aqueous) phase was transferred to a fresh eppendorf and 100 μl of 7.5 M Ammonium Acetate were added. After mixing 750 μl of ethanol were added. The DNA was pelleted by centrifuging at 13000 rpm for 15 min, washed in 70% ethanol and eluted in TE buffer.

2.3.3 Determination of nucleic acid concentration and quality

Determinaton of nucleic acid concentration and quality was performed using a micro-volume UV-visible spectrophotometer (Nanodrop 2000, ThermoScientific). In brief,

1 μl was loaded onto an optical pedestal and the absorbed light from the sample measured at a wavelength of 260 nm. The ratio of readings at 260 nm and 280 nm provided an estimate of the purity of DNA. The appropriate constant was selected to quantify double-stranded DNA, single-stranded DNA or RNA samples.

2.3.4 Polymerase Chain Reaction (PCR)

Genomic sequence and annotation data were downloaded from the Ensembl site (http://www.ensembl.org) and the University of California Santa Cruz genome site (http://genome.ucsc.edu). In all cases, PCR primers were designed using the Primer3 programme (http://frodo.wi.mit.edu/primer3/). Stock primers were diluted to 100 μM, with working stocks diluted at 1:10.

A typical 25 μl PCR reaction contained 30-50 ng of template DNA, 0.4 pmoles of each primer, 1x Mg^{2+} free PCR buffer (Promega), 2 mM $MgCl_2$ (Promega), 0.2 mM of each dNTP (Amersham) and 1 unit of Taq DNA polymerase (Bioline). A standard PCR reaction consisted of an initial denaturation step at 95^{o}C for 5 min, 35 cycles of 94^{o}C for 1 min, 55^{o}C for 1 min and 72^{o}C for 1 min and a final extension step at 72^{o}C for 10 min. PCR reactions were carried out on a PTC-225 thermocycler (MJ Research). Depending on the primer pair and target size, variations of several conditions (Mg^{2+} concentration, additives, annealing temperature) were necessary. PCR products were analysed using agarose gel electrophoresis. The agarose gels were stained with ethidium bromide and were run alongside a 1 kb DNA ladder using Tris-Borate EDTA (TBE) running buffer.

Table 2.1 shows primers used for genotyping.

Primer Name	Primer Sequence 5'-3'	Product Size (bp)
Cre F	CGGTCGATGCAACGAGTGATGAGG	600
Cre R	CCAGAGACGGAAATCCATCGCTCG	
Fbxw7 null F	CAGTCGAGTGAAGTACAACTCTGG	floxed 394
Fbxw7 null R	GCATATTCTAGAGGAGGGTATCGG	wildtype 287
Fbxw7 Δ	GGCCAGCCTGGTCTGTATAGAG	deleted 744
R482Q F 1	TTCCTCACTTCCCATTCCAG	(1,3) floxed 477
R482Q R 3	TCTCTGGATCCCACACCTTC	(1,3) wildtype 322
R482Q F 5	CGCGGATCTAGAGATCTGATAA	(5,8) neo deleted 237
R482Q R 6	GATTGGCCAGTACTGAACCT	(1,6) deleted 294
R482Q R 8	AACACTGGCCGGTCTCAATA	
Apc^{Min} 9	GCCATCCCTTCACGTTAG	wt 618
Apc^{Min} 15	TTCCACTTTGGCATAAGGC	mut 327
Apc^{Min} MT	TGAGAAAGACAGAAGTTA	
Apc^{1322T} F	CCCTCCATCAACCAAGAAAC	wt 217
Apc^{1322T} R2	TGGGTTTGGCTCTAGCATTC	tar 430
Apc^{1322T} R3	AAGAGTGCCTCCCAAAATGA	

Table 2.1: Genotyping primers

2.3.5 Long-range PCR screening

To identify homologous recombinants in the ES cells and to amplify full length *Fbxw7* cDNA, the Roche Long-Range Expand long template PCR system was used following manufacturer's instructions. The primers used for ES screening are shown in Table 2.2.

Primer Name	Primer Sequence 5'-3'	Product Size
5' F	GGCCAAGCAGAGAAAACAAG	5' tar 5371bp
5' Rtar	GAGCTTAACGTCACCGGTTC	
5' Rwt	GCATCTACCAGTCCCCAGAA	
3' Ftar	GCCTGAAGAACGAGATCAGC	3' tar 5533bp
3' Fwt	TGCTCAAATATGGGGTCCTC	
3' R3	ACCTGTGCCTTGCTCTCTGT	

Table 2.2: ES cell screening primers

2.3.6 Sequencing

In order to sequence a specific area of DNA or cDNA, first a standard PCR reaction was carried out with the appropriate primer sets. 5 μl of PCR product were used for verification by agarose gel electrophoresis. 5 μl of PCR product were incubated with 2 μl of EXOSAP-IT (Affymetrix), and run on a thermocycler at 37^{o}C for 15 min followed by 80^{o}C for 15 min (to inactivate enzymes). EXOSAP-IT contains hydrolytic enzymes exonuclease I and shrimp alkaline phophatase that clean up unused dNTPs and primers from the initial PCR reaction. For the second round of amplification, a 20 μl reaction contained 30-50 ng of template DNA, 0.4 pmoles of forward or reverse primer and 2x Big Dye Terminator v3.1 reagent (Applied Biosystems). The sequencing reaction consisted of an initial denaturation step at 96^{o}C for 5 min, followed by 35 cycles of 96^{o}C for 30 s, 50^{o}C for 45 s and 60^{o}C for 4 min. Unincorporated dye terminators were removed with the DyeEx 2.0 Spin kit (Qiagen) using gel-filtration technology following manufacturer's instructions and the purified products were run on the ABI 3730 DNA analyzer (Applied Biosystems) by the Zoology department sequencing service, Oxford University. All sequences were analysed by eye for alterations using the ApE programme (A plasmid Editor by M. Wayne Davis). Primers used for sequencing are shown in Table 2.3 and Appendix B.2.

Primer Name	**Primer Sequence 5'-3'**	**Product Size (bp)**
R482Q cDNA F	TTGTGGCAACCGCATAGTTA	208
R482Q cDNA R	ACCCTCCTGCCATCATACTG	
Fbxw7 seq1	GGAGGAAGAGGAGGAAGAGG	439
Fbxw7 seq2	AGCCAGCAACTTCTCTGGTC	
Fbxw7 seq3	ACCCACAGGCCTTCAAGAGT	448
Fbxw7 seq4	ATGCCCTTTCAGCACCTTAG	
Fbxw7 seq5	GGGTTGTTAGTGGAGCTTATGA	400
Fbxw7 seq6	ACCGTTCCGTCGTCTGAG	
Fbxw7 seq7	CGGGTGAATTTATCCGAAAC	227
Fbxw7 seq8	GGGGGAAGGGTAGGGAGTAT	
Fbxw7 seq mut	AGGTTCACTAGTACTGGCCAATC	
HA tag	GATCCGGTACTAGAGGAACTGAAAAAC	

Table 2.3: Sequencing primers

2.3.7 Southern blotting

Southern blotting was used to confirm correct integration of the *Fbxw7* R482Q mouse construct into genomic DNA of a clone of ES cells that were positive for construct integration from PCR screening. The probes were provided by Taconic and digested with EcoRI. The probes were then radioactively labelled by random priming with α^{32}P dCTP using the random primed labelling kit (Roche) as previously described [176] and purified using NICK^{TM} Columns Sephadex G-50 DNA grade (GE Healthcare). 20 μg of genomic DNA were digested to completion with EcoRI enzyme. The digested DNA was electrophoresed on 0.8% gels in 1x TBE overnight. After denaturation, the gels were blotted onto Hybond N^{+} membrane (Amersham Pharmacia) overnight, UV crosslinked (Stratalinker, Stratagene) and hybridised with the appropriate radiolabelled probes. Hybridisation and washing of Southern blots was performed as described previously by Church *et al* [177].

2.3.8 Array comparative genomic hybridisation

DNA was extracted from a formalin-fixed-paraffin-embedded R482Q/+ tumour using the phenol-choloform DNA extraction method described in section 2.3.2.2. aCGH was performed by collaborators at the Medical University of Gratz. The Agilent 4x44k platform was used, following manufacturer's instructions. One exception from the protocol was that the BioPrime array CGH genomic labelling system (Invitrogen) was used rather than the Agilent labelling kit. Genomic DNA from a female C57Bl/6J mouse was used as reference DNA.

2.4 RNA / cDNA

2.4.1 RNA extraction

RNA was isolated from frozen tissue with the RNeasy minikit (Qiagen) according to manufacturer's instructions. A hand-held electrical tissue homogeniser (Polytron PT1200E, Kinematica) was used to homogenise mouse tissue samples, typically in 350 μl of tissue lysis buffer. Cell pellets were incubated in 350 μl RLT tissue lysis buffer and were disrupted by pipetting up and down. Ethanol was added to lysates creating conditions that promote selective binding of RNA to the membrane in the RNeasy column. Contaminants were washed away and purified RNAs were eluted. These were then treated with DNase I (Fermentas) to degrade residual DNA, according to the manufacturer's protocol. The RNeasy kit was also used to purify RNA following DNase treatment. RNA samples were quantified with the Nanodrop spectrophotometer (section 2.3.3).

2.4.2 RNA extraction from individual crypts

RNA was isolated from individual crypts with the RNeasy microkit (Qiagen) according to manufacturer's instructions. Carrier RNA (poly-A RNA) was added to sample lysates to improve recovery of RNA. On-column DNase digestion was carried out following manufacturer's instructions.

2.4.3 Reverse transcription of RNA into cDNA

Complementary DNA (cDNA) was reverse transcribed *in vitro* from extracted RNAs, using the High Capacity cDNA Reverse Transcription Kit (Applied Biosystems), according to the manufacturer's protocol. cDNA samples were purified from oligo-dT primers with the QIAquick purification kit (Qiagen) following manufacturer's instruc-

tions and sample concentration was determined using the NanoDrop spectrophotometer (section 2.3.3).

2.4.4 *In situ* hybridisation

Briefly, templates for riboprobe synthesis were generated by PCR using the following primers: Hes1F 5'-AGTCGAGCTCACCCCAGCCAGTGTCAAC-3' and Hes1R 5'-TGCAGCATGCTCTGGGTCATGCAGTTGG-3'. Accuracy of the 400 bp PCR product was confirmed by sequencing. The PCR product was cloned into pGEM3Z using SacI and SphI restriction sites. Maxipreps were linearised with EcoRI. Isotopic *in situ* hybridisation (ISH) was performed by the ISH facility at Cancer Research UK, London Research Institute following the protocol described by Poulsom *et al* [178]. ^{35}S-labelled riboprobes were generated by *in vitro* transcription using the RNA polymerase Sp6 and hybridised to 4 μm sections, cut from formalin-fixed, paraffin-embedded specimens. A β-actin probe, generated by the ISH facility, was used as a hybridisation control in all cases. The slides were investigated using a Nikon ME6000 microscope with dark-field epi-illumination and images were acquired with a Micropublisher 5.0 RTV digital camera, with Qimaging software.

2.4.5 Quantitative real time-PCR (qRT-PCR): TaqMan (ABI)

Absolute quantification qRT-PCR was performed on the ABI 7900HT cycler (Applied Biosystems) for each sample (at least in duplicate, but in triplicate whenever possible) and data were analysed using standard protocols to calculate relative expression with the dCT method described in Livak *et al* [179], with *GAPDH* serving as an endogenous control . Percentage knockdown of gene expression is calculated by 100 multiplied by (1-(2^{-ddCT})).

TaqMan Gene Expression Assays were used for each gene of interest and are shown in Table 2.4. These pre-prepared assays contain primer pairs and probe that have

already been tested for optimal PCR efficiency by Applied Biosystems. A reporter dye (FAM dye in all cases in this thesis) is linked to the 5' end of the probe and a non fluorescent quencher is at the 3' end of the probe. To confirm high amplification efficiency of commercially designed probes, standard curves were conducted over a 6-log dilution range using cDNA derived from the tissue of interest. CT values were plotted against the cDNA log concentration and the slope of the curve used to calculate amplification efficiency ($10^{(-1/slope)}$-1)(Figure 2.1).

A typical reaction contained 10 ng of purified cDNA, 0.5 μl of Gene Expression Assay for the gene of interest, 5 μl of TaqMan FAST Universal Mastermix and dH_20 to the total volume of 10 μl. The samples were run on the ABI PRISM 7900HT with the following conditions: 95^{o}C for 20 s followed by 40 cycles of denaturation at 95^{o}C for 1 s and simultaneous annealing and extension at 60^{o}C for 20 s.

Gene	**TaqMan Probe**
Fbxw7	Mm00504445ml
Mnd1	Mm01703074m1
Trim2	Mm03053379s1
Tigd4	Mm01702361s1
Lgr5	Mm00438890m1
Gapdh	Mm99999915g1
Olfm4	Mm01320261ml
GAPDH	Hs99999905ml
FBXW7	Hs00217794ml

Table 2.4: TaqMan probes

2.4.5.1 Pre-amplification of cDNA

When using cDNA generated from individual crypts, pre-amplification of these cDNAs were necessary prior to qRT-PCR. A pooled mix of TaqMan probes was generated by adding 1 μl of each desired probe and adjusting to a final volume of 100 μl with TE. Pre-amplification reaction mixes were prepared as follows; 12.5 μl TaqMan PreAmp mastermix (2x) (ABI), 6.25 μl pooled assay mix (0.2x each assay), 6.25 μl

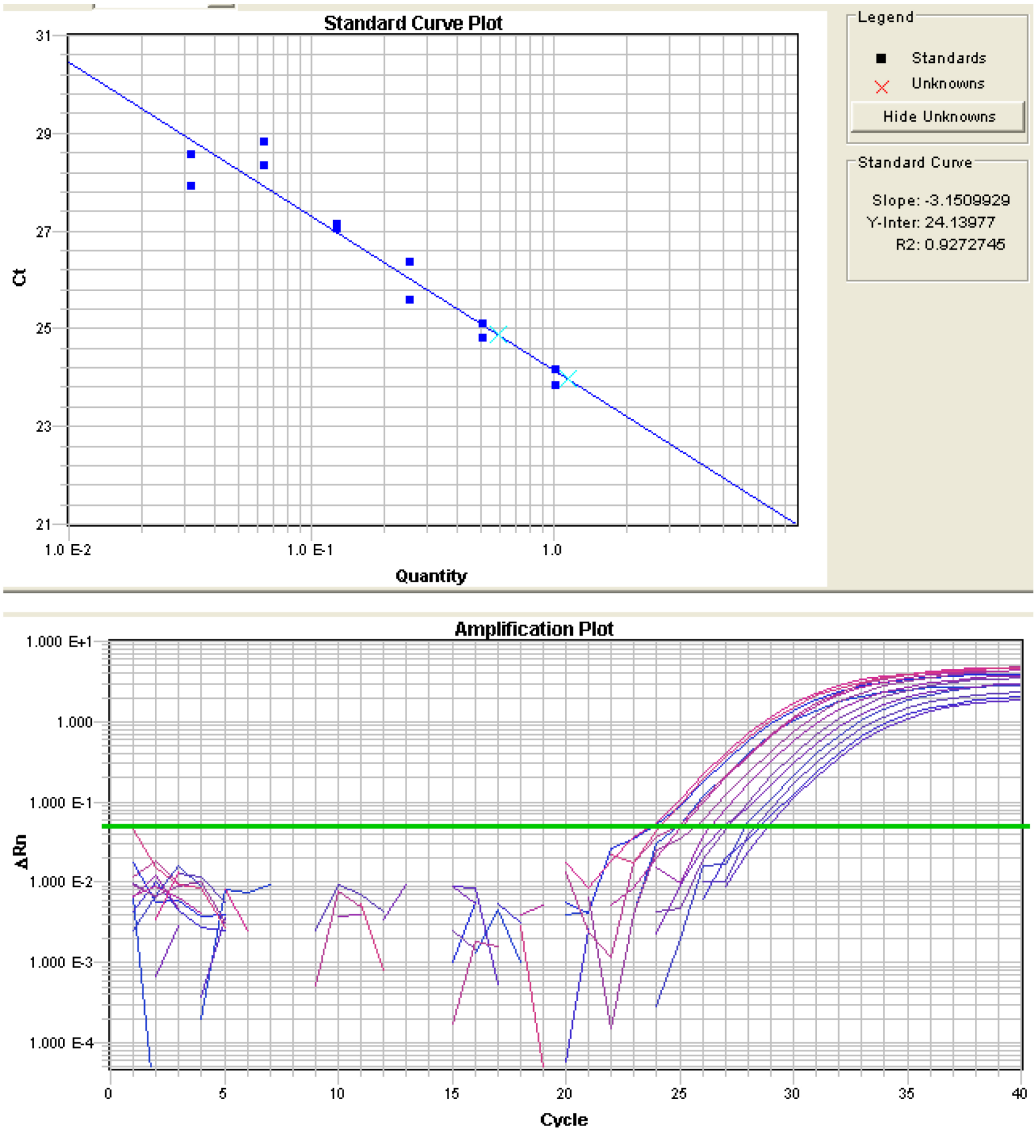


Figure 2.1: Confirming amplification efficiency of TaqMan probes, example testing the *Fbxw7* Mm00504445ml probe. The upper graph plots the CT value against the log concentration over a 6-log dilution of cDNA generated from E18.5 lungs. The slope of the curve is used to generate the amplification efficiency ($(10^{(-1/-3.15)}\text{-}1) = 107\%$). The lower panel represents the amount of amplicon present over the dilution range.

cDNA sample (25 μl reaction). The pre-amplification reaction was run on a thermocycler with the following programme: initial step at 95^{o}C for 10 min, followed by 14 cycles of 95^{o}C for 15 s and 60^{o}C for 4 min. Upon completion the reaction was immediately placed on ice. The pre-amplification product was diluted 1 in 20 in dH_20. A typical reaction contained 2.5 μl of diluted cDNA, 0.5 μl of Gene Expression Assay for the gene of interest, 5 μl of TaqMan FAST Universal Mastermix and dH_20 to a total volume of 10 μl. The samples were run on the ABI PRISM 7900HT with the following conditions; 95^{o}C for 20 s followed by 40 cycles of denaturation at 95^{o}C for 1 s and simultaneous annealing and extension at 60^{o}C for 20 s. For each TaqMan Gene Expression Assay used a comparison of pre-amplified cDNA and normal (non pre-amplified) cDNA was carried out to ensure uniformity in the amplification of amplicons. For all assays the difference between the ddCT value for the normal cDNA and pre-amplified cDNA samples was less than 1.5.

2.4.6 SYBR-Green RT-PCR

The SYBR-Green Dye I is used to detect PCR product by binding to double-stranded DNA products formed during PCR. When the mastermix is added to the sample, SYBR-Green Dye I binds to all dsDNA. During PCR, the DNA polymerase in the mastermix amplifies the target sequence creating a PCR product, the SYBR-Green dye I then binds to all the newly formed double-stranded PCR product. As SYBR-Green dye I binds to all dsDNA, the fluorescence intensity is proportional to the amount of PCR product produced.

A typical reaction contained 10 ng of purified cDNA, 10 μl of FAST SYBR-Green Mastermix, 300 nM of both forward and reverse primer and dH_20 to a total volume of 20 μl. The samples were run on the ABI PRISM 7900HT with the following conditions: 95^{o}C for 20 s followed by 40 cycles of denaturation at 95^{o}C for 1 s and simultaneous annealing and extension at 60^{o}C for 20 s.

As SYBR-Green dye I detects any dsDNA, I routinely checked for non-specific product formation by producing a dissociation curve. Directly following the PCR reaction, samples were run with the following conditions: 95^{o}C for 15 s followed by 50^{o}C for 1 min and 95^{o}C for 15 s. The dissociation curve shows changes in fluorescence plotted against temperature and a single narrow peak is expected (Figure 2.2). Primers used for SYBR-Green RT-PCR can be found in Appendix B.1.

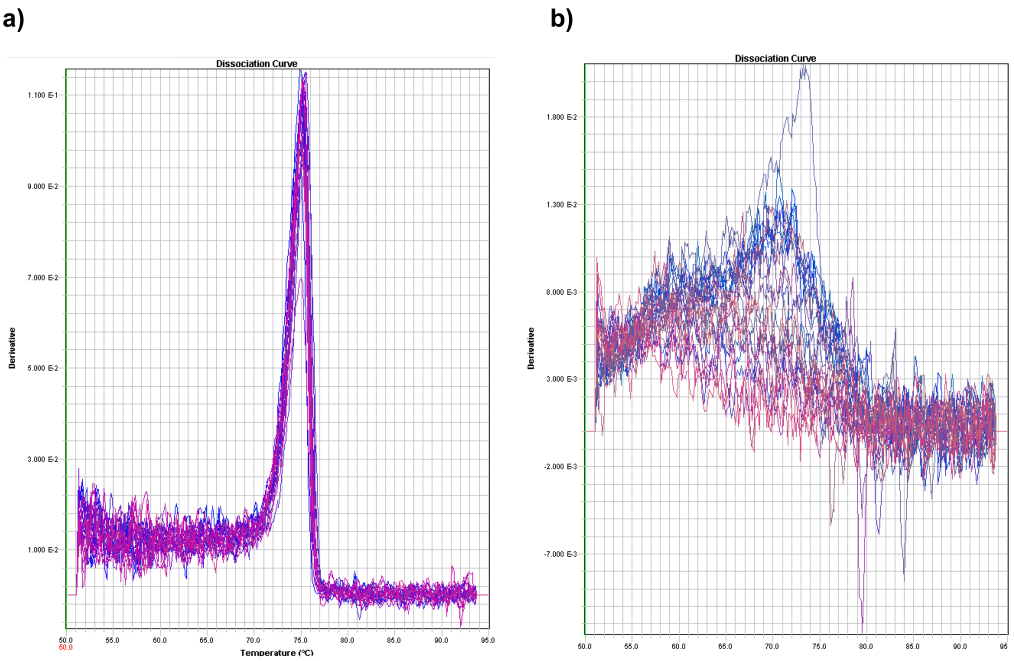


Figure 2.2: SYBR-Green RT-PCR: Dissociation curve. a) Dissociation curve with a discrete peak for Fbxw7α isoform showing a specific PCR product with no primer dimers. b) Example of a non-specific dissociation curve.

2.5 Protein

2.5.1 Immunohistochemistry

Formalin-fixed, paraffin-embedded tissue sections (4 μm) were de-waxed in xylene and rehydrated through graded alcohols to water for 3-5 min each. Endogenous peroxidase was blocked using 1.6% H_2O_2 for 20 min. For antigen retrieval, sections were pressure

cooked in 10 mM citrate buffer (pH6.0) for 5 min. Sections were blocked with 10% normal serum for 30 min. Slides were incubated with primary antibody for 2 h (for antibody dilutions see Table 2.5). Sections were washed in PBS prior to applying biotinylated secondary antibody for 1 h at room temperature. Sections were washed in PBS and then incubated in ABC (contains avidin and biotinylated horseradish peroxidase) (Vector labs) for 30 min prior to washing. DAB solution was applied for 2-5 min and development of the colour reaction was monitored microscopically. Slides were washed in PBS, counterstained with Haematoxylin, dehydrated, cleared and then mounted with a coverslip using DPX. For Caspase3 staining, digit apoptosis found in E12.5 embryos was used as a positive control.

Primary Antibody	Manufacturer	Dilution	Block	Secondary Antibody
Alkaline Phosphatase AB65834 (Rabbit)	Abcam	1:50	Goat	Goat anti-rabbit
β-catenin 610154 (Mouse)	BD	1:50	Horse	Horse anti-mouse
Caspase3 AF835 (Rabbit)	R and D Systems	1:800	Goat	Goat anti-rabbit
CC10 sc-9772 (Goat)	Santa Cruz	1:250	Horse	Horse anti-goat
Chromogranin A AB15160 (Rabbit)	Abcam	1:1250	Goat	Goat anti-rabbit
Ki-67 TEC-3 (Rat)	DAKO	1:125	Rabbit	Rabbit anti-rat
Lysozyme EC3.2.1.17 (Rabbit)	DAKO	1:500	Goat	Goat anti-rabbit
proSP-C AB3786 (Rabbit)	Millipore	1:1000	Goat	Goat anti-rabbit

Table 2.5: Antibodies used for immunohistochemistry

2.5.1.1 Immunohistochemistry quantification

Chapter 3: Figure 4.9; to quantify proliferation in E18.5 lungs, two independent images of Ki67 immunohistochemistry were captured at 20x magnification, then randomly within these images three equally sized sections were selected. Within these sections the percentage of total cells which were Ki67 positive were calculated.

Figure 4.9; to quantify alveolar type II cells in E18.5 lungs, images of pro SP-C were captured at 20x magnification, then an defined area (half the field of view) were selected. Within these areas, the percentage of total cells which were pro SP-C cells were calculated.

Chapter 4: Figure 4.8; In morphologically normal intestinal tissue of *Fbxw7*-

mutant mice, abundance of enteroendocrine cells was determined by counting the number of Chromogranin-A positive cells in SB3 in 100 villus-crypt units.

Figure 4.9; In morphologically normal intestinal tissue of *Fbxw7*-mutant mice, to assess proliferation, the percentage of Ki67 positive cells per crypt was quantified in 200 crypts from SB3. To assess apoptosis the number of positive Caspase3 cells per crypt-villus unit in SB1, SB2 and SB3 were counted for 100 crypt-villus units.

Chapter 5: Figure 5.4; To quantitate Ki67 immunohistochemistry of R482Q/+ Apc^{1322T} compound and Apc^{1322T} tumours, images of the centre of each tumour were captured at 20x magnification, followed by random selection of an equally-sized area conducted blindly by an independent person and then the percentage of total cells which were Ki67 positive were calculated.

2.5.2 Immunofluorescence

Formalin-fixed paraffin-embedded tissue sections (4 μm) were de-waxed in xylene and rehydrated through graded alcohols to water for 3-5 min each. Endogenous peroxidase was blocked using 1.6% H_2O_2 for 20 min. For antigen retrieval, sections were pressure cooked in 10 mM citrate buffer (pH6.0) for 5 min. Sections were blocked with 10% goat serum for 30 min. Slides were incubated with primary phospho-Smad2 (Ser465/467) rabbit polyclonal antibody (AB3849, Millipore) for 1 h, at a 1:1000 dilution. Secondary antibody goat anti-rabbit FITC (1: 200 dilution Abcam) was applied for 30 minutes and slides were washed and stained with DAPI-containing vectashield (Vector Labs) and a coverslip was added. Images were captured using a Zeiss 510 MetaHead confocal microscope.

2.5.3 Western blotting

Tissue samples were homogenised in Mega9 (0.5% NP40, 0.5% Mega9 (Sigma), 150 mM NaCl, Tris-EDTA (100X) up to 50 ml in H_20) or RIPA (Tris-Hcl 50 mM, NaCl

150 mM, 0.5% sodium deoxylcholate, 1% Triton-X, 0.1% SDS, 5 mM EDTA, pH 7.4) lysis buffer with the addition of protease and phosphatase inhibitors (Complete Mini and PhosSTOP, Roche). Volume of lysis buffer varied depending on the size of tissue/cell pellet (typically 100-400 μl). Lysis was allowed to occur on ice for 20 min and the samples were centrifuged to precipitate cell debris at maximum speed for 2 min in a tabletop centrifuge.

2.5.3.1 Quantification of protein lysates

Protein lysates were quantified using the bicinchoninic acid (BCA) assay, based on the biurect reaction. This assay allows colorimetric detection and quantitation of total protein content. The principle of the assay is the reduction of Cu^{+2} to Cu^{+1} by proteins in an alkaline environment, followed by reaction of Cu^{+1} with BCA to produce a purple product. This product exhibits a strong absorbance at 562 nm, showing a linear correlation with protein concentration. In order to quantify unknown samples, a standard curve is was generated by diluting a known protein (bovine serum albumin) to defined dilutions. 5 μl of lysates were diluted in 45 μl H_20. Kit reagents A and B were mixed at 1:50 ratio and 1 ml of mixed reagents added to diluted lysates and incubated at 37^{o}C for 30 min, before reading the absorbance at 562 nm on a spectrophotometer (NovaspecII, Pharmacia Biotech). The known standards were used to plot a standard curve of known protein concentrations from which the protein contents of unknown lysates were calculated. Typically 35 μg of protein per sample were loaded for western blot analysis.

2.5.3.2 Running western gel and transfer

Lysates were diluted in an appropriate amount of 4x loading dye (Invitrogen) and denatured at 95^{o}C for 5 min.

Western blotting was performed using the NuPAGE Gel system, (Invitrogen) ac-

cording to manufacturer's protocol. Briefly, denatured lysates were loaded onto a 4-12% NuPAGE Novex Bis-Tris Mini Gel and ran at 100V for at least 2 h in MOPS SDS running buffer (Invitrogen). 10 μl of anti-oxidant were added to the running buffer in the small chamber. Proteins were run alongside a protein ladder (Spectra Multicolour, Fermentas). The gels were transferred onto PVDF membrane (Immobilon P, Millipore) in a semi-dry tank (120mA for at least 2 h) and blocked by incubating for 1 h at room temperature in PBS or TBS containing 10% milk (Marvel) or TBS-BSA.

The membranes were then incubated overnight in the appropriate primary antibody in PBS or TBS with 5% milk. The antibodies and dilutions used are summarised in Table 2.6. After washing, the membranes were incubated with the appropriate secondary antibody and the HRP-conjugated anti-β actin antibody (Abcam 8226, 1:10 000 dilution, as loading control) for 1 h at room temperature. After further washes, the blots were incubated in ECL reagents (GE healthcare) and chemiluminescence was detected by developing chemiluminescence film (GE Healthcare) with a developer (Compact X4, Xograph). To quantify band intensity, an area of constant size surrounding each band was selected and the pixels were counted (ImageJ). After taking into account the value for the background, the intensity of the band was normalised to its loading control.

Primary Antibody	**Manufacturer**	**Dilution**	**Secondary Antibody**	**Manufacturer**	**Dilution**
AuroraA kinase (610938)	BD biosciences	1:600	Goat anti-mouse-HRP	DAKO	1:10000
Cyclin E1 (sc-481)	Santa Cruz	1:600	Goat anti-rabbit-HRP	DAKO	1:10000
Anti-FLAG M2 (F1804)	Sigma-Aldrich	1:5000	Goat anti-mouse-HRP	DAKO	1:10000
c-Jun (sc-44)	Santa Cruz	1:200	Goat anti-rabbit-HRP	DAKO	1:10000
Klf5 (ab24331)	Abcam	1:250	Goat anti-rabbit-HRP	DAKO	1:10000
Lamin B1 (H-90 sc-20682)	Santa Cruz	1:1000	Goat anti-rabbit-HRP	DAKO	1:10000
c-Myc (9E11) (sc-47694)	Santa Cruz	1:200	Goat anti-mouse-HRP	DAKO	1:10000
c-Myc Epitope tag (S1826)	Clontech	1:75	Goat anti-mouse-HRP	DAKO	1:10000
p-c-Myc (Thr58/Ser62) (sc-8000R)	Santa Cruz	1:500	Goat anti-rabbit-HRP	DAKO	1:10000
Activated Notch1 (Nicd1) (ab8925)	Abcam	1:1000	Goat anti-rabbit-HRP	DAKO	1:10000
Smad4 (sc-7966)	Santa Cruz	1:200	Goat anti-mouse-HRP	DAKO	1:10000
Tgif (H-171) (sc-9084)	Santa Cruz	1:200	Goat anti-rabbit-HRP	DAKO	1:10000

Table 2.6: Antibodies used for western blotting

2.5.3.3 Epithelial isolation of cells from intestinal tissue

For intestinal tissue, isolation of epithelial cells was carried out. The gut was dissected out and flushed with PBS. A 2 cm long piece of SB1 was opened longitudinally and incubated in PBS supplemented with 30 mM EDTA for 2 h with agitation at 4^{o}C. During the incubation, the falcon was vortexed every 30 min to aid villus-crypt shedding. After 2 h, most villus-crypt units had shed and the remaining muscle layer was removed with forceps. The shedded epithelial tissue was centrifuged at 3000 rpm for 10 min and the supernatant was aspirated. Cell pellets were then frozen at -80^{o}C, prior to lysis for western blotting.

2.5.3.4 Cell fractionation for western analysis

Nuclear fractions were generated using lysis buffer A (HEPES 1000 mM, KCL 1000 mM, EDTA 1000 mM, DTT 1 mM, PMSF, NP40 10%, protease and phosphatase inhibitors) and spinning for 5 min. The pellets were then resuspended and lysed with buffer B (HEPES 20 mM, NaCl 400 mM, EDTA 1 mM, glycerol 10%, DTT 1 mM, PMSF, protease and phosphatase inhibitors) and agitated at 4^{o}C for 2 h. The samples were spun and the supernatant, containing the nuclear fraction was removed.

2.5.4 Co-immunoprecipitation

Cells were transiently transfected (section 2.6.3) with *Fbxw7* mutant FLAG-tagged and *Fbxw7* wildtype Myc-tagged expression plasmids, then grown for 72 h. Prior to harvesting, cells were washed twice with cold PBS. Cells were then scraped into 150 μl of ice cold coIP buffer (Tris 20 mM, NaCl 100 mM, EDTA 1 mM, Triton 0.1%, protease inhibitor tablet).

2.5.4.1 Myc Co-IP

20 μl protein G Dynabeads (Invitrogen) were used per sample and transferred into an eppendorf. 2 μg Myc antibody (Clontech) diluted in 200 μl PBST (1x PBS supplemented with 1% Tween) were added to the Dynabeads and incubated with rotation for 20 min at 4^{o}C to allow the Dynabeads and antibody to bind. After 20 min the supernatant was removed, by using the DynaMag (Invitrogen) before the Dynabeads were washed twice with PBST supplemented with 0.5% BSA. 20 μl of cell lysate were added to the Dynabead-antibody complex and incubated with rotation for 2.5 h at room temperature to allow antigen binding. The eppendorf was placed on the DynaMag and the supernatant was discarded. The dynabead-antibody-antigen complex was washed 3 times with PBST/BSA, before a final wash in PBS. Then 20 μl NuPage sample buffer + DTT (Invitrogen) were added and samples boiled at 100^{o}C for 10 min. The samples were placed on the DynaMag, precipitated proteins were collected and loaded on to 4-12% NuPAGE Novex Bis-Tris Mini Gel (Invitrogen) and ran as a normal western (section 2.5.3.2). Whole cell lysates were run alongside the co-IP samples as a reference for detection of each protein. Blots were probed with anti-FLAG antibody (Sigma-Aldrich) at 1:5000 dilution.

2.5.4.2 FLAG co-IP

30 μl Anti-Flag M2 magnetic beads (Sigma-Aldrich) were used per sample and transferred into an eppendorf. The eppendorfs were put on the DynaMag and the supernatant removed. Beads were washed twice with 300 μl of TBS. 100 μl cell lysate and 900 μl coIP buffer were added to the beads and incubated with rotation for 2 h at room temperature to allow antigen binding. The eppendorf was placed on the DynaMag and the supernatant discarded. The bead-antigen complex was washed 3 times with 600 μl TBS. Then 40 μl NuPage sample buffer was added, and samples were boiled at 100^{o}C for 10 min. The samples were diluted in a further 60 μl of

co-IP buffer and the precipitated proteins were loaded on to 4-12% NuPAGE Novex Bis-Tris Mini Gel (Invitrogen) and ran as a normal western (section 2.5.3.2). Blots were probed with Myc anitbody (Clontech) at 1:75 dilution.

2.6 Cell culture

2.6.1 Maintenance of cell lines

All cell culture protocols were carried out in a class II laminar flow hood. All cell lines were grown from frozen stocks, by thawing cells rapidly at 37^{o}C, pelleting and resuspending cells in appropriate tissue culture media. All cell lines used were maintained in DMEM medium plus L-Glutamine (PAA) supplemented with 10% foetal bovine serum (FBS) (PAA) and 1% penicillin-streptomycin (PAA) with the exception of the colorectal cancer cell line SW1463 which was maintained in RPMI 1640 (PAA) supplemented with 10% FCS and 1% penicillin-streptomycin. Cells were grown at 37^{o}C with 5% CO_2 and were passaged before they reached confluence. In order to subculture the cells, they were detached with trypsin-EDTA (Invitrogen). When not in use, cells were stored in liquid nitrogen. In preparation for storage, cells were harvested in the log phase of growth, then resuspended in freezing medium (90% FBS, 10% DMSO).

2.6.2 Counting cells

Cell numbers were counted using a FastRead102 disposable haemocytometer (Immune Systems). The number of cells per ml were calculated by the following calculation: (Number of cells / No of 4x4 grids counted) x 10^4 x sample dilution. Cells were typically seeded at the following densities: 1 x 10^5 cells per well of a 6-well plate, 2.5 x 10^4 cells per well of a 24-well plate and 5 x 10^3 cells per well of a 96-well plate depending on experiment.

2.6.3 Transient transfections

Plasmid DNA was transiently transfected with the lipid reagent Lipofectamine 2000 (Invitrogen), according to manfacturer's protocol. In brief, in a 6-well plate format, 10 μl of Lipofectamine 2000 was diluted in 240 μl of antibiotic and serum free medium and incubated for 5 min at room temperature. 4 μg of DNA were diluted in 250 μl antibiotic and serum free media. The diluted DNA and lipid were then mixed in the same eppendorf and incubated at room temperature for 20 min. After 20 min the newly formed complexes were added in a dropwise fashion to the cells. The medium was changed to normal cell culture growth medium after 6 h. When co-transfection of two plasmids was required, the same protocol was used and equal amounts of both plasmids were included in the reaction. Typically for mRNA experiments, cells were collected 48 h after transfection, whereas for protein experiments cells were collected 72 h after transfection.

2.6.4 Measurement of cell viability

Cell viability was measured using the CellTiter 96 Aqueous One Solution Cell Proliferation Assay (Promega) according to manufacturer's instructions. The assay uses a colorimetric method whereby a tetrazolium compound (MTT) is bioreduced by metabolically active cells into a coloured formazan product that is soluble in tissue culture medium. Colour variation was measured with a spectrophotometer plate reader (Molecular Devices) at 490 nm wavelength and is directly proportional to cell number.

2.6.5 Derivation of mouse embryonic fibroblasts (MEFs)

E13.5 embryos were dissected out of the mother and the head, tail and internal organs were removed. Cells from embryo carcasses were then dissociated by incubating in

trypsin (Invitrogen) for 30 min. The cells were then washed and grown in DMEM medium (PAA) with 5% FCS. Cells were grown for up to four passages.

2.6.6 Synchronising cells by serum starvation

Cells were serum starved by maintaining cells with the following medium: DMEM/ RPMI with 0.5% FBS and 1% penicillin-strepomycin for 48 h (this enriches for cells at G0/G1). Cells were re-stimulated with the following media: DMEM/RPMI with 30% FBS and 1% penicillin-strepomycin. Cells were serum starved for 48 h, then re-stimulated for 3-11 h, this protocol was modified from Jackson *et al* [180].

2.7 *In vitro* shRNA knockdown of *FBXW7*

pLKO.1 lentiviral constructs expressing shRNA to human *FBXW7* (RHS4533-NM-033632) were purchased from Open Biosystems as glycerol stocks. Four clones were tested; TRCN0000006555, TRCN0000006556, TRCN0000006557 and TRCN0000006558, for ease these clones will be referred to as clones 5, 6, 7 and 8 respectively. The hair-pin, mature sense and antisense sequences are shown in Table 2.7 as well as their *FBXW7* exon targets. Note that clone 8 targets exon 9 but in a different part of the sequence to that which is mutated in LOVO and SW1463 cell lines. These stocks were streaked out onto ampicillin agar plates. Individual colonies for each separate clone were grown up in LB with carbenicillin resistance and endotoxin free maxipreps (Qiagen) were performed (section 2.8.1.4). To test shRNA efficiency transient transfection of target cell lines was carried out (section 2.6.3) and knockdown assessed by TaqMan qRT-PCR using *FBXW7* and *GAPDH* probes (section 2.4.5).

Clone	Hairpin Sequence	Mature Sense	Mature Antisense	Exon
5	CCGGCCTAAAGAGTTGGCACTCTATCTCG AGATAGAGTGCCAACTCTTTAGGTTTTT	CCTAAAGAGTTGGC ACTCTAT	ATAGAGTGCCAACT CTTTAGG	5
6	CCGGCCAGAGAAATTGCTTGCTTTACTCG AGTAAAGCAAGCAATTTCTCTGGTTTTT	CCAGAGAAATTGCT TGCTTTA	TAAAGCAAGCAAT TTCTCTGG	4
7	CCGGCCAGTCGTTAACAAGTGGAATCTCG AGATTCCACTTGTTAACGACTGGTTTTT	CCAGTCGTTAACAA GTGGAAT	ATTCCACTTGTTAA CGACTGG	10
8	CCGGCCAGAGACTGAAACCTGTCTACTCG AGTAGACAGGTTTCAGTCTCTGGTTTTT	CCAGAGACTGAAAC CTGTCTA	TAGACAGGTTTCAG TCTCTGG	9

Table 2.7: Sequences of pLKO.1 shRNA *FBXW7* Clones.

2.7.1 Production of lentiviral particles

All lentiviral cell culture was carried out in a designated class II laminar flow hood. Protective oversleeves were worn, as well as two pairs of gloves. All waste was double bagged and discarded in clinical waste disposal bags. HEK 293T cells were plated out in 10 cm plates at a density of 4 x 10^6 cells per plate in Iscove's Modified Dulbecco's Medium (IMDM) supplemented with 10% FBS and 1% penicillin-streptomycin. The following day the cells were at 70-80% confluency ready for transfection. I used the polyethylenimine (PEI) transfection method. The following plasmids were required for viral packaging: an envelope glycoprotein-encoding plasmid (pMD2.VSVG (vesicular stomatitis virus G glycoprotein), pREV, packaging plasmid ΔR: pCMVΔ8.74).

15 μg of FBXW7 targeting plasmid DNA, 6.5 μg of ΔR, 3.5 μg of VSVG and 2.5 μg of pREV DNA were prepared in one tube and the volume was made up to 2.5 ml with medium without FCS or penicillin/streptomycin. 100 μl of 10 μM PEI (Sigma) were diluted in a total volume of 2.5 ml medium without FCS or penicillin/streptomycin in a separate tube. The DNA/medium tube was vortexed whilst adding the PEI/medium mixture in a dropwise fashion. This mix was then incubated at room temperature for 20 min before being added to the cells. The cells were incubated at 37^{o}C for 4 h, after which the transfection mix was removed and 5 ml of fresh medium with FBS and penicillin/streptomycin were added to the cells. Cell medium containing virus particles was collected 48 h later, centrifuged and the supernatant was filtered with a 0.45 μm filter and frozen at -80^{o}C in 1 ml aliquots.

2.7.2 Titration of lentiviral stocks

Virus titres were assessed using the Lenti-X p24 Rapid Titer Kit (Clontech). This is a standard ELISA kit which quantifies p24, an HIV-1 virus core capsid protein (Figure 2.3).

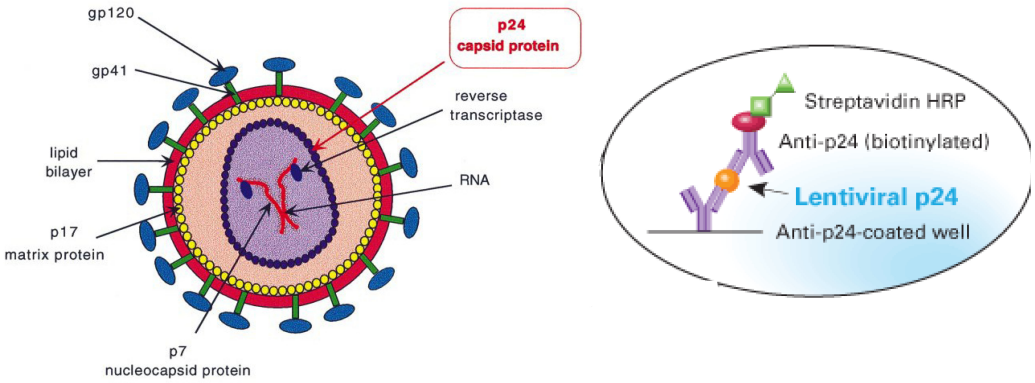


Figure 2.3: Schematic representation of the HIV-1 Virion and p24 ELISA. The left side of the figure shows a representation of the HIV-1 Virion highlighting the p24 capsid (figure reprinted by permission from Macmillan Publishers Ltd: [EMBO J] (ref [181]), copyright (1999)). The right side of the figure illustrates p24 ELISA. First virus particles were lysed to generate soluble p24. The wells of the plate are coated with anti-p24 antibody. Bound p24 was detected using a biotinylated anti-p24 secondary antibody, a streptavidin-horseradish peroxidase (HRP) conjugate and a colour producing substrate. Colour intensity was measured spectrophotometrically to indicate the level of p24 in the viruses and quantitation was performed by comparing test samples to the standard curve.

2.7.3 Transduction of cell lines

Target cell lines were transduced by adding 100 ng (LOVO) or 75 ng (SW1463) of packaged virus to cells in a 1x polybrene mix. Polybrene is a polycation that neutralises charge interactions to increase binding between the pseudoviral capsid and the cellular membrane. Transduced cells were then selected by adding puromycin dihydrochloride (Sigma). Appropriate concentration of puromycin for selection was pre-determined by performing a kill curve for each cell line; LOVO required 4.5 μg/μl and SW1463 required 3 μg/μl.

2.8 Cloning

2.8.1 Standard cloning

2.8.1.1 Ligation

Purified PCR products and vectors were digested overnight with the appropriate restriction enzymes (described in each chapter) according to manufacturer's protocol. All enzymes were from New England Biolabs (NEB). For the last hour of digestion, the vector was treated with 1 μl Calf Intestinal alkaline Phosphatase (CIP) (NEB), preventing re-circularisation of the vector by catalysing the removal of 5' phosphate groups. The digested products and vectors were purified by gel extraction and their concentration determined by spectrophotometry (section 2.3.3). A mixture of insert and vector (at a molecular ratio of 3:1) was ligated with T4 DNA ligase at 4^oC overnight.

2.8.1.2 Blunt-ended ligation

In order to perform blunt-ended ligation, the following reaction was carried out in triplicate: 42 μl of plasmid, 5 μl of buffer 2 (NEB), 1 μl dNTPs, 2 μl Klenow (NEB), at room temperature for 15 min, followed by a standard clean-up using a QIAquick (Qiagen) column. The blunt-ended reaction product was then re-ligated and transformed following standard procedures.

2.8.1.3 Transformation

XL-10 Gold UltraCompetent cells (Stratagene) were transformed in 14 ml BD Falcon polypropylene round-bottomed tubes by adding 10 μl of the ligated mix to the cells, incubating on ice for 30 min, heat-shocking the cells at 42^oC for 30 s, recovering in LB medium for 1 h at 37^oC with agitation and plating out onto LB agar plates with 100 μg/ml ampicillin. For white/blue colour screening, 80 μg/ml X-gal and 20 mM

IPTG were added to the LB agar prior to pouring plates.

2.8.1.4 Amplification of DNA products from bacteria

Single colonies were grown in small volumes and DNA was extracted using the QIAprep miniprep kit (Qiagen) following manufacturer's instructions. The principle of this kit is based on alkaline lysis of bacterial cells followed by adsorption of DNA onto silica in the presence of high salt, followed by washing and elution of the plasmid DNA. The DNA was then tested for presence of the insert by restriction enzyme digest or by DNA sequencing.

Positive clones were grown in larger 200 ml cultures and DNA used subsequently in tissue culture was extracted using the Endotoxin free Maxiprep kit (Qiagen). This kit is based on a modified alkaline lysis procedure, followed by binding of plasmid DNA to a resin under low salt and pH conditions. Prior to binding of DNA to the resin the lysate is treated with an endotoxin removal buffer, this is an important step as endotoxins from bacterial cell membrane components reduce transfection efficiencies. Impurities were removed by medium salt washes, and plasmid DNA was eluted in a high-salt buffer and then concentrated and de-salted by isopropanol precipitation.

2.8.2 Site-directed mutagenesis

In vitro site-directed mutagenesis was carried out with the QuikChange multi site-directed mutagenesis kit (Agilent) following manufacturer's instructions. The primer was designed following the guidelines outlined in the kit and was as follows:

Fbxw7 knockin G1445A (R482Q) mutation:

5'-GTTGTAAGCGGTTCTC**A**AGATGCCACTCTCAG-3'

Removal of PCR mutation in pCMV-HA *Fbxw7* plasmid (chapter 6):

5'-GTTGGACCATGGTTCTGAAGTTCGTTCCTTTTCTTTGGG-3'.

The reaction was set to the following programme on a thermocycler; 95^{o}C for 30

s, 12 cycles of 95^oC for 30 s, 55^oC for 1 min and 68^oC for 12 min.

2.9 Statistical Analysis

Data were analysed with Student t-test, Fisher's Exact test, Wilcoxon rank sum test, χ^2 test and logistic regression analysis using the statistical package Stata or Excel. P$\leq$0.05 was considered statistically significant.

In brief, Student t-test was used to compare the means of two groups of samples, assuming the observations were normally distributed. Fisher's Exact test was used to determine if there was a non-random association between two variables, by calculating the exact probability of getting a result (or more extreme). It was used when a categorical test was more appropriate than a continuous variable test. χ^2 test was used to determine the fit between a theoretical frequency distribution and a frequency distribution of observed data. The Wilcoxon rank sum test, a non-parametric test, was used as an alternative to the Student t-test when the distribution of data was unknown. Logistic regression analysis was used as method of predicting the outcome of a categorical variable based on a predictor variable (e.g. can you predict the genotype depending on the number of polyps observed? (Chapter 5)). This method requires a large sample size but makes no assumptions about the distribution of the data and can take into consideration other variables (such as gender or age) as covariates.

Chapter 3

Investigation of a constitutive *Fbxw7* propellor-tip mutation

3.1 Introduction

FBXW7 is the substrate recognition component of an SCF-type E3 ubiquitin ligase, which degrades a multitude of critical proteins in developmental and signalling pathways. *FBXW7* has been proposed as a tumour suppressor gene (TSG) [91], with mutations occurring at a moderate frequency in cancers of several anatomical sites including the colorectum, stomach, blood, bile duct and endometrium [1]. Our group previously reported that in most colorectal cancers with *FBXW7* mutations, these mutations do not inactivate the protein, but are mono-allelic missense changes at specific arginine residues involved in substrate binding [19]. These findings were confirmed by evaluating mutation data from the COSMIC database, which shows most mutations are mono-allelic with the 'second hits' typical of a TSG occurring rarely. Furthermore, it is not clear that the most commonly occurring mutations - missense changes at arginine residues at propellor-tips - result in loss of protein function and only about 15% of mutations are predicted to lead to truncated FBXW7 protein. It

is possible that the arginine propellor-tip mutations are haploinsufficient or abolish FBXW7 function by acting as dominant negatives [1; 70].

3.1.1 Existing *Fbxw7* mutant mice

To date, several mouse models targeting *Fbxw7* have been generated [171; 172]. These models were generally straightforward knockouts, targeting exons encoding the critical F-box domain (which allows association with the rest of the SCF complex) and therefore generating null alleles. In a model developed by Tsunematsu *et al* [172], in a heterozygous state, mice appeared normal with no tumour formation up to 1 year of age. In a homozygous state, the mutation caused embryonic lethality at stage E10.5 due to compromised vascular and cardiovascular development. Elevated protein levels of Notch 1 and 4 leading to stimulation of downstream pathways involving *Hes1* were observed. Another *Fbxw7*-null model was generated by Tetzlaff *et al* [171] and used a construct that replaced the first five exons of *Fbxw7* with a neomycin cassete. Homozygous *Fbxw7*-null embryos all died *in utero* at E10.5-E11.5 and also displayed defective vascular development. Notch4 accumulated in homozyogus null embryos, leading to the expression of *Hey1*, which encodes a transcriptional repressor that acts downstream of Notch signalling and is implicated in vascular development. Elevated protein cyclin E levels were found by Tetzlaff *et al* but not Tsunematsu *et al*, the latter suggesting that Fbxw7 was dispensable for cyclin E degradation at least until mid-embryogenesis [172].

Conditional *Fbxw7*-null models have also been developed and used to study the role of Fbxw7 in haematopoietic cells [153; 155; 173] mouse embryonic fibroblasts [154], liver cells [152] and gut lineages [151]. These models, along with the novel propellor-tip mutant *Fbxw7* model are discussed in greater detail in Chapter 4.

3.1.2 Possible mechanisms behind characteristic mutation spectrum

As discussed in section 1.3.6, a mutational hotspot has been identified in the WD40 substrate recognition domain of *Fbxw7*. The mutations found here are mostly missense and only observed in one allele with no loss of heterozygosity [19]. This suggests that *FBXW7* does not function as a standard tumour suppressor gene through the two-hit mechanism of inactivation described by Knudson *et al* [82]. No colorectal tumour was found to carry two *FBXW7* mutations predicted to abolish protein function and therefore only partial loss of FBXW7 function may cause tumorigenesis [19]. The underlying reason for this observation needs to be identified. Possibilities include:

- Haploinsufficiency: According to the genetic data, a few cases of *in trans* truncating and missense mutations occur, therefore, simple haploinsufficiency cannot explain the mutation spectrum [18].
- Dominant negative effect: As FBXW7 contains an N-terminal dimerisation domain and can form dimers [70], it could act as a dominat negative, whereby a mutant gene product adversely affects the wildtype gene product by dimerising with it [1].
- Selective loss-of-function: of particular substrates only or in a tissue-specific fashion.
- Partial loss-of-function: whereby mutant FBXW7 is not optimal in substrate degradation.
- Gain-of-function: This is not probable considering the genetic data show that *FBXW7* inactivating mutations do occur albeit at a low frequency.
- 'Just-right' model: in which simple inactivation of FBXW7 is not selected in human tumours but rather mutations that disrupt FBXW7 function but do not

abolish it are selected.

- Other forms of inactivation of the wildtype allele, such as methylation.

3.1.3 Conservation of FBXW7 protein sequence between human and mouse

Appendices C.1, C.2, C.3 shows conservation of the protein sequence between human and mouse Fbxw7 for all three isoforms (α, β, γ) with 96-98% identity observed. Sequences have been downloaded from Ensembl and aligned using BLASTP software. Figure 3.1 shows complete conservation of the protein sequence between mouse and human surrounding the human R479Q mutation site. Note that human arginine residue 479 is equivalent to mouse residue 482.

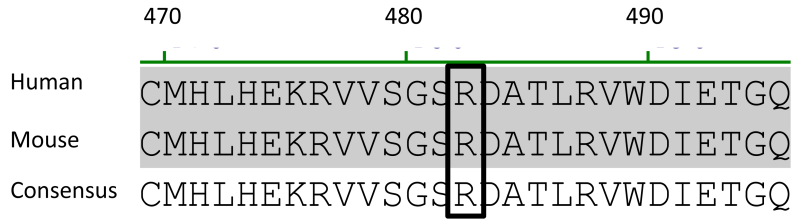


Figure 3.1: Alignment of FBXW7 protein sequence surrounding a common mutation site in the WD40 domain in human and mouse. Sequences were obtained from Ensembl and aligned using BLASTP software. The boxed region shows an arginine residue (human R479, mouse R482) within the WD40 domain which is commonly mutated in cancers. There is 100% homology in the sequence shown surrounding human R479.

Figure 3.2 shows a molecular model of the WD40 domain of FBXW7, in which the arginine at amino acid position 479 (482 in mouse) is at the apex of one of the β-sheets and is critical in substrate recognition. Two *in silico* prediction programs, SIFT (http://sift.jcvi.org) and Polyphen (http://genetics.bwh.harvard.edu/pph) also predicted that R479Q substitution, from a basic to an uncharged polar amino acid, affects protein function and may be damaging.

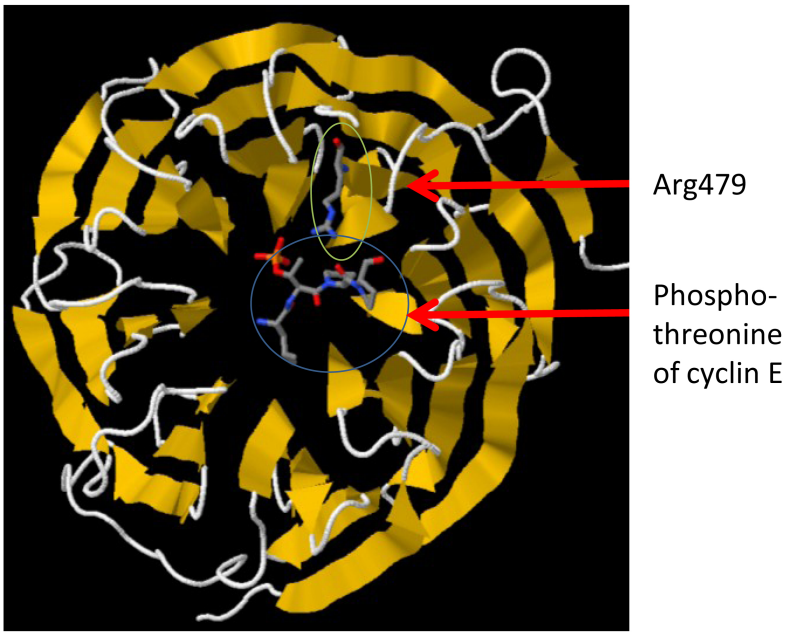


Figure 3.2: Interaction of FBXW7 WD40 propellor domain with FBXW7 substrates. This molecular model of the FBXW7 WD40 propellor domain shows the structure and interaction of arginine 479 and a phosphorylated substrate (cyclin E). Arginine 479 is found at the apex of one of the β-sheets and directly interacts with the phosphothreonine of cyclin E. This interaction is abolished if this arginine is mutated to a glutamine. This model was generated using RasMol software.

3.2 Aims of chapter

Given the *FBXW7* mutation status observed in human cancers, it was hypothesised that these mutations are selected for reasons other than haploinsufficiency or full loss-of-function. It was speculated whether arginine propellor-tip mutations in *FBXW7* provide a selective advantage for tumorigenesis. Given that existing *Fbxw7* mutant mice have null alleles, I aimed at creating a model carrying one of the commonly occurring point mutations (human R479Q). Using this model I aimed to search for phenotypic and functional differences from *Fbxw7*-null alleles. Specific aims included:

- Generation of R482Q targeting construct for constitutive knock-in of R482Q mutation (this chapter) and tissue or developmental specific knock-in of R482Q mutation (Chapter 4)

- Generation of constitutive R482Q knock-in mouse model by *PGK*-Cre crosses
- Investigation of observed phenotypes
- Comparison of R482Q mouse model with existing *Fbxw7*-null models to investigate the observation that *FBXW7* mutations often occur in the heterozygous and 'non-null' state in human tumours.

3.3 Results

Results presented in this chapter have been published in Davis *et al* [182].

3.3.1 Generation of *Fbxw7* R482Q construct

Figure 3.3 shows the targeting construct used to generate *Fbxw7* R482Q knock-in mice. Dr Annabelle Lewis designed this construct and it was cloned by an commercial company (Taconic). I took over the project from this point onwards.

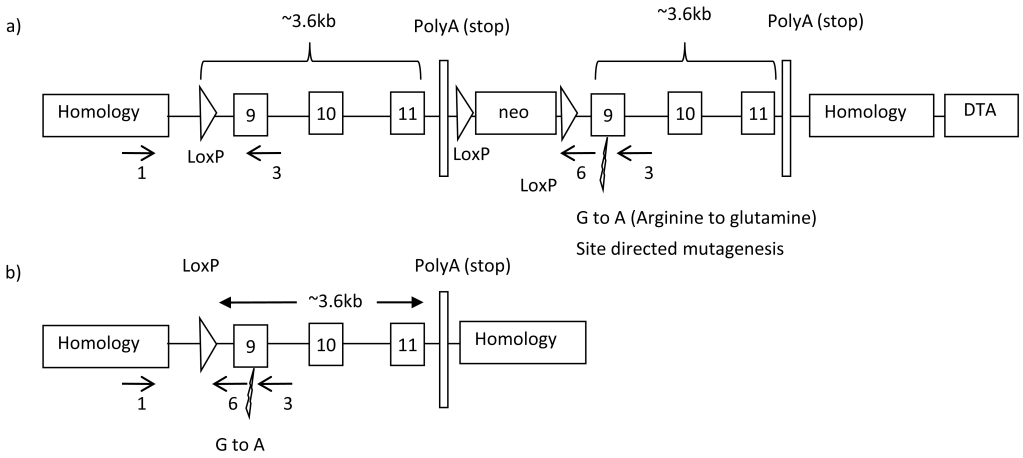


Figure 3.3: *Fbxw7* targeting construct and recombined alleles. Representative diagram of targeting scheme used to generate R482Q mouse model. a) Schematic showing the targeting construct with regions of homology, LoxP sites, genomic *Fbxw7* exon 9-11, a neomycin selection cassette and repeated exon 9-11 in which a mutation in exon 9 has been introduced by site-directed mutagenesis (G1445A). b) Schematic that represents the allele after Cre-mediated recombination. The arrows with corresponding numbers depict the position and direction of the primers used to genotype R482Q mice.

The targeting construct is based on the bacteriophage derived Cre-LoxP recombination system. Cyclization recombination (Cre) recombinase enzyme is a 38 kDa protein that recognises LoxP (locus of chromosomal crossover from Bacteriophage P1) sequences. LoxP sequences are 34 bp motifs consisting of two 13 bp inverted repeats separated by an 8 bp asymmetric spacer region. Exogenous LoxP sequences are not found in the mammalian genome and therefore if a DNA segment is surrounded by two LoxP sites in the same orientation, when exposed to Cre recombinase this segment of DNA is removed. A gene segment which is flanked by LoxP sites prior to Cre-mediated recombination is called a 'floxed' gene.

The *Fbxw7* R482Q targeting construct contained one LoxP site upstream of *Fbxw7* exon 9 and two other sites, flanking a neomycin cassette, downstream of exon 11. On the other side of the distal LoxP, a repeated genomic region containing exons 9-11 was inserted, but with an R482Q allele created by site-directed mutagenesis within exon 9 (G1445A). A neomycin cassette allowed neomycin resistance in those embryonic stem (ES) cells in which recombination had occurred and a diptheria toxin (DTA) cassette allowed negative selection of those cells in which non-homologous recombination had occurred.

It was anticipated that Cre-mediated recombination would generally remove the genomic sequence between the most proximal and distal LoxP sites, removing the neomycin cassette and endogenous exon 9, 10 and 11 (and polyA stop signal), thus allowing transcription of the knock-in mutated exon 9; recombination had occurred between these outer LoxP sites in all the mice subsequently reported in this chapter.

The targeting construct was electroporated into ES cells which were then screened for homologous recombination. Long-range PCR amplification (section 2.3.5) was initially used to screen for 5' and 3' integration using primers shown in Table 2.2. For 5' screening, the forward primer was designed outside the 5' region of homology and the reverse primer to a specific part of the targeted allele that was not present

in the wildtype allele. For 3' screening the forward primer was designed in a specific part of the neo/LoxP sequence which was not found in the wildtype and the reverse primer was designed outside the 3' region of homology. Figure 3.4a shows that three colonies were positive by 5' PCR and only two of these were positive by 3' PCR. The H3 clone had therefore only half integrated, losing its 3' end. 5' Southern blotting (section 2.3.7) was used to confirm positive clones (Figure 3.4b). Colony A10 was selected for subsequent introduction into mouse blastocysts to generate a chimera. Germline transmission occurred and the offspring were back-crossed onto a C57Bl/6J genetic background for six generations prior to being used for experiments.



Figure 3.4: Homologous recombination of targeting construct in electroporated ES cells. a) Long range PCR screening of electroporated ES cell clones showing clones with positive 5' (A10, F12, H3) and 3' (A10, F12) integration. The band sizes of the 5' and 3' PCR products were 5371 and 5533 bp respectively. b) 5' Southern blot screening showing wildtype and targeted bands.

3.3.2 Generation of constitutive R482Q model

Genotype abbreviations of R482Q mice used in this chapter are summarised in Table 3.1, with nomenclature of all mice used in this thesis shown in Appendix A.1.

Mice carrying 'floxed' R482Q alleles were identified by PCR-based genotyping (Figure 3.5). Separate PCRs have been used to identify floxed mice (R482Qfl/+) and knock-in (R482Q/+) mice. Neomycin cassette deletion was also confirmed by PCR analysis (section 4.2.1). Primer sequences are shown in Table 2.1 and position of these primers are depicted in Figure 3.3. No abnormal phenotype was seen in the R482Qfl/+ and R482Qfl/R482Qfl animals up to 13 months of age.

Abbreviated Genotype	Full Genotype	Explanation
R482Qfl/+	$Fbxw7^{R482Qfl/+}$	Heterozygous floxed Fbxw7 R482Q (G1445A) allele, *PGK*-Cre^{-}
R482Qfl/R482Qfl	$Fbxw7^{R482Qfl/R482Qfl}$	Homozygous floxed Fbxw7 R482Q (G1445A) allele, *PGK*-Cre^{-}
R482Q/+	$Fbxw7^{R482Q/+}$	Heterozygous R482Q (G1445A) knock-in allele, *PGK*-Cre^{+},
R482Q/R482Q	$Fbxw7^{R482Q/R482Q}$	Homozygous R482Q (G1445A) knock-in allele, *PGK*-Cre^{+}

Table 3.1: Nomenclature of R482Q mice used in this study. Note that in this chapter all Cre-mediated crosses used *PGK*-Cre, a ubiquitously expressed Cre [183].

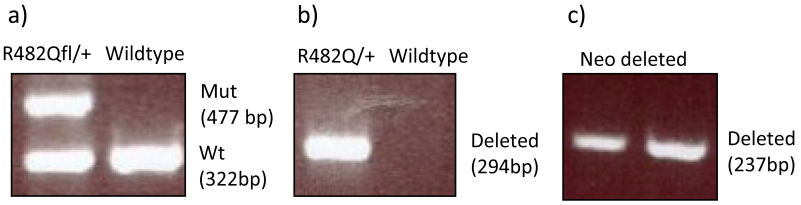


Figure 3.5: PCR genotype screening for *Fbxw7* R482Q mice. Bands show the PCR product present when using: a) primer pair 1 and 3 to identify the R482Q floxed and wildtype alleles; b) primer pair 1 and 6 to identify the R482Q knock-in allele; and c) primer pair 5 and 6 or 8 to show the neomycin cassette was removed. Primer positions are depicted in Figure 3.3.

To investigate the effect of germline *Fbxw7* R482Q mutation, I attempted to generate constitutively mutant R482Q/+ mice by breeding R482Qfl/+ animals with ubiquitously-expressing *PGK*-Cre mice [183]. In this transgenic mouse strain, Cre recombinase is driven by the *Phosphoglycerate kinase-1* (*PGK*) promoter which has early and uniform expression. This Cre recombinase is under dominant maternal control [183], therefore, by mating *PGK*-Cre females with R482Qfl/+ males, even those offspring that do not inherit *PGK*-Cre, knock-in the target R482Q mutation. *PGK*-Cre male mice however, can only transmit site-specific recombination to their Cre positive offspring.

The offspring from R482Qfl/+ and *PGK*-Cre crosses were genotyped and Table 3.2 shows that none (n=0/64) were of the R482Q/+ genotype (p=2.086 x 10^{-5}, χ^2 test).

Genotype	Male	Female	Total
Wildtype, *PGK*-Cre$^-$	9	10	19
Wildtype, *PGK*-Cre$^+$	15	12	27
R482Qfl/+, (*PGK*-Cre$^-$)	11	7	18
R482Q/+, (*PGK*-Cre$^+$)	0	0	0
Total	35	29	64

Table 3.2: No R482Q/+ offspring resulted from R482Qfl/+ x *PGK*-Cre crosses. The number and genotype of offspring from R482Q/+ x *PGK*-Cre males crosses are shown (p=2.086 x 10^{-5}, χ^2 test). Mice were counted from 12 litters from 5 different breeding pairs (n=64).

To determine if the R482Q allele caused embryonic lethality, embryos were collected at various stages of development and genotyped using their yolk sacs or tails. As shown in Table 3.3, embryos were observed at the expected 1:1 Mendelian ratio of heterozygous (R482Q/+, neo$^-$) and wildtype embryos up to E18.5 (p=0.984, χ^2 test). Therefore, it was concluded that embryos must be dying at or shortly after birth. On closer inspection it was noted that mutant embryos were in fact dying shortly after birth and being cannibalised by the mother. It was, of course, impossible to generate homozygous mutants (R482Q/R482Q) due to lethality in the heterozygous state.

Stage	Wildtype	R482Q/+
E12.5	5	7
E13.5	9	11
E14.5	3	5
E16.5	6	3
E17.5	4	5
E18.5	25	22

Table 3.3: Expected Mendelian ratios of R482Q/+ embryos found at all embryonic stages of development (p=0.984, χ^2 test). Number and genotype of embryos from various embryonic stages of R482Q/+ male x *PGK*-Cre female crosses are shown.

3.3.3 Confirmation that observed phenotype was specific to targeted *Fbxw7* R482Q mutation

To confirm accurate targeting of *Fbxw7*, E13.5 R482Q/+ embryos were collected. RNAs were extracted and reverse transcribed to generate cDNA. These cDNA were amplified using sequencing primers shown in Table 2.3. Figure 3.6 shows chromatograms confirming the presence of the G1445A (R482Q) mutation. Both wildtype (G) and mutated (A) residues were seen at base pair position 1445 (residue 482) in R482Q/+ embryos demonstrating presence of the mutation in the heterozygous state.

To date, there is not an efficient antibody available to analyse Fbxw7 at the protein level. However, Figure 3.7 shows no significant difference in *Fbxw7* mRNA expression between R482Q/+ and wildtype E13.5 whole embryos (p=0.636, Student t-test). *In vitro* work using epitope-tagged Fbxw7 R482Q plasmids showed that R482Q protein was stable (Chapter 6).

The genomic region surrounding *Fbxw7* is shown in Figure 3.8. To evaluate if any nearby genes were disrupted in the targeting of *Fbxw7*, mRNA expression of *Tigd4* (tigger transposable element derived 4: function not known), *Trim2* (tripartite motif-containing 2: function not known) and *Mnd1* (meiotic nuclear division 1 homolog: required for functional meiotic recombination) were analysed. Figure 3.9 shows that no significant differences were observed between wildtype and R482Q/+ embryos in *Mnd1* (p=0.830, Student t-test) and *Trim2* (p=0.170, Student t-test). The difference in expression of *Tigd4* between wildtype and R482Q/+ was also not considered biologically important as the CT values were very high (>34) and thus the gene was expressed at a low level (p=0.015, Student t-test).

Various tissues were dissected from E18.5 embryos and the expression of *Fbxw7* analysed by qRT-PCR. Figure 3.10 shows that *Fbxw7* was most highly expressed in brain and lung tissue. There were no significant differences in expression of *Fbxw7* between R482Q/+ and wildtype in any of the tissues analysed.

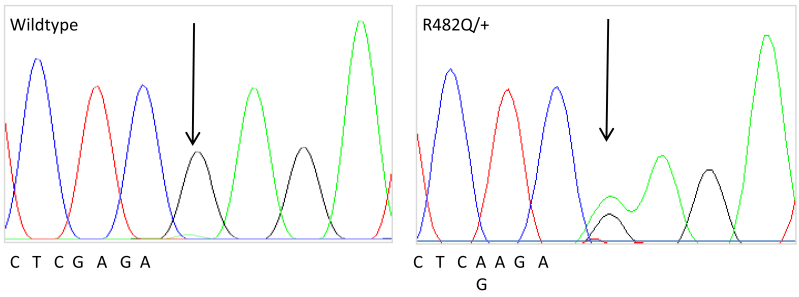


Figure 3.6: Confirmation of heterozygous *Fbxw7* R482Q mutation in R482Q/+ mice. RNA were extracted from E13.5 embryos, reverse transcribed and sequenced. Sequence traces were analysed with the ApE programme. Details of primers used are shown in Table 2.3.

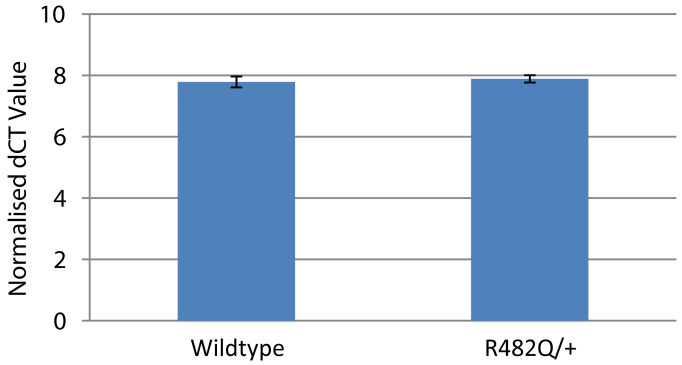


Figure 3.7: No difference in *Fbxw7* mRNA expression in R482Q/+ mice (p=0.636, Student t-test). Analysed by qRT-PCR using TaqMan probes shown in Table 2.4. CT values were normalised to *Gapdh*. Error bars represent the SEM. Wildtype (n=7) and R482Q/+ (n=14) samples were run in duplicate.

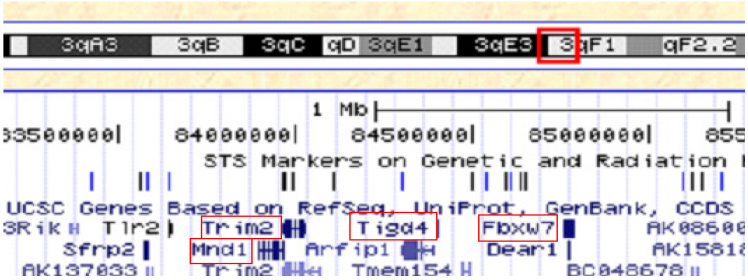


Figure 3.8: Genes surrounding *Fbxw7*. Snapshot of genes surrounding *Fbxw7* on mouse chromosome 3q, modified from UCSC.

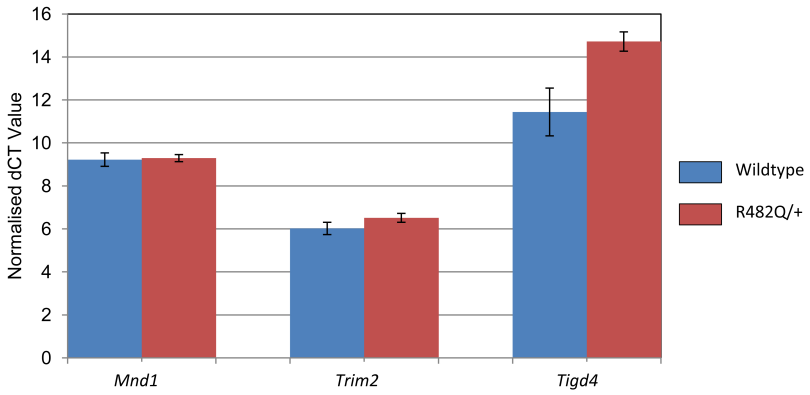


Figure 3.9: No biologically significant changes in mRNA expression in genes surrounding *Fbxw7* (p=0.830 for *Mnd1*, p=0.170 for *Trim2* and p=0.015 for *Tigd4*, Student t-tests). Note for *Tigd4* CT values were very high (>34) demonstrating low expression levels. The statistical significance observed was therefore not considered to be biologically important. Analysed by qRT-PCR using TaqMan probes (Table 2.4), CT values were normalised to *Gapdh*. Wildtype (n=7) and R482Q/+ (n=14) samples were run in duplicate. Error bars represent the SEM.

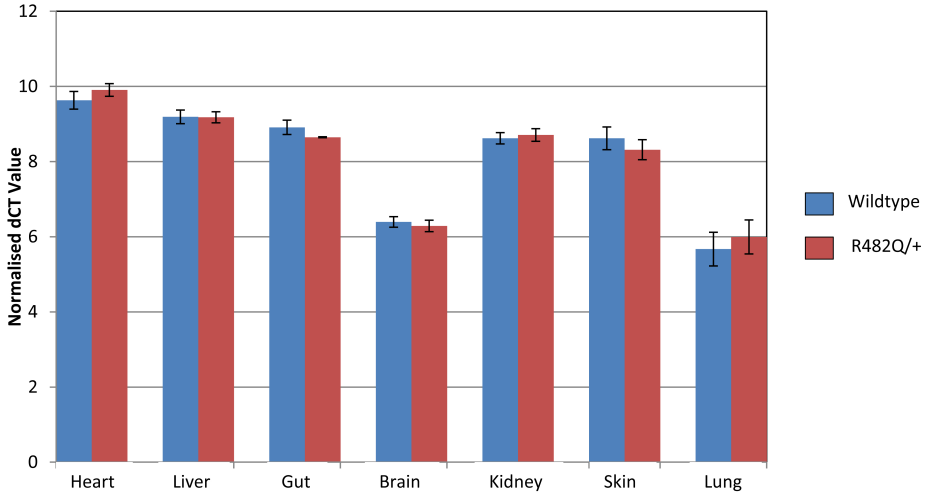


Figure 3.10: High expression of *Fbxw7* mRNA in the brain and lung at E18.5. Analysed by qRT-PCR using TaqMan probes (Table 2.4), CT values were normalised to *Gapdh*. Wildtype (n=4) and R482Q/+ (n=4) samples for each tissue were run in duplicate. Error bars represent the SEM. There were no difference between *Fbxw7* expression in wildtype and R482Q/+ samples in all tissues (p>0.05, Student t-test in all cases).

Section 1.3.2 discussed that Fbxw7 has three isoforms (α, β, γ). The abundance of individual isoforms have been analysed by SYBR-Green qRT-PCR using primers that were designed to the unique first exons reported by Hoeck *et al* [149]. Figure 3.11 shows that in the lung, the most abundant Fbxw7 species present was the α isoform. Again, there were no differences observed between R482Q/+ and wildtype lung tissue (p>0.05, Student t-test in all cases).

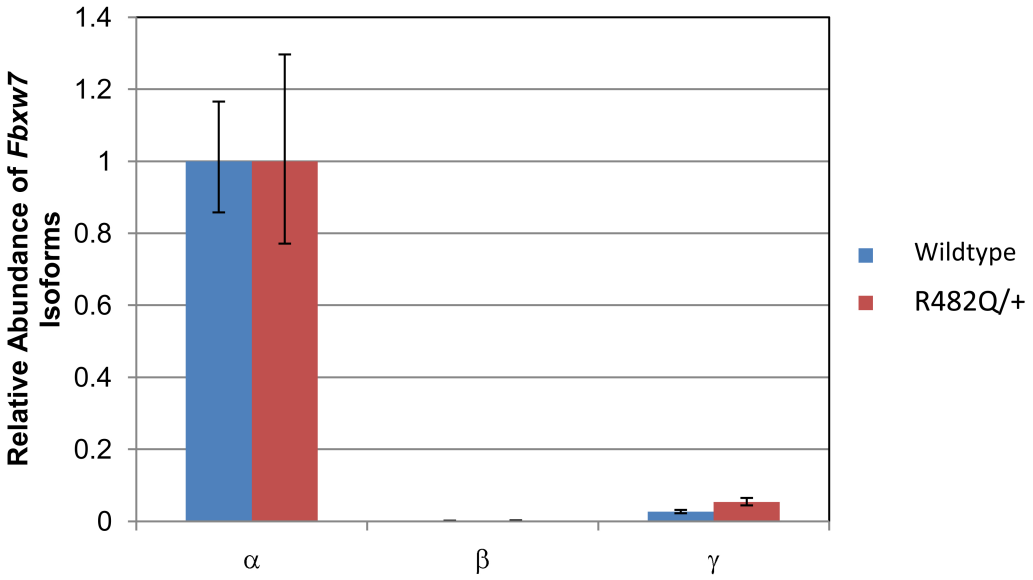


Figure 3.11: *Fbxw7α* is the most abundant isoform in the lung at E18.5. Isoform expression was analysed by qRT-PCR using SYBR-Green technology, primer sequences are shown in Appendix B.1. CT values were normalised to *Gapdh*. Wildtype (n=4) and R482Q/+ (n=4) samples were run in triplicate. Error bars represent the SEM. There were no difference between *Fbxw7* isoform expression in wildtype and R482Q/+ samples (p>0.05, Student t-test in all cases).

3.3.4 Defect in lung development in R482Q/+ mice

Embryos were collected at a late developmental stage (E18.5) to analyse physiological and histological abnormalities to explain the perinatal lethality. As shown in Figure 3.12, no significant difference in embryo weight at E18.5 was observed (p=0.200, Student t-test). Also no obvious differences could be noted on gross external appearance of wildtype and R482Q/+ embryos (Figure 3.13).

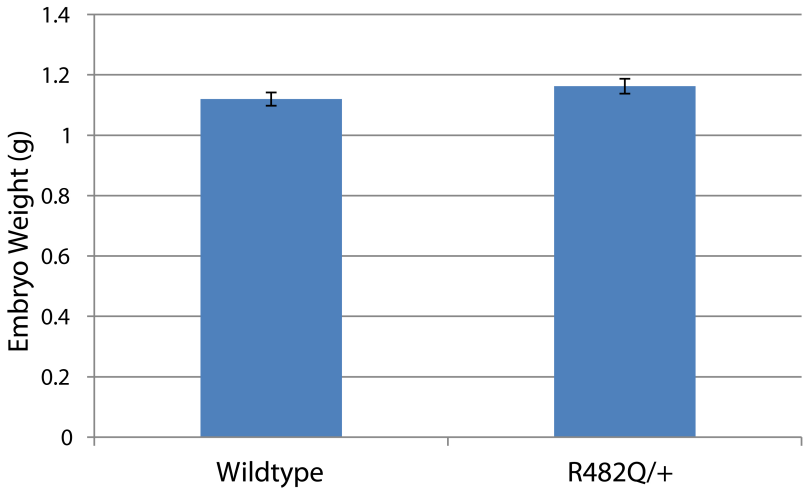


Figure 3.12: No difference in the weight of R482Q/+ and wildtype E18.5 whole embryos (p=0.200, Student t-test). 29 Wildtype and 25 R482Q/+ embryos were analysed, the error bars represent the SEM.

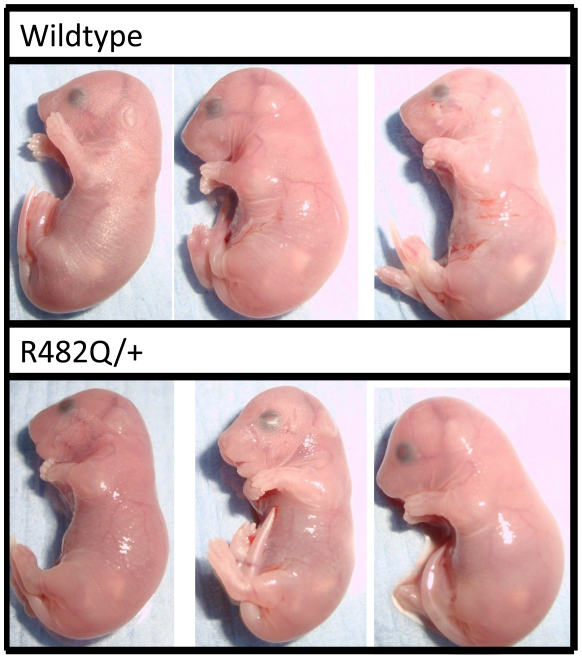


Figure 3.13: Normal gross external appearance of E18.5 R482Q/+ embryos.

However, histopathologic review of embryonic lungs identified a striking difference between E18.5 R482Q/+ and wildtype animals (Figure 3.14a). R482Q/+ embryos had thickened alveolar septa in comparison to wildtype littermates. Quantification of alveolar septa was conducted on wildtype (n=7) and R482Q/+ (n=4) mice as described in section 2.2.4.1. Wildtype lung septa measured on average 16.95 μm (range 8.89 - 29.11 μm) and R482Q/+ lung septa measured on average 29.69 μm (range 18.40 - 50.23 μm) (p=0.002, Student t-test) (Figure 3.14b and Table 3.4).

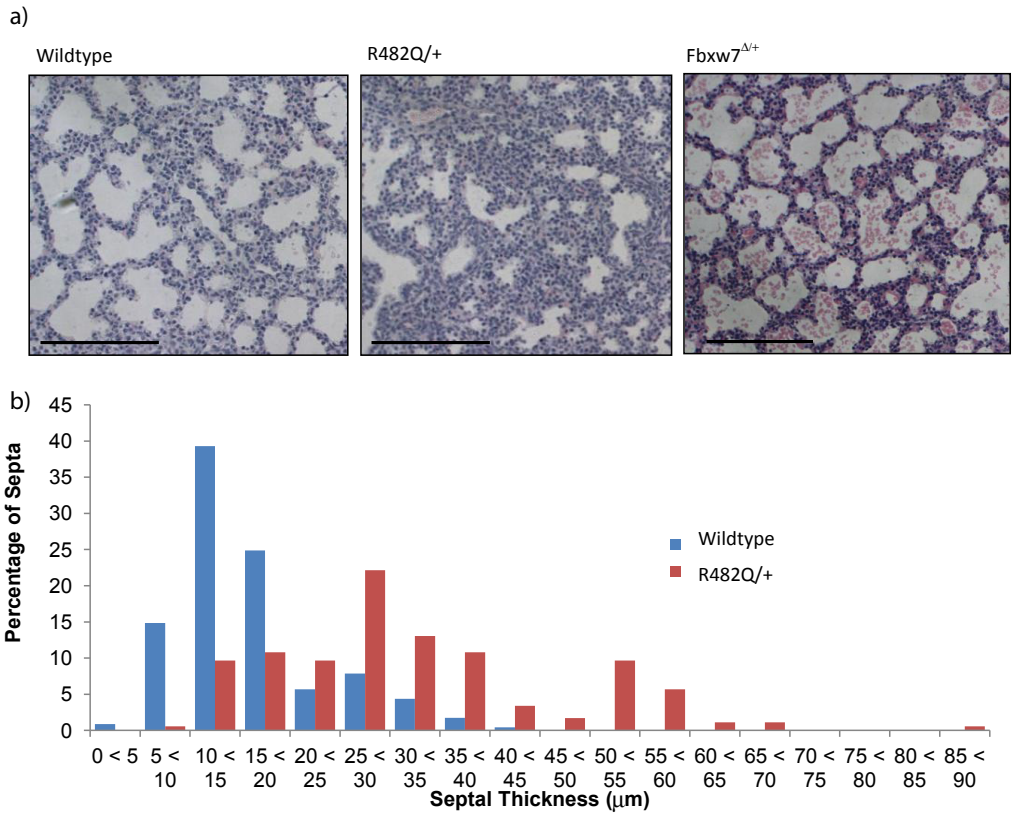


Figure 3.14: Alveolar septal thickening in R482Q/+ E18.5 embryos. a) Representative H and E stained sections of E18.5 wildtype, R482Q/+ and $Fbxw7^{\Delta/+}$ lungs. $Fbxw7^{\Delta/+}$ mice are described in section 3.3.8. Scale bars represent 150 μm. b) Histogram of alveolar septal thickness in E18.5 wildtype (n=7) and R482Q/+ (n=4) lungs. H and E images were captured at 20x magnification and all alveolar septae were quantified in a randomly selected quandrant (section 2.2.4.1).

Genotype	Mean thickness (μm)	Min (μm)	Max (μm)
Wildtype 1	22.84	11.32	31.13
Wildtype 2	17.63	5.66	33.96
Wildtype 3	13.09	8.49	19.81
Wildtype 4	16.47	8.49	28.30
Wildtype 5	15.57	8.49	33.96
Wildtype 6	12.89	5.66	25.47
Wildtype 7	20.13	14.15	31.13
Mean wildtype	**16.95**	**8.89**	**29.11**
R482Q/+ 1	28.71	22.64	39.62
R482Q/+ 2	28.77	11.32	56.60
R482Q/+ 3	38.81	25.47	56.60
R482Q/+ 4	22.48	14.15	48.11
Mean R482Q/+	**29.69**	**18.40**	**50.24**

Table 3.4: Increased alveolar septal thickness in E18.5 R482Q/+ lungs (p=0.002, Student t-test). For quantification of alveolar septal thickness see section 2.2.4.1.

3.3.4.1 Molecular characterisation of lung developmental defect in R482Q/+ mice

Ki67 immunohistochemistry shown in Figure 3.15 demonstrated significantly increased level of proliferation in R482Q/+ E18.5 lungs compared with wildtype lungs (p=0.028, Student t-test). For quantification of lung proliferation see section 2.5.1.1. Figure 3.15b shows that very few lung cells had undergone apoptosis in either R482Q/+ or wildtype E18.5 lungs, as indicated by Caspase3 immunohistochemistry.

To determine the cause of septal overgrowth analysis was carried out on distinct lung cell types. Immunohistochemistry for CC10, a marker of Clara cells [184] showed no significant difference in the number, architecture or location of these cells between R482Q/+ and wildtype samples (Figure 3.16a). Also immunohistochemistry for lung prosurfactant protein C (pro SP-C), a specific marker for alveolar type II cells, showed no difference in the percentage of pro SP-C positive cells between R482Q/+ (n=5) and wildtype (n=5) samples (Figure 3.16b) (p=0.324, Student t-test, for quantification see section 2.5.1.1).

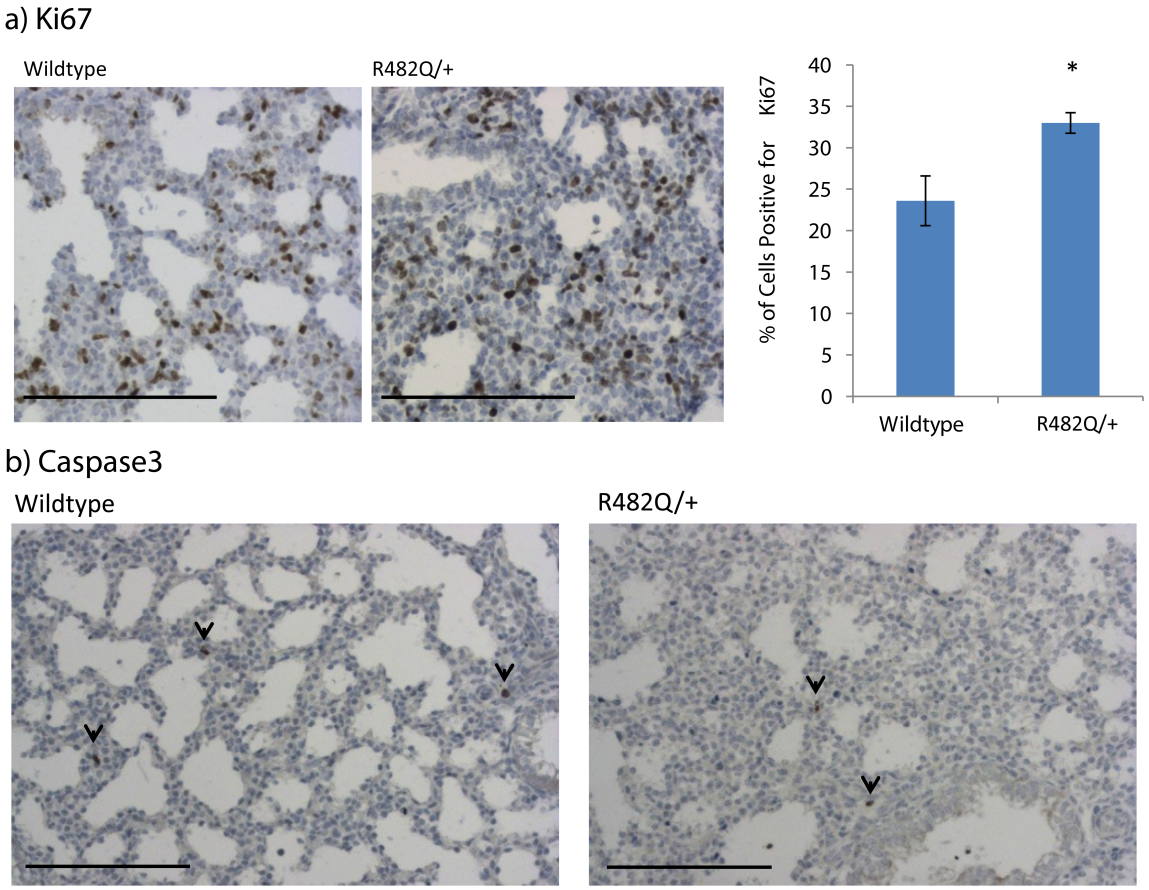


Figure 3.15: Increased proliferation in E18.5 R482Q/+ lungs. a) Ki67 immunohistochemistry on E18.5 wildtype and R482Q/+ lungs (p=0.028, Student t-test). Error bars represent the SEM. b) Caspase3 immunohistochemistry in E18.5 wildtype and R482Q/+ lungs. Very low levels of apoptosis were identified in both genotypes, arrowheads highlight positive cells. Antibody details are shown in Table 2.5. All scale bars represent 150 μm.

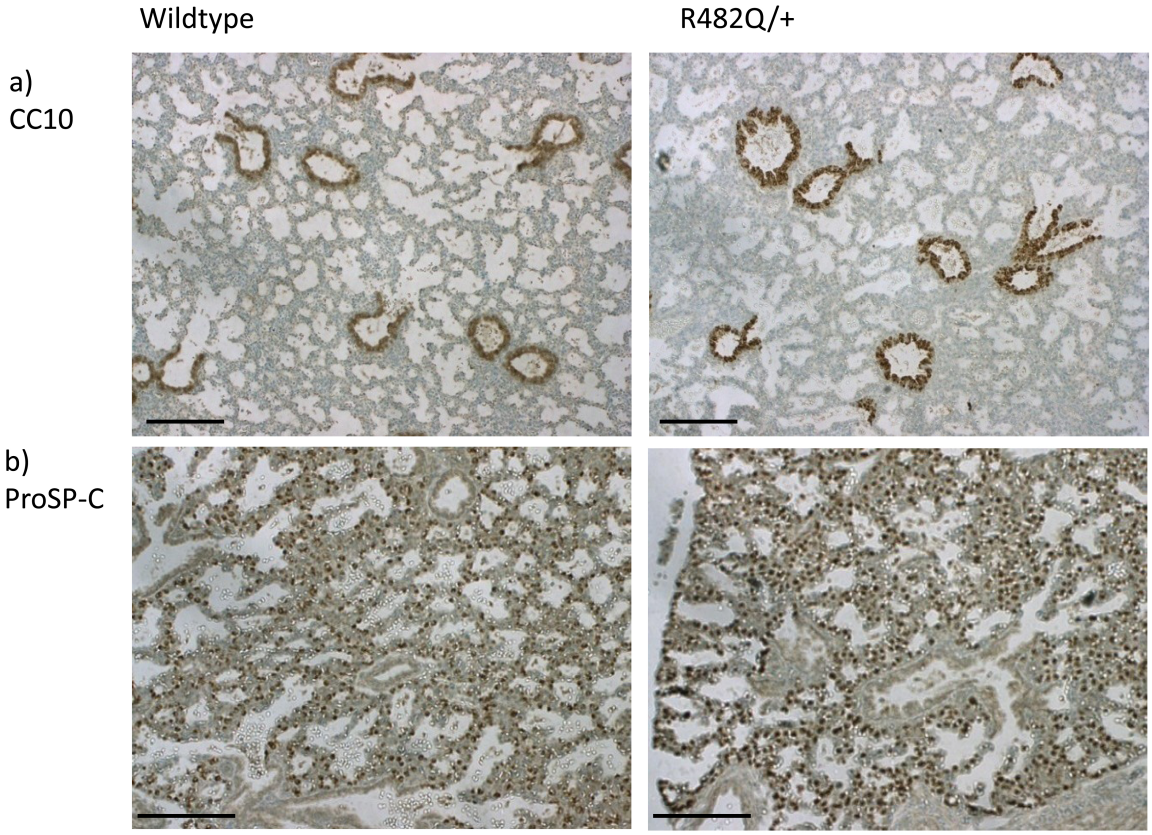


Figure 3.16: Analysis of lung cell-lineage markers in R482Q/+ E18.5 lungs. a) CC10 immunohistochemistry marking Clara cells. There was no significant difference in the number, architecture or location of these cells between wildtype and R482Q/+ samples. b) Prosurfactant protein C (Pro SP-C) immunohistochemistry staining marking alveolar type II cells. There was no difference in the number of these cells between wildtype and R482Q/+ samples (p=0.324, Student t-test). Antibody details are shown in Table 2.5. All scale bars represent 150 μm.

Figure 3.17 shows H and E stained sections of R482Q/+ and wildtype lungs at E16.5, prior to thinning down of the alveolar septa. At this developmental stage, both R482Q/+ and wildtype lung samples were indistinguishable, therefore the pseudoglandular stage of development (E9.5 to E16.6) proceeded normally but there was disruption at the canalicular (E16.6-E17.6) and/or terminal sac stage (E17.6-P5) (section 3.4.3).

3.3.4.2 Assessment on FBXW7 substrate protein abundance in R482Q/+ lungs

As Fbxw7 is involved in the ubiquitination and subsequent degradation of its substrates, I sought to determine if the R482Q mutation, predicted to abrogate substrate binding, led to any notable accumulation of protein substrates. Fbxw7 substrates (AuroraA, cyclin E, Nicd1, c-Jun and c-Myc) were investigated by western blot on E18.5 lungs. Figure 3.18 shows there were no significant differences observed in protein levels between wildtype and R482Q/+ samples ($p>0.05$, Student t-test in all cases). The antibodies and their dilutions used are summarised in Table 2.6.

In view of the lack of differential expression of these proteins, two more recently identified Fbxw7 substrates, Klf5 [127; 128] and Tgif1 [135], were analysed by western blot. Klf5 is an nuclear transcription factor so cell fractionation of lung lysates was conducted and western blots were performed on the nuclear fraction (section 2.5.3.4). Figure 3.19a shows a significantly increased amount of Klf5 protein in the nuclear fraction of R482Q/+ E18.5 lungs compared to wildtype samples ($p=0.015$, Student t-test). Figure 3.19b shows Tgif protein was detected as a double band as previously reported, with the upper band representing the hyper-phosphorylated form [135]. Quantification of both bands to assess total protein levels demonstrated a significant increase in Tgif protein in R482Q/+ E18.5 lungs ($p=0.010$, Student t-test). As CPD phosphorylation is required for Fbxw7 recognition and degradation

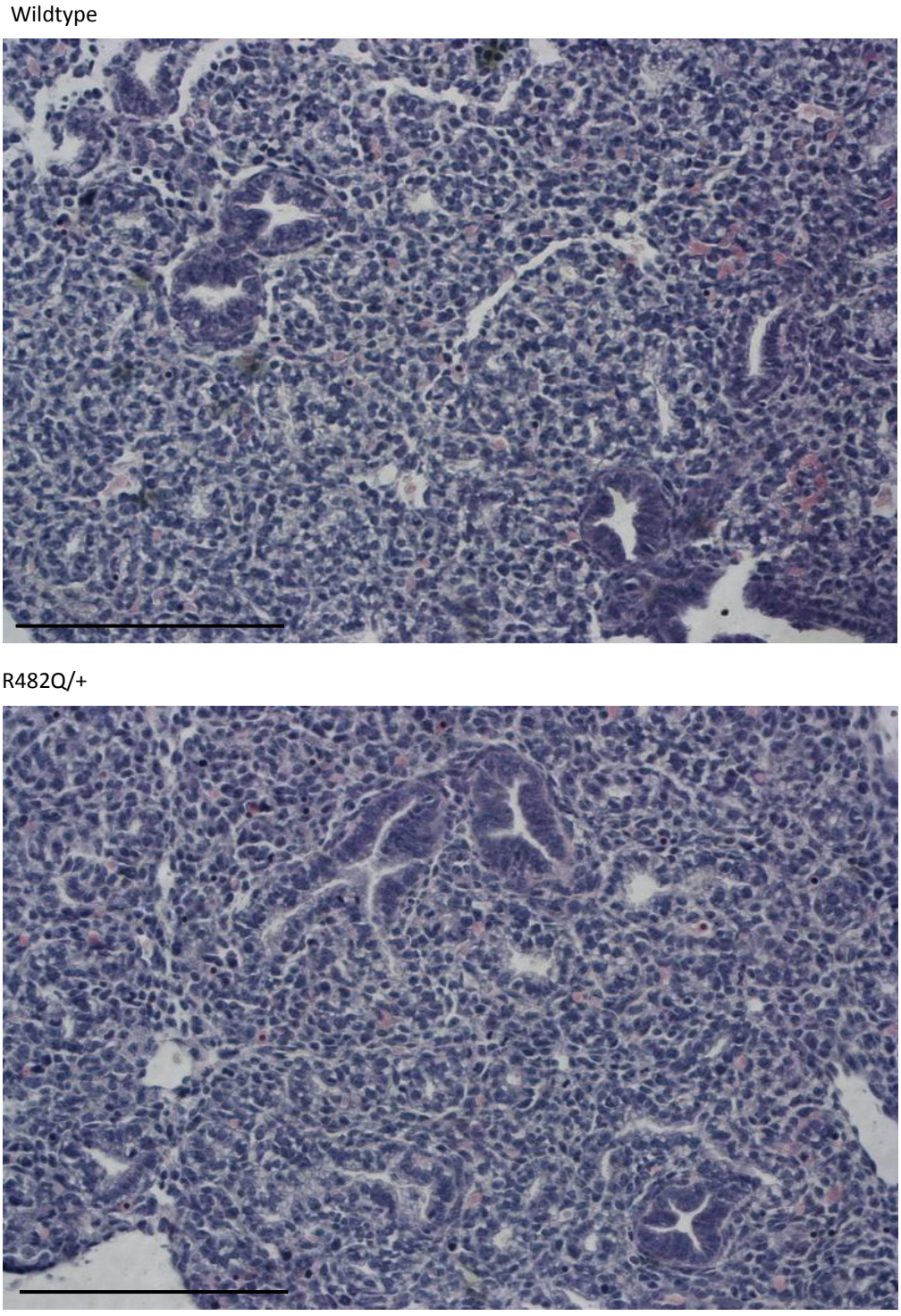


Figure 3.17: No difference in lung architecture in E16.5 R482Q/+ lungs. Representative H and E stained sections of wildtype and R482Q/+ E16.5 lungs. Scale bars represent 150 μm.

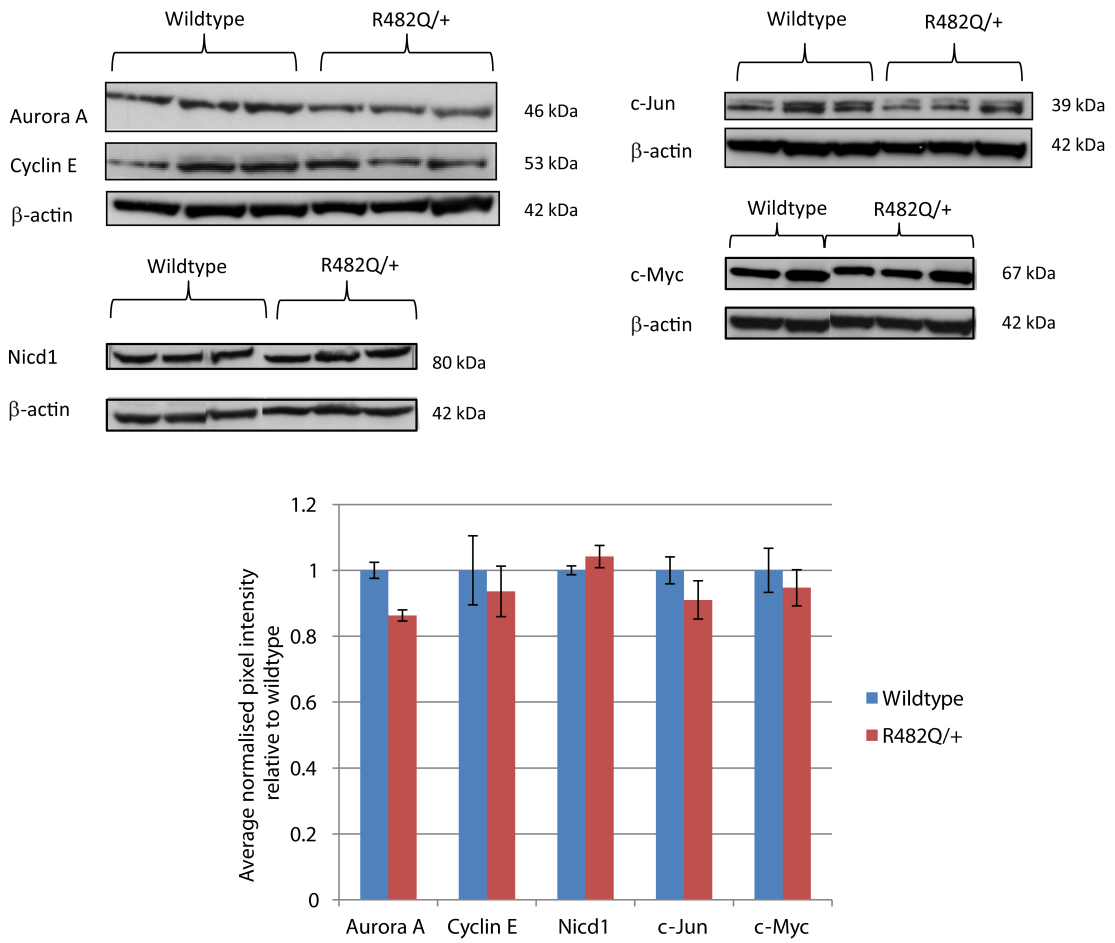


Figure 3.18: No difference in protein levels of several Fbxw7 substrates in E18.5 R482Q/+ lungs (p>0.05 in all cases, Student t-test). Antibodies used are summarised in Table 2.6. β-actin has been used as a loading control. Protein sizes in kDa are indicated. All westerns have been run at least in duplicate. The graph shows average normalised pixel intensities relative to wildtype samples. Error bars represent the SEM.

of substrates, both upper (hyper-phosphorylated) and lower (hypo-phosphorylated) bands were next quantified independently. Elevation of Tgif protein in R482Q/+ samples compared to wildtype samples was evident in both bands (p=0.006, p=0.023 respectively, Student t-test).

It was confirmed there were no differences in expression of *Klf5* and *Tgif1* mRNA and in E18.5 lungs (p=0.589 and p=0.704 respectively, Student t-test) (Figure 3.20). This is consistent with elevated levels of these proteins mediated by altered Fbxw7 ubiquitin ligase activity.

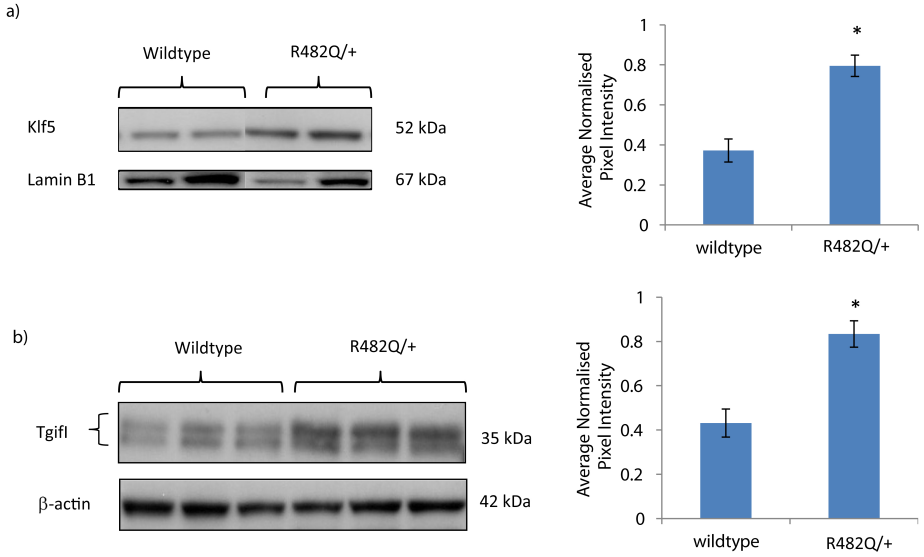
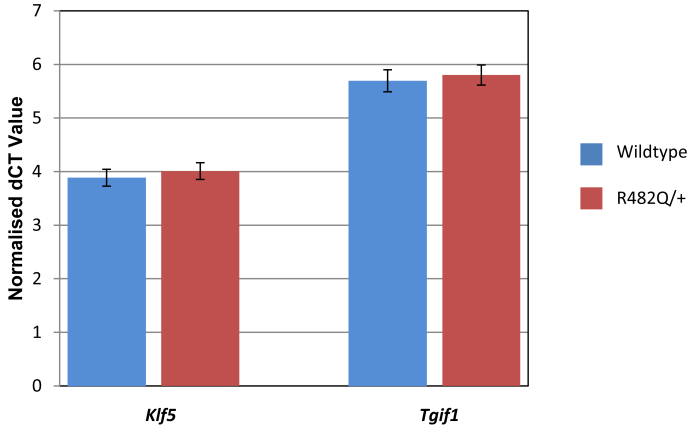


Figure 3.19: Elevation of Klf5 and Tgif protein levels in E18.5 R482Q/+ lungs. a) Western blot for Klf5 using the nuclear fraction of lung lysates (p=0.015, Student t-test). Lamin B1 has been used as loading control. b) Tgif upper band represents hyper-phosphorylated Tgif1 and the lower band represents hypo-phosphorylated Tgif1 (bands were quantified together, p=0.010, Student t-test). β-actin has been used as a loading control. Antibody details are summarised in Table 2.6. Graphs show average normalised pixel intensities. Error bars represent the SEM. Western blots were repeated at least in duplicate.



p]

Figure 3.20: No increase in mRNA expression of *Klf5* and *Tgif1* in E18.5 R482Q/+ lungs (p=0.589 and p=0.704 respectively, Student t-test). Analysed by qRT-PCR using SYBR-Green technology, CT values were normalised to *Gapdh*, using primers detailed in Appendix B.1. Wildtype (n=10) and R482Q/+ (n=13) samples were run in triplicate. Errors bars represent the SEM.

3.3.5 Assessing potential tissue-specificity of R482Q/+ mutation

In order to assess if elevated protein levels of Klf5 and Tgif were restricted to the lung, mouse embryonic fibroblasts (MEFs) were derived from E13.5 wildtype and R482Q/+ embryos using standard methods (section 2.6.5). Figure 3.21 shows that Tgif1 protein was increased in R482Q/+ MEFs in comparison to wildtype MEFs. Quantification of both Tgif bands demonstrated a significant increase in Tgif protein in R482Q/+ MEFs (p=0.037, Student t-test). Both hyper and hypo-phosphorylated bands were quantified independently and a greater increase in Tgif protein level between R482Q/+ and wildtype samples was seen with the hyper-phosphorylated band (upper band, p=0.015, lower band p=0.242, Student t-test). This was consistent with the paradigm that Fbxw7 substrates are phosphorylated prior to ubiquitination by Fbxw7.

Klf5 was not detectable in MEFs; it is only expressed at high levels at later stages of embryonic development [185].

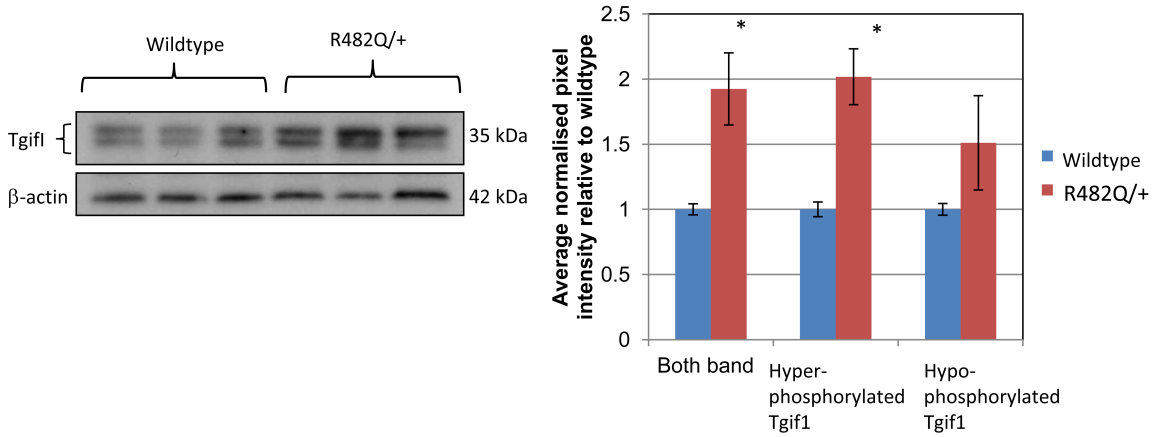


Figure 3.21: Elevation of protein level of Tgif in R482Q/+ MEFs (p=0.037, p=0.015, p=0.242 for total Tgif1, hyper- and hypo-phosphorylated Tgif1 respectively, Student t-test). Antibody details are shown in Table 2.6. Western blots were run in duplicate. β-actin was used as a loading control. Graph shows the average normalised pixel intensities relative to wildtype samples. Note that every lane on the western blot represents MEFs derived from independent embryos.

3.3.6 Additional developmental abnormalities in R482Q/+ E18.5 embryos

Review of the available literature on mouse models exhibiting perinatal lung developmental defects highlighted an association with disruption of the Tgf-β pathway (section 3.4.5). R482Q/+ E18.5 embryos were therefore assessed for additional phenotypes characteristic of Tgf-β defects.

Figure 3.22 shows the gross appearance of the cleft palate phenotype in E18.5 R482Q embryos, as well as H and E stained sections which highlight that palatal shelves had failed to fuse (section 3.4.4). 30% (n=12/40) of R482Q/+ embryos displayed this phenotype. It was found that 42% (n=17/40) of R482Q/+ mice had an 'eyes-open-at-birth' (EOB) phenotype, whereby eyelids failed to fuse (Figure 3.23).

60% (n=24/40) of R482Q/+ embryos showed EOB and/or cleft palate developmental phenotypes. One of the two phenotypes were observed in 47.5% (n=19/40) of embryos and both phenotypes were observed in 12.5% (n=5/40) of embryos. The incidence of additional developmental abnormalities are shown visually in Figure 3.24. Neither the cleft palate nor the EOB phenotype were present in wildtype embryos.

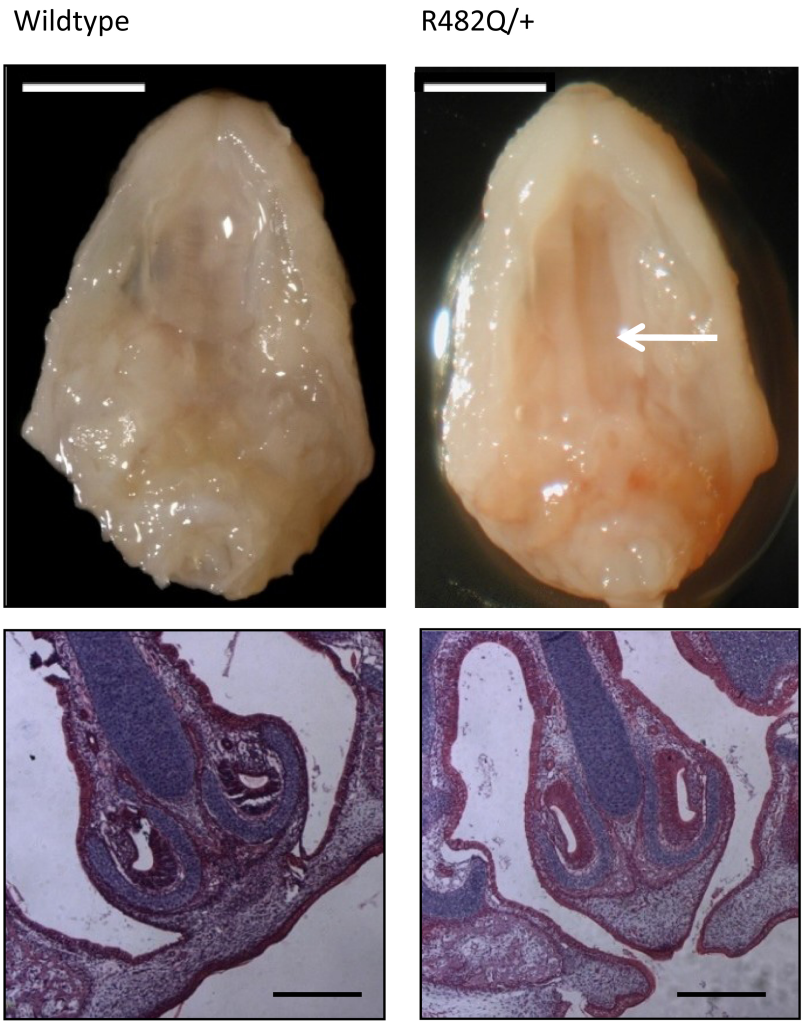


Figure 3.22: Identification of cleft palate phenotype in E18.5 R482Q/+ embryos. The upper left panel shows the gross appearance of a normal palate in an E18.5 wildtype embryo. The upper right panel shows the gross appearance of the R482Q/+ palate with the arrow highlighting the position of the cleft palate. The scale bars represent 0.5 cm. Lower panels shows H and E stained sections, the scale bars represent 300 μm.

.

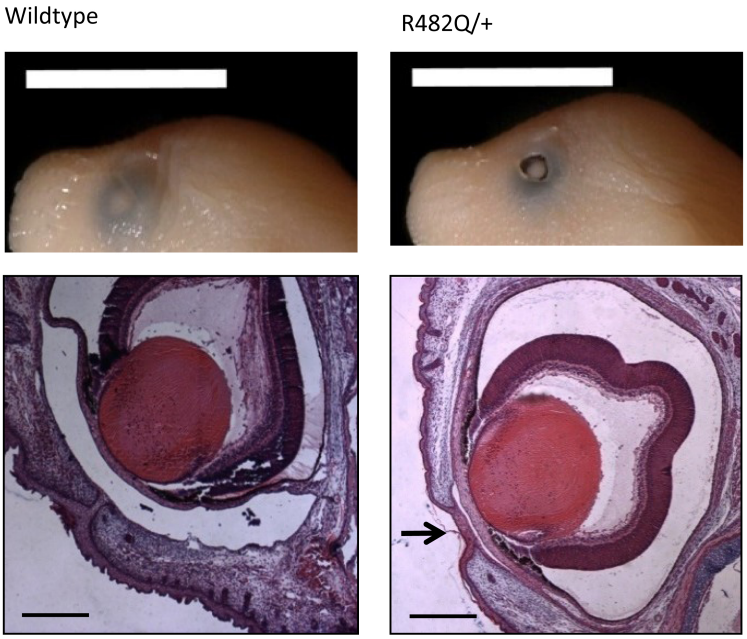


Figure 3.23: Eyes-open-at-birth phenotype found in R482Q/+ E18.5 embryos. The upper left panel shows the gross appearance of normal eyelid fusion in wildtype E18.5 embryos. The upper right panel shows the EOB phenotype in E18.5 R482Q/+ embryos, the scale bars represent 0.5 cm. The lower panel shows H and E stained sections, the scale bars represent 300 μm. The arrow highlights the failure in eyelid fusion in R482Q/+ embryos.

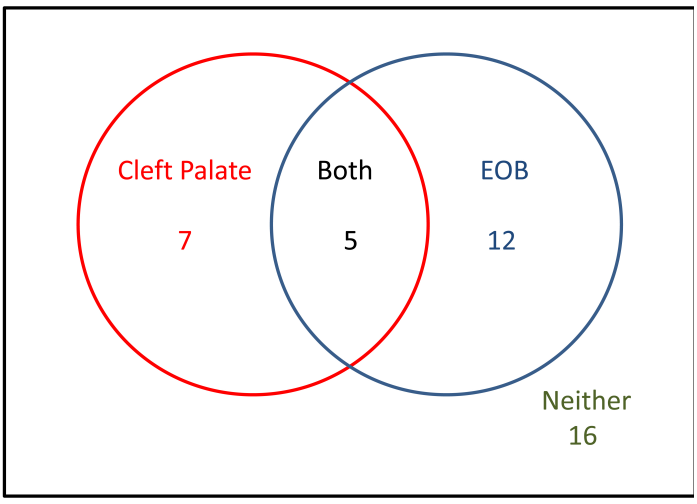


Figure 3.24: Occurrence of other developmental abnormalities in R482Q/+ embryos (n=40).

3.3.7 Analysis of specific signalling pathways

3.3.7.1 Tgf-β pathway

The characteristic phenotypes of EOB, cleft palate and developmental lung defects suggested deregulation of the Tgf-β signalling pathway. Analysis of several key components in the Tgf-β signalling were subsequently undertaken. There were no notable differences in phospho-Smad2 protein location or intensity of staining analysed by immunofluorescence (Figure 3.25).

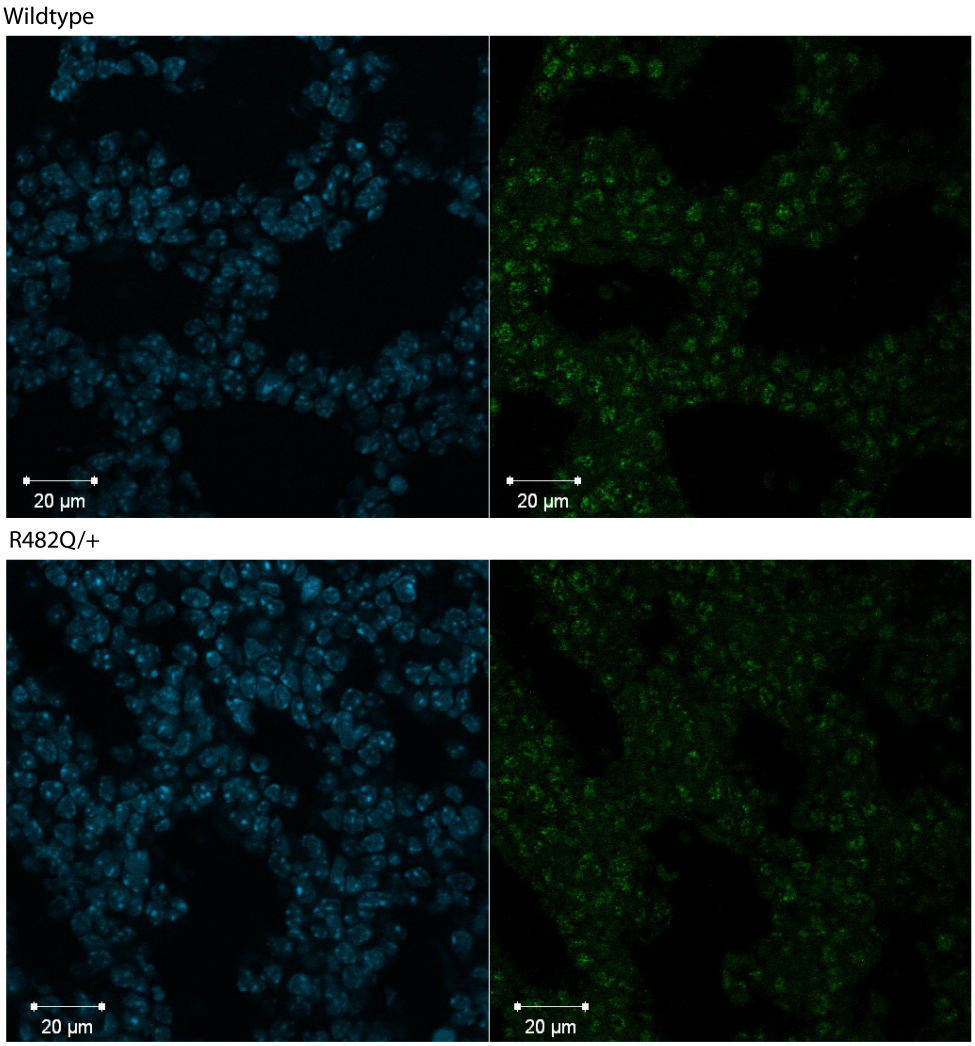


Figure 3.25: No difference in location or intensity of phospho-Smad2 in R482Q/+ E18.5 lungs. Left hand images show DAPI staining and right hand images show fluorescent phospho-Smad2 staining (FITC filter). Antibody details are shown in section 2.5.2.

Nor was there any difference in mRNA expression of selected downstream targets analysed by qRT-PCR (p>0.05 in all cases, Student t-test) (Figure 3.26). Finally nuclear Smad4 protein levels analysed by western blot on the nuclear fraction of lung lysates also remained unchanged between R482Q/+ and wildtype samples (Figure 3.27) (p=0.698, Student t-test).

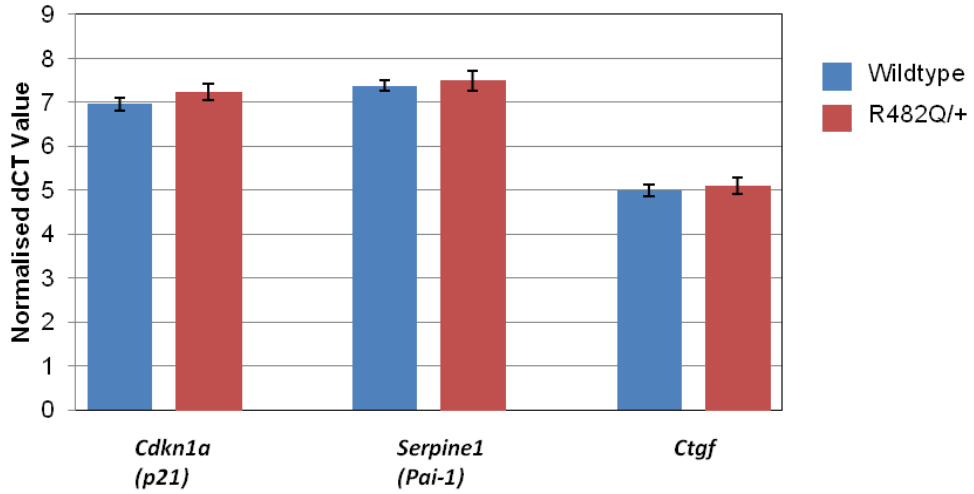


Figure 3.26: No change in mRNA expression of selected downstream targets of the Tgf-β pathway in E18.5 wildtype and R482Q lungs (p=0.302 for *Cdkn1a*, p=0.682 for *Serpine1* and p=0.666 for *Ctgf*, Student t-tests). Wildtype (n=10) and R482Q/+ (n=13) samples were run in triplicate. Primers used are detailed in Appendix B.1. Analysed by qRT-PCR using SYBR-Green technology, CT values were normalised to *Gapdh*. Error bars represent the SEM.

3.3.7.2 Notch pathway

As early embryonic lethality (E10.5-11.5) in homozygous *Fbxw7*-null mice is associated with defects in Notch signalling [171; 172], assessment of components of this pathway was also conducted. Figure 3.18 showed no difference in the protein level of Nicd1 in wildtype and R482Q/+ E18.5 lung samples. Investigation of Hairy/enhancer of split1 (*Hes1*), a downstream target of Notch signalling, by *in situ* hybridisation (ISH), found no difference in mRNA expression between wildtype and R482Q/+ E18.5 lung samples (Figure 3.28).

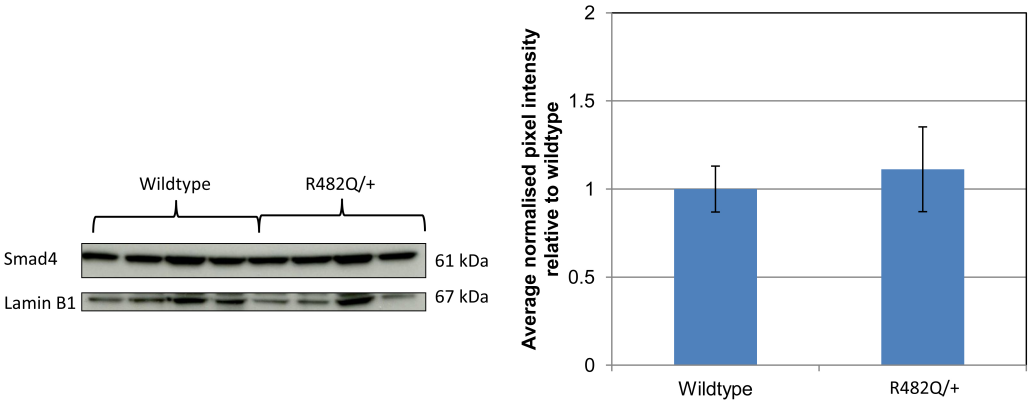


Figure 3.27: No difference in Smad4 protein levels in the nuclear fraction of E18.5 R482Q/+ lungs (p=0.698 Student t-test). Lamin B1 has been used as the loading control.

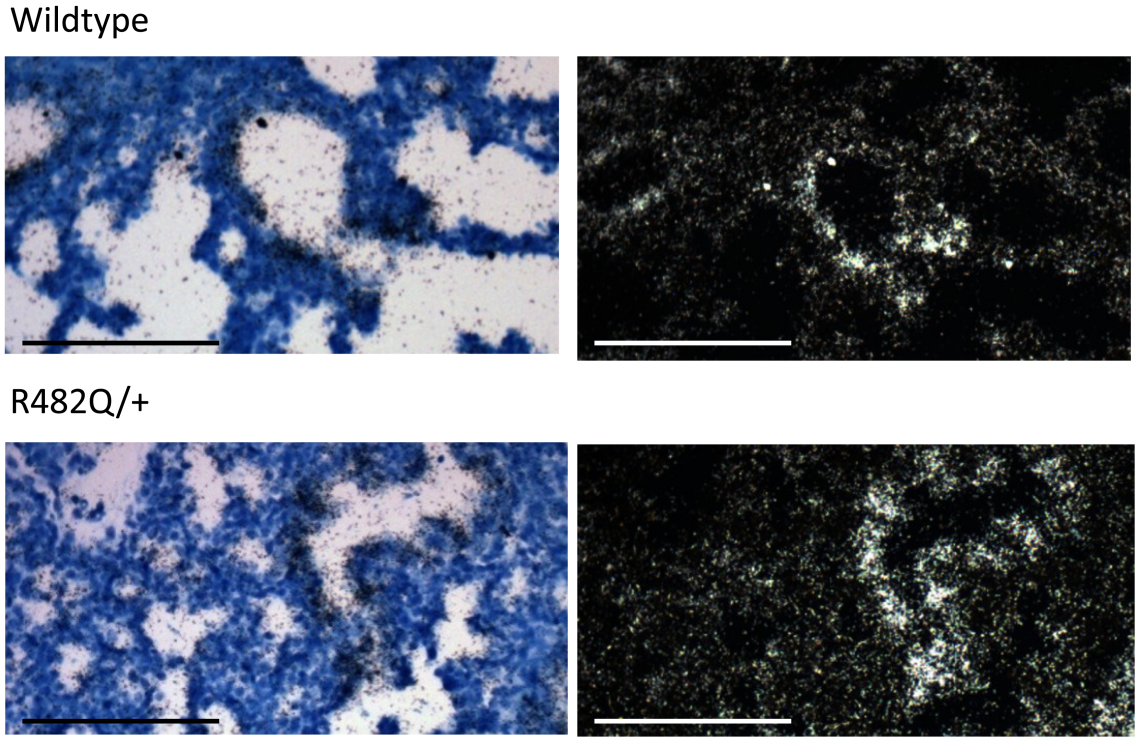


Figure 3.28: No difference in *Hes1* mRNA expression in E18.5 R482Q/+ lungs. *In situ* hybridisation was carried out with ^{35}S labelled *Hes1* riboprobe. Brightfield images shown on the left hand side and darkfield images showing silver granules counterstained with Giemsa shown on the right. Scale bars represent 150 μm.

3.3.7.3 Retinoic acid pathway

The retinoic acid signalling pathway is well recognised as playing a pivotal role in lung development [186]. Hundreds of genes have been proposed as downstream targets of the retinoic acid pathway, 27 of which have been validated [187]. A selection of these were analysed by SYBR-Green qRT-PCR, including: *Rara* (retinoic acid receptor α), *Stra6* (a retinoic acid binding protein receptor gene) and *Crabp2* (cellular retinoic acid binding protein; involved in storage, transport and degradation of retinoic acid). Figure 3.29 shows there was no difference in these selected downstream targets of the retinoic acid pathway between wildtype and R482Q/+ E18.5 lung samples (P>0.05 Student t-test in all cases).

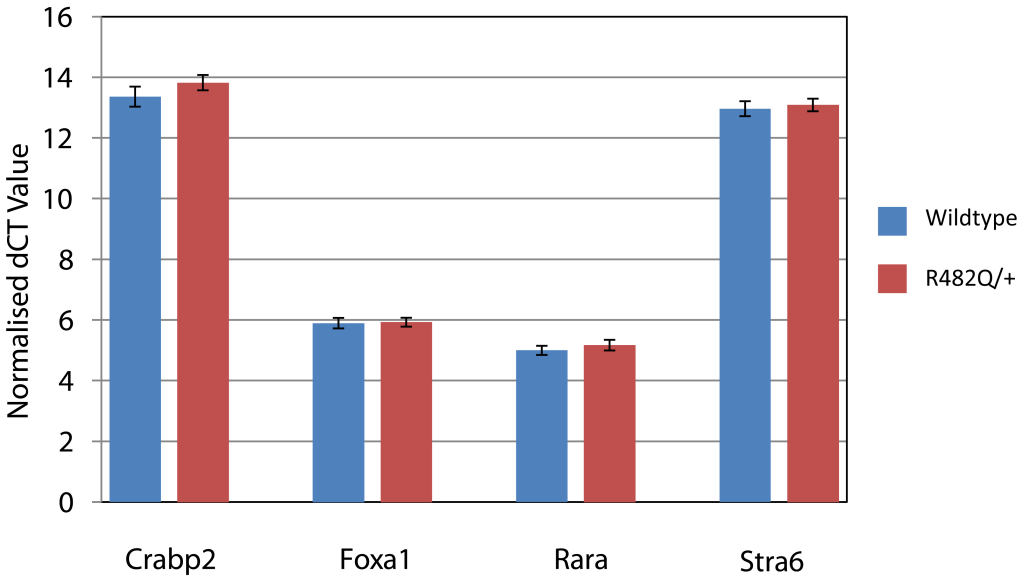


Figure 3.29: No change in mRNA expression of selected retinoic acid pathway targets in R482Q/+ E18.5 lungs (p=0.271, 0.891, 0.481, 0.706 for *Crabp2*, *Foxa1*, *Rara* and *Stra6* respectively, Student t-tests). Assessed by qRT-PCR using primers detailed in Appendix B.1. Wildtype (n=10) and R482Q/+ (n=13) samples were run in triplicate.

3.3.8 Comparison to *Fbxw7*-null mouse model

Professor Axel Behrens (Cancer Research UK, London Research Institute) provided us with a conditional *Fbxw7*-null mutant mouse model [151]. In this model, *Fbxw7*

exon 5, which encodes the critical F-box domain, is flanked by LoxP sites and thus deleted when crossed with Cre-recombinase expressing mice. The open reading frame of Fbxw7 is subsequently disrupted and Fbxw7 protein is unstable and not detectable. The genotype abbreviations for this strain are shown in Appendix A.1. Genotyping PCRs were carried out using primers shown in Table 2.1 following reported protocols [151]. Studies were carried out on this null $Fbxw7^{\Delta/+}$ model to see if the phenotypes observed in the R482Q/+ model were mutation specific. Figure 3.14 shows the $Fbxw7^{\Delta/+}$ lungs do not have thickened alveolar septa or any other lung abnormalities. This demonstrates that the epithelial developmental defects observed in R482Q/+ mice were not a result of *Fbxw7* haploinsufficiency. $Fbxw7^{\Delta/\Delta}$ E18.5 lungs could not be assessed due to early embryonic lethality (previously reported [188]).

3.4 Discussion

3.4.1 Generation of informative *Fbxw7*-mutant mice

It is important to note that FBXW7 has been highly evolutionary conserved, with 96-98% protein identity between human and mouse across isoforms. The DNA sequence and protein sequence surrounding the common sites of *FBXW7* mutations are also highly conserved between human and mouse and elucidation of murine phenotypes is likely to provide mechanistic insights into human disease. Although several *Fbxw7* models have already been created to study Fbxw7 function *in vivo*, these models, to date, are all null alleles and thus not reminiscent of predominant *FBXW7* missense mutations found in human cancers. The *Fbxw7* R482Q mutant mouse model more faithfully recapitulates *FBXW7* mutations observed in human CRC and other cancers.

3.4.2 Constitutive *Fbxw7* R482Q model

Like many cancer related genes, *Fbxw7* is also important in developmental pathways, for example in vascular and cardiovascular development [171; 172].

Using the R482Q mouse model, it was shown that a specific propellor-tip mutation resulted in a different phenotype in comparison to *Fbxw7*-null heterozygous or homozygous alleles. The R482Q mutant model affected embryonic epithelial development in the heterozygous state with a combination of defects in lung maturation, palatogenesis and eyelid fusion causing perinatal lethality within a few hours of birth. The cause of death was almost certainly due to the lung phenotype, as EOB is not life threatening and cleft palate does not usually lead to death this early. The relatively high level of *Fbxw7* mRNA expression in developing lungs suggest a particularly important role in this organ and may explain the presence of the lung phenotype in all R482Q/+ embryos. By contrast, the cleft palate and eyelid fusion phenotypes were incompletely penetrant. *Fbxw7*α was the most abundant isoform in E18.5 lung tissue (Figure 3.11), consistent with previous reports indicating *Fbxw7*α as the most abundant isoform in most adult mouse tissues [60]. *Fbxw7*β is only expressed highly in the brain and testis and *Fbxw7*γ is only expressed highly in the heart and skeletal muscle [60].

Homozygous *Fbxw7*-null mice displayed earlier embryonic lethality at E10.5-E11.5 due to compromised vasculogenesis [171; 172]. The heterozygotes were reported to survive to adulthood with no apparent defects, thus R482Q/+ animals show a novel intermediate phenotype. Disruption of Notch was considered the primary contributor to the phenotype in homozygous null animals. I neither found the level of Nicd1 protein elevated in the lungs of R482Q/+ embryos, nor observed effects on c-Jun protein levels (Figure 3.18) previously found when *Fbxw7* inactivation was targeted to the gut [151]. Conversely, since the epithelial phenotypes were not observed in the heterozygous *Fbxw7*-null models, these must directly result from the specific

propellor-tip R482Q mutation. It is of note to mention here that all *Fbxw7* models discussed were on a C57Bl/6J genetic background and thus differential effects are not attributable to presence of modifier loci between strains [189].

3.4.3 Lung development

Murine lung development can be described in four phases as summarised in Table 3.5 [190].

Phase	Time	Details
Pseudoglandular	E9.5 - E16.6	Bronchial and respiratory tree develops to form an undifferentiated primordial system
Canalicular	E16.6 - E17.4	Terminal lung bud dilation and vascularisation
Saccular	E17.4 - P5	Formation of distal airways sacs, thinning down of mesenchyme layer, vascularisation and differentiation of pneumocytes
Alveolar	P5-P30	Terminal sacs develop into alveolar ducts and alveoli

Table 3.5: Stages of murine lung development. E denotes embryonic day, whereas P is postpartum age in days.

The pseudoglandular stage of level development (E9.5 to E16.6) appears to proceed normally as E16.5 R482Q/+ lungs were indistinguishable from wildtype lungs (Figure 3.17). However, there was disruption in the canalicular (E16.6-E17.6) and/or terminal sac stage (E17.6-P5) resulting in the differences in alveolar septa thickness shown in Figure 3.14.

3.4.4 Additional developmental abnormalities

During murine development there is temporary fusion of the eyelids; the eyelids start to form at E11.5, grow across the eye from E14 and eyelid fusion is complete by E16. In R482Q/+ embryos the eyelids do not reach each other in order to allow fusion.

Figure 3.30 represents the multi-step nature of murine palatogenesis. To sum-

marise, palatal shelves grow downwards from maxillary processes followed by elevation above the tongue and fusion of the palatal shelves. These processes occur between E12.5 and E15.5. Defects in any aspect of this process can lead in a phenotypic cleft palate such as observed in R482Q/+ embryos.

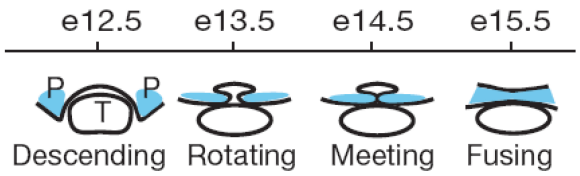


Figure 3.30: Schematic representation of murine palatogenesis. P: Palatal shelves, T:Tongue. Figure modified by permission from Macmillan Publishers Ltd: [Nature] (ref [191]), copyright (2007).

3.4.5 Comparable mouse models / Critical signalling pathways

There are several mouse models which display similar developmental phenotypes to the R482Q/+ model, a selection of these are summarised in Table 3.6.

A mouse model that also exhibits all three developmental defects observed in R482Q/+ mice (though in a homozygous state) interestingly targets another F-box E3 ubiquitin ligase encoded by *Fbxo11* [192]. To date, the substrates of Fbxo11 have not been characterised. This mutant model was identified from a deafness mouse mutagenesis screen and contains a non-conservative glutamine to leucine change at amino acid 491 of Fbxo11 [193]. Phospho-Smad2, a component of the Tgf-β signalling pathway, was significantly upregulated in the epithelia of homozygous mutant *Fbxo11* mice.

The models highlighted in Table 3.6 indicate that multiple signalling pathways are critical for lung/epithelial embryonic development. Many of the models show deregulated Tgf-β signalling and suggest that this pathway, amongst others, is critical in epithelial embryonic development [125; 194; 195; 197].

Model	Lung Defect	Cleft	EOB	Details	Ref.
Knockout of *Cebpa*	✓ at birth		✓	↑ Tgf-β2	[194; 195]
Defective *Foxa2*	✓ within 1st 2 days postpartum			Alveolar thickened. Immature cuboidal type II cells	[196]
Knockout of Nuclear factor I-B (*Nfib*)	✓ at birth		✓	↑ thickness of alveolar septa Cannicular phase delay ↑ Tgf-β1	[197]
↑ *Klf5* in epidermis		✓	✓	Altered p63	[198]
Null *Jun* in epidermis			✓	Altered EGFR signalling	[199; 200]
Knockout of *Tgfb3*	✓	✓			[201; 202]
Knockout of *Klf5* in lung	✓ at birth			Saccular phase disrupted ↑ Tgfβ2	[125]
Mutant *Fbox11*	✓	✓	✓	↑ pSmad2	[192; 193]
↑ *Hoxa7* expression		✓	✓		[203]
Knockout of *Rara*	✓				[204]
Gsk3b mutant		✓			[191]

Table 3.6: Mouse models with developmental phenotypes similar in those observed in the R482Q/+ model.

Notch signalling also plays a major role in lung development [205]. The moderate hypotrophic phenotype of lungs from animals with an *Hes1* mutation and the expression of Notch components in the distal lung bud during branching morphogenesis, together suggest that Notch may play a role in normal lung growth, especially in Clara cell precursors. I did not however, establish any obvious signs of Notch signalling deregulation in the components in which I analysed at E18.5. As investigation were conducted at a late embryonic stage I cannot exclude Notch deregulation at earlier developmental stages.

The retinoic acid signalling pathway plays an important role in all stages of lung development especially during terminal maturation which gives rise to alveoli. Figure 3.31 schematically represents the role of this pathway in embryonic lung development.

A mouse model studying retinoic acid receptor deficient mice displayed defective alveolarisation, thus indicating the importance of the retinoic acid pathway in lung development. Klf5 and Tgif1 are both components of the retinoic acid signalling pathway; Klf5 has been shown to directly interact with the retinoic acid receptor [122] and Tgif1 can bind a retinoid response motif in DNA thus inhibiting RXR binding by steric hinderance [206].

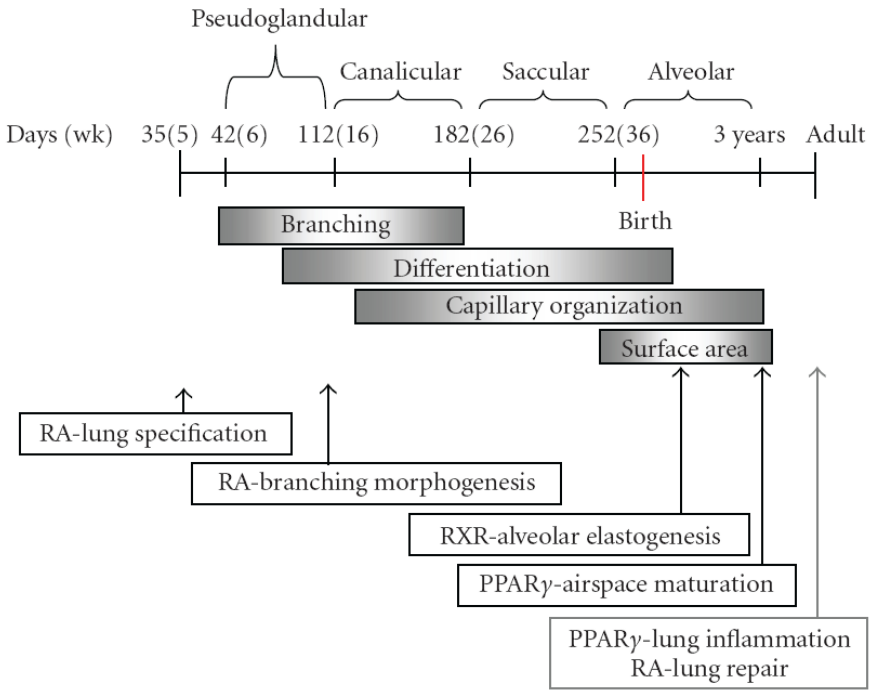


Figure 3.31: Retinoic acid signalling is essential at many points during lung development. The schematic shows the multiple stages, critical processes and multiple regulatory factors of lung development. Although this schematic represents the timeline for human lung development, murine lung development occurs in similar stages. Figure taken from ref [186].

Additional pertinent observations regarding similar mutant mouse models include:

- *Gsk3b* mutant mice develop cleft palates [191]. GSK3-β is the kinase responsible for the phosphorylation of the majority of FBXW7 substrates.

- *Jun* deficient mice developed an EOB phenotype due to a decrease in epidermal growth factor (EGFR) signalling [199; 200].

- PGC-1α (Peroxisome proliferator-activated receptor gamma (PPARγ) coactivator 1 alpha) is a substrate of FBXW7. Pparγ contributes to normal lung maturation as conditional disruption of *Pparg* resulted in enlarged airspaces consistent with a deficiency in postnatal lung maturation [207].

3.4.6 Fbxw7 substrates

Although R482Q is predicted to abrogate substrate binding and hence their subsequent ubiquitination and degradation, protein levels of many Fbxw7 substrates remained unaltered between R482Q/+ and wildtype samples. This could partially be explained by the fact that many Fbxw7 substrates are regulated by other E3 ligase complexes. For example, Myc is also regulated by the Skp2 SCF E3 ligase [106] (at a different motif) and Notch is also regulated by the E3 ubiquitin ligase Itch [118]. Stability of Fbxw7 substrates may additionally be regulated in part by deubiquitinating enzymes (e.g USP28) that remove ubiquitin from proteins post-ubiquitination to release them from planned degradation [107].

Fbxw7 appears to target substrates for degradation in a tissue-specific manner. For example, Fbxw7 deficiency in immature T-cells leads to thymic hyperplasia and lymphoma development attributed to the accumulation of c-Myc [153]. The abnormalities in lipid metabolism and cell differentiation seen with liver specific deficiency of Fbxw7 is attributed to the accumulation of Srebp1 [152]. Whereas, in human Wilms' tumours, N-MYC is proposed to be the critical substrate deregulated [208]. Results presented in this chapter have shown that Klf5 and Tgif1 appear the critical Fbxw7 substrates for embryonic lung development and Tgif1 was found to be important in MEFs.

3.4.6.1 Tgif1

Tgif1 knockdown *in vitro* causes disruption of both Tgf-β and retinoic acid pathways [209], both critical for lung development. Tgif1 is a transcriptional repressor that negatively regulates the Tgf-β pathway via several mechanisms. Tgif1 acts as a repressor by recruiting specific repressor complexes to Smad2 to repress Smad2 mediated transcription and by competing with coactivator p300 for Smad interaction. It regulates a number of Tgf-β dependent processes, including transcription, proliferation and

cell migration. Tgf-β signalling is involved in growth inhibition [32], therefore, elevated levels of Tgif1, a Tgf-β signalling repressor, could contribute to the enhanced proliferation rate identified in R482Q/+ lungs.

TGIF1 also regulates retinoid responsive gene expression by interacting directly with ligand binding domain of the RXRα retinoid receptor and by recruiting the corepressor CtBP to RXRα [131; 206].

3.4.6.2 Klf5

Klf5, an Fbxw7 substrate elevated in R482Q/+ mice, has previously been reported to be implicated in lung development. When *Klf5* was conditionally deleted in respiratory epithelial cells, there was inhibition of maturation of the lung during the saccular stage of development [125]. Homozygous *Klf5*-null mice died of respiratory distress immediately after birth and a group of genes known to be involved in Tgf-β signalling were altered in the lungs of these mice, including increased expression of *Tgfb2*. Additionally, in a conditional transgenic model in which *Klf5* is overexpressed in the basal layer of the epidermis, embryonic craniofacial defects have been identified [198]. Partial clefting of the palate and EOB due to lack of eyelid formation have been observed amongst other abnormalities. The authors explained these abnormalities arise as a result of disrupted epithelial-mescenchymal interactions necessary for craniofacial development and attributed them to altered levels of p63.

Klf5 is a zinc finger domain-containing transcription factor that plays roles in Tgf-β, retinoic acid and Protein kinase C (PKC) signalling pathways among others [123]. To date hundreds of genes regulated by Klf5 have been identified, associated with processes including cell cycle regulation, apoptosis, migration, differentiation, angiogenesis and lipid metabolism [124; 125]. KLF5 has many pro-proliferative effects [210; 211] and some of the important target genes are *CCND1*, *CCNB1*, *PDGFA* and *FGFBP1* [123]. Elevated protein levels of Klf5 therefore, may contribute to the

increased proliferation rate in E18.5 R482Q/+ lungs assessed by Ki67 immunohistochemistry.

3.4.7 Heterozygous propellor-tip mutation

Several studies have proposed that *Fbxw7* acts in a haploinsufficient manner in cancers and there is some evidence for this: heterozygous *Fbxw7*-null mutants have a greater susceptibility to radiation-induced tumorigenesis [91] and enhanced intestinal tumorigenesis in an *Apc*-mutant background (although not when *Fbxw7* alone is mutated) [151].

However, in human cancers, the predominance of missense propellor-tip mutations over protein-truncating mutations or other missense mutations argues against simple haploinsufficiency and the data presented here clearly show functional differences between heterozygous null and R482Q alleles. Mutated Fbxw7 protein has also been proposed to act in a dominant negative fashion [1]. Fbxw7 contains a dimerisation domain near the N-terminus and dimers may target specific substrates for degradation. Proteins containing missense mutations or nonsense mutations that leave the dimerisation domain intact are still able to dimerise with wildtype Fbxw7. This reduces the number of active dimers and might be expected to have more detrimental effects than simple haploinsufficiency, comparable to the severe homozygous *Fbxw7*-null phenotype. However, R482Q/+ mice have shown that the R482Q mutant protein does not function as a simple dominant negative. It is therefore possible that this allele results in a level of protein function between that of the heterozygous and homozygous null states. This allele may even differ in some specific way in terms of substrate specificity or, whilst unlikely, gain of activity against non-physiological substrates.

To summarise this chapter, a novel Fbxw7 mouse model with a knock-in R482Q mutation was generated. When this mutation was knocked-in constitutively in all tissues using the *PGK*-Cre transgenic line, heterozygous mice died perinatally due

to a defect in lung development and in some cases showed cleft palate and eyelid fusion defects. In contrast, whilst *Fbxw7*$^{\Delta/+}$ mice were viable, developed normally and showed no signs of epithelial developmental defects, *Fbxw7*$^{\Delta/\Delta}$ mice exhibited vascular problems causing lethality at E10.5-E11.5. Known Fbxw7 substrates were screened for signs of protein accumulation (deregulated degradation) in R482Q/+ embryonic lungs and Tgif1 and Klf5 proteins were found to be increased. It can be concluded that *Fbxw7* R482Q alleles are not functionally equivalent to heterozygous or homozygous *Fbxw7*-null alleles.

Chapter 4

Investigation of an intestinal-specific *Fbxw7* propellor-tip mutation

4.1 Introduction

4.1.1 Role of *FBXW7* in cancers of diverse tissue type

FBXW7 mutations are found in cancers of diverse origin with the highest frequencies occurring in the bile duct, blood, endometrium, stomach and colorectrum [1]. The most critical FBXW7 substrates vary in a tissue-specific manner, for example Nicd1 and c-Jun in mouse embryonic fibroblasts [91; 154] and c-Jun in haematopoietic stem cells [155] (section 1.3.10). However, three isoforms of FBXW7 exist and their abundance also varies in different tissues, with *Fbxw7*β mRNA restricted to the brain and testis and *Fbxw7*γ mRNA restricted to the heart and skeletal muscle [60]. A critical question, for which an answer will require accumulated evidence, is whether mutations affect a common set of critical targets in each tumour type.

Mice with a constitutively expressed *Fbxw7*-null allele resulted in embryonic lethal-

ity [171; 172]; therefore conditional knockout systems have been employed to study the role of Fbxw7 protein in a tissue-specific manner. As *FBXW7* mutations are abundant in T-cell acute lymphoblastic leukaemias, one focus of study has been investigating the role of null *FBXW7* in the haematopoietic system. Fbxw7 has been identified as an essential protein in maintenance of the haematopoietic stem cell compartment [155; 173]. Conditional *Fbxw7* knockout in the thymus led to the formation of lymphoma in approximately half of the mice studied [153], with c-Myc accumulation leading to significantly increased proliferation rates. Matsuoka *et al* [173] reported that with the additional loss of p53, mice developed lymphomas with increased penetrance and reduced latency.

Fbxw7-null alleles have also been studied conditionally in the liver, whereby liver cell differentiation was altered and increased triglycerides deposits on the liver were observed as well as the development of hamartomas [152]. Onoyama *et al* [152] reported Notch1 and Srebp1 as the critical substrates involved in the development of these phenotypes.

Several studies have recently reported on conditional *Fbxw7* deficiency in the brain [149; 150]. Hoeck and co-workers have identified impaired stell cell development and increased progenitor cell death in embryonic development, attributed to deregulated c-Jun and Notch [149]. Conditional *Fbxw7*-null in the cerebellum decreased cerebellular size and abundance of Purkinje cells and again c-Jun and Notch were reported as the most critical substrates [150].

4.1.2 Role of Fbxw7 in intestinal tissue

As discussed in section 1.3.5.2, *FBXW7* mutations are found in approximately 10% of cases of CRC [18; 19; 20]. The most commonly occurring mutations are arginine missense mutations found at propellor-tips in the WD40 domain. It has also been reported that low levels of *FBXW7* mRNA expression in CRC were associated with

poor prognosis [212]. In this study Iwatsuki *et al* found elevated protein levels of c-Myc and cyclin E in tumour tissue from cases with low *FBXW7* expression. In 65% of CRCs in which low *FBXW7* mRNA expression was detected, no copy number change in *FBXW7* was observed by aCGH.

Two studies have focused on conditional *Fbxw7*-null in the mouse gut [151; 188], showing that Fbxw7 controls the differentiation and proliferation of both intestinal progenitor cells and tumour cells. In the work of Sancho *et al* [151], *Fbxw7* exon 5, encoding the critical F-box domain, was deleted conditionally in the gut, thus disrupting the Fbxw7 ORF and preventing production of detectable protein. This study showed that wildtype *Fbxw7* mRNA was highly expressed in the transit-amplifying progenitor cell compartment, with a 3-fold increase in *Fbxw7* mRNA in the crypt compared to the villus [151]. Homozygous *Fbxw7*-null resulted in impaired intestinal cell differentiation with a reduction in the number of goblet and Paneth cells present. There was an accumulation in protein levels of intracellular domain of Notch1 (Nicd1) and phosphorylated c-Jun in normal intestinal tissue. Heterozygous *Fbxw7*-null resulted in an accumulation of Nicd1 but not p-c-Jun. Notch is a key regulator in the binary decision of transit-amplifying cells to differentiate into secretory or absorptive cells and therefore elevated Nicd1 protein levels in *Fbxw7*-null cells were reported as the likely cause of the differentiation phenotype observed. *Fbxw7* has thus been reported to be a critical regulator in secretory fate decisions in the gut. Despite the accumulation of actively proliferating progenitor cells in the guts of homozygous null allele mice, no intestinal tumours were reported up to 11 months of age (n=15).

Another group (Babaei *et al*) has studied the same conditional *Fbxw7*-null mouse model and observed a small number of adenomas in the colons of $Fbxw7^{\Delta/\Delta}$ mice at 9-10 months of age [188]. Increased crypt budding and fission but no polyps were observed in the small intestine. This study additionally found *DEK*, a phospho-proto-oncogene, to be elevated in *Fbxw7*-null/Apc^{Min} compound tumours, leading to

increased cell division and altered splicing of tropomyosin RNA. Although the studies were conducted in different laboratories, both used the same *Fbxw7*-null model and method of Cre-mediated recombination and the mice were also maintained on the same genetic background. Inconsistencies between the occurrences of polyps between these two studies have not been explained.

To date, no *in vivo* studies to investigate the common propellor tip *FBXW7* mutations, as opposed to *FBXW7*-null alleles, have been conducted despite the fact that, as previously discussed, mutations that result in absence of FBXW7 protein occur infrequently in CRC.

4.1.3 Aims of chapter

The aims of the work in this chapter included:

- Generation of conditional (gut-specific) R482Q knock-in mice by breeding R482Qfl/+ (refer to Appendix A.1 for nomenclature) mice with *Vil1*-Cre mice
- Evaluation of any phenotypes that arose
- Comparison of R482Q (*Vil1*-Cre$^+$) mice with *Fbxw7*-null (*Vil1*-Cre$^+$) mice

4.2 Results

4.2.1 Generation of conditional R482Q knock-in mice

The targeting construct described in Chapter 3 (Figure 3.3) was also used to generate conditional R482Q floxed mice. It has previously been reported that targeting alleles which retain selectable markers can alter gene expression [213], therefore the neomycin selection cassette needed to be removed in all tissues. To this end, ES cells expanded from a clone in which homologous recombination had occurred (section

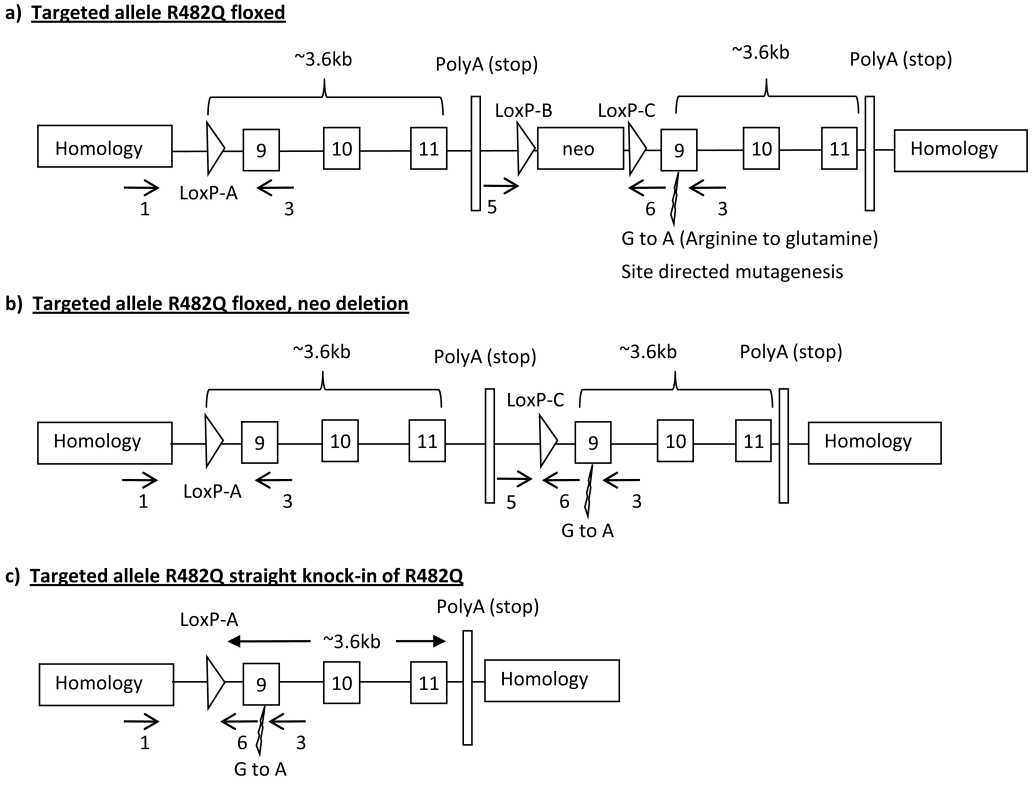


Figure 4.1: *Fbxw7* targeting construct showing Cre-mediated neomycin cassette deletion and recombined alleles. a) Schematic diagram of Fbxw7 targeted allele; regions of homology, LoxP sites, *Fbxw7* exon 9-11, a neomycin selection cassette and repeated exon 9-11 in which a mutation in exon 9 has been introduced by site-directed mutagenesis are highlighted. b) Scheme representing the allele after Cre-mediated removal of the neomycin cassette. c) Scheme representing the straight knockin R482Q targeted allele. The arrows with corresponding numbers depict the position and direction of the primers used to genotype R482Q ES clones and subsequently R482Q mice.

3.3.1), were further electroporated with the Cre-recombinase expressing pMC1-Cre plasmid. These ES clones were screened to identify removal of the neomycin cassette using a PCR-based screening method. The primers used are detailed in Table 2.1, with their positions within the targeting construct highlighted in Figure 4.1. In brief, primer set 1 and 3, with the forward primer designed in the intronic region upstream of exon 9 and the reverse primer in exon 9, amplified a PCR product of 433 bp in the targeting allele and 322 bp in the wildtype allele. The difference in size between these alleles accounts for the additional LoxP and plasmid sequence in the targeted allele. Primer set 5 and 6 identified removal of the neomycin cassette; in clones where

this had occurred the PCR product amplified was 135 bp and when the neomycin cassette was not removed no PCR product was detected. Forty eight colonies were analysed and as shown in Figure 4.2, Cre-mediated deletion of the neomycin cassette occurred in one of these colonies (A). Recombination between LoxP A and C, excising endogenous exons 9-11 as well as the neomycin cassette was a more common event and occurred in five clones (C-F). PCR screening with primers 1 and 3 amplified only the wildtype allele in clone B (Figure 4.2); only 30 out of the 48 clones screened had the targeted allele. This highlighted that the original expanded ES clone must have been a mixed clone. Colony A was selected for subsequent introduction into mouse blastocysts to generate a chimera. Germline transmission occurred and the offspring were continuously back-crossed onto a C57Bl/6J genetic background for at least six generations prior to mice being used for experiments.

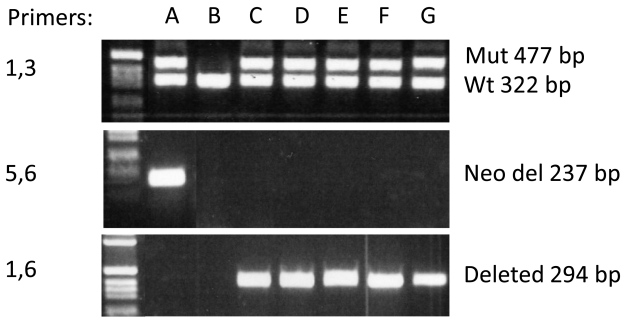


Figure 4.2: Removal of neomycin cassette in an ES cell clone. ES cells were screened by PCR-analysis using primers detailed in Table 2.1. Primer set 1 and 3 identified wildtype and floxed alleles, primer set 5 and 6 identified removal of neomycin cassette (clone A) and primer set 1 and 6 identified Cre-mediated deletion removing both the non-mutated exons 9-11 and the neomycin cassette (clones C-F).

4.2.2 Characterisation of tissue-specific recombination mediated by *Vil1*-Cre crosses

In order to ascertain whether R482Q could induce intestinal tumorigenesis I wished to breed R482Qfl/+ (neo^{-}) mice (hereafter refered to as R482Qfl/+) with a gut-specific

Cre. There are several Cre recombinase-expressing mouse transgenic strains available to induce recombination in the intestine [214; 215; 216; 217]. Here, R482Qfl/+ mice were crossed with the *Vil1*-Cre model [216]. In this model, Cre recombinase is expressed under the control of a 9-kb regulatory region of the murine *Villin* (*Vil1*) gene [216]. Villin, an actin bundling cytoskeletal protein, is broadly expressed in every cell of the intestinal epithelium on the vertical (crypt to villus) and the horizontal axis (duodenum to colon) [218]. *Vil1*-Cre stocks were also maintained on a C57Bl/6J background. After breeding R482Qfl/+ and *Vil1*-Cre mice, subsequent interbreeding of offspring was carried out to obtain R482Q/+, R482Q/R482Q and wildtype littermates.

In order to confirm efficient recombination specifically in the intestines of R482Q mice, a range of tissues were collected from mature (6-weeks old) R482Q/+ and R482Qfl/+ mice. DNA was extracted from the proximal (SB1), middle (SB2) and distal (SB3) small intestine, colon, kidney, liver, lung and tail. Recombination was assessed using a PCR-based method as described for identifying recombination in ES colonies exposed to pCM1-Cre *in vitro* (section 4.2.1). Primer positions are highlighted on the schematic of the R482Q targeting construct in Figure 4.1.

As shown in Figure 4.3a, primer pair 1 and 3 amplified both the wildtype and targeted PCR product in all tissues analysed in R482Qfl/+ and R482Q/+ mice. Primer pair 1 and 6 shows Cre deletion of the repeated section of exons 9 - 11 (section 3.3) and thus knock-in of R482Q mutation in intestinal tissue from SB1 through to the colon in R482Q/+ but not R482Qfl/+ mice, as expected. As 20 ng of DNA from each tissue were used in PCR amplification, the strength of the PCR product observed was semi-quantitative. A band of lower intensity suggesting a lower level of recombination was also observed in the kidney (as previously reported [216]) and the lung. As expected, there was no recombination observed in liver, tail or ear tissue.

In R482Q/R482Q mice recombination also occurred in intestinal tissue (SB3) but

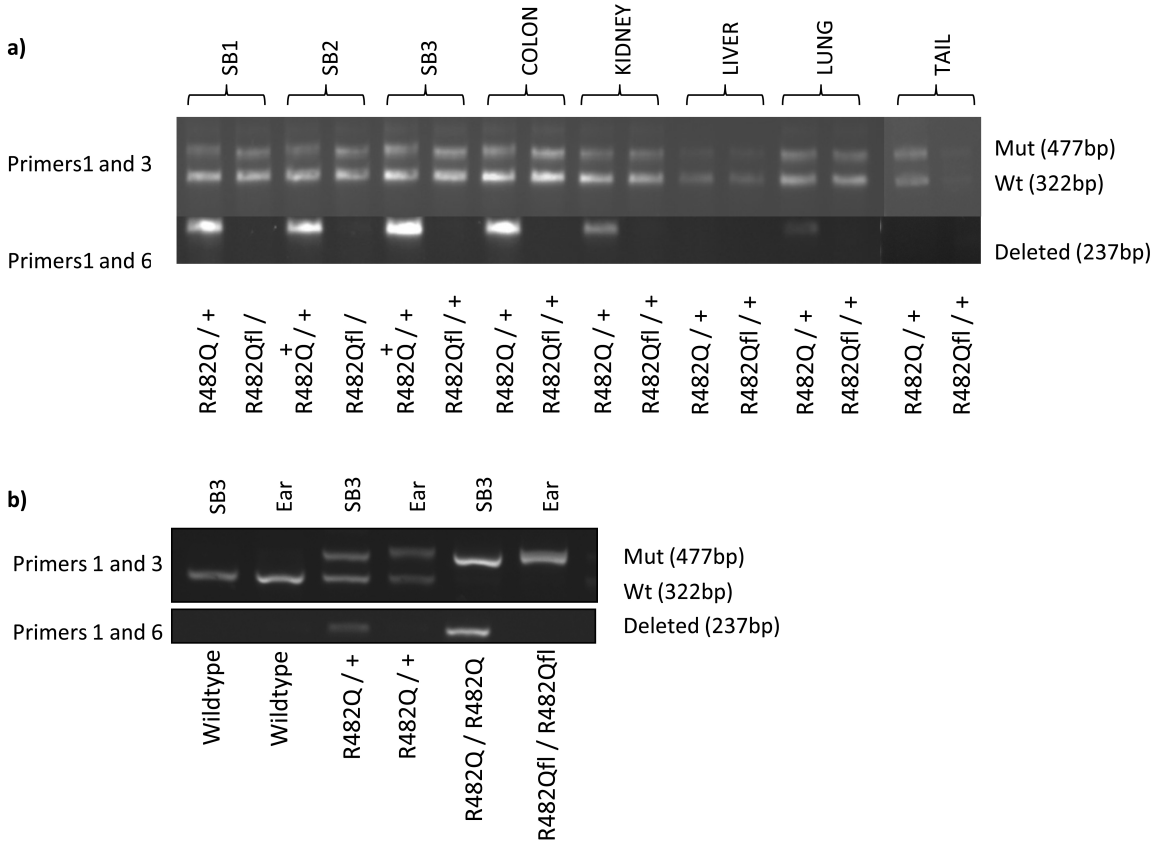


Figure 4.3: Tissue-specific knock-in of R482Q mutation mediated by *Vil1*-Cre recombination. DNA extracted from mature mice at 6-weeks old. PCR products were amplified using primers shown in Table 2.1. Primer pair 1 and 3 showed presence of the R482Q floxed allele whereas primer pair 1 and 6 highlighted Cre-mediated knock-in of the R482Q mutation. The positions of these primers are highlighted in Figure 4.1. 20 ng of DNA were used to amplify PCR products from a range of tissues. a) Recombination in R482Q/+ (*Vil1*-Cre^{+}) and R482Qfl/+ (*Vil1*-Cre^{-}) mice. b) Recombination from wildtype and R482Q/R482Q (*Vil1*-Cre^{+}) mice.

not in tissue taken from an ear biopsy (Figure 4.3b).

4.2.3 Tissue-specific recombination of *Fbxw7*-null allele mediated by *Vil1*-Cre crosses

Fbxw7 (floxed exon 5) mice described in section 4.1.2 were supplied by Professor Axel Behrens (Cancer Research UK, London Research Institute) and were used as a comparison to R482Q mice. The nomenclature used for this mouse strain is summarised

in Appendix A.1. $Fbxw7^{fl/+}$ had been maintained on C57Bl/6J background for 6+ generations and I continued to maintain stocks on this genetic background. Genotyping PCRs on this strain were performed as described by Sancho *et al* [151], with primer sequences shown in Table 2.1.

Previous reports have shown efficient *Vil1*-Cre mediated recombination, but no tumour formation in homozygous *Fbxw7*-null mice up to 11 months old [151]. In order to confirm efficient recombination using the available *Vil1*-Cre stock, $Fbxw7^{fl/+}$ and $Fbxw7^{fl/fl}$ were crossed with *Vil1*-Cre mice and intestines from mature wildtype, $Fbxw7^{\Delta/+}$ and $Fbxw7^{\Delta/\Delta}$ mice were collected for analysis. Figure 4.4 shows PCR products of the expected sizes were amplified using the primers detailed in Table 2.1; primer set 'Fbxw7 null' forward and reverse primer amplified products of 394 bp and 287 bp identifying floxed and wildtype alleles respectively. Primer set 'Fbxw7 null' forward and 'Fbxw7 Δ' reverse amplified PCR products of 744 bp when Cre-mediated deletion of floxed exon 5 had occurred. Figure 4.4 shows the amplified PCR product identifying Cre-mediated deletion in intestinal tissue from SB1 through to the colon in both $Fbxw7^{\Delta/+}$ and $Fbxw7^{\Delta/\Delta}$ mice, as expected, but not in wildtype mice. No recombination was observed in tail tissue from these mice as expected.

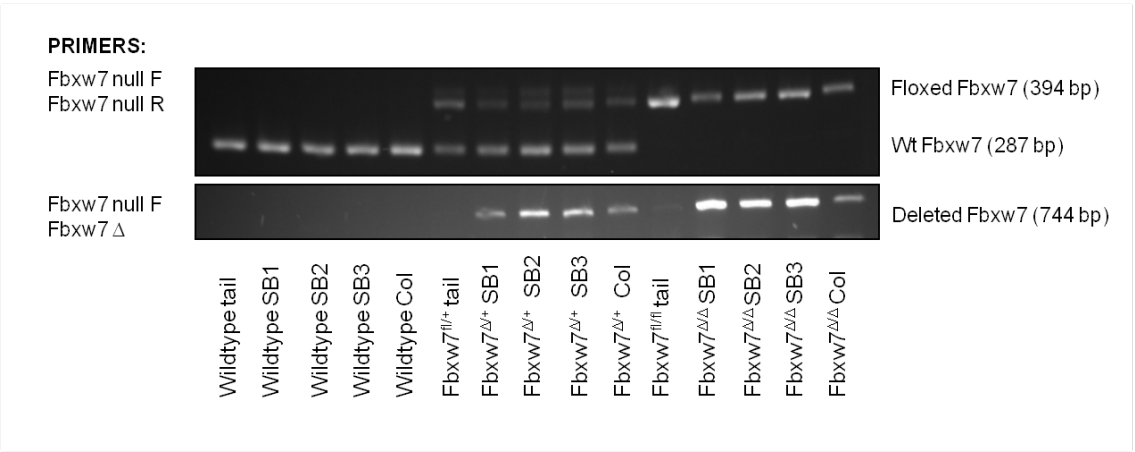


Figure 4.4: Intestinal recombination in $Fbxw7^{\Delta/+}$ and $Fbxw7^{\Delta/\Delta}$ mice mediated by *Vil1*-Cre crosses. Deletion of the floxed exon 5 occurred in all intestinal tissue from SB1 through to the colon, but not in tail tissue. 20 ng of DNA were used for PCR amplifications using primers shown in Table 2.1.

4.2.4 Gross morphological analysis of R482Q mice

A cohort of R482Q mice was sacrified when mice reached maturity at 6-weeks old and intestinal tissue was collected. At least three mice of each genotype group (R482Q/+, R482Q/R482Q and wildtype) were analysed and at this time point all mice were asymptomatic. Intestines were assessed for presence of gross intestinal abnormalities using a dissection microscope and no polyps were observed in R482Q/+, R482Q/R482Q or wildtype mice at this age.

Mice were aged and monitored for signs of intestinal phenotype, including anaemia (white feet), hunching and inactive behaviour. No polyps were detected in a cohort of R482Q/+ mice aged 100-215 days (n=8) and R482Q mice appeared asymptomatic up to one year of age. A R482Q/+ mouse showed signs of distress and thus was sacrificed and a gut sample collected at 409 days old. Upon analysis it was observed that this mouse exhibited a large small intestinal polyp (Figure 4.5a/b). Upon further histological analysis this polyp was found to be an invasive adenocarcinoma, as shown in H and E stained sections in Figure 4.5d/e, there was invasion into the muscle layer indicating this was an advanced stage polyp.

In order to determine the incidence of polyps in R482Q/+ mice, a cohort of mice were aged at least to 300 days old and gut preparations analysed. Twenty-nine percent (n=12/41) of R482Q/+ mice exhibited a low number (1-3) of small intestinal polyps (Table 4.1). Ages of asymptomatic aged mice are shown in Appendix D.1. Table 4.1 shows polyps were evenly distributed throughout the small intestine, with polyps detected in SB1, SB2 and SB3. Sixty seven percent (n=18, from 12 mice) of polyps were greater than 3 mm in diameter.

Wildtype mice of a similiar age did not show any intestinal phenotype (n=10). Comparison of polyp number in R482Q/+ and wildtype is not formally significant (p=0.092, Fisher's exact test), due to the low number of wildtype samples. A small number of R482Q/R482Q mice are currently aging, to date none have been analysed.

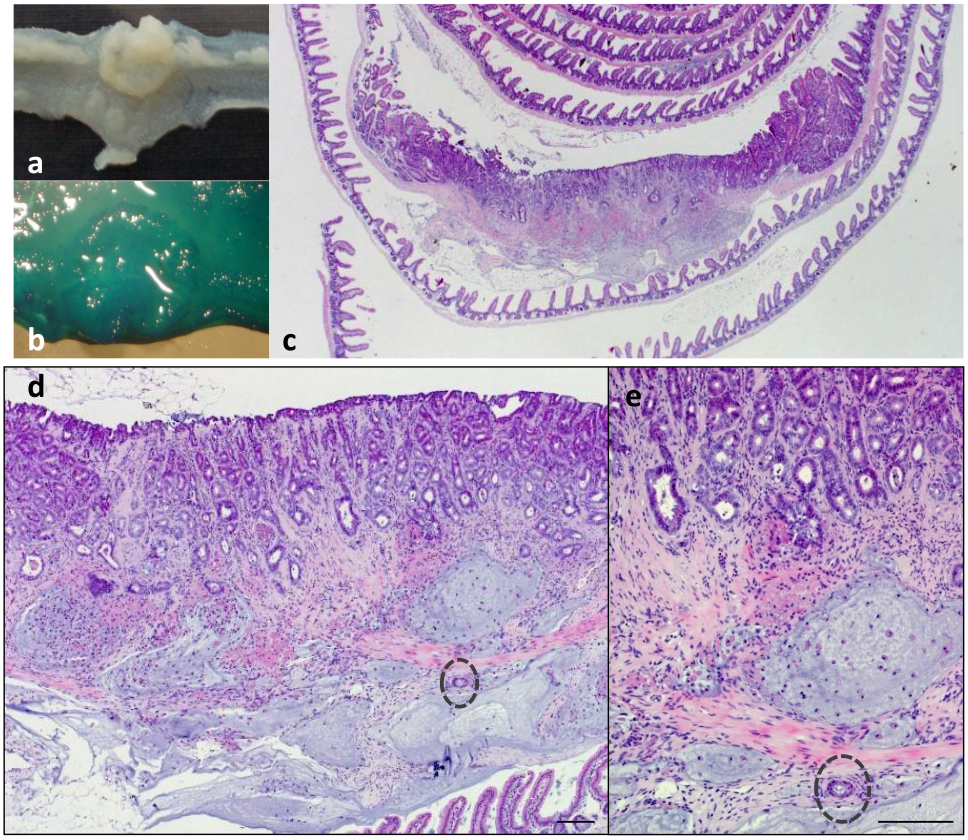


Figure 4.5: Invasive adenocarcinoma in the small intestine of a R482Q/+ mouse. a) Gross appearance of tumour, b) Methylene blue stained tumour, c-e) H and E stained sections of tumour showing invasion into the muscle layer (dotted circle). Scale bars represent 150 μm.

Mouse	Age (days)	No of Polyps	Polyp Location	Size
1	409	1	SB3	3 mm+
2	453	1	SB3	3 mm+
3	453	3	SB3	1-2 mm, 3 mm+, 3 mm+
4	488	2	SB1	3 mm+, 3 mm+
5	488	1	SB3	2-3 mm
6	383	1	SB2	3 mm+
7	383	1	SB2	1-2 mm
8	359	1	SB2	3 mm+
9	383	1	SB1	3 mm+
10	376	1	SB2	2-3 mm
11	378	3	SB1	1-2 mm, 1-2 mm, 3 mm+
12	394	2	SB1	3 mm+, 3 mm+

Table 4.1: Summary table of R482Q/+ mice with intestinal polyps. Twelve R482Q/+ mice showed intestinal polyps out of 41 mice analysed. Age, intestinal location and size of polyps are shown.

Apart from the tumour shown in Figure 4.5, histological analysis on all other polyps showed them to be non-invasive, H and E stained sections on four of these tumours are shown in Figure 4.6.

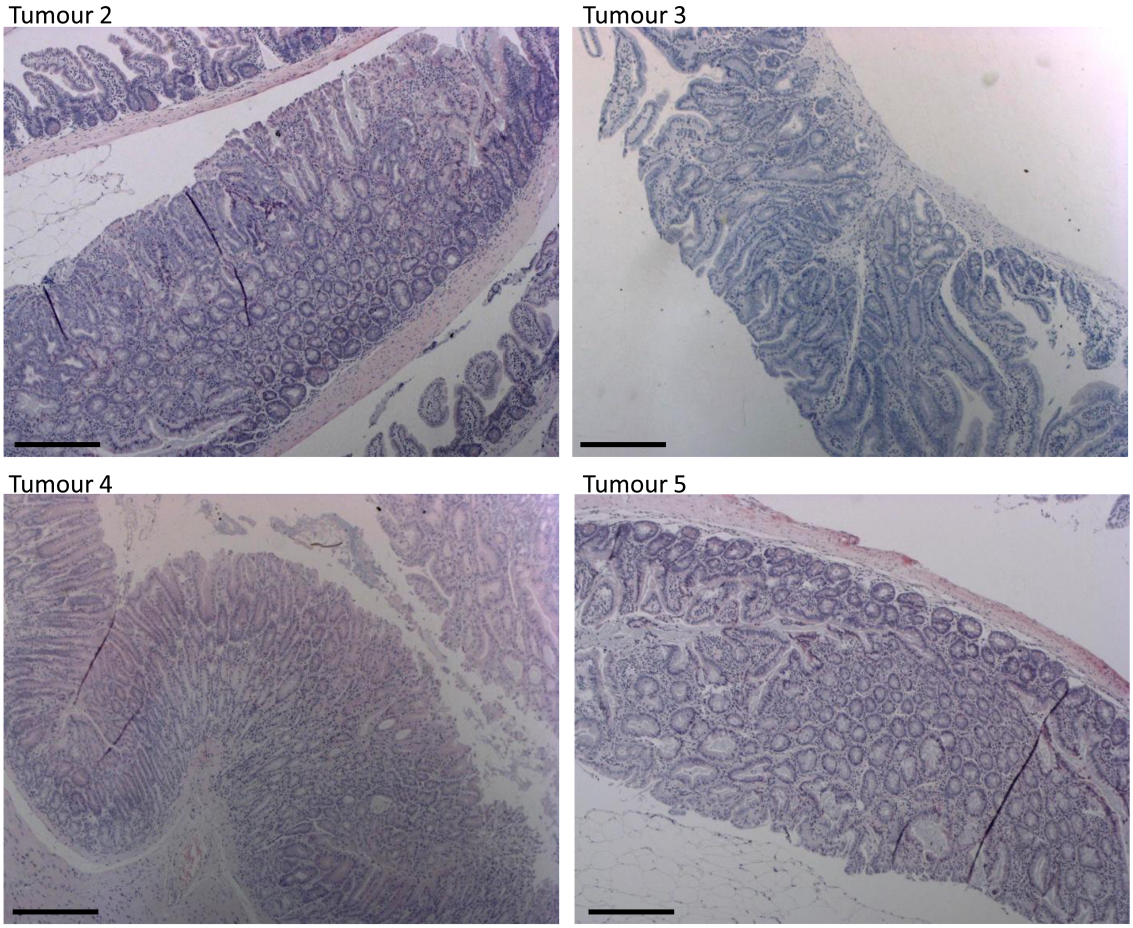


Figure 4.6: Non-invasive polyps in small intestine of a R482Q/+ mice. H and E stained sections, scale bars represent 300 μm.

4.2.4.1 Intestinal polyp analysis on *Fbxw7*-null mice

$Fbxw7^{\Delta/\Delta}$, $Fbxw7^{\Delta/+}$ and wildtype littermates (at least three of each genotype) were also collected at 6-weeks old, with no gross abnormalities in the intestines observed.

A cohort of 13 $Fbxw7^{\Delta/+}$ mice aged over 300 days were analysed. Fifteen percent (n=2/13) displayed an intestinal tumour, at 310 and 400 days of age. Both polyps were greater than 3 mm in diameter, located in SB2 and SB3 and were non-invasive.

Ages of asymptomatic aged mice are shown in Appendix D.1. There was no significant difference in the incidence of polyps between R482Q/+ and $Fbxw7^{\Delta/+}$ mice (linear regression, p=0.377, OR: 1.94, 95% confidence intervals 0.44 - 8.5). To date, no $Fbxw7^{\Delta/\Delta}$ mice have been analysed.

4.2.5 Molecular analysis of *Fbxw7* mutant mice

4.2.5.1 Intestinal cell lineage analysis in morphologically normal *Fbxw7* mutant mice

To ascertain whether all differentiated intestinal cell types were present in normal intestinal tissue from *Fbxw7* mutant mice, immunohistochemistry analysis was conducted for a range of markers of intestinal cell lineage on morphologically normal samples collected from mature 6-weeks old mice (at least three mice for each genotype group), for quantification parameters see section 2.5.1.1. Figure 4.7 shows alcian blue and fast acid red staining (section 2.2.4.2) used to identify goblet cells, the average number of goblets cells per villus varied subtly from 7 to 10 positive cells across all genotypes assessed (Figure 4.8). By grouping all *Fbxw7* mutant mice (R482Q/+, R482Q/R482Q, $Fbxw7^{\Delta/+}$, $Fbxw7^{\Delta/\Delta}$) together to compare them to wildtype mice, there was a significant decrease in the number of goblet cells (p=0.030, Wilcoxon rank test). Individual genotype analysis compared to wildtype were as follows (Wilcoxon rank test): R482Q/R482Q p=0.049; R482Q/+ p=0.130; $Fbxw7^{\Delta/\Delta}$ p=0.279; and $Fbxw7^{\Delta/+}$ p=0.049. Therefore, there was no significant decrease in goblet cells in $Fbxw7^{\Delta/\Delta}$ and R482Q/+ mice compared to wildtype.

Chromogranin-A immunohistochemistry was used to stain enteroendocrine cells (Figure 4.7). By grouping all *Fbxw7* mutant mice, there was not a significant difference in the number of enteroendocrine cells compared with wildtype mice (p=0.190, Wilcoxon rank test). There was a trend towards an increased number of enderoendrocine cells in R482Q/+ (p=0.091) and R482Q/R482Q (p=0.025) mice (Wilcoxon

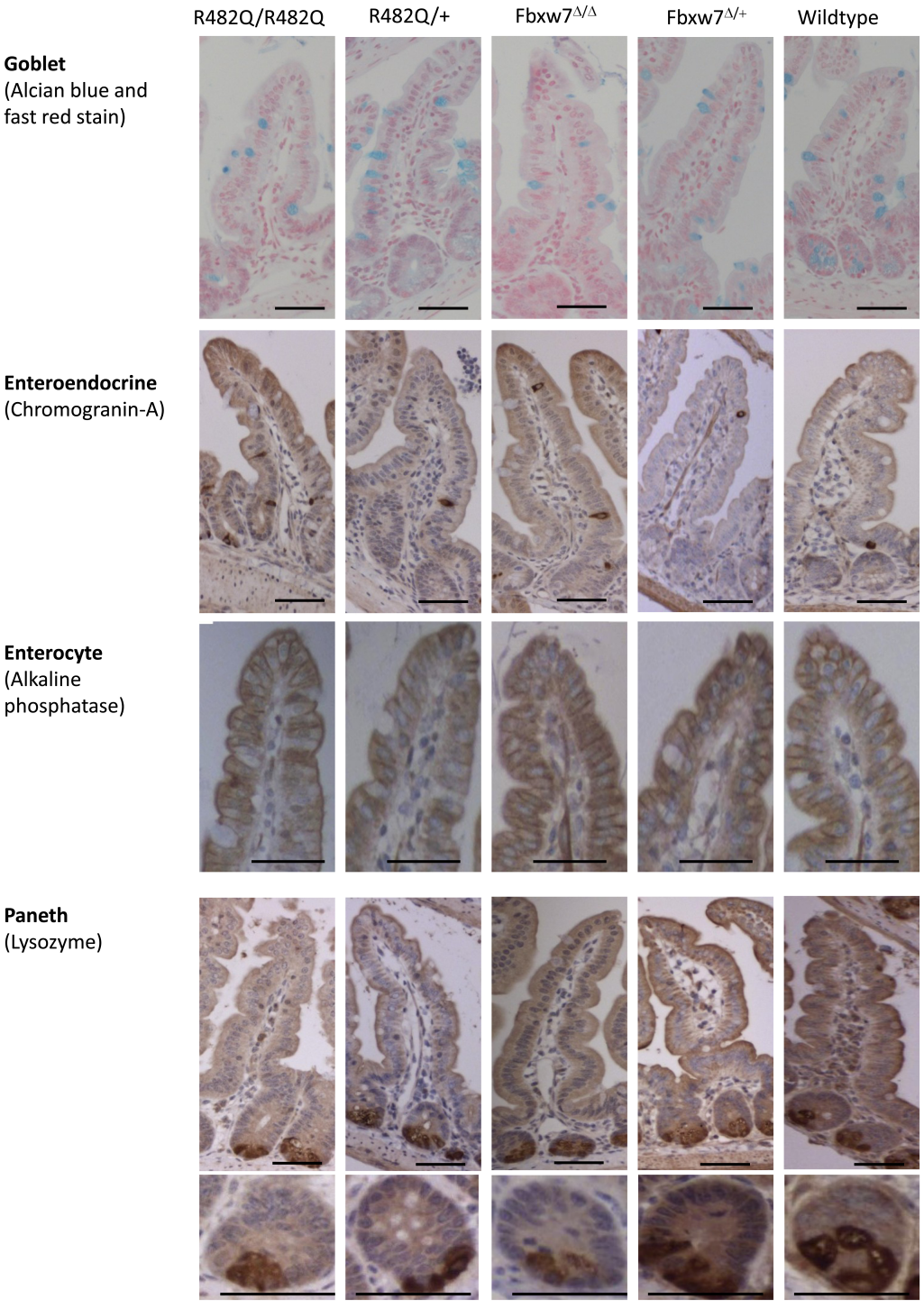


Figure 4.7: Differentiated cell types in the intestines of *Fbxw7* mutant and wildtype 6-weeks old mice. Alcian blue and fast red staining identified goblet cells. Immunohistochemistry identified enteroendocrine (Chromogranin-A), enterocytes (alkaline phosphatase) and Paneth (lysozyme) cells. Scale bars represent 50 μm. Details of antibodies used are shown in Table 2.5.

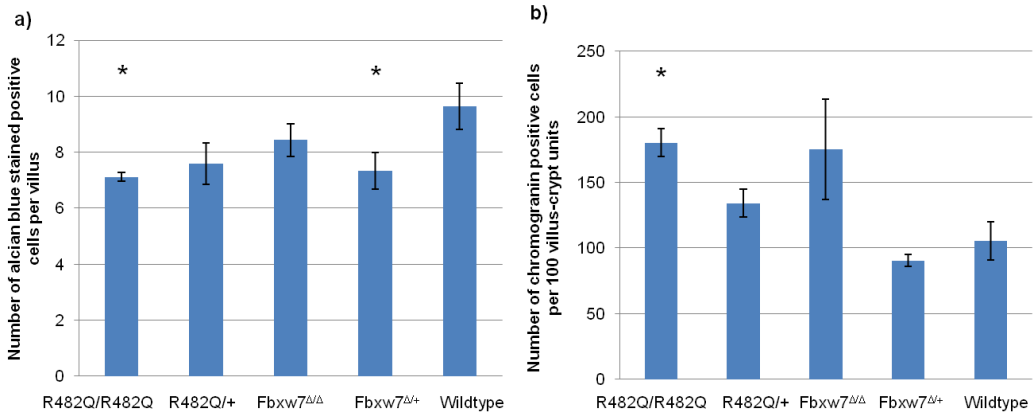


Figure 4.8: Quantification of goblet and enteroendocrine cells in the small intestine of *Fbxw7* mutant and wildtype 6-weeks old mice. a) The average number of goblet (alcian blue stained positive) cells per villus has been quantified by counting 100 villi from SB3 in at least 3 mice of each genotype. p=0.049 in R482Q/R482Q and p=0.049 in $Fbxw7^{\Delta/+}$, p>0.05 in all other cases (Wilcoxon rank test). b) Enteroendocrine cells have been quantified by counting number of Chromogranin-A positive cells in SB3 in 100 villus-crypt units in at least 3 mice of each genotype. p=0.025 for R482Q/R482Q mice, p>0.05 for all other cases (Wilcoxon rank test).

rank test). Though not statistically significant, there was an elevation of enteroendocrine cells in $Fbxw7^{\Delta/\Delta}$ mice (p=0.178) and a slight decrease in $Fbxw7^{\Delta/+}$ (p=0.220) mice in comparison to wildtype (Wilcoxon rank test).

There were no gross differences in the abundance and distribution of enterocytes (alkaline phosphatase stained) and Paneth (lysozyme stained) cells (Figure 4.7). Intense staining of Paneth cells precluded accurate quantification despite optimisation of antibody concentration and immunoperoxidase staining. However, Paneth cells were present in the expected location in the crypt and there was no obvious differences in the number of positive cells per crypts of different genotypes.

4.2.5.2 Proliferation and apoptosis in morphologically normal tissue in *Fbxw7* mutant mice

As many of Fbxw7 substrates are critical proteins in the control of cell-cycle, proliferation and apoptosis, these processes were assessed in morphologically normal intestinal tissue from at least three mice for each genotype group. Proliferation was assessed by

Ki67 immunohistochemistry (Figure 4.9a). The percentage of Ki67 positive cells per crypt was quantified (section 2.5.1.1) and no differences in proliferation were observed in any of the Fbxw7 mutant genotypes in comparison to the wildtype control (Figure 4.9b, p>0.05, Student t-test in all cases).

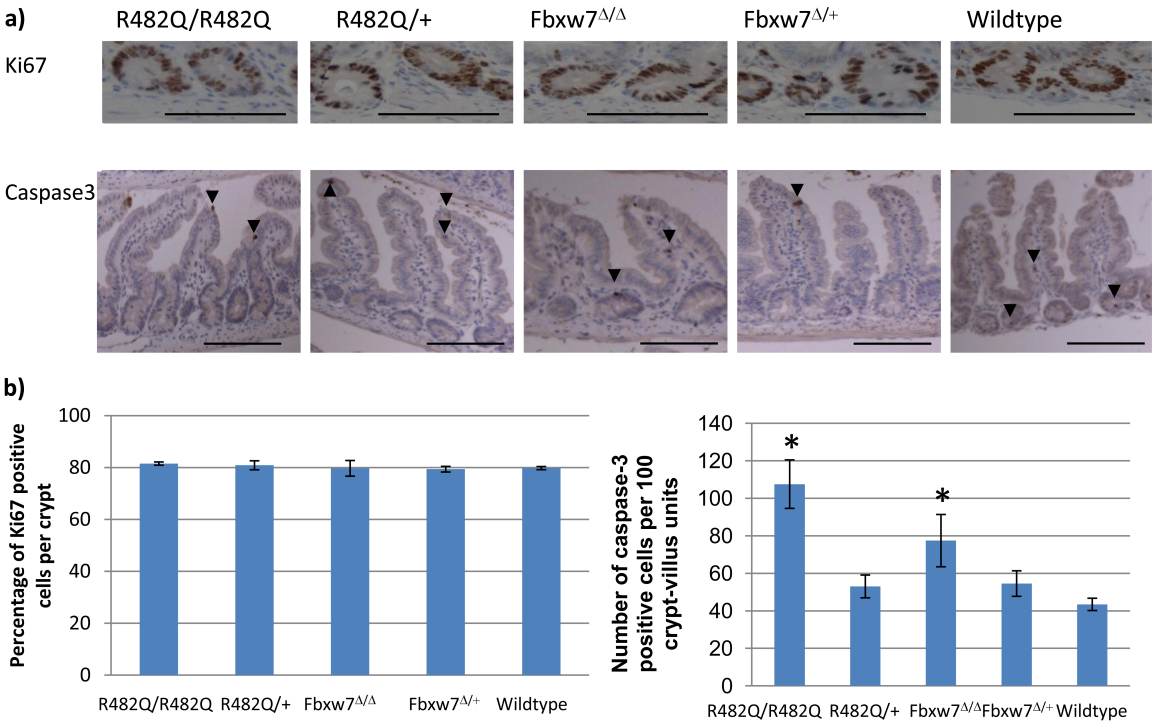


Figure 4.9: Proliferation and apoptosis analysis in *Fbxw7* mutant and wildtype 6-weeks old intestines, assessed by Ki67 and Caspase3 immunohistochemistry respectively. a) Scale bars represent 150 μm. Antibody details shown in Table 2.5. Arrowheads indicate Caspase3 positive cells. b) The percentage of Ki67 positive cells per crypt was assessed in 200 crypts in SB3, for at least 3 mice for each genotype (p>0.05 in all cases, Student t-test). The number of positive Caspase3 cells per crypt-villus unit in SB1, SB2 and SB3 in 100 crypt-villus units were assessed in at least 3 mice of each genotype. (p=0.0001 for R482Q/R482Q mice and p=0.014 for $Fbxw7^{\Delta/\Delta}$ mice, Wilcoxon rank test). Error bars represent the SEM.

Apoptosis was assessed by Caspase3 immunohistochemistry (Figure 4.9), for quantification see section 2.5.1.1). There was a significant increase in apoptosis in both R482Q/R482Q and $Fbxw7^{\Delta/\Delta}$ mice (p=0.0001 and p=0.014 respectively, Wilcoxon rank test) whilst R482Q/+ and $Fbxw7^{\Delta/+}$ mice showed elevated apoptosis, these results were not statistically significant (p>0.05, Wilcoxon rank test).

4.2.6 Molecular analysis of R482Q/+ tumours

In tumours loss of heterozygosity (LOH), with loss of the remaining wildtype allele of a tumour suppressor gene, is a common event, although not often observed in *FBXW7* mutations [19]. LOH of *Fbxw7* was investigated in R482Q/+ tumours (n=4). PCR amplification of wildtype and R482Q alleles from tumour and matched normal DNA from R482Q/+ mice showed bands of equivalent intensity indicating that LOH had not occurred (Figure 4.10a). Figure 4.10b also shows confirmation of the presence of both wildtype and R482Q alleles (base pair position 1445) by sequencing.

In order to test for chromosomal deletions or gains, array comparative genomic hybridisation (aCGH) was carried out on DNA extracted from the paraffin-embedded R482Q/+ invasive adenocarcinoma (section 2.3.8). No copy number variations were identified.

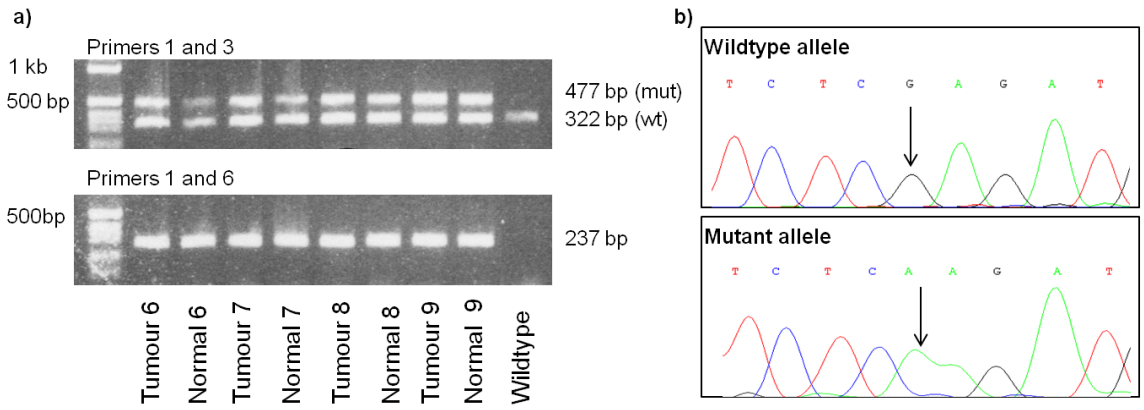


Figure 4.10: No loss of heterozygosity was observed in R482Q/+ tumours. a) PCR detection of both wildtype and R482Q mutant alleles (primers 1 and 3) in both tumour and normal samples at the same intensity indicating no LOH. Primer pair 1 and 6 confirm knock-in of R482Q mutation in tumour samples. Tumour and corresponding normal tissue were analysed using 20 ng of DNA in the PCR reaction. b) Chromatograms of Fbxw7 wildtype and R482Q allele, using primers detailed in Table 2.1.

4.2.6.1 Assessment of Wnt signalling pathway

The late age of onset of tumorigenesis in R482Q/+ mice and the incomplete penetrance of the phenotype suggested that accumulation of additional mutations was necessary for tumorigenesis. In colorectal tumorigenesis, deregulated Wnt signalling resultant from *APC* mutation typically occurs as an early event. In order to assess the Wnt signalling pathway, I investigated localisation of β-catenin protein by immunohistochemistry. As shown in Figure 1.3, in the absence of a Wnt signal, β-catenin is usually associated with membrane bound E-cadherin and the level of free intracellular β-catenin is minimised by targeting it for proteasomal degradation. Figure 4.11 shows Ki67 and β-catenin immunohistochemistry in R482Q/+ tumours. Cytoplasmic and a low level of nuclear staining of β-catenin were observed suggesting deregulation of the Wnt signalling pathway.

To determine if there was a genetic cause for activation of the Wnt-signalling pathway, primers were designed to amplify mutational hotspots of both *Apc* (exon 15) [219] and *Ctnnb1* (exon 2). For *Ctnnb1*, primers were designed in the intronic regions to allow amplification of the full sequence of exon 2. For *Apc*, primer pairs were designed to amplify approximately 300-400 bp overlapping regions (primer sequences are shown in Appendix B.2). Tumour tissue was microdissected by laser-capture microscopy prior to DNA extraction (section 2.2.4) to avoid contamination by normal tissue. No *Apc* mutations were found in the R482Q/+ tumours analysed (n=11). Sequencing analysis focused on the mutation cluster region of *Apc* so it is possible that mutations occurred outside of the regions sequenced.

Figure 4.12 shows that the same missense *Ctnnb1* (C122T) mutation resulting in T41I mutant protein was identified in two R482Q/+ tumours from two different mice. Corresponding normal intestinal tissue from these mice was also analysed and was mutation free. This mutation has previously been reported (in humans) and shown to mutate a Gsk-3β phosphorylation site. Mutant β-catenin protein therefore may

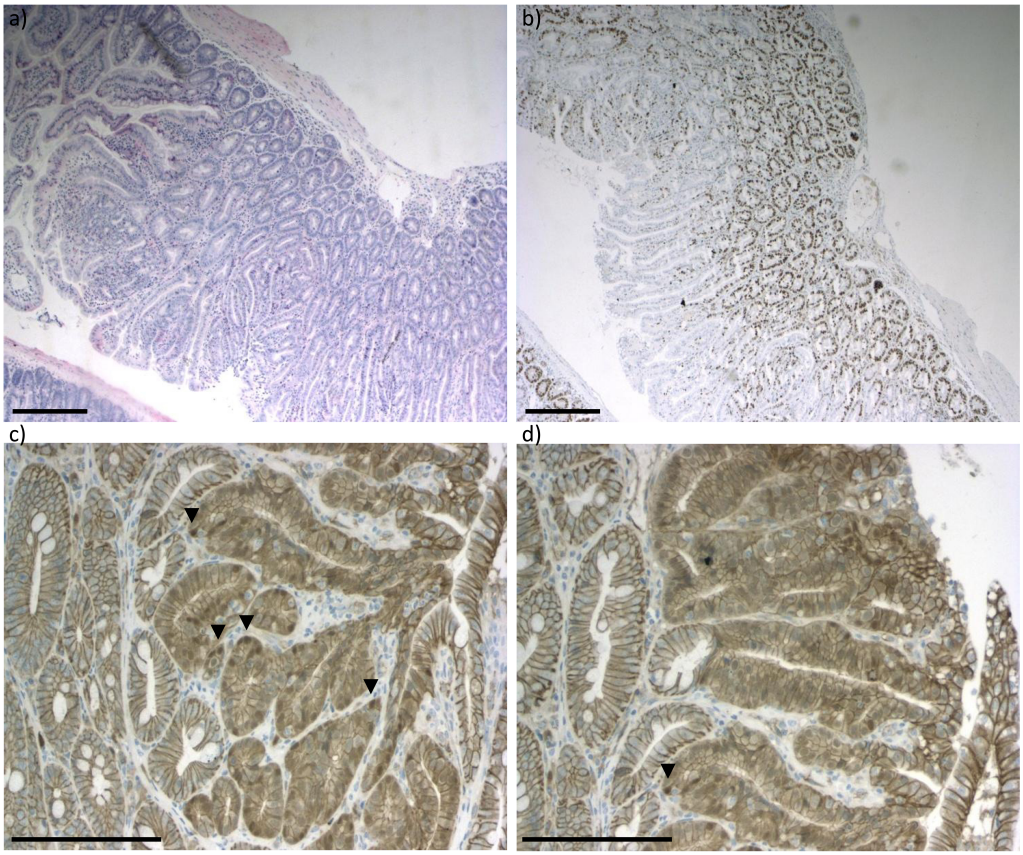


Figure 4.11: Ki67 and β-catenin immunohistochemistry staining on R482Q/+ polyp. a) H and E stained section, scale bars represent 300 μm b) Ki-67 stained section, scale bars represent 300 μm, c)-d) β-catenin stained sections, scale bars represent 150 μm, arrowheads highlight nuclear staining.

be resistant to phosphorylation by Gsk-3β which usually tags it for ubiquitination and subsequent degradation. β-catenin levels may accumulate and translocate into the nucleus where it will act as a co-activator for TCF-responsive genes (see Figure 1.3). *Ctnnb1* mutations were present in heterozygous state, consistent with oncogene activation. The low amplitude of the mutant chromatograms compared to that of the wildtype suggested that the mutation may not have been present in all tumour cells indicating polyclonality of the tumours. Deregulation of Wnt signalling (assessed by β-catenin immunohistochemistry) was also observed in tumours in which no *Ctnnb1* (nor *Apc*) mutations had been identified, again suggesting that mutations were undetected or that Wnt signalling was activated via an alternative mechanism.

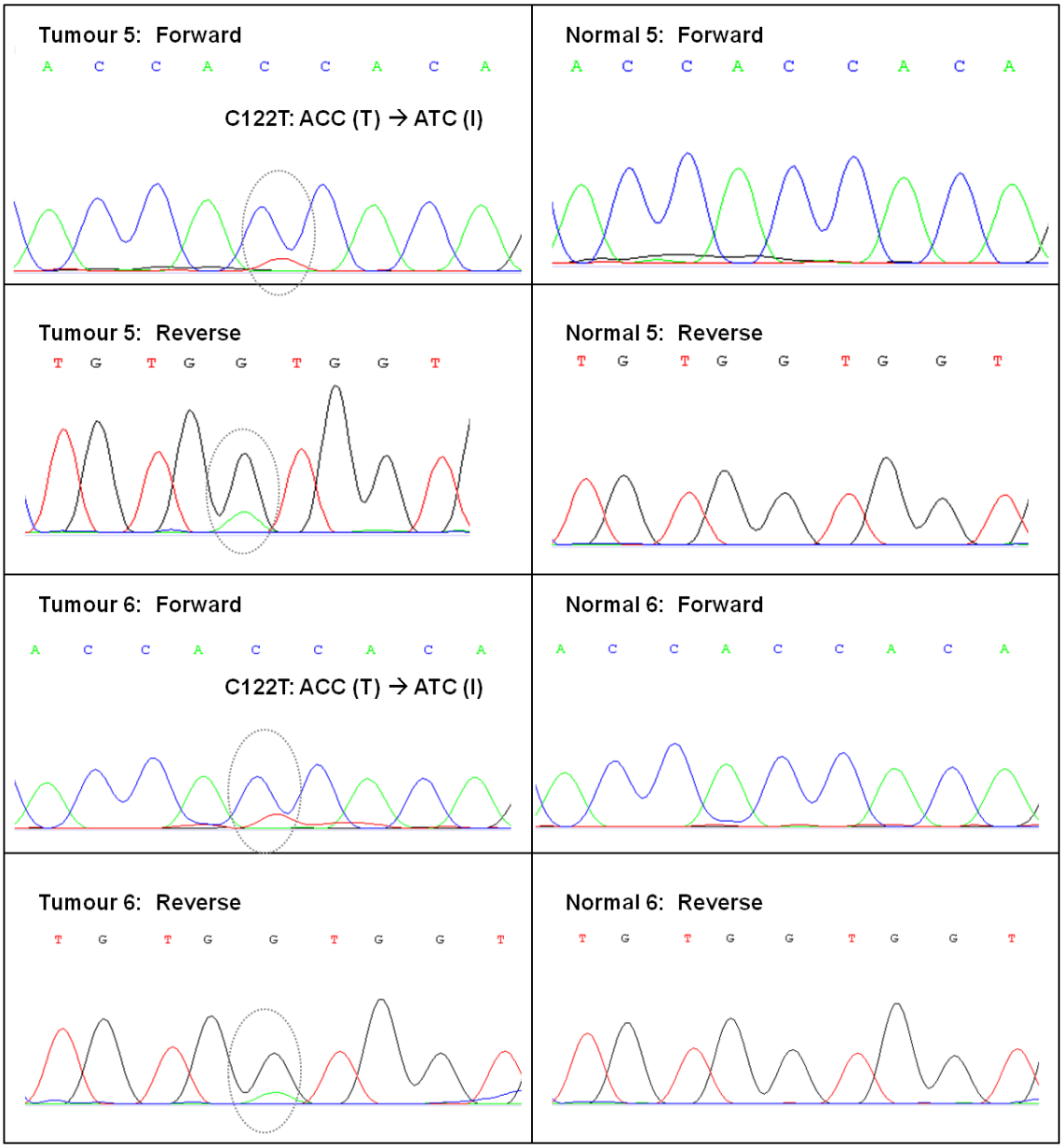


Figure 4.12: *Ctnnb1* mutation in R482Q/+ tumours. Corresponding normal intestinal tissue was used as a control in both cases. Sequencing primers used are detailed in Appendix B.2. Sequencing traces were analysed using the ApE programme. Note the lower intensity of mutant chromatograms in comparison to wildtype, suggesting the mutations were not present in all tumour cells.

In order to assess if mutations in other commonly mutated genes in colorectal tumorigenesis could be identified, primers were designed to amplify mutational hotspots of *Tp53* (exons 5-8 [220]) and *Kras* (exons 1-2). Primers sequences are shown in Appendix B.2. No mutations were identified in either of these genes (n=11). No mutations were identified in the common mutational hotspots of *Apc*, *Ctnnb1*, *Kras* or *Tp53* in $Fbxw7^{\Delta/+}$ tumours (n=2).

To investigate any increase in the number of cells in the stem cell compartment, 10 individual crypts from SB3 from three R482Q/R482Q, R482Q/+, $Fbxw7^{\Delta/\Delta}$ and wildtype genotypes were isolated (section 2.1.6). Markers of stem cells in the small intestine (*Lgr5* and *Olfm4*) were assessed by qRT-PCR and no significant differences in stem cell numbers were found in comparison to wildtype mice in all genotypes analysed (p>0.05, Student t-test in all cases) (Figure 4.13).

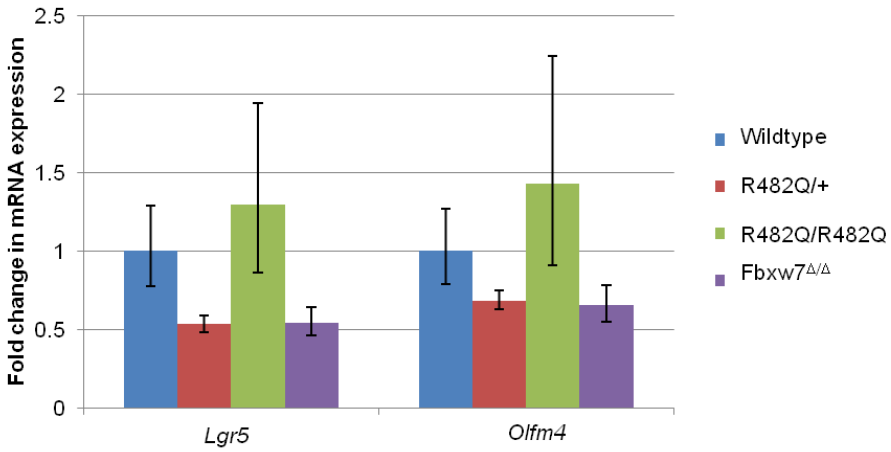


Figure 4.13: No significant change in mRNA expression of stem cell lineage markers in *Fbxw7*-mutant small intestinal crypts relative to wildtype crypts. Ten individual crypts from SB3 were analysed for three mice from each genotype. Assessed by qRT-PCR using TaqMan probes (Table 2.4), CT values were normalised to *Gapdh*. p>0.05, Student t-test in all cases. Error bars represent the SEM.

4.2.7 Protein abundance of Fbxw7 substrates in morphologically normal R482Q mice

Fbxw7 regulates a plethora of substrates and I wished to determine if the R482Q mutation deregulates any of these substrates in the intestine. Intestinal samples were collected from three R482Q/+, R482Q/R482Q and wildtype mature 6-weeks old mice. Epithelial cell isolation was conducted on a 2 cm section of proximal SB1 tissue as described in section 2.5.3.3. Western blots for several Fbxw7 substrates were performed. As discussed in Chapter 3, as Tgif and Klf5 are transcriptional factors, western blots were conducted on the nuclear fraction (section 2.5.3.4) for these targets. All western blots were run at least in triplicate. All western blots were quantified by normalising pixel intensity to the loading control (β-actin or Lamin B1 in cases of nuclear fraction) and shown relative to wildtype samples. Figure 4.14a shows no significant difference in the protein level of Aurora A, Nicd1, c-Myc, p-c-Myc or c-Jun between intestinal tissue from wildtype, R482Q/+ and R482Q/R482Q mice. Elevated levels of cyclin E in R482Q/R482Q tissue compared to wildtype tissue (p=0.046, Wilcoxon test) were found, although no increase in protein expression was seen in R482Q/+ tissue compared to wildtype.

Figure 4.14b shows a dosage dependent elevation of Tgif1 protein in R482Q/R482Q and R482Q/+ tissue compared to wildtype (p=0.017, non parametric trend test). The same trend was observed for Klf5, whereby elevated protein levels were observed in R482Q/+ compared to wildtype and to a greater extent in R482Q/R482Q compared to wildtype (p=0.024, non parametric trend test).

I wished to see if Tgif and Klf5 proteins were also differentially expressed in *Fbxw7*-null mice (Figure 4.14b). No dosage dependent elevation in Tgif1 protein in *Fbxw7*-null mice was seen (p=0.102, non parametric trend test) and similar results were found for Klf5 (p=0.229, non parametric trend test). Interestingly, however there was an increase in the protein level of Tgif in $Fbxw7^{\Delta/\Delta}$ compared with wildtype

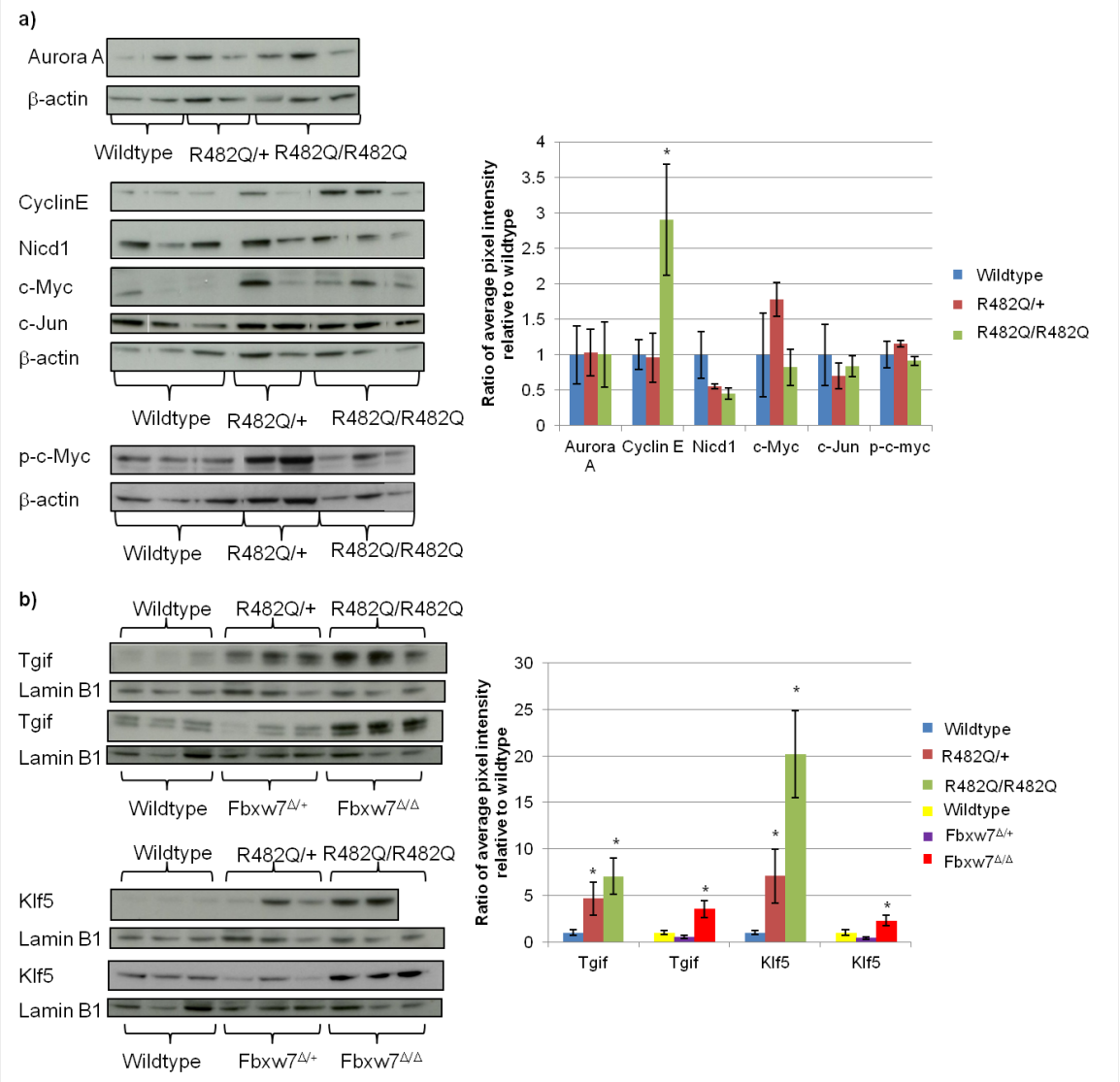


Figure 4.14: Protein expression of Fbxw7 protein targets in intestines from *Fbxw7* mutant 6-weeks old mice, Klf5 and Tgif show elevated levels in *Fbxw7*-mutant mice compared to wildtype mice. Antibodies used are detailed in Table 2.6. β-actin was used as a loading control in most cases, with Lamin B1 used as a control for Tgif and Klf5 when the nuclear fraction was assessed. Graphs show quantification of western blots with the ratio of normalised pixel intensity relative to wildtype mice. Asterisks indicate significant results (see text for details). Western blots for each antibody were performed on three separate occasions.

(p=0.051, Student t-test) but not $Fbxw7^{\Delta/+}$ tissue (p=0.165, Student t-test). Similiarly there was an increase in the protein level of Klf5 in $Fbxw7^{\Delta/\Delta}$ compared to wildtype (p=0.033, one tailed Student t-test), but not in $Fbxw7^{\Delta/+}$ compared to wildtype (p=0.311, one tailed Student t-test).

4.3 Discussion

4.3.1 R482Q/+ mutation causes intestinal tumorigenesis

Twenty-nine percent of R482Q/+ mice exhibited small intestinal adenoma formation at a low frequency following a long latency period. The propensity of mouse models of colorectal cancer to manifest predominantly small intestinal lesions in contrast to colonic lesions has previously been reported extensively. The incomplete penetrance of this phenotype and low number of adenomas observed suggested that additional mutations were required for tumorigenesis. Wnt signalling was deregulated in these adenomas as highlighted by cytoplasmic and low level nuclear β-catenin staining. Activation of the Wnt signalling pathway is an early event in most intestinal tumours, typically occurring through truncating *Apc* mutations. No mutations were identified in the mutational cluster region of *Apc*, although it is possible that mutations were present outside the region sequenced. Two tumours from R482Q/+ mice had *Ctnnb1* mutations, whereby a Gsk-3β phosphorylation site was altered.

FBXW7 mutations have been identified in human adenomas, even in those less than 1 cm in diameter [18]. It has been postulated that *FBXW7* mutations occur at the transition from intermediate to late adenoma [221] and may occur prior to *TP53* disruption [91]. The cooperative effect of *Tp53* and *Fbxw7* mutations has also been demonstrated in the tumours observed in the heterozygous *Fbxw7*-null and heterozygous *Tp53*-null mice [91]. It has been hypothesised that there is a genetic association between *Fbxw7* and *Tp53* mutations, whereby, mutation of *Fbxw7* leads

to increased levels of oncoproteins resulting in p53 dependent oncogene-induced apoptosis or sensescence [222]. Cells therefore, may be selectively pressured to inactivate *Tp53* in order to enable continued proliferative capacity and survival. No mutations were observed in the commonly mutated sites in *Kras* or *Tp53* in R482Q/+ tumours perhaps supporting the hypothesis that *Fbxw7* mutations occur as an early event in colorectal tumorigenesis.

Adenomas develop in R482Q mice in a heterozygous state, reminscient of the heterozygous *FBXW7* mutations observed in human tumours. No homozygous *FBXW7* propellor-tip mutations have been observed in humans. To date, no homozygous R482Q samples have been analysed, although a small cohort of mice are currently aging and are greater than 250 days old, suggesting there is not a significant enhancement of phenotype observed if any.

$Fbxw7^{\Delta/+}$ mice also exhibit adenoma formation at a lower frequency than R482Q mutation, although the difference in frequency was not statistically significant (15% vs 29%). Sancho *et al* [151] and Babaei *et al* [188] reported absence of adenomas in $Fbxw7^{\Delta/+}$ mice up to 11 months [151]. As only very few intestinal polyps develop per mouse, these mice often do not display typical signs of intestinal phenotype, such as anaemia and hunching and therefore it is possible that collection of these samples may have been missed by these groups.

4.3.2 R482Q/+ invasive adenocarcinoma

One R482Q/+ tumour was identified as an invasive adenocarcinoma (6%, n=1/18), whilst at low frequency, such tumours are found infrequently in mouse models of colorectal cancer. Table 4.2 shows examples from the literature whereby invasive adenocarcinomas have been reported. It is notable that the majority of these cases were compound models which also had mutant *Apc* alleles.

Model	Incidence of adenocarcinomas (%)	Ref.
$Pten^{+/-}$ $Apc^{+/-}$	56%, 150-200 days post induction	[223]
Apc^{Min}, SWR/BR hybrids	24-87%, age 1 year+	[224]
$Muc^{-/-}$		[225]
$Kras^{V12G}$ / $Apc^{1638N/+}$	47%, by 105 days	[226]
$p53^{-/-}$ / Apc^{Min}	5%, 90 days	[227]
$Smad3^{-/-}$	30%, C57Bl/6J x 129/Sw hybrid	[228]

Table 4.2: Mouse models that exhibit invasive small intestinal adenocarcinomas

4.3.3 R482Q/+ mutation in morphologically normal intestinal tissue

In R482Q mutant mice, all differentiated cell types of the small intestine were identified (enterocytes, goblet, enteroendocrine, Paneth cells). A subtle, but significant decrease in the number of goblet cells was observed in some *Fbxw7* mutant genotypes (R482Q/R482Q, $Fbxw7^{\Delta/+}$). Two previous studies on *Fbxw7*-null mice reported defective differentation in $Fbxw7^{\Delta/\Delta}$ mice, with marked reduction in the number of goblet and Paneth cells [151; 188]. Although results reported in section 4.2.5.1 indicate that subtle changes in the abundance of epithelial cells occur between *Fbxw7* mutant genotype groups, they do not replicate the drastic reduction in the number of goblet and Paneth cells previously reported [151; 188]. Colonies of mice have been maintained in different animal facilties and thus may be subject to differences in husbandry and environmental factors. As goblet cells are more abundant in the distal intestine, ileal (SB3) tissue was assessed. The previously reported studies also investigated ileal (SB3) tissue, though the method of defining intestinal sections may have differed between studies. It is also important to highlight that opposing effects have been observed on neuroendrocrine (Chromogranin-A positive) cell number in these two previous studies, suggesting inconsistencies in staining protocols and methods of quantification.

In the intestine, Notch signalling is critical for the differentiation of progenitor cells

into absorptive or secretory cells. No difference in protein levels of Nicd1 was seen in the intestine of morphologically normal R482Q/+ and R482Q/R482Q intestinal cells in comparison to wildtype cells, suggesting that Notch signalling is not deregulated, possibly justifying why only minor alterations in intestinal cell lineage have been observed.

There were no differences in proliferation of crypts from morphologically normal *Fbxw7* mutant mice assessed by Ki67 immunohistochemistry. However, there were increased levels of apoptosis observed in R482Q/R482Q and $Fbxw7^{\Delta/\Delta}$ intestines. These data suggests mutant Fbxw7 modulates apoptosis to a greater extent than proliferation.

4.3.4 Possible role of elevated Klf5 and Tgif proteins in intestinal tumorigenesis

In morphologically normal intestinal tissue, a trend for elevated levels of Klf5 and Tgif1 in both R482Q/+ and R482Q/R482Q mice was found. However, in the *Fbxw7*-null model, Klf5 and Tgif1 levels were only found to be elevated in $Fbxw7^{\Delta/\Delta}$ mice. This suggests that the heterozygous R482Q mutation is sufficient to induce deregulation of these Fbxw7 substrates, whereas inactivation of both alleles in a null setting is required to induce Klf5 and Tgif deregulation. This finding supports the 'Just Enough' model (discussed in section 7.2.1) that I have proposed to explain the mutation spectrum of *FBXW7* from the human data, whereby *FBXW7* heterozygous propellor-tip mutations are observed more frequently than two-hit mutations as they allow sufficient ('Just Enough') disruption of gene function [229].

KLF5 is a zinc finger family transcription factor that plays a role in multiple cellular processes including cell cycle regulation, proliferation and angiogenesis [123]. KLF5 is primarily expressed in proliferative crypts in the intestinal epithelium and not in differentiated cells in the villi [210]. Overexpression of *KLF5* in fibroblasts has

stimulatory effects on proliferation [210] and these cells also showed features of a transformed phenotype, including loss of contact inhibition and gain of serum-independent growth. KLF5 exhibits pro-proliferative effects through activation of cell cycle regulatory proteins, including cyclin B1 and cyclin D1, leading to increased G1-S phase transition [124]. KLF5 is also thought to repress expression of cell cycle inhibitory proteins. There is some contradictory evidence that whilst *KLF5* overexpression in non-transformed epithelia cells induces proliferation, *KLF5* overexpression plays an inhibitory role on cell growth in a colon cancer cell line (DLD1) [230]. It has been postulated that the timing of *Klf5* deregulation may be critical: *Klf5* overexpression is growth promoting early on in tumour growth, whereas at later stages of cancer, loss in expression may aid tumour cell survival. In morphologically normal tissue from R482Q/+ and R482Q/R482Q mice, no changes in proliferation were observed, indicating that elevated protein levels of Klf5 at this stage do not result in increased cell proliferation. However, it is possible the elevated levels of Klf5 may contribute to tumorigenesis after adenoma initiation (see Chapter 5).

TGIF1 is a negative regulator of the TGF-β signalling pathway, acting as a co-repressor in Smad2/3 complexes [231]. TGIF1 can recruit histone deacetylases to aid transcriptional repression therefore setting the maximal level to which a TGF-β signal can activate transcription. Typically, TGF-β ligand binding leads to growth inhibition via transcriptional regulation of a cyclin-dependent kinase inhibitor, resulting in cell cycle arrest. Experiments to overexpress *TGIF1* in human keratinocyte cells have demonstrated repression of Smad-activated transcription of cyclin-dependent kinase inhibitor p15 and thus attentuation of growth inhibition [231]. As TGIF1 antagonises the TGF-β anti-proliferative response, elevated Tgif1 levels may contribute to the increased proliferation necessary for tumorigenesis, however this is not detected in morphologically normal intestinal cells in R482Q/R482Q and R482Q/+ mice.

Enhanced apoptosis may not be directly mediated by Klf5, as previous reports

show that Klf5 suppresses apoptosis by increasing the expression of *Survivin*, an inhibitor of apoptosis [232]. Also, TGF-β signalling induces apoptosis through the Fas receptor, thus increased levels of TGF-β signalling repressor alone are unlikely to result in elevated apoptosis.

I can conclude that heterozygous R482Q mutation caused tumorigenesis although accompanying spontaneous mutations that activate the Wnt signalling pathway were required. The critical Fbxw7 substrates in the intestine appeared to be Klf5 and Tgif1; elevated protein levels of both of these substrates were observed in R482Q/+ and R482Q/R482Q tissues, but only in $Fbxw7^{\Delta/\Delta}$ and not $Fbxw7^{\Delta/+}$ tissues. Further analysis is required to investigate tumorigenesis in R482Q/R482Q mice. Additional work that investigates R482Q mutations in the background of *Apc*-mutant alleles is presented in Chapter 5.

Chapter 5

Investigation of an *Fbxw7* propellor-tip mutation in an *Apc*-mutant background

5.1 Introduction

5.1.1 *Apc* mutant mouse models

As discussed in section 1.1.4, multiple mutations are necessary for carcinogenesis. As *APC* mutations occur in a large majority of human colorectal cancers, *FBXW7* mutations are found mostly in the context of *APC* mutant alleles. To address whether Fbxw7 mutant propellor-tip protein could affect the development of intestinal polyposis, I wished to cross R482Q/*Vil1*-Cre mice to *Apc*-mutant mice.

In humans, the first and second *APC* hits are non-random with respect to each other and are selected to generate an optimal/'Just-Right' level of Wnt signalling [27; 28]. Figure 5.1 highlights the protein domains of APC including seven 20 amino acid repeats (AARs) that are important in β-catenin binding and degradation. In FAP, patients with a germline mutation at codon 1309 (1 20 AAR retained) exhibit

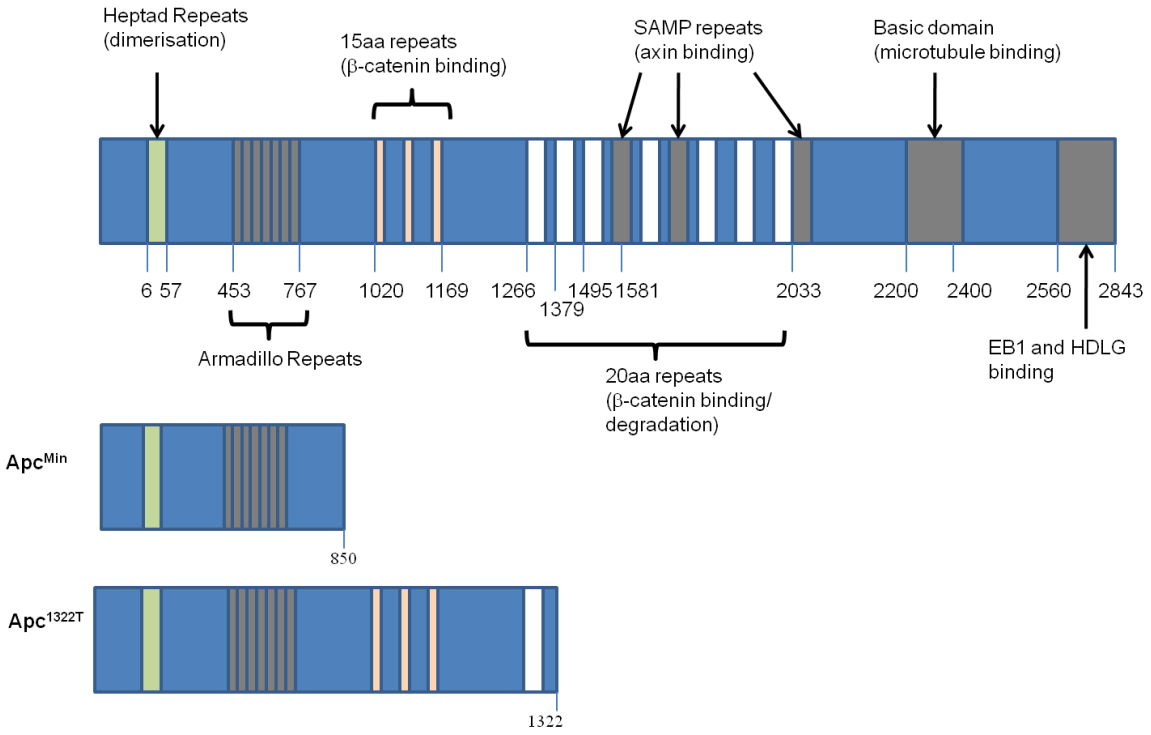


Figure 5.1: Protein domains of APC, codon numbers are indicated for human APC, although the positions vary little in mouse Apc protein. The retained Apc protein domains in Apc^{Min} mice (truncating codon 850 mutation) and Apc^{1322T} mice (truncating 1322 mutation) are indicated.

a more severe polyposis phenotype.

Many *Apc* mutant mouse models have been generated by either gene targeting or chemical mutagenesis. The Apc^{Min} mouse was generated from an N-ethyl-N-nitrosourea (ENU) screen; ENU is a powerful germline mutagen that induces point mutations in a genome-wide manner [233]. This mouse developed 'multiple intestinal neoplasia', with a large but varying number of small intestinal adenomas dependent on genetic background. The causative mutation was identified as a truncating mutation at codon 850 of *Apc* [233; 234]. The Apc^{Min} model is the most widely used *Apc* mutant mouse model.

Truncated APC proteins in colorectal tumours are generally stable and usually retain a total of one to two 20 AARs (over two alleles), with very few human colorectal tumours retaining zero AARs. Our laboratory has generated a mouse model more rep-

resentative of the mutations found in human colorectal tumours, the Apc^{1322T} model, which carries a truncating mutation at *Apc* codon 1322 [235]. Figure 5.1 shows the retained protein domains of mutant Apc proteins in Apc^{Min} and Apc^{1322T} models. In both Apc^{Min} and Apc^{1322T} mice, the mutations are rendered homozygous in tumours following loss of heterozygosity by mitotic recombination [235; 236]. Therefore, the Apc^{1322T} protein retains one of the 20 AARs, while the Apc^{Min} protein retains none.

Typically about 200 polyps are found in the small intestine of Apc^{1322T} mice by 10-12 weeks of age [235]. Apc^{1322T} has markedly more severe polyposis, with earlier-onset and larger, more numerous and more highly dysplastic adenomas in comparison with the Apc^{Min} mouse model. The Apc^{1322T} mutation produces a sub-maximal β-catenin level that promotes early tumour growth more effectively then the Apc^{Min} mutation [237].

5.1.2 Aims of chapter

The aim of the work in this chapter was to breed R482Q/*Vil1*-Cre and *Apc* mutant mice and evaluate any modification of phenotype observed in R482Q/+ *Apc*-mutant compound mice compared with *Fbxw7*-wildtype *Apc*-mutant control animals.

5.2 Results

5.2.1 Crosses with *Apc*-mutant mice and subsequent evaluation of phenotype modification

R482Q mice were crossed with *Apc* mutant (both Apc^{Min} and Apc^{1322T}) mice. In order to generate mice with R482Q/+ *Apc*-mutant compound genotypes, breeding pairs were set up in various combinations using the available mice (Appendix E.1, E.2). Both *Apc*-mutant models are embryonic lethal in the homozygous state so all

Apc-mutant mice analysed were heterozygous. Offspring were genotyped for R482Q and *Vil1*-Cre alleles as described in sections 3.3.2 and 4.2.2. *Apc* mutant alleles were genotyped using primers detailed in Table 2.1, following previously reported protocols [234; 235]. R482Q/+ *Apc*-mutant compound (test) mice and *Fbxw7*-wildtype *Apc*-mutant (control) mice were aged. Test animals were culled and samples collected when they exhibited a 'hunched' appearance, became less active and showed signs of anaemia (white feet). Within each litter control mice were sacrificed at the same time as test mice. Intestines were analysed using a dissection microscope and polyps were counted and categorised according to size. Total polyp counts assessed tumour initiation, whereas polyp size assessed tumour growth. I also recorded polyp distribution throughout the intestine and investigated tumour invasion.

5.2.1.1 R482Q/+ Apc^{Min} compound mice

R482Q/+ Apc^{Min} (n=8) and Apc^{Min} control (n=5) mice were collected from multiple breeding pairs which used mice with the best genotype combinations available at the time. Examples of breeding pairs used to generate desired genotypes are shown in Appendix E.1. Low numbers of R482Q Apc^{Min} compound mice were obtained per litter as expected due to the complicated nature of the desired compound genotype. Note that: R482Qfl/+ *Vil1-*Cre^{-} Apc^{Min}; *Fbxw7*-wildtype *Vil1-*Cre^{+} Apc^{Min}; and *Fbxw7*-wildtype *Vil1-*Cre^{-} Apc^{Min} genotypes were considered as Apc^{Min} controls.

The R482Q/+ Apc^{Min} compound mice were culled when they exhibited signs of intestinal phenotype at 87-105 days, in comparison to approximately 200 days in Apc^{Min} mice. To date there have been insufficient numbers of mice to allow aging of control mice until symptomatic for formal survival analysis; an indication of symptomatic age has been deduced from previous work on these mice in our laboratory.

Intestines were stained with methylene blue (section 2.2.1) to allow easier visualisation and quantitation of polyp burden according to size (Figure 5.2b). Figure 5.2a

shows an increase in total tumour burden in the R482Q/+ Apc^{Min} compound mice in comparison to Apc^{Min} mice, with the median total polyp count of 80 polyps in R482Q/+ Apc^{Min} compound mice in comparison to 29 polyps in Apc^{Min} mice (raw polyp counts are shown in Appendix F.1). Very few colon polyps were identified in both genotype groups and thus these data have been excluded from further analysis.

Figure 5.2c shows the distribution of small intestinal polyps by representing the percentage of total polyps present in each small intestinal location. As with Apc^{Min} control mice, R482Q/+ Apc^{Min} compound mice displayed the greatest frequency of polyps in SB3. However, in R482Q/+ Apc^{Min} compound mice there was a significant increase in the proportion of polyps found in SB1 compared with Apc^{Min} control mice (p=0.002, Fisher's exact test, Table 5.1).

Location	**R482Q/+ Apc^{Min}**	Apc^{Min}	**Total**
SB1	131	25	156
SB2	206	75	281
SB3	286	124	410
Total	623	224	847

Table 5.1: Number of polyps at each intestinal location in R482Q/+ Apc^{Min} compound and Apc^{Min} mice. An increase in the proportion of SB1 polyps in R482Q/+ Apc^{Min} compound mice in comparison to Apc^{Min} mice was seen (p=0.002, Fisher's exact test).

Figure 5.2d shows small intestinal polyps categorised by size. In Apc^{Min} control mice the largest proportion of tumours (58%) were <1 mm in diameter. In R482Q/+ Apc^{Min} compound mice the polyps were larger, with the largest proportion of tumours (58%) between 1 and 2 mm in diameter. Note that no R482Q/+ Apc^{Min} polyps showed signs of invasion into the muscle layer; this finding was probably due to polyps not having sufficient time to progress within the shortened lifespan of these mice before they were sacrified due to tumour load.

Conducting logistic regression analysis with polyp size as the independent variable and presence or absence of R482Q mutation as the dependent variable, stratified by

age and sex, highlighted that the presence R482Q mutation had a significant positive impact on tumour size (p=0.000, Z=10.02, OR=6.448, 95% confidence intervals 4.5-9.3).

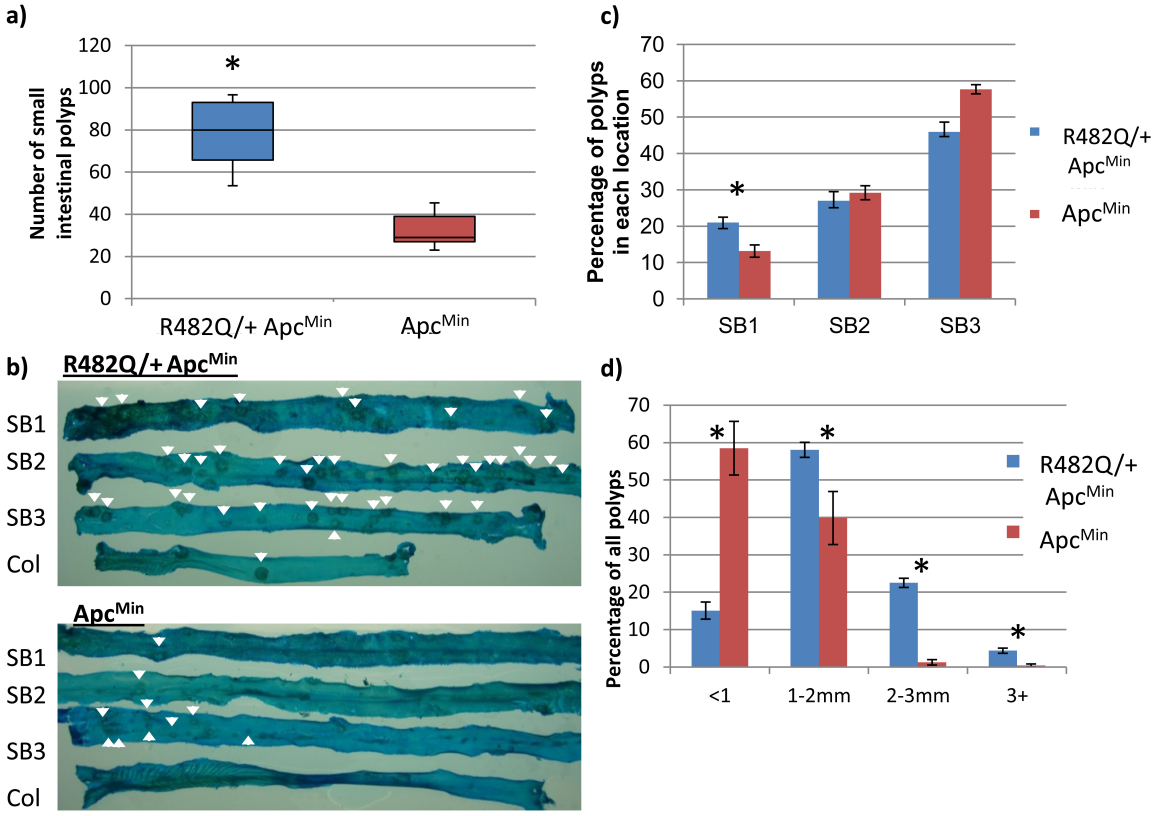


Figure 5.2: R482Q mutation enhances tumorigenesis in R482Q/+ Apc^{Min} compound mice. Eight R482Q/+ Apc^{Min} mice and five Apc^{Min} mice were analysed, both test and control mice within each litter were collected when test mice showed signs of an intestinal phenotype, aged 87-105 days. a) Box and whiskers plot of the polyp burden in the small intestines. The line within the box represents the median, lines at the ends of the box represent 25th and 75th centile and lines at the end of the whiskers represent 5th and 95th centile. b) Representative images of methylene blue stained intestines, arrowheads highlight polyps. c) Percentage of total small intestinal polyps found at each intestinal location. d) Percentage of polyps categorised according to size. Error bars represent the SEM. Asterisks depicts significant results (see text for details).

5.2.1.2 R482Q/+ Apc^{1322T} compound mice

R482Q/+ Apc^{1322T} (n=13) and Apc^{1322T} (n=9) were collected from multiple breeding pairs which used mice with the best genotype combinations available at the time. Examples of breeding pairs used to generate desired genotypes are shown in Appendix E.2. As previously reported, female Apc^{1322T} mice do not breed well, so where possible male Apc^{1322T} were used in breeding pairs. As Apc^{1322T} mice become symptomatic at a relatively young age it was necessary to replace breeding males often. Breeding males were paired with two females in order to increase the number of offspring. Note that: R482Qfl/+ *Vil1-Cre*$^{-}$ Apc^{1322T}; *Fbxw7*-wildtype *Vil1-Cre*$^{+}$ Apc^{1322T}; and *Fbxw7*-wildtype *Vil1-Cre*$^{-}$ Apc^{1322T} genotypes were considered as Apc^{1322T} controls.

The R482Q/+ Apc^{1322T} compound mice were culled when they displayed signs of intestinal phenotype at 71-127 days, in comparison to approximately 150 days for Apc^{1322T}. Methylene blue stained intestines shown in Figure 5.3b allow visualisation of tumour burden. Figure 5.3a shows a slight increase in total tumour number in R482Q/+ Apc^{1322T} compound mice in comparison to Apc^{1322T} controls (raw polyp counts are shown in Appendix F.2). However, performing logistic regression analysis with polyp number as the independent variable and presence or absence of R482Q mutation as the dependent variable, stratified by age and sex, showed no evidence that presence of R482Q mutation had an effect on total tumour number (p=0.300, Z=1.04, OR=1.026, 95% confidence intervals 0.98-1.08). Very few colon polyps were identified in both genotype groups and thus have been excluded from further analysis.

Figure 5.3c shows the distribution of small intestinal polyps in Apc^{1322T} mice, with the greatest frequency observed in SB1. Tumours from R482Q/+ Apc^{1322T} compound mice show the same distribution pattern, with R482Q mutation not effecting location.

Figure 5.3d shows that there was a greater proportion of larger tumours in the R482Q/+ compound mice in comparison to Apc^{1322T} control mice. Conducting logistic regression analysis with polyp size as the independent variable and presence

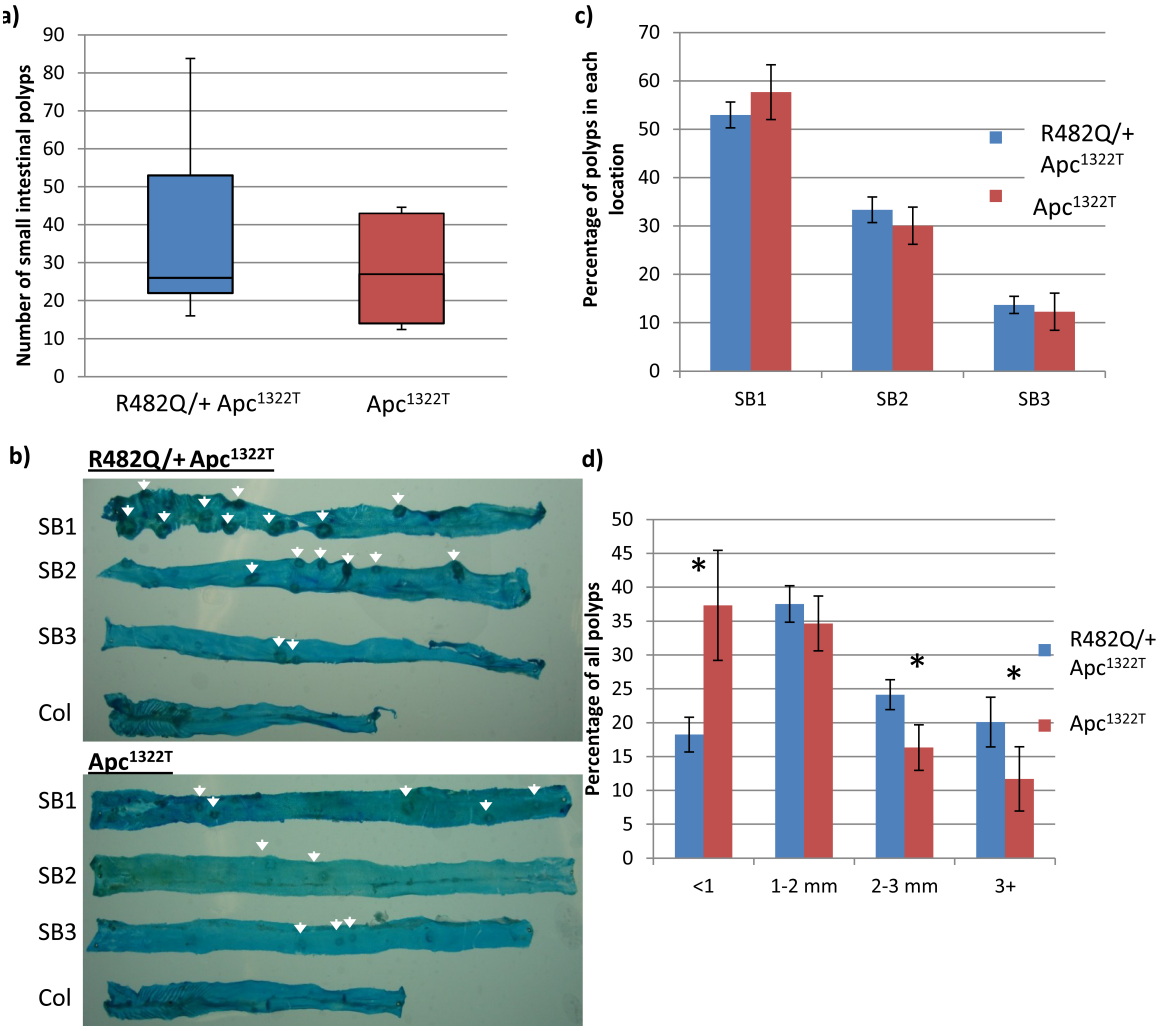


Figure 5.3: R482Q mutation enhances tumorigenesis in R482Q/+ Apc^{1322T} compound mice. Thirteen R482Q/+ Apc^{1322T} mice and nine Apc^{1322T} mice were analysed, both test and control mice within each litter were collected when test mice showed signs of phenotype, aged 71-127 days. a) Box and whiskers plot of the polyp burden in the small intestine. The line within the box represents the median, lines at the ends of the box represent 25th and 75th centile and lines at the end of the whiskers represent 5th and 95th centile. b) Representative image of methylene blue stained intestines, arrowheads highlight polyps. c) Percentage of total small intestinal polyps found at each small intestinal location. d) Percentage of polyps categorised according to size. Asterisks depicts significant results (see text for details). Error bars represent the SEM.

or absence of R482Q mutation as the dependent variable, stratified by age and sex, highlighted that the presence R482Q mutation had a significant positive impact on tumour size (p=0.000, Z=5.06, OR=1.551, 95% confidence intervals 1.3-1.8). Therefore, although there was not a dramatic increase in polyp number in R482Q/+ Apc^{1322T} compound mice, the tumours were significantly larger and thus must be growing more quickly. Note that no invasive adenomas were detected in R482Q/+ Apc^{1322T} compound mice; this may be due to the shortened lifespan of mice due to tumour burden, which prevents the accumulation of the somatic mutations necessary for tumour progression.

When both *Apc* mutant models were grouped together for analysis with *Apc* mutation as a co-variate, the total number of polyps in R482Q *Apc* mutant mice was significantly increased in comparison to *Apc* mutant control mice (logisitic regression analysis, p=0.009, Z=2.61, OR=1.06, 95% confidence intervals 1.01 - 1.11). Also polyps were larger in R482Q/+ *Apc* mutants compared to *Apc* mutant controls (logistic regression, p=0.000, Z=10.78, OR=2.337, 95% confidence intervals 2.0-2.7).

5.2.1.3 Molecular analysis: R482Q/+ Apc^{1322T} compound tumour proliferation

All further analysis was conducted on R482Q/+ Apc^{1322T} compound tumours as insufficient numbers of R482Q/+ Apc^{Min} compound mice impeded tumour collection.

As results presented in section 5.2.1 showed that presence of R482Q mutation increased tumour size, I decided to assess the proliferation rate in R482Q/+ Apc^{1322T} compound tumours. Ki67 immunohistochemistry was carried out on tumours from R482Q/+ Apc^{1322T} compound mice and Apc^{1322T} control symptomatic mice (Figure 5.4) (note that Apc^{1322T} control mice used were symptomatic mice and not those age-matched). In order to quantitate proliferation, 21 tumours from 7 R482Q/+ Apc^{1322T} compound mice and 11 tumours from 4 Apc^{1322T} mice were assessed (section 2.5.1.1).

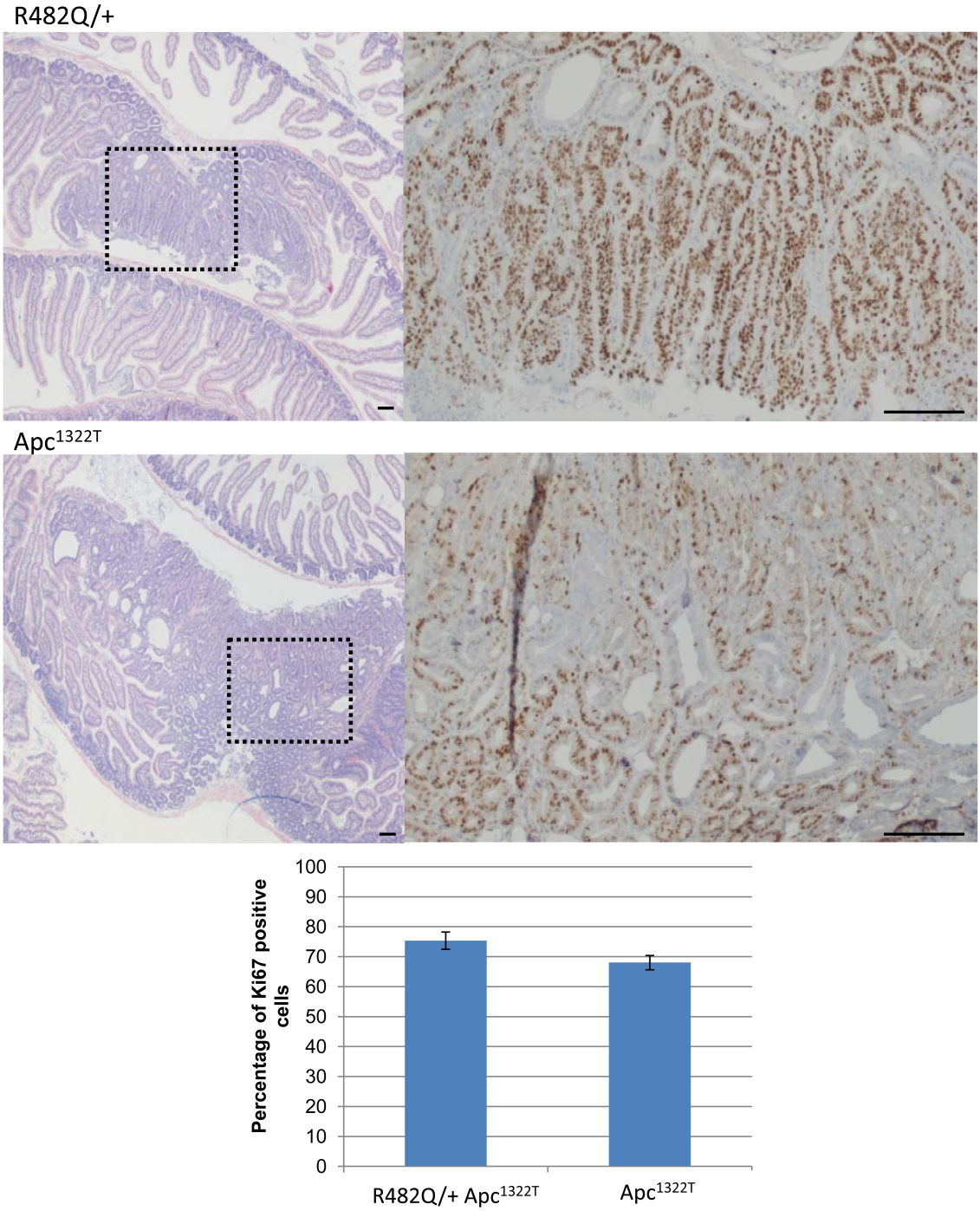


Figure 5.4: Proliferation in R482Q/+ Apc^{1322T} compound tumours assessed by Ki67 immunochemistry. Representative H and E and Ki67 immunohistochemistry images. Scale bars represent 100 μm. The graph shows the mean percentage of proliferating cells in R482Q/+ Apc^{1322T} compound and Apc^{1322T} tumours from symptomatic mice. Twenty-one tumours from seven R482Q/+ Apc^{1322T} compound mice and eleven tumours from four Apc^{1322T} mice were assessed, (p=0.102, Student t-test). Error bars represent the SEM.

There was a slight trend towards an increased percentage of proliferating cells per tumour as assessed by Ki67 immunohistochemistry, however this was not statistically significant (p=0.102, Student t-test).

β-catenin immunohistochemistry shows some cytoplasmic and low level of nuclear β-catenin in R482Q/+ Apc^{1322T} compound tumours, comparable to that seen in Apc^{1322T} tumours (Figure 5.5).

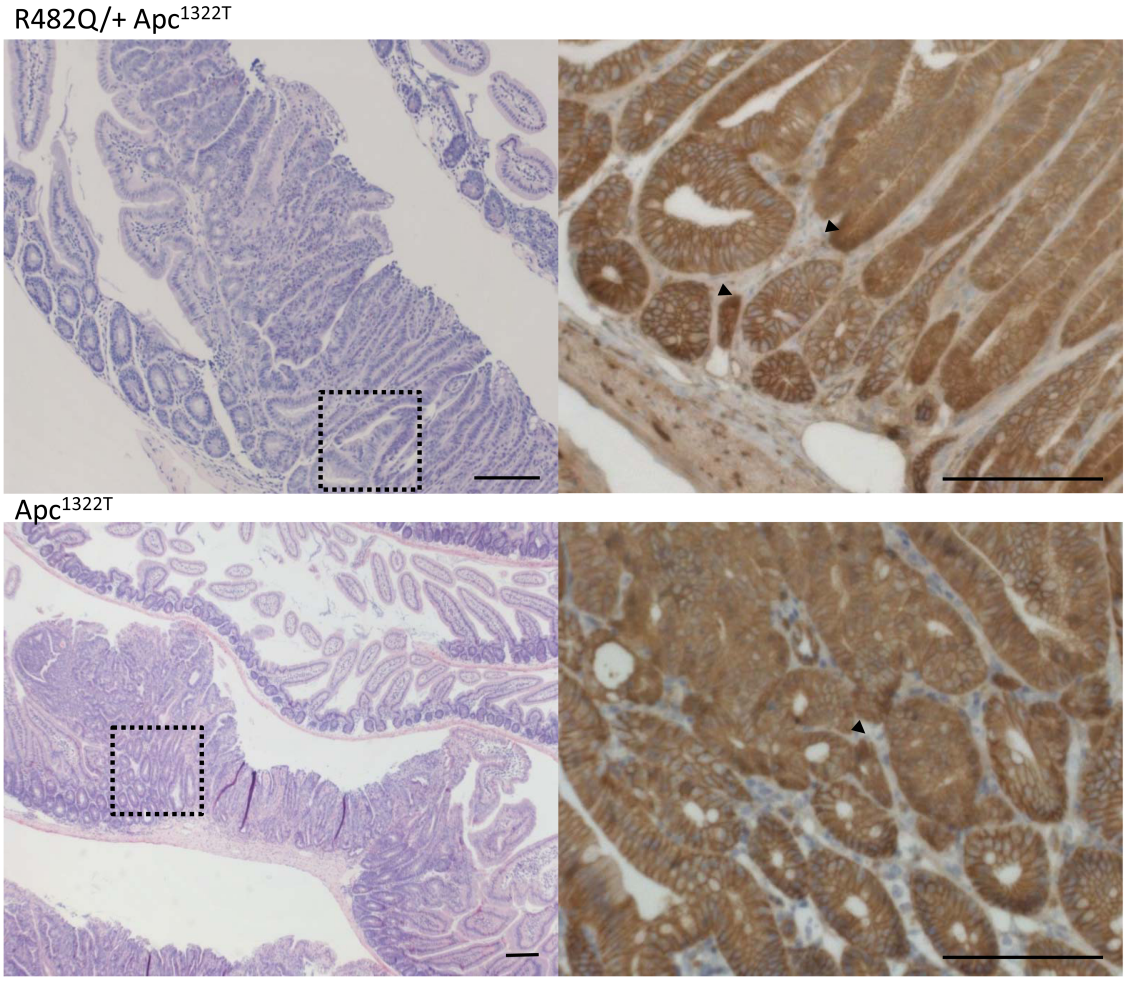


Figure 5.5: β-catenin immunohistochemistry on R482Q/+ Apc^{1322T} compound and Apc^{1322T} tumours. Antibody details shown in Table 2.5. Scale bars represent 100 μm. Arrowheads highlight cells with nuclear β-catenin staining.

To assess the stem cell proportion in R482Q/+ Apc^{1322T} and Apc^{1322T} tumours *Lgr5*, a marker of stem cells, was assessed by qRT-PCR in 10 large (>2mm) polyps

from SB1 from each genotype group. There was no significant difference in the expression of *Lgr5* between R482Q/+ Apc^{1322T} and Apc^{1322T} tumours (Figure 5.6) (p=0.473, Student t-test). *Lgr5* has already been reported to be up-regulated in Apc^{1322T} tumours and the additional R482Q mutation showed no further increase in *Lgr5* levels.

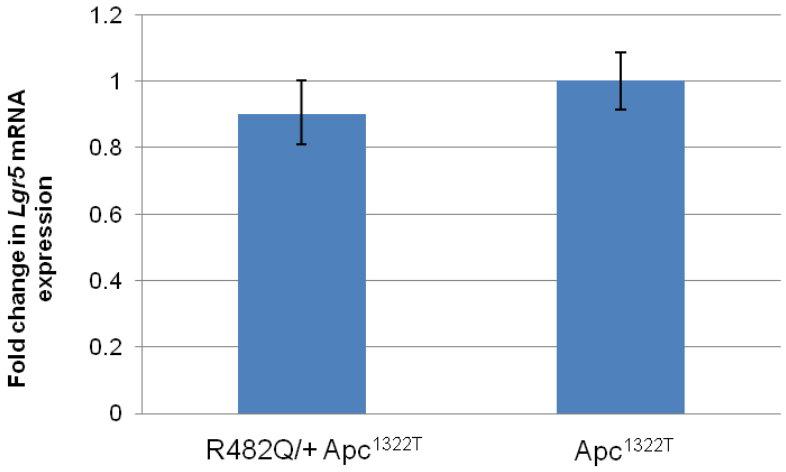


Figure 5.6: No significant difference in *Lgr5* mRNA expression between R482Q/Apc^{1322T} and Apc^{1322T} tumours (p=0.473, Student t-test), as assessed by qRT-PCR using TaqMan probes. CT values were normalised to *Gapdh*, fold change relative to Apc^{1322T} samples. Ten large (>2 mm) polyps from SB1 of both genotypes were analysed in duplicate.

5.2.1.4 Fbxw7 protein substrate analysis in R482Q/+ Apc^{1322T} compound tumours

The protein levels of selected Fbxw7 substrates were analysed in R482Q/+ Apc^{1322T} compound tumours and Apc^{1322T} tumours from symptomatic mice. Four large (>2 mm) tumours from SB1 of each genotype group were analysed. As shown in Figure 5.7a, there was no significant elevation in the levels of c-Jun, Aurora A, Nicd1, cyclin E or p-c-Myc between R482Q/+ Apc^{1322T} and Apc^{1322T} tumours (p>0.05, Student t-test in all cases). To assess the protein level of Klf5 and Tgif1 western blots were run on the nuclear fraction (section 2.5.3.4) of four large (>2mm) tumours from SB1 from R482Q/+ Apc^{1322T} and Apc^{1322T} mice. Protein expression of Klf5 and Tgif1

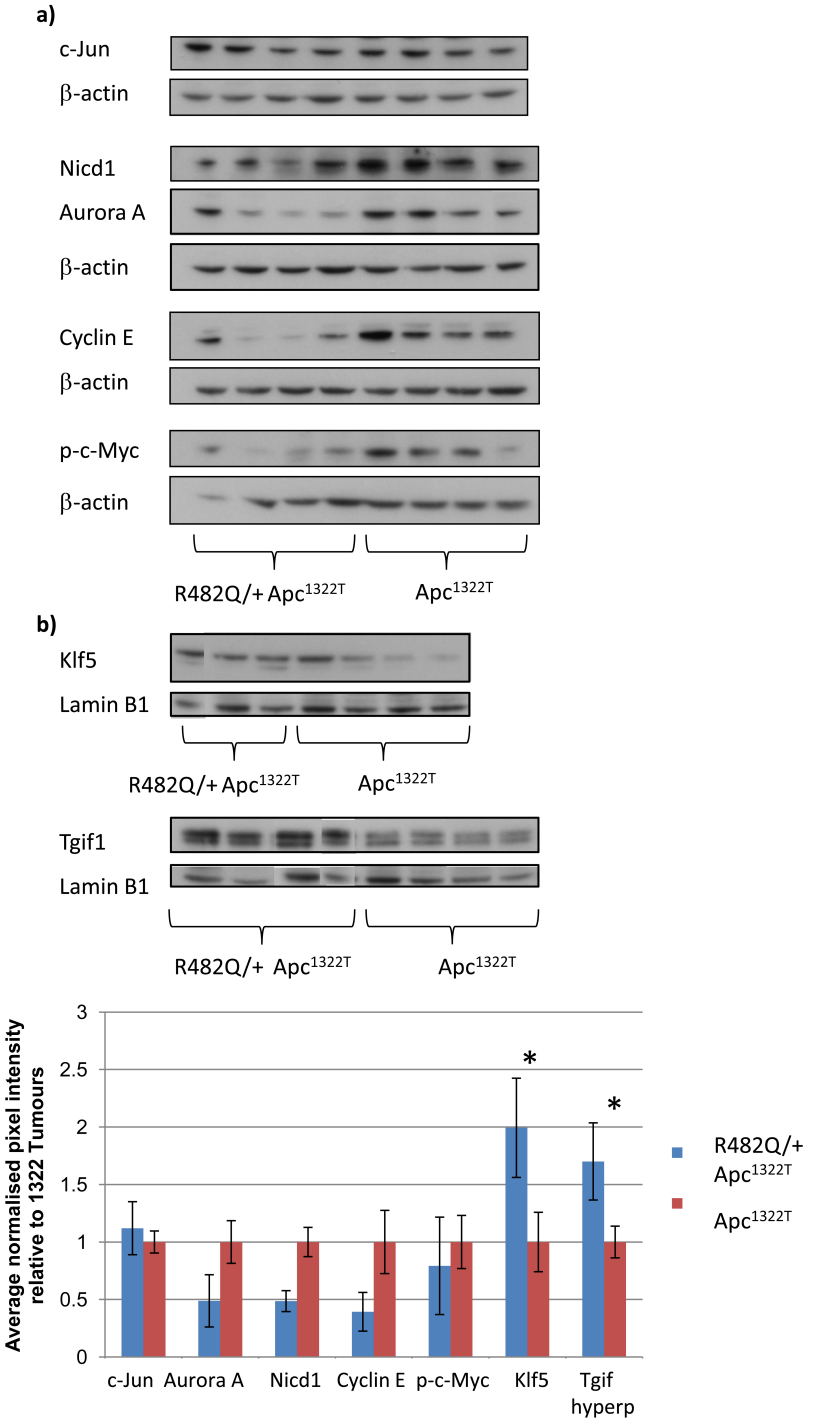


Figure 5.7: Elevated protein levels of Klf5 and Tgif1 in R482Q/Apc^{1322T} tumours, other Fbxw7 substrates were not elevated. a) Antibody details are shown in Table 2.6, β-actin has been used as a loading control. b) Nuclear fractionation (section 2.5.3.4) was carried out for Klf5 and Tgif analysis. Lamin B1 was used as a loading control. The graph shows the ratio of average normalised pixel intensities, relative to Apc^{1322T} tumours. As resolution allowed, the hyper-phosphorylated band of Tgif was quantified. Asterisks depicts significant results, (p=0.045 for Klf5 and p=0.042 for Tgif1, all other cases p>0.05, one tailed Student t-test). Western blots were all repeated at least in duplicate.

was increased in R482Q/+ Apc^{1322T} compared to Apc^{1322T} tumours (p=0.045 and p=0.042, one-tailed Student t-tests respectively, Figure 5.7b).

As Klf5 and Tgif operate in both the Tgf-β and the retinoic acid signalling pathway, selected downstream targets of these pathways (section 3.3.7) were analysed in 9 large (>2 mm) R482Q/+ Apc^{1322T} and Apc^{1322T} tumours from SB1. No significant differences were observed in expression levels of downstream targets of the Tgf-β signalling pathway (p>0.05, Student t-test in all cases) and only one downstream target of the retinoic acid pathway (*Stra6* (retinoic acid binding protein receptor gene)) showed elevated mRNA expression in R482Q/+ Apc^{1322T} tumours (p=0.0003, Student t-test) (Figure 5.8).

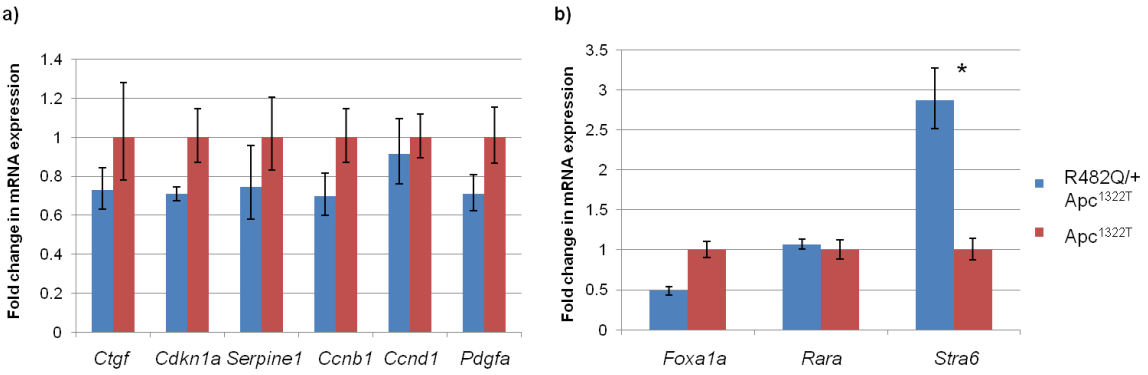


Figure 5.8: Fold change in mRNA expression of selected downstream targets of the Tgf-β and retinoic acid signalling pathways in R482Q/+ Apc^{1322T} and Apc^{1322T} tumours. Assessed by SYBR green qRT-PCR, primer details are shown in Appendix B.1. CT values were normalised to *Gapdh*, relative to Apc^{1322T} samples. Nine large (>2 mm) polyps from SB1 of both genotypes were analysed in duplicate. Asterisk denotes significant result (*Stra6*, p=0.0003 Student t-test).

5.3 Discussion

5.3.1 R482Q/+ mutation enhances intestinal tumorigenesis in *Apc*-mutant mice

R482Q/+ Apc^{Min} compound mice showed an increased tumour burden at the time of sample collection in comparison to Apc^{Min} control mice, whereas an increase in total polyp number was not associated with R482Q mutation in the Apc^{1322T} model. Apc^{Min} mice typically exhibit slower intestinal tumorigenesis compared with Apc^{1322T} mice [235; 237]. Therefore it is possible that at the time of sample collection in Apc^{Min} control mice, tumours may not have been detectable using a dissection microscope and thus they have not been counted in the analysis.

In both R482Q/+ *Apc*-mutant compound mice models, tumours were larger compared to control mice, suggesting that R482Q plays a role in accelerating tumour growth rather than enhancing tumour initiation. I conducted analysis of tumour proliferation by quantifying Ki67 immunohistochemistry on R482Q/+ Apc^{1322T} and Apc^{1322T} tumours, but only observed a slight increase in proliferation rate, which was not statistically significant (p=0.102, Student t-test). It is possible that the method used for quantifying proliferation was sub-optimal in detecting fairly small differences in already high levels of proliferation. Given further time, other methods of assessing proliferation (e.g. BrdU incorporation in replicating cells) would have been investigated, as well as consideration of automated quantification methods to allow greater numbers of cells to be assessed. It is possible that elevated levels of tumour proliferation occur at an early stage of tumour growth and thus were not detected in the samples investigated (from mice at symptomatic age).

As discussed in section 1.1.3, Lgr5 has been identified as an intestinal stem cell marker. I assessed *Lgr5* mRNA in R482Q/Apc^{1322T} and Apc^{1322T} tumours by qRT-PCR and observed no significant difference (Figure 5.6). *Lgr5* mRNA expression is

reported to be up-regulated in Apc^{1322T} tumours cells [237] and may already by elevated to a maximal level, therefore the additional R482Q mutation shows no increased involvement of the stem cell compartment.

As well as increased numbers of proliferating cells, an increased level of crypt fission (the division of a parental crypt into two daugther crypts) has been proposed as a mechanism of early tumorigenesis [238]. Apc^{1322T} mice already show an elevated level of crypt fission in comparison to the Apc^{Min} model and it will be important to investigate if the level of crypt fission is elevated even further in R482Q/+ Apc^{1322T} compound tumours.

It is also possible that tumour growth is enhanced by altered apoptosis. Elevated levels of apoptosis found in morphologically normal intestinal tissue in *Fbxw7* mutant mice (Figure 4.9) suggests that apoptosis is deregulated by *Fbxw7* mutations and thus this should be investigated further in R482Q/+ *Apc* mutant compound tumours.

It is interesting to note that, in R482Q/+ Apc^{Min} compound mice there was a significant increase in the number of SB1 polyps, although the greatest tumour burden was still observed in SB3. Polyps are more proximally distributed in Apc^{1322T} mice, thus no changes in distribution of polyps in R482Q/+ Apc^{1322T} compound mice were identified. Several mouse models have been reported to alter the distribution of Apc^{Min} polyps, including $Kras^{V12}$ Apc^{Min} mutant compound mice, which exhibit a more dramatic proximal shift in polyp distribution [239]. Despite studies suggesting that regional distribution of intestinal tumours reflects the major mechanism by which Apc function is lost, this is not fully understood at this time [240].

5.3.2 Elevated levels of Klf5 and Tgif1; implications for tumorigenesis

Elevated protein expression of the Fbxw7 substrates Klf5 and Tgif1 were identified in R482Q/+ Apc^{1322T} compound tumours. As previously discussed in section 4.3.4,

Klf5 and Tgif1 are transcriptional activators/repressors that play critical roles in regulating many cellular processes, including cell proliferation. Hundreds of genes regulated by KLF5 have been identified and it has been shown that KLF5 promotes cell proliferation and tumorigenesis primarily by upregulating *CCND1*, *PDGFA* and *FBFBP* [124].

Additionally, work by McConnell and colleagues [241] has demonstrated that Klf5 contributes to intestinal adenoma initiation and growth, as a heterozygous *Klf5*-null allele in conjunction with a Apc^{Min} allele led to a 96% reduction in the number of tumours observed. Klf5 has been reported to interact with β-catenin facilitating its nuclear localisation and transcriptional activity [241]. *Klf5*-null heterozygosity in a compound Apc^{Min} and mutant *Kras* model also led to significantly reduced tumour burden, reiterating the critical role of Klf5 in modulation of intestinal tumorigenesis [239]. Elevated levels of Klf5 thus may contribute to the enhanced tumorigenesis observed in R482Q *Apc*-mutant compound mice.

The TGF-β signalling pathway plays a dual role in cancer as both a tumour suppressor and a tumour promoter [33]. Perturbed TGF-β signalling at early stages of cancer progression can lead to rapid growth through loss of TGF-β growth inhibitory properties [32], which are in part mediated by transcriptional control of *CDKN1A*. Elevated Tgif1 protein, as a repressor of Tgf-β signalling, were observed even in morphologically normal tissue in R482Q/+ mice (Figure 4.7) and therefore suppression of this pathway may occur as an early event contributing to the enhanced tumour growth observed in R482Q/+ *Apc*-mutant compound mice.

5.3.3 Retinoic acid pathway in intestinal tumorigenesis

Klf5 and Tgif1 are both components of the retinoic signalling pathway; Klf5 has been shown to directly interact with the retinoic acid receptor [122] and Tgif1 can bind the retinoic receptor (RXR) response element, inhibiting RXR binding by steric

hinderance [206]. I have identified upregulation of mRNA expression of *Stra6* (a retinoic acid binding protein receptor gene), a downstream target of the retinoic acid pathway. Retinoids have been shown to have an inhibitory effect on tumour cell growth [242]. Dillard *et al* [243] have reported that disruption of the retinoic acid receptors can alter the degradation of β-catenin as well as inhibiting β-catenin mediated gene transcription. It therefore may be of interest to further explore the potential deregulation of retinoic acid pathway in intestinal tumorigenesis using the R482Q mouse model.

5.3.4 Comparison to *Fbxw7*-null tumorigenesis in an *Apc*-mutant background

I also have conducted crosses of *Fbxw7*-null mouse models to *Apc*-mutant models in order to compare the differences between *Fbxw7*-null mutations versus *Fbxw7* propellor-tip mutation in the context of *Apc* deficiency. To date, I have insufficient numbers of mice to allow informative analysis. It has been reported that crossing *Fbxw7*-null allele mice with Apc^{Min} mice causes accelerated tumorigenesis [151; 188]. As these mice have been maintained in different animal facilities and samples have been collected at differing ages and severity of disease, it is difficult to draw any firm conclusions from comparisons between the *Fbxw7*-null and R482Q mutant models. In brief, it was reported than $Fbxw7^{\Delta/\Delta}$ Apc^{Min} mice had dramatically enhanced intestinal adenoma formation with an increase in size and number and had to be sacrificed at 6-weeks of age. $Fbxw7^{\Delta/+}$ Apc^{Min} also had a reduced average survival of 12-weeks with an increase in adenoma number but not size. Levels of c-Jun and Nicd1 were also differentially regulated between $Fbxw7^{\Delta/\Delta}$ Apc^{Min} and $Fbxw7^{\Delta/+}$ Apc^{Min}; p-c-Jun, c-Jun and Nicd1 were dramatically increased in $Fbxw7^{\Delta/\Delta}$ Apc^{Min} tumours whereas $Fbxw7^{\Delta/+}$ Apc^{Min} tumours showed an accumulation in Nicd1 and not in c-Jun and p-c-Jun. The authors therefore summarised that *Fbxw7* dose can differentially affect

Notch and c-Jun to influence tumour initiation and progression. It is possible to speculate that homozygous *Fbxw7*-null Apc^{Min} mice have the most severe phenotype, followed by R482Q/+ /Apc^{Min} and then heterozygous *Fbxw7*-null. A controlled experiment directly comparing *Fbxw7*-null and *Fbxw7* propellor-tip mutant models in *Apc*-mutant backgrounds is necessary to assess if R482Q and *Fbxw7*-null mutations result in comparable severities of tumorigenesis.

I can conclude that the R482Q mutation enhances tumorigenesis in conjunction with mutant Apc proteins and that protein levels of Tgif and Klf5 were found to be upregulated in R482Q/+ Apc mutant compound tumours.

Chapter 6

Investigating consequences of *FBXW7* propellor-tip mutations in cell-based systems

6.1 Introduction

Results in Chapter 3 have shown that a heterozygous propellor-tip missense mutation in *Fbxw7* (resulting in R482Q protein) had a severe effect on lung development and this phenotype was not observed in *Fbxw7*-null mutant mice. Results in Chapters 4 and 5 have also shown the R482Q heterozygous mutation enhances intestinal tumorigenesis and it is possible to speculate that this mutation is different to *Fbxw7*-null alleles both in the heterozygous and homozygous state. I wished to further understand the mechanism of action of propellor-tip mutant FBXW7 protein in comparison to wildtype FBXW7 and absence of protein. Here I have taken an *in vitro* approach specifically by using colorectal cancer cell lines.

6.1.1 FBXW7 dimerisation and potential dominant negative effect

As discussed previously, *FBXW7* is mutated in approximately 6% of tumours in a broad range of tissues [1], with a unique mutation spectrum. Mutational hotspots have been identified in the WD40 domain at arginine residues in the propellor blades, which are the points of contact between FBXW7 and the substrates which it degrades. In colorectal cancer, *FBXW7* mutations are frequently mono-allelic propellor-tip missense mutations, showing no loss of heterozygosity [19], suggesting this gene does not function as a standard tumour suppressor through the two-hit mechanism of inactivation [82]. Bi-allelic inactivating mutations are very rare and it remains possible that complete loss-of-function is disadvantageous. I hypothesised that *FBXW7* propellor-tip mutations provide sufficient derangement and a selective advantage and I wished to elucidate the mechanism of action for this.

It has been noted that FBXW7 can act as a dimer [69; 70] and therefore it has been postulated that mutant FBXW7 has the potential to act by a dominant negative mechanism, in which mutant FBXW7 binds and sequesters or inactivates wildtype FBXW7 [1].

FBXW7 binds to itself through a dimerisation domain that has been mapped just upstream of the F-box [69; 70] (see Figure 1.7). Regulation of certain substrates, especially in those with sub-optimal phosphodegrons (CPDs), may require FBXW7 dimerisation possibly functioning by reducing the distance between the substrate and the SCF catalytic site [70]. As it has previously been shown that wildtype FBXW7 can dimerise with itself, I wished to confirm that in the R482Q mouse model, propellor-tip R482Q mutant Fbxw7 was also capable of directly interacting with wildtype Fbxw7.

6.1.2 Distinguishing *FBXW7* propellor-tip mutations from *FBXW7*-null setting

Several studies, using various *in vitro* systems, have been carried out to study the consequences of *FBXW7*-null. A selection of these studies are briefly summarised below.

Koepp *et al* [53] reported a reduction in cyclin E protein level when transfecting 293T cells with pCMV-cyclin E and pCMV-FBXW7 tagged plasmids. Conversely, an elevated level of cyclin E protein was detected following small-interfering RNA (siRNA) knockdown of *FBXW7* [53]. It was additionally reported that retroviral knockdown of *FBXW7* in HEK 293T resulted in expression of cyclin E at inappropriate times in the cell cycle, for example in telophase cells [97]. This was assessed by cyclin E immunofluorescence (using cyclin A as a control for proliferative state) and flow cytometry analysis of cyclin E and propidium iodide to assess DNA content and thus cell cycle stage.

siRNA has been used as a tool to knockdown expression of *FBXW7* mRNA in a human salivary gland cell line by Rajagopalan *et al* [18]. Although in this study only 40% knockdown of mRNA expression was achieved, both elevated cyclin E and micronuclei formation were noted. By conducting experiments in which cyclin E protein was overexpressed, similar micronuclei formation was observed and thus the authors concluded that chromosomal instability in *FBXW7* knockdown cells resulted from cyclin E over-abundance.

To investigate the functional effect of FBXW7 protein absence in colorectal cells, a study was carried out in which homologous recombination disrupted both alleles of *FBXW7* in HCT116, a colorectal carcinoma cell line [18]. In this cell line, which was now effectively *FBXW7*-null, an elevated level of cyclin E was detected. This cell line had normal growth compared with the parental HCT116 cell line, although cytological abnormalities, including micronuclei and an increased formation of multipolar

spindles were identified. These features resulted in misalignment and segregation of chromosomes in mitosis and therefore CIN.

These studies all demonstrate the consequences of loss of FBXW7, mostly by analysing cyclin E abundance; there are many other FBXW7 substrates which have yet to have been fully explored. It is important to reiterate that *FBXW7* mutations which result in null FBXW7 (absence of FBXW7 protein) occur much less frequently than missense propellor-tip mutations in human cancer. Less literature is available focusing on the functional effect of missense propellor-tip mutant FBXW7. Fujii *et al* [120] conducted experiments in which protein levels of several substrates (cyclin E, c-Myc and Aurora A) were assessed in a panel of cell lines with and without *FBXW7* mutations. The *FBXW7* mutant cell lines used were as follows; SUM149PT (breast; nonsense mutation within WD40 repeats), MDAH2774 (ovarian; nonsense mutation, terminated before F-box domain, effectively null), SKOV3 (ovarian; R505L missense mutation) and CCRF-CEM (lymphoid; R465C missense mutation). Aurora A, c-Myc and cyclin E were elevated to varying degrees in the mutant cell lines and overexpression of wildtype FBXW7 subsequently reduced these substrate levels. The authors conducted short-hairpin RNA (shRNA) knockdown experiments of each of the three substrates independently in *FBXW7*-mutant cell lines and deduced that all three substrates were required for efficient proliferation and anchorage-independent growth. No colorectal cancer cell lines were analysed in this panel and the authors did not make the distinction between different categories of *FBXW7* mutations.

Iwatsuki *et al* [212] performed siRNA knockdown of *FBXW7* in colorectal LOVO (FBXW7 propellor-tip mutant) and colo201 (FBXW7 wildtype) cells, showing elevated cyclin E and c-Myc protein levels in both lines, as well as increased proliferation. The authors did not attempt to distinguish differential effects between these wildtype and propellor-tip mutant cell lines.

In another study using the *FBXW7*-null HCT116 cell line developed by Ra-

jagopalan *et al* [18], a series of transient transfections with tagged propellor-tip missense mutant overexpression plasmids were carried out [1]. When co-expressing wildtype FBXW7 with mutant R465C or R479Q FBXW7, alongside an overexpressing cyclin E plasmid, an accumulation of cyclin E was found in comparison to co-expression of wildtype FBXW7 and cyclin E plasmids alone. Elevated levels of cyclin E in cells in which both wildtype/mutant FBXW7 were expressed suggested that a dominant negative effect was observed. Cycloheximide-chase experiments revealed that elevated levels of cyclin E were a consequence of increased protein half life and thus stability. However, it is important to note that in this study, even extreme over-expression of propellor-tip mutant FBXW7 did not cause cyclin E levels close to those obtained in a null system, bringing into question the extent of the dominant negative effect observed.

I wished to conduct a more systematic study of *FBXW7* propellor-tip mutations in colorectal cell lines in an attempt to ascertain whether is it preferable to retain propellor-tip mutant FBXW7 protein over complete absence of FBXW7 protein. Propellor-tip mutant FBXW7 protein may not be preferable, just functionally similar to absence of FBXW7 protein (FBXW7-null) and simply occur at a higher incidence as it is less difficult to acquire one hit mutation in *FBXW7* than it is to have two hits.

6.2 Aims of chapter

The overall aim of this chapter was to investigate the mechanism of *FBXW7* propellor-tip mutations using *in vitro* systems. Specific aims included:

- Confirmation that murine Fbxw7 wildtype and R482Q mutant proteins can interact by generating appropriately-tagged mouse constructs in mammalian expression systems and conducting co-immunoprecipitation experiments.

  - If dimerisation was confirmed between Fbxw7 wildtype and Fbxw7 propellor-tip mutant (R482Q) protein, further investigation of any evidence that Fbxw7 R482Q acts in a dominant negative fashion.

- shRNA knockdown of *FBXW7* in colorectal cancer cell lines with *FBXW7* propellor-tip mutations (to generate effectively '*FBXW7*-null' cells).
  - Comparison of *FBXW7*-knockdown cells with parental *FBXW7* propellor-tip missense mutant cells.

- Overexpression of wildtype FBXW7 protein in *FBXW7*-mutant colorectal cancer cell lines in order to assess regulation of FBXW7 substrate abundance.

6.3 Results

6.3.1 Cell-based system to test Fbxw7 wildtype and R482Q dimerisation and potential dominant negative effect

The aim was to generate appropriately-tagged mammalian expression plasmids that contained either murine wildtype or mutant (R482Q) full length *Fbxw7* cDNA. The aim was to subsequently co-express these plasmids in appropriate cell lines to assess if wildtype and propellor-tip mutant Fbxw7 were capable of interacting to form dimers.

6.3.1.1 Generation of tagged Fbxw7 wildtype and R482Q mutant mammalian expression vectors

pCMV-HA and pCMV-Myc mammalian expression plasmids (Clontech) were selected in order to clone the cDNA of interest fused to either a haemagglutinin (HA) or c-Myc N-terminal epitope tag. The key features of these plasmids are shown in Figure 6.1. c-Myc and HA are well-characterised and highly immunoreactive tags. They are

also relatively small and unlikely to interfere with protein function. Both vectors use the CMV promoter for constitutive, high-level expression. As c-Myc is a substrate of Fbxw7, it is important to note that the c-Myc epitope tag is distinct from the native CPD recognition site (Section 1.3.4). Also the c-Myc antibody used to detect the c-Myc tag was reported not to detect endogenous c-Myc.

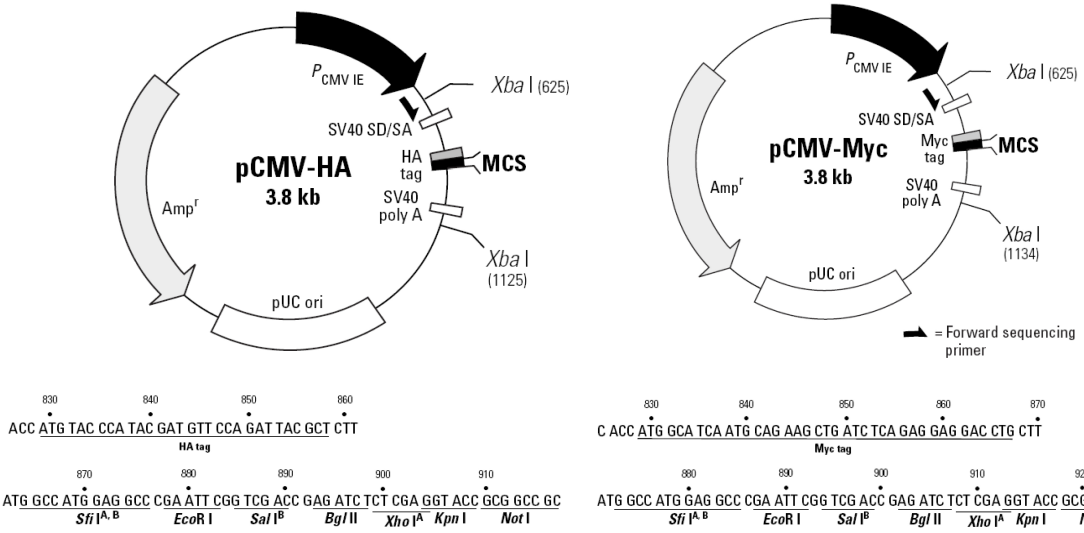


Figure 6.1: Restriction map of pCMV-HA and pCMV-Myc plasmids. Key features include; P CMV IE: Human cytomegalovirus immediate/early promoter and enhancer, SV40 splice donor/acceptor site, MCS (multiple cloning site), polyadenylation signal from SV40 and the ampicillin resistance gene for selection in *E.coli*.

Primers were designed to amplify full length *Fbxw7* cDNA and allow cloning into SalI and KpnI restriction sites in the MCS. The annotated sequences of these primers are shown in Figure 6.2a. The SalI restriction site sequence was added to the 5' end of the forward primer sequence with an extra base pair in between to ensure the correct ORF. Extra base pairs were included prior to the restriction site sequence to ensure an intact restriction site was amplified. The reverse primer sequence included a KpnI restriction site sequence.

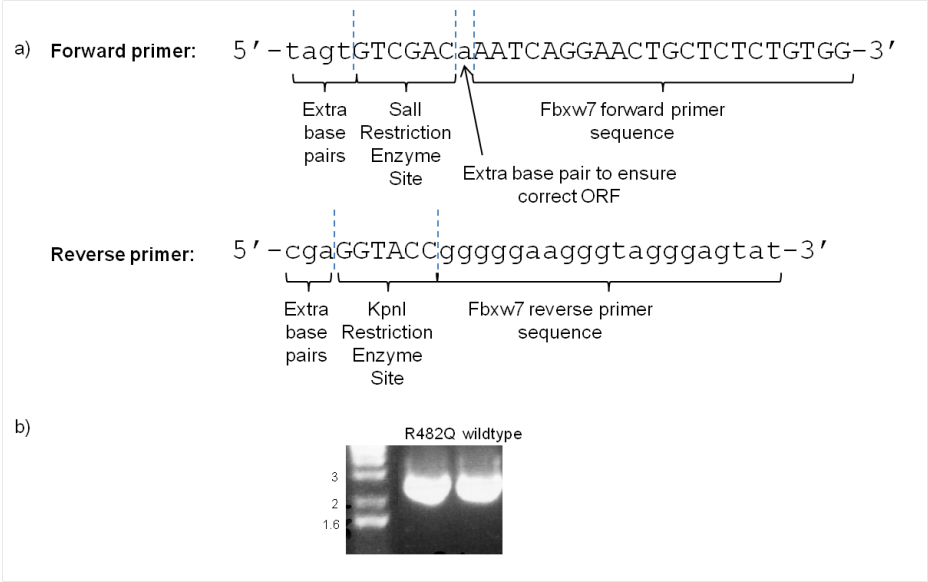


Figure 6.2: Amplification of *Fbxw7* R482Q and wildtype cDNA. a) Annotated primers used for amplification of wildtype and mutant Fbxw7 cDNA. SalI and KpnI restriction sites were added to the appropriate primers to allow subsequent cloning into pCMV-Myc and pCMV-HA expression vectors. b) Amplified Fbxw7 PCR product, size 2.2 kb. cDNA used as starting material was extracted from E12.5 embryos. A DNA ladder was run alongside samples with known band sizes shown in kb.

RNA was extracted from E12.5 R482Q and wildtype embryos (Chapter 3), DNase treated and reverse transcribed into cDNA. This cDNA was used in a long-range PCR reaction with the primers shown in Figure 6.2a, to give a product size of 2.2 kb, which contains the complete Fbxw7 translated region (Figure 6.2b). Note that wildtype and mutant *Fbxw7* amplification products were of identical size, as expected, consistent with a missense mutation. Wildtype and mutant *Fbxw7* cDNAs were cloned into KpnI and SalI restriction sites of pCMV-Myc and pCMV-HA plasmids respectively.

All correct clones were carefully sequenced for *Fbxw7* (using sequencing primers detailed in Table 2.3), to ensure there were no PCR mutations, as well as to confirm the presence of the G1445A (R482Q) mutation in the pCMV-HA vector. Figure 6.3 shows a C**G**A codon (arginine) was present in the wildtype sequence and a C**A**A codon (glutamine) was present in the mutant sequence.

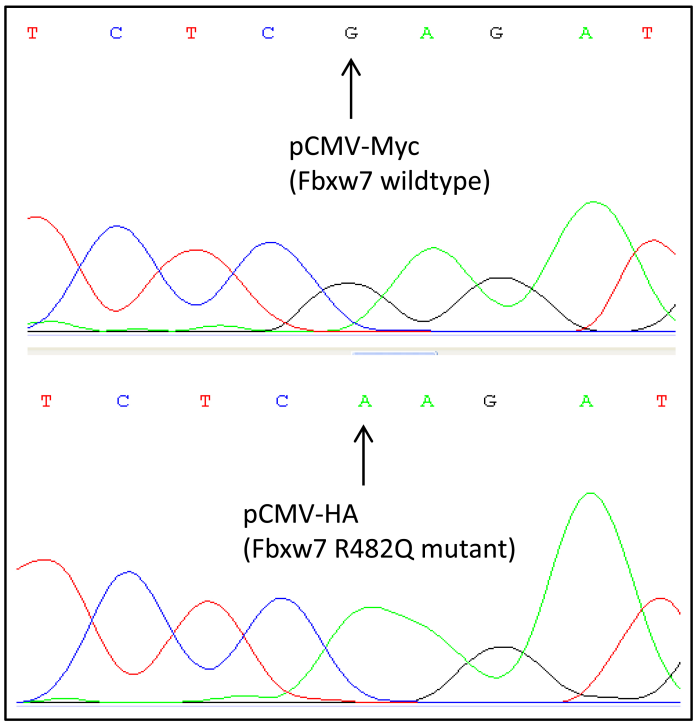


Figure 6.3: *Fbxw7* R482Q mutation in pCMV-HA Fbxw7 R482Q plasmid. PCR products were amplified from plasmids using primers detailed in Table 2.3 and subsequently sequenced and analysed with the ApE programme. Arrows highlight the G to A bp change (G1445A) causing the R482Q mutation.

Initially, NIH3T3 mouse fibroblast cells were transiently transfected with pCMV-HA and pCMV-Myc Fbxw7 plasmids, as well as a GFP-expressing control plasmid, pEGFP-C3 (Clontech) to assess transfection efficiency. Only low levels of GFP-fluorescence were detected in NIH3T3 cells co-transfected with the GFP control plasmid indicating a low transfection efficiency (Figure 6.4). Despite attempting to optimise transfection efficiency by altering cell density, lipid concentration and lipid to DNA ratio, an acceptable level of transfection was not achieved using this cell line. Other mouse cell lines (colo26, MC38, MC26) gave similar results. I then attempted to transfect a human colorectal cancer cell line (RKO) which I had previously transfected successfully, in order to identify if the root of the problem was due to the cell lines or the plasmids themselves. When using RKO cells, approximately 70% were transfected successfully, assessed by GFP-fluorescence in cells co-transfected with a

GFP plasmid (Figure 6.4).

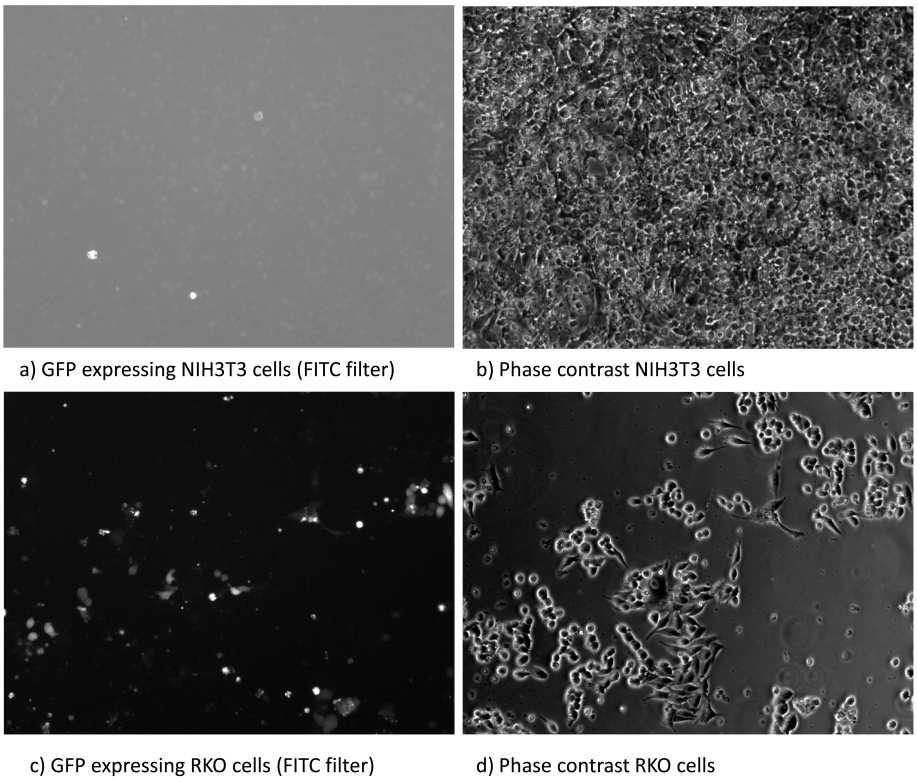


Figure 6.4: Efficient transfection of RKO but not NIH3T3 cells. Transfection efficiencies were assessed by co-transfection of the GFP-expressing plasmid pEGFP-C3. a) Positively transfected NIH3T3 cells were detected by GFP-fluorescence (FITC filter). b) Phase contract image showing total NIH3T3 cell number. A low percentage of NIH3T3 were successfully transfected. c) Positively transfected RKO cells were detected by GFP fluorescence (FITC filter). d) Phase contrast image showing total RKO cell number. Approximately 70% of RKO cells were successfully transfected.

qRT-PCR analysis was carried out on cDNA derived from cells collected 72 h post-transfection to assess for elevated *FBXW7* mRNA expression. Analysis showed a drastic increase (20-30 fold) in *Fbxw7* mRNA in comparison to cells treated with only the lipid reagent (Figure 6.5). Control cells were treated with the lipid reagent rather than left untreated, as cell toxicity may result from the transfection reaction.

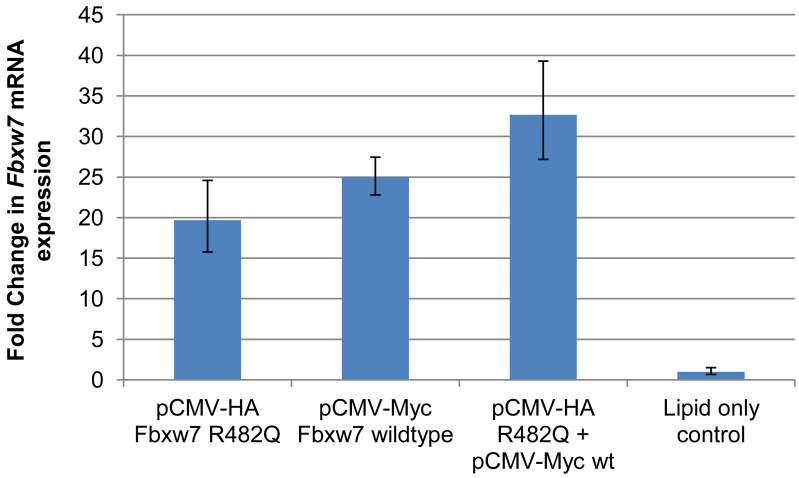


Figure 6.5: Elevated *Fbxw7* mRNA expression in RKO cells following transient transfection of pCMV-HA Fbxw7 and pCMV-Myc Fbxw7 plasmids. Fold change in mRNA expression measured by qRT-PCR using mouse *Fbxw7* probe and human *GAPDH* to normalise samples. Cells were collected 72 h post-transfection and RNA was DNase-treated prior to reverse transcription to generate cDNA. Biological triplicates were run. Error bars represent the SEM.

Cells were also collected 72 h post-transfection to test detection of the epitope-tags via western blot with HA and Myc antibodies (Clontech). Cells transfected with the pCMV-HA Fbxw7 R482Q plasmid failed to show a band of the appropriate size by western blot when probed with HA antibodies (Clontech and Roche). The HA epitope tag was sequenced (primers details shown in Table 2.3) and was intact and accurate. The HA-tag could have destabilised the Fbxw7 protein and led to its degradation. Alternatively, the HA antibodies used may have been ineffective in detecting the HA-epitope tag.

In order to proceed, I decided to remove the HA-tag and replace it with a FLAG-tag. To do this, the pCMV-HA Fbxw7 R482Q plasmid was digested with restriction enzymes ApaI and KpnI, removing both the HA-tag and the Fbxw7 R482Q insert. Fbxw7 cDNA was re-amplified using a new forward primer which included a 3x FLAG in its sequence (the same reverse primer was used). Figure 6.6 shows the annotated forward primer sequence. The PCR product was re-ligated into ApaI and KpnI sites in the digested pCMV-HA plasmid. Sequencing of resultant clones identified

one PCR mutation in all samples, which was rectified by site-directed mutagenesis (section 2.8.2). The corrected plasmid shall now be referred to as pCMV-FLAG Fbxw7 R482Q.

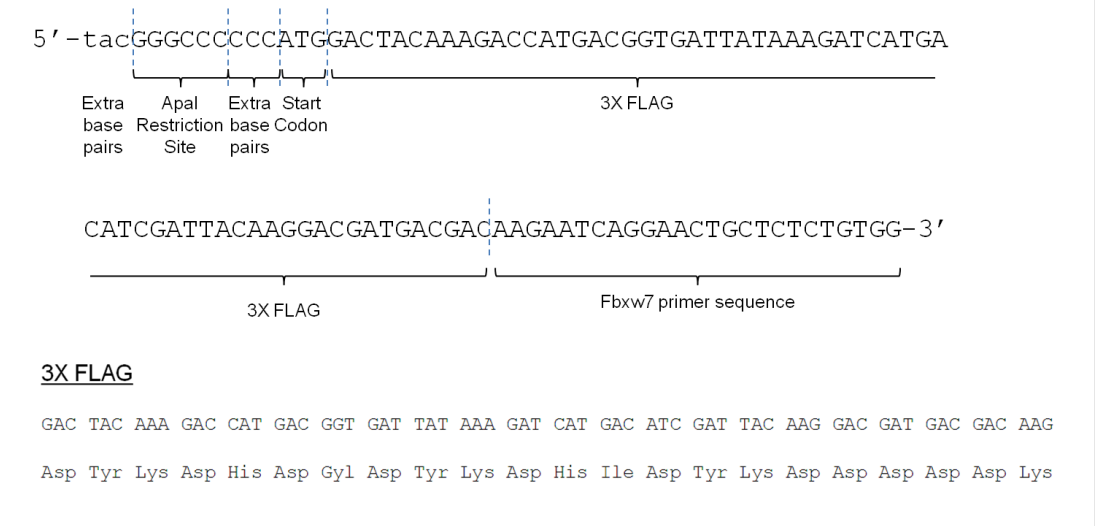


Figure 6.6: Forward primer for amplification of Fbxw7 R482Q cDNA with an N-terminal FLAG tag. ApaI restriction enzyme site was added to the 5' end of primer to allow subsequent cloning into pCMV-HA plasmid. The residues encoded by the 3x FLAG tag are indicated.

pCMV-FLAG Fbxw7 R482Q and pCMV-Myc Fbxw7 wildtype plasmids were co-transfected into RKO cells and FLAG (Sigma) and Myc (Clontech) antibodies were tested by western blot 72 h post-transfection. Proteins of approximately 100 kDa were detected by FLAG and Myc antibodies, confirming their suitability for detection of the epitope tags (Figure 6.7).

6.3.1.2 Fbxw7 R482Q and wildtype interaction

Both FLAG and Myc co-immunoprecipitation experiments were conducted on transiently transfected RKO cells in order to assess Fbxw7 R482Q and Fbxw7 wildtype interaction (Figure 6.8). When co-immunoprecipitating proteins with the FLAG antibody in cells which had been co-transfected with both pCMV-FLAG Fbxw7 R482Q and pCMV-Myc Fbxw7 wildtype plasmids, Myc-tagged Fbxw7 was detected, high-

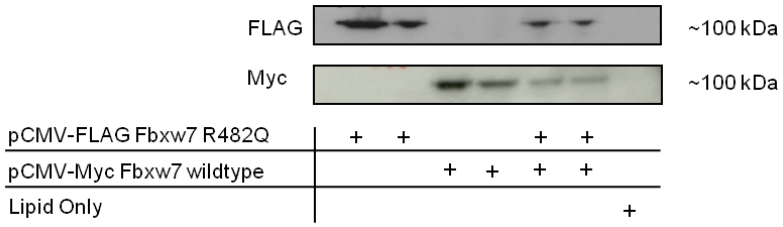


Figure 6.7: FLAG and Myc-tagged Fbxw7 detected in RKO cells. Western blot run on cells 72 h post-transfection of pCMV-FLAG Fbxw7 R482Q and pCMV-Myc Fbxw7 wildtype plasmids. FLAG antibody detects FLAG-tagged Fbxw7 protein in cells transfected with pCMV-FLAG Fbxw7 R482Q plasmid at a size of approximately 100 kDa. Myc antibody detects Myc-tagged Fbxw7 in cells transfected with pCMV-FLAG Fbxw7 plasmid at a size of approximately 100 kDa. Both tags were detected in cells co-transfected with both plasmids. As expected, no bands were observed in cells transfected with only the lipid reagent and no plasmid DNA, this confirmed the Myc antibody does not detect endogenous c-Myc (as reported).

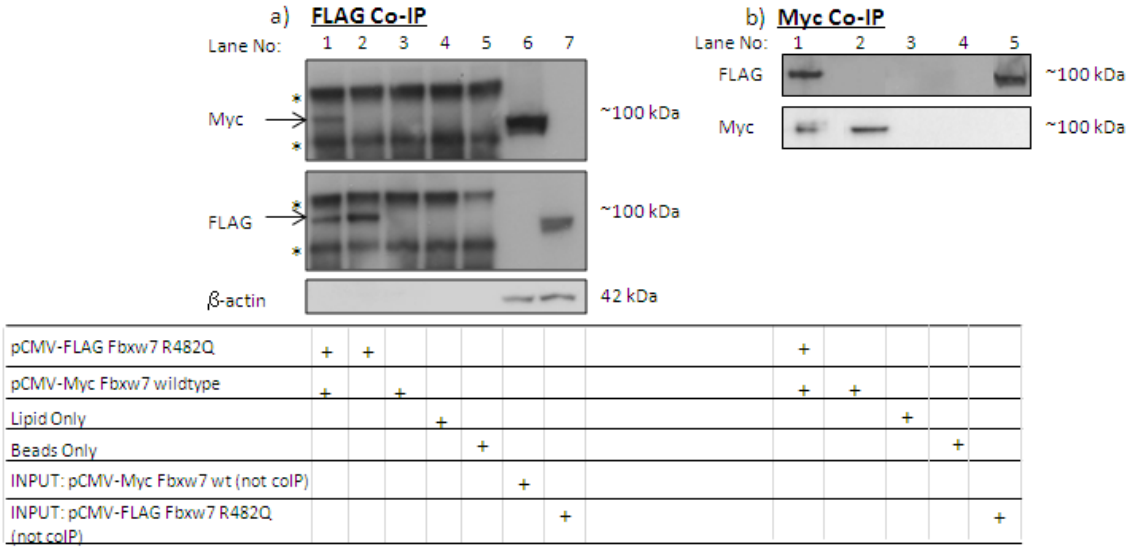


Figure 6.8: Interaction of wildtype and R482Q Fbxw7 protein. a) FLAG co-IP of RKO cells transiently transfected with pCMV-FLAG Fbxw7 R482Q and pCMV-Myc Fbxw7 wildtype plasmids. Asterisks denote non-specific bands. In lane 1, cells were transfected with both plasmids and FLAG co-immunoprecipitation identifies Myc-tagged Fbxw7, indicating that R482Q mutant and wildtype Fbxw7 proteins interact. b) Myc co-IP of RKO cells transiently transfected with pCMV-FLAG Fbxw7 R482Q and pCMV-Myc Fbxw7 wildtype plasmids. Lane 1 shows that Myc co-IP in cells transfected with both plasmids identified FLAG-tagged Fbxw7, re-confirming that Fbxw7 wildtype and Fbxw7 R482Q protein interact.

lighting that Fbxw7 R482Q mutant protein interacts with Fbxw7 wildtype protein (Figure 6.8a, lane 1). In lane 2, cells were transfected only with pCMV-FLAG Fbxw7 mutant plasmid, so that co-immunoprecipitating proteins with FLAG antibody only detected FLAG-tagged protein and not Myc-tagged protein, as expected. In lane 3, cells were transfected only with pCMV-Myc Fbxw7 wildtype plasmid and as expected no FLAG-tagged or Myc-tagged proteins were precipitated by FLAG co-IP. Lanes 4 and 5 show no tagged proteins detected in lipid reagent and beads only controls. Lane 6 was a positive control for the Myc antibody in cells transfected with pCMV-Myc Fbxw7 plasmid and lane 7 shows a positive control for the FLAG antibody in cells transfected with pCMV-FLAG Fbxw7 plasmid. The β-actin control was only detected in lanes 6 and 7, in those samples that were not co-immunoprecipitated, as β-actin does not interact with Fbxw7. Note the detection of background bands present in all FLAG co-immunoprecipitated samples. The origin of these bands remains unclear, although they could represent non-specific binding to the FLAG antibody, or impurities or immunoglobulins as a result of immunoprecipitation.

When co-immunoprecipitating proteins with the Myc antibody in cells which had been co-transfected with both plasmids, FLAG-tagged Fbxw7 protein was detected (Figure 6.8b, lane 1), re-confirming interaction of Fbxw7 wildtype and Fbxw7 R482Q protein.

6.3.1.3 Assessment of dominant negative effect of propellor-tip mutant Fbxw7

I wished to determine whether the propellor-tip mutant protein exerted a dominant negative effect when both Fbxw7 wildtype and R482Q were co-transfected. To this end, I assessed the protein levels of selected FBXW7 substrates (NICD1, cyclin E and TGIF) in RKO cells, 72 h post-transfection. Figure 6.9 shows there were no significant differences in protein levels of NICD1, cyclin E and TGIF between cells transfected

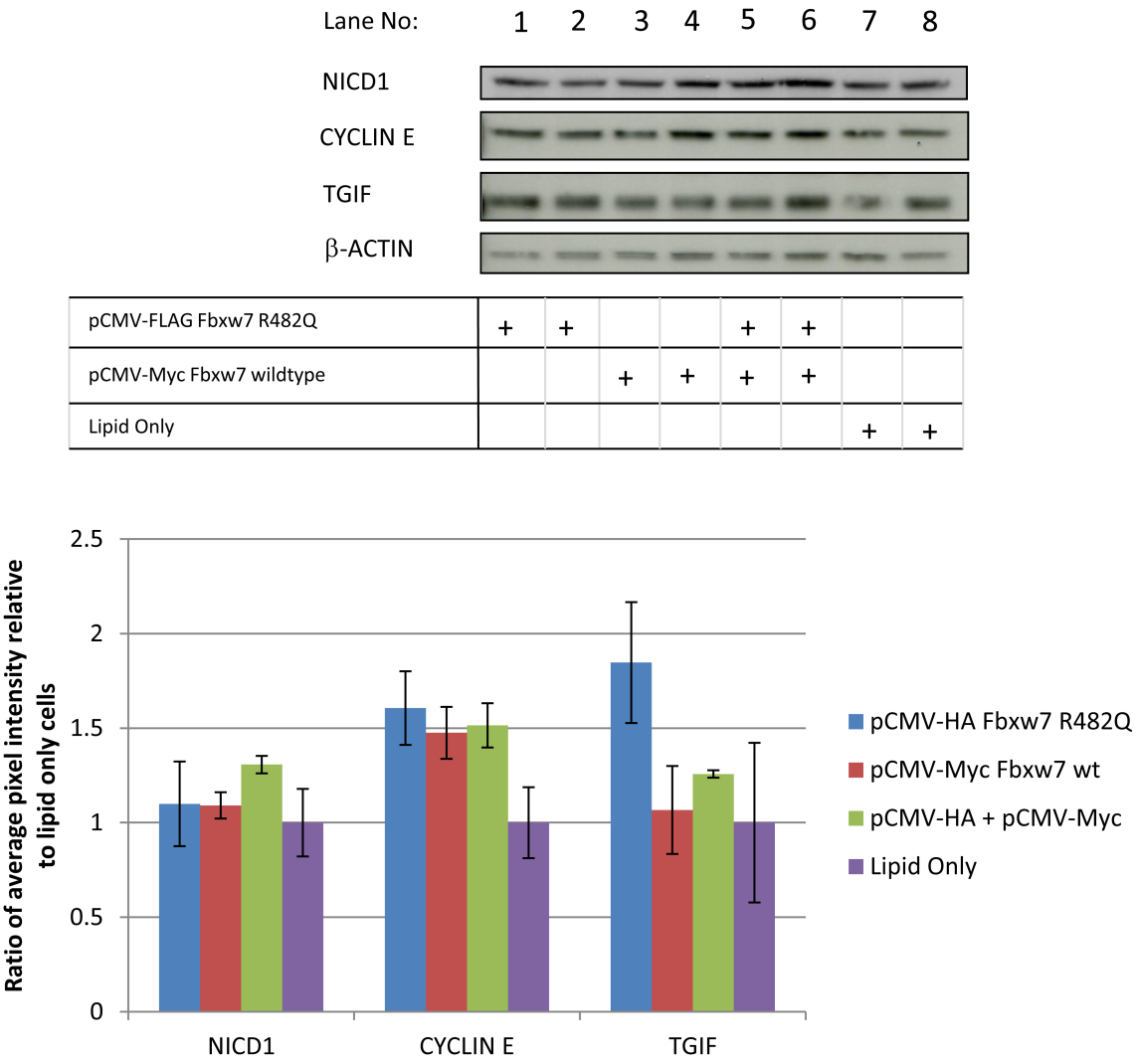


Figure 6.9: No significant changes in NICD1, cyclin E and TGIF protein levels were seen in RKO cells overexpressing Fbxw7 R482Q and wildtype plasmids, as assessed by western blot. Cells analysed 72 h post-transfection. Cells in lanes 1-2 were transfected with pCMV-FLAG Fbxw7 R482Q, lanes 3-4 with pCMV-Myc Fbxw7, lanes 5-6 with both plasmids and lanes 7-8 with the lipid reagent only (no plasmids). Transfection efficiency was determined by assessing *Fbxw7* mRNA expression, shown in Figure 6.5. Western blots were quantified and the ratio of average pixel intensities relative to cells transfected with lipid only are shown in the graph. Error bars represent the SEM. $p>0.05$ in all cases, Student t-test.

with either or both plasmids, $p>0.05$ in all cases (Student t-test). This could suggest Fbxw7 R482Q does not alter protein levels of the selected substrates, possibly due to multiple factors, including the presence of other endogenous ubitiquitin ligases that can regulate protein degradation in these cells. *In vivo* studies described in Chapters 4 and 5 suggested that cyclin E and NICD1 were not critical substrates in the intestine, however, in these studies TGIF was found to be deregulated by R482Q protein. These data could imply that Fbxw7 R482Q does not exert a dominant negative effect, or that overexpressing Fbxw7 does not alter substrate levels to a greater extent than endogenous Fbxw7. Although there is 96% identity between human and mouse Fbxw7 protein (Appendix C.1), as mouse proteins were expressed in a human cell line, these results must be treated with caution. I therefore did not assess further the potential dominant negative effect of the Fbxw7 R482Q mutant using this system.

6.3.2 Targeted *FBXW7* shRNA knockdown in colorectal cancer cell lines

I conducted a preliminary screen of TGIF, one of the most interesting FBXW7 substrates that arose from *in vivo* work reported in Chapters 3-5, by western blot in a panel of colorectal cancer cell lines with propellor-tip missense mutations, non propellor-tip mutations and wildtype *FBXW7* (Figure 6.10).

TGIF levels were very variable both within and between mutation categories. This could be explained by many factors altering TGIF mRNA and protein transcription and translation and by differing abundance of regulatory factors including protein kinases and other ubiquitin ligases between cell lines.

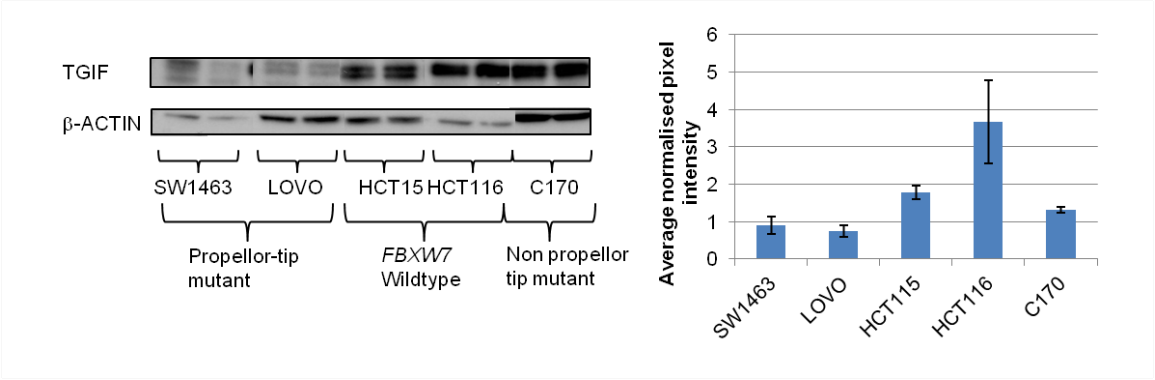


Figure 6.10: Variable TGIF protein levels in a panel of CRC cell lines assayed by western blot. The graph shows average pixel intensities, normalised to β-actin control. Error bars represent the SEM.

To create a system that allows more accurate comparison of null and mutant propellor-tip *FBXW7* cell lines, I aimed to knockdown *FBXW7* using stable lentiviral shRNA in cells from colorectal cancer cell lines with propellor-tip mutations. Direct comparison of the *FBXW7* shRNA knocked-down cells (effectively FBXW7-null) could be conducted with parental *FBXW7* mutant cells. These tools could be then used to study the effects of *FBXW7* propellor-tip mutations on endogenous substrate levels instead of using overexpression of substrates at non-physiological levels, as many previous studies have reported.

6.3.2.1 Colorectal cancer cell lines with *FBXW7* mutations

Our laboratory sequenced an extensive panel of colorectal cancer cell lines for *FBXW7* mutations [19] and both LOVO and SW1363 were identified as *FBXW7* mutants. I confirmed the presence and nature *FBXW7* mutations in these lines (Figure 6.11): LOVO, a hyperdiploid (49) cell line, which is MSI positive, carries a heterozygous propellor-tip missense (R505C) mutation and also carries *APC*, *KRAS* and *MSH2* mutations (COSMIC ID 907790). SW1463, an MSI-negative hypertriploid cell line [244], carries a heterozygous propellor-tip missense (R479Q) as well as *APC*, *KRAS* and *TP53* mutations (COSMIC ID 909748).

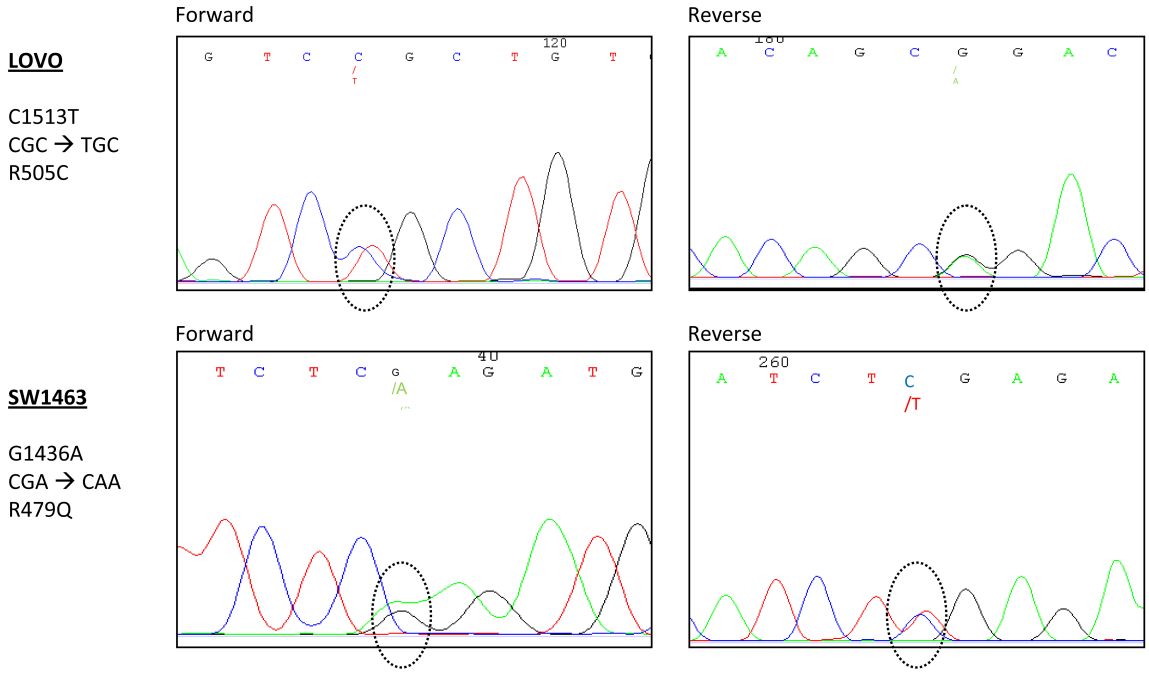


Figure 6.11: *FBXW7* mutations in LOVO and SW1463 cells. PCR products were amplified using primers detailed in Table 2.3. Products were then sequenced and analysed using ApE programme. The chromatograms show the R505C heterozygous mutation in LOVO cells and R479Q heterozygous mutation in SW1463 cells.

6.3.2.2 Testing *FBXW7* shRNA efficiency by transient transfection

pLKO.1 lentiviral constructs (clones 5, 6, 7 and 8) expressing shRNA to human *FBXW7* (Open Biosystems) were amplified (section 2.7) and tested by transient transfection in LOVO cells. Each clone targets a different exon (Table 2.7) of *FBXW7*, although all clones target the common exons of *FBXW7*, thereby affecting all isoforms. 72 h post-transfection, DNase-treated RNA was reverse transcribed to generate cDNA, which was then assayed by qRT-PCR to determine *FBXW7* mRNA expression. Figure 6.12 shows that shRNA clones resulted in 30-55% knockdown of *FBXW7* expression levels.

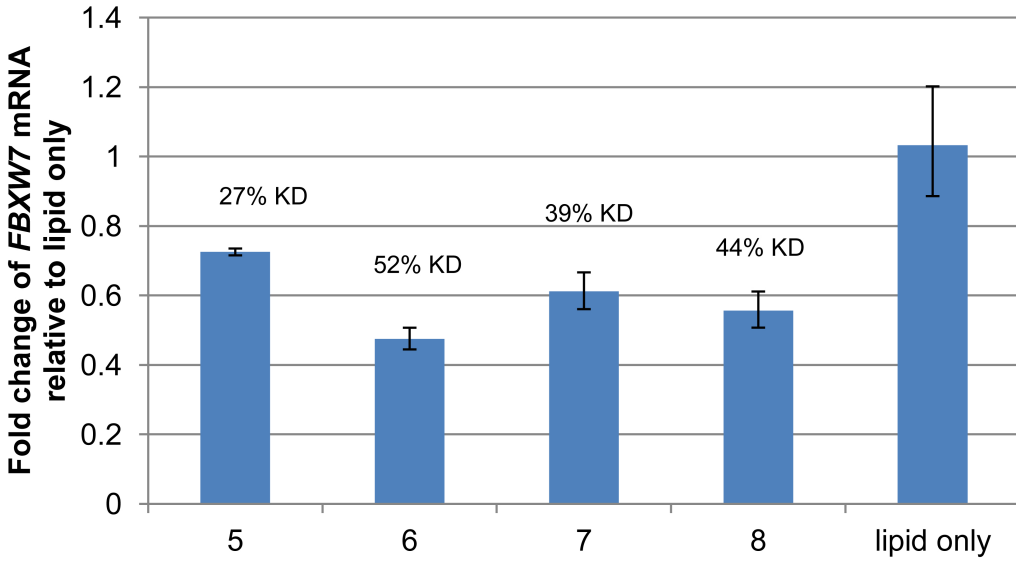


Figure 6.12: shRNA-mediated knockdown of *FBXW7* mRNA expression in transiently transfected LOVO cells, analysed 72 h post-transfection by qRT-PCR using TaqMan probes shown in Table 2.4. Expression was normalised using *GAPDH* and calculated relative to cells transfected with the lipid reagent only. The error bars represent the SEM. Each clone was run in triplicate. Percentage knockdown of *FBXW7* mRNA expression are stated (relative to cells transfected with lipid reagent only).

6.3.2.3 Comparison of *FBXW7* shRNA knocked-down and *FBXW7* propellor-tip mutant cells

As previous studies have reported downstream effects observed in cases of 40% *FBXW7* knockdown [18], I proceeded to package lentiviral particles for all four clones, as well as a shRNA non-targeting scramble control (Sigma-Aldrich), using a PEI transfection method (section 2.7.1). The non-targeting scramble control has a short hairpin sequence that does not match any known human or mouse gene. Titration of virus particles was performed using a p24 ELISA (section 2.7.2). LOVO and SW1463 cells were transduced, selected with puromycin (Sigma-Aldrich) and grown for four cell passages prior to confirmation of *FBXW7* mRNA expression knockdown by qRT-PCR. Figure 6.13 shows that LOVO clones 6 and 7 achieved 75% and 67% knockdown respectively and SW1463 clones 7 and 8 achieved 82% and 73% knockdown respectively. *FBXW7* mRNA expression levels in parental SW1463 cells were lower than

those in LOVO cells. This could be due to endogenous regulation of *FBXW7* in SW1463 cells, for example by presence of microRNAs (it has been recently reported *FBXW7* is targeted by miR-223 and miR-27a [158; 160]).

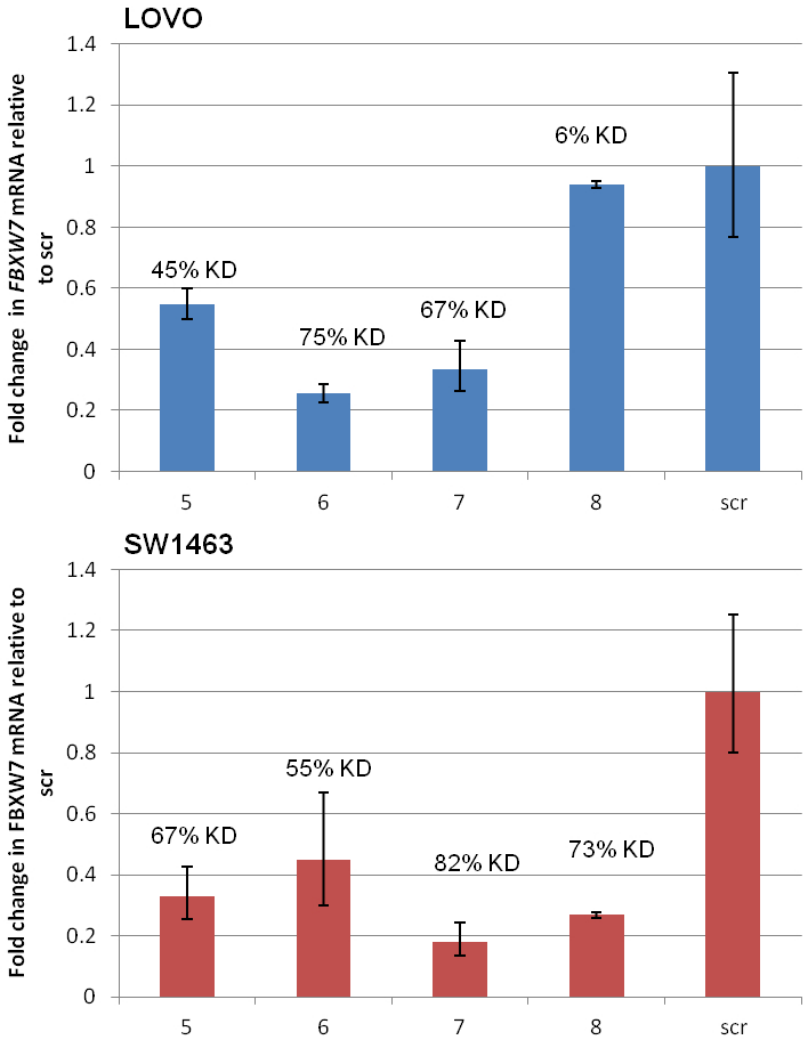


Figure 6.13: shRNA-mediated knockdown of *FBXW7* mRNA expression in LOVO and SW1463 cells. Analysed by qRT-PCR using TaqMan probes shown in Table 2.4, CT values were normalised to shRNA scramble cells. The error bars represent the SEM. All samples were run in triplicate. Percentage knockdown of *FBXW7* mRNA expression relative to scramble cells are stated.

It would have been preferable to additionally check the knockdown of FBXW7 protein level by western blot, but I tested several FBXW7 antibodies on parental cell lines and scramble control cells (Abcam, Abnova, Orbigen, Invitrogen, Thermo Scientific) and none worked successfully.

The identified clones were expanded and cells were collected to perform western blots on selected FBXW7 substrates to ascertain whether *FBXW7* shRNA knockdown (effectively rendering the cells FBXW7-null) caused a differential effect on protein abundance of substrates compared with propellor-tip FBXW7 mutant protein (Figure 6.15). Unfortunately, SW1463 clone 8 failed to grow and therefore only clone 7 underwent further analysis.

I wished to assess if *FBXW7* shRNA knocked-down cells exhibited an alteration in proliferation rate. Figure 6.14 shows there was no significant difference in the proliferation of shRNA knockdown or scramble control cells in one clone of both LOVO and SW1463 (p=0.600 and p=0.351 respectively, Student t-tests) assessed using an MTT proliferation assay.

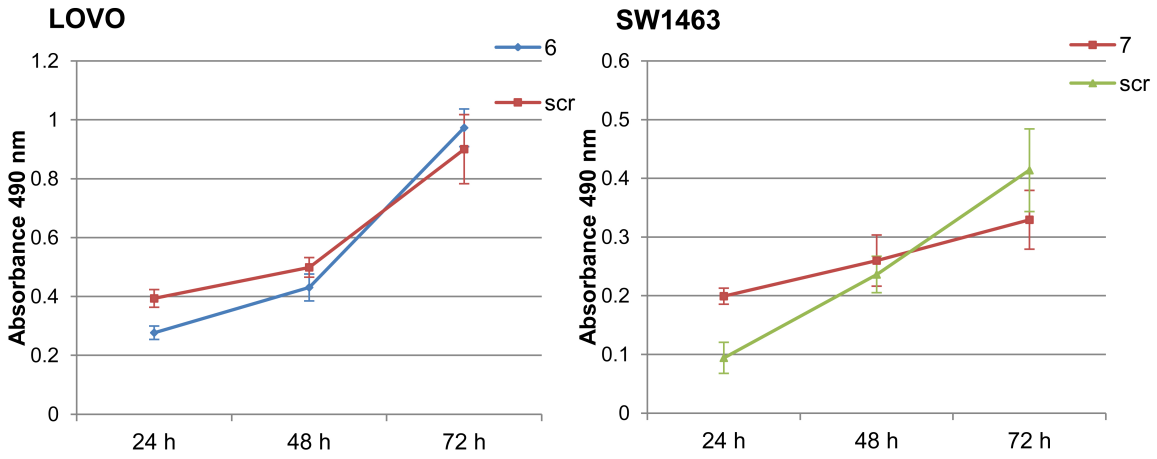


Figure 6.14: Unaltered cell proliferation in *FBXW7* shRNA knocked-down LOVO and SW1463 cells. shRNA knockdown cells were assayed with the CellTiter 96 aqueous one solution cell proliferation assay at 24, 48 and 72 h. The error bars represent the SEM. Assays were repeated in three independent experiments.

With *FBXW7* shRNA knockdown cells, one might expect the levels of FBXW7 substrates to be elevated in comparison to the scrambled control as FBXW7 is involved in the ubiquitination and degradation of its substrates. Hence, with lower levels of FBXW7 protein present, the substrates of FBXW7 may accumulate. In the LOVO experiment, the only substrate for which this was the case was c-Myc (clone

6), but this result was not confirmed with clone 7 and I therefore considered this to be an artefact (Figure 6.15). In SW1463 cells, cyclin E was elevated (less than 1.5 fold change) in comparison to the scramble control but this increase was not statistically significant (p=0.366, Student t-test). As work in Chapter 4 demonstrates, it is unclear whether cyclin E is a critical FBXW7 substrate in colorectal cells.

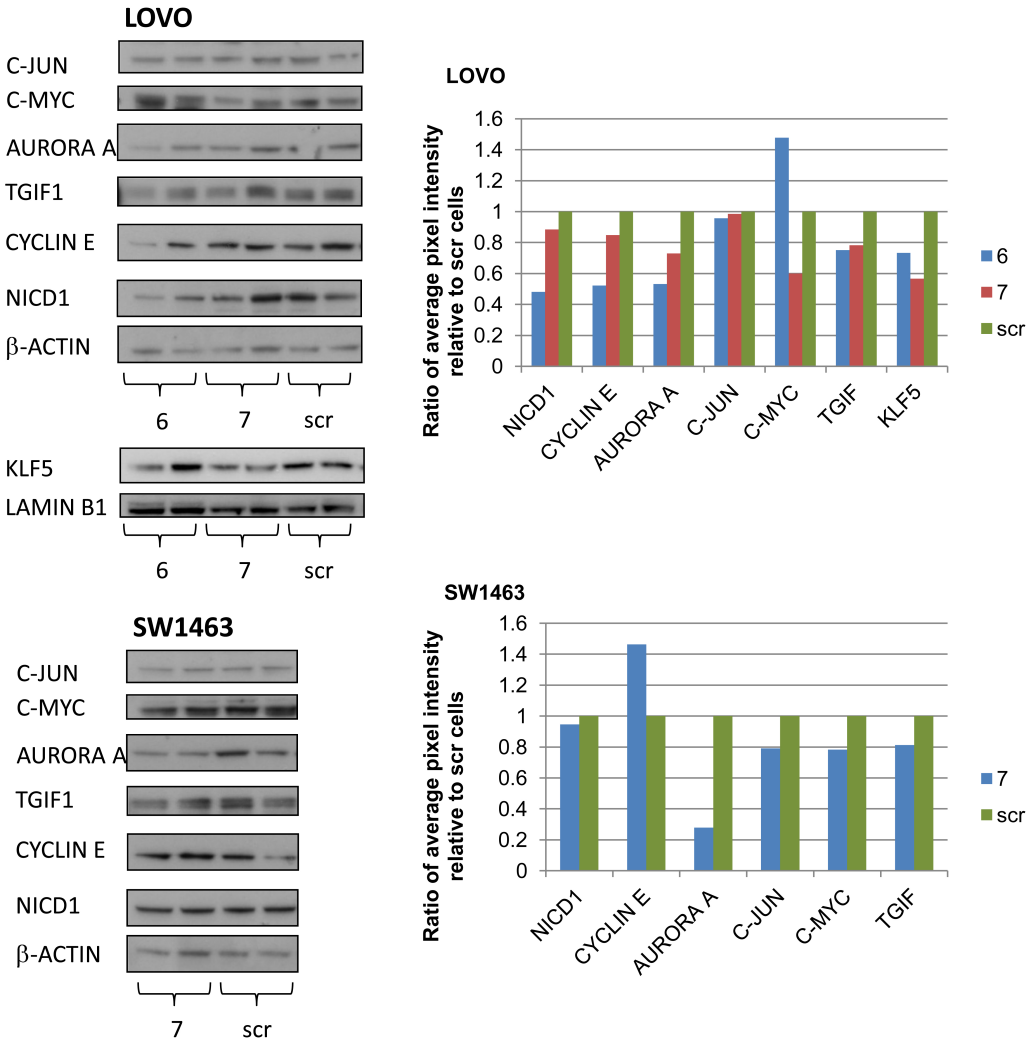


Figure 6.15: No significant differences in protein levels of FBXW7 substrates between *FBXW7* shRNA knocked-down and propellor-tip mutant parental LOVO and SW1463 cells, as assayed by western blot (p>0.05 in all cases, Student t-tests). Antibody details are summarised in Table 2.6. The graphs show the ratio of normalised pixel intensities (using β-actin as the loading control, or Lamin B1 in the case of KLF5), relative to the scramble control cells.

To summarise, no significant differences in the protein levels of any the FBXW7

substrates assayed, nor any changes in proliferation were observed between *FBXW7* shRNA knocked-down and parental propellor-tip mutant cells. It is possible that I was unable to achieve sufficient knockdown of FBXW7 at a protein level (unable to assess). Alternatively, it is plausible that I was able to knockdown FBXW7 protein levels, but in propellor-tip FBXW7 mutant cells, the endogenous FBXW7 was sufficient in exerting substrate deregulation to a comparable level to shRNA FBXW7 knocked-down cells, as detailed in section 7.2.1, further work is required to determine if total absence of FBXW7 protein is functionally equivalent or more tumorigenic than propellor-tip mutant FBXW7.

6.3.3 Overexpression of wildtype FBXW7 in propellor-tip mutant cell lines

I aimed to analyse FBXW7 substrates when overexpressing wildtype FBXW7 in FBXW7 propellor-tip mutant cells. This was the opposing experiment to the previous section and could determine if overexpression of wildtype FBXW7 could overcome any possible dominant negative effect of propellor-tip mutant FBXW7.

6.3.3.1 Method of overexpressing FBXW7 in colorectal cancer cell lines: Plasmid details

Bruce Clurman (Fred Hutchinson Cancer Research Center, Seattle) kindly provided the expression vector p3xFLAG-myc-CMV-24 (Sigma) with human *FBXW7* (α isoform) cDNA cloned into the HindIII and EcoRI restriction sites [245]. This plasmid will be refered to as pFLAG FBXW7α.

In order to generate an empty vector plasmid which could be used as a control, the *FBXW7* cDNA insert was excised with a HindIII/EcoRI double digest. The 'sticky-ends' from the restriction enzyme digest were then blunt-ended (section 2.8.1.2), re-ligated and transformed. I will refer to this empty vector plasmid as pEV.

6.3.3.2 Assessment of wildtype FBXW7 overexpression on selected FBXW7 substrates in unsynchronised propellor-tip mutant cells

LOVO and SW1463 cell lines were transiently transfected with pFLAG FBXW7α and pEV plasmids and selected FBXW7 substrates were assessed. Figure 6.16 shows no notable differences in the protein levels of TGIF when wildtype FBXW7 is overexpressed in LOVO and SW1463 cells (p>0.05, Student t-test). Figure 6.16 shows no notable differences in the protein level of cyclin E when wildtype FBXW7 is overexpressed in LOVO cells, however, a decrease in cyclin E protein levels were observed in SW1463 cells (p=0.034, Student t-test). As LOVO and SW1463 are both propellor-tip mutant cell lines, I expected both cell lines to show similar effects with regards to substrate regulation. I therefore decided to continue assessment of FBXW7 substrates using methods to enrich for cells in which specific protein substrates would be expressed.

Western blots were probed with the FLAG antibody to give an indication of transfection efficiency. It was noted that western blots on SW1463 cells required a greater exposure time for FLAG-tagged protein to be detected. This could suggest extrinstic or intrinstic degradation of FBXW7 in this cell line.

6.3.3.3 Assessment of cyclin E levels in synchronised FBXW7 propellor-tip mutant cells with wildtype FBXW7 overexpression

Cells in culture grow asynchronously and thus when collected for analysis they may be at any point of their cell cycle. Briefly, the cell cycle is divided into four phases: G1, S, G2 and M. Chromosomal duplication (S-phase) is preceded by a gap phase (G1). In G1 the cell makes a critical decision whether to progress through the cell cycle and initate DNA synthesis. S phase is followed by another gap phase (G2), where the cell prepares for cell division/mitosis (M). Cells in G1 that are not committed to cell division, can withdraw from the cell cycle and enter G0 (quiescence). Cells in G0 can

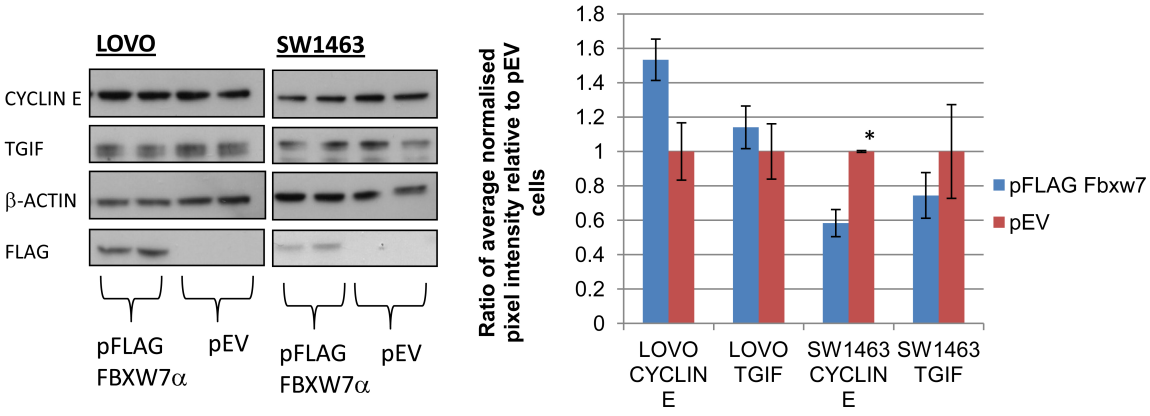


Figure 6.16: Cyclin E and TGIF protein levels in FBXW7-overexpressing LOVO and SW1463 cells. Western blot analysis of cyclin E and TGIF protein levels 72 h post-transfection with pFLAG FBXW7α or pEV plasmids. β-actin was used as a loading control and FLAG used to assess transfection efficiency. Asterisk denotes significant result (p=0.034, Student t-test).

be stimulated by external growth factors to re-enter the cell cycle. As levels of cyclin E alter periodically throughout the cell cycle, transfected cells were synchronised and collected at the G1-S transition at which cyclin E levels peak [93] (Figure 6.17). Cells were synchronised in G0/G1 by serum starvation for 48 h, then restimulated with serum and collected at 3 h, 6h and 11 h time points, in which time they would have progressed through to S-phase.

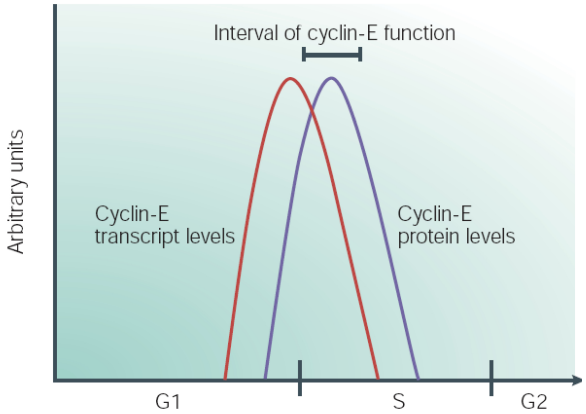


Figure 6.17: Periodicity of cyclin E mRNA and protein expression relative to cell cycle stage. Cyclin E levels peak at the G1-S transition and fall during S-phase. Schematic reprinted by permission from Macmillan Publishers Ltd: [Nat Rev Mol Cell Biol] (ref [246]), copyright (2003).

Figure 6.18 shows that in LOVO cells, the level of cyclin E is very low in serum

starved-cells transfected with wildtype FBXW7 (pFLAG FBXW7α) in comparison to a higher level of cyclin E detected in cells transfected with pEV (p=0.007, Student t-test). Cyclin E should be undetectable in all serum starved cells, as cells should be synchronised at G0/G1 and cyclin E is not expressed at this cell cycle stage. In LOVO propellor-tip FBXW7 mutant cells, cyclin E is thus deregulated relative to cell cycle stage. Several cell lines have been reported to inappropriately or constitutively express cyclins [247]. It has been reported that temporal misregulation of cyclin E in cells could be as detrimental as cyclin E overexpression [97].

When restimulated for 3 h, the levels of cyclin E in wildtype FBXW7 overexpressing LOVO cells increased to a level equivalent to that seen in pEV cells (p=0.556, Student t-test). At 6 and 11 h post-stimulation, there was still no difference between cyclin E levels in cells transfected with pFLAG FBXW7α and pEV (p>0.05 on both instances, Student t-test). FLAG-tagged FBXW7 protein was detected in all lanes transfected with pFLAG FBXW7α, showing that transient transfections were successful.

Similar synchronisation experiments for cyclin E were carried out in propellor-tip mutant SW1463 cells, as well as in HCT116 (wildtype *FBXW7*) and C32 cells (nonsense R278X *FBXW7* mutation, hypertriploid, *APC* mutation and LOH) (Figure 6.18). As stimulation of cells 3 h post serum starvation was sufficient to detect cyclin E levels in LOVO cells, this 3 h time point was used in all subsequent experiments.

No cyclin E was detected in serum starved SW1463 cells when transfected with pFLAG FBXW7α or pEV, as expected in G0/G1 cells. When restimulated for 3 h, cyclin E protein was detected in those cells with only endogenous FBXW7 (both wildtype and mutant, as heterozygous mutation), compared to an undetectable level of cyclin E in those which had wildtype FBXW7 overexpressed. This could suggest that overexpression of wildtype FBXW7 can rescue the putative dominant negative effect of propellor-tip mutant FBXW7 in these cells.

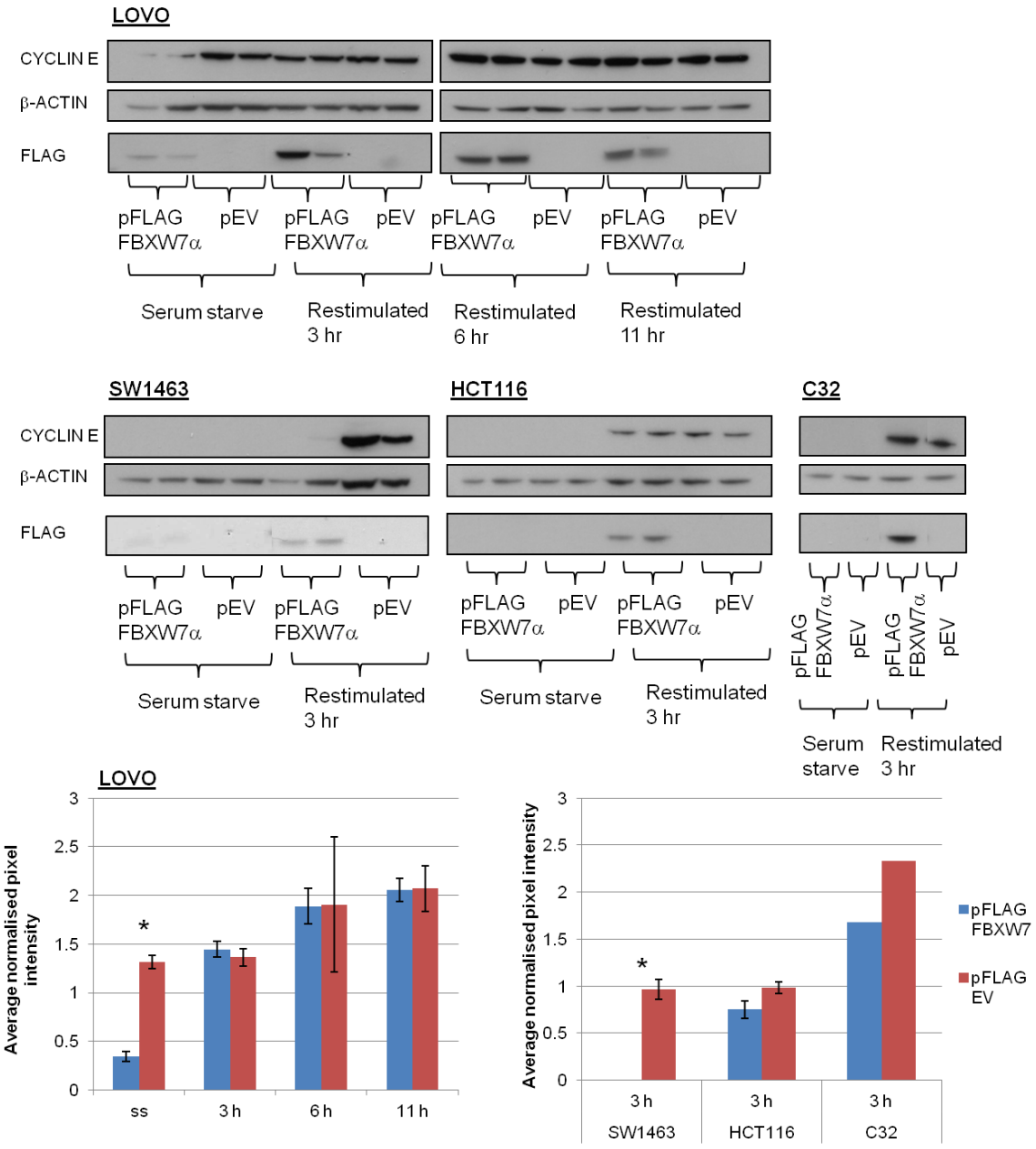


Figure 6.18: Protein levels of cyclin E in a panel of synchronised cells overexpressing wildtype FBXW7. Cells were synchronised by 48 h serum starvation followed by serum restimulation for 3 h, 6 h or 11 h in LOVO cells, and just 3 h in all other cell lines. Antibodies details are shown in Table 2.6. β-actin was used as a loading control. Probing western blots with FLAG antibody showed transfection efficiency. The graphs show average normalised pixel intensities. Error bars represent the SEM. Askerisks denote significant results. Experiments were repeated on three separate occasions. A large proportion of C32 cells died post-transfection and therefore these samples were not run in duplicate.

In HCT116 cells, no cyclin E was detected in serum starved cells as expected and there was no difference in the levels of cyclin E detected 3 h post-serum stimulation when pFLAG FBXW7α or pEV were transfected (p>0.05, Student t-test). This is perhaps expected as HCT116 already has wildtype FBXW7 so cyclin E is already degraded to an appropriate level.

In C32, no cyclin E was detected in serum starved cells, as expected and there was no difference in the level of cyclin E 3 h post-serum stimulation when pFLAG FBXW7α or pEV were transfected (p>0.05, Student t-test). This finding highlights a difference between heterozygous *FBXW7* propellor-tip and heterozygous truncating mutations.

To summarise, overexpressing wildtype FBXW7 in SW1463 cells led to degradation of cyclin E 3 h post-stimulation, whereby endogenous propellor-tip mutant FBXW7 and FBXW7 wildtype alone, cannot degrade (or fully degrade) cyclin E. In HCT116 (FBXW7 wildtype) cells, overexpressing wildtype FBXW7 further has no effect and similarly no effect is seen in C32 cells, which carry a nonsense *FBXW7* mutation. In LOVO cells, overexpressing wildtype FBXW7 does not effect cyclin E abundance in restimulated cells, however in this cell line, serum starvation did not lead to a complete absence of cyclin E in cells with endogenous levels of FBXW7.

6.3.3.4 Assessment of p-c-Myc levels in synchronised FBXW7 propellor-tip mutant cells with wildtype FBXW7 overexpressed

c-Myc promotes cell cycle progression. It is known that in quiescent (G0) cells *in vitro*, protein levels are virtually undetectable [102]. However, following serum starvation, c-Myc mRNA and protein are rapidly induced as cells enter the G1 phase of the cell cycle. mRNA and protein levels decline to low but detectable, steady state levels in proliferating cells. If serum or growth factors are removed c-Myc declines to undetectable levels and cells arrest. Figure 6.19 shows that in LOVO cells there was

no p-c-Myc expressed in serum starved cells as expected and when restimulated for 3, 6 and 11 h there were no significant differences between the level of p-c-Myc in the cells in which wildtype FBXW7 was overexpressed (pFLAG FBXW7α) and in pEV transfected cells (p>0.05 in all cases, Student t-test). As no differences were observed in LOVO, I decided not to assess p-c-Myc in other FBXW7 mutant cell lines.

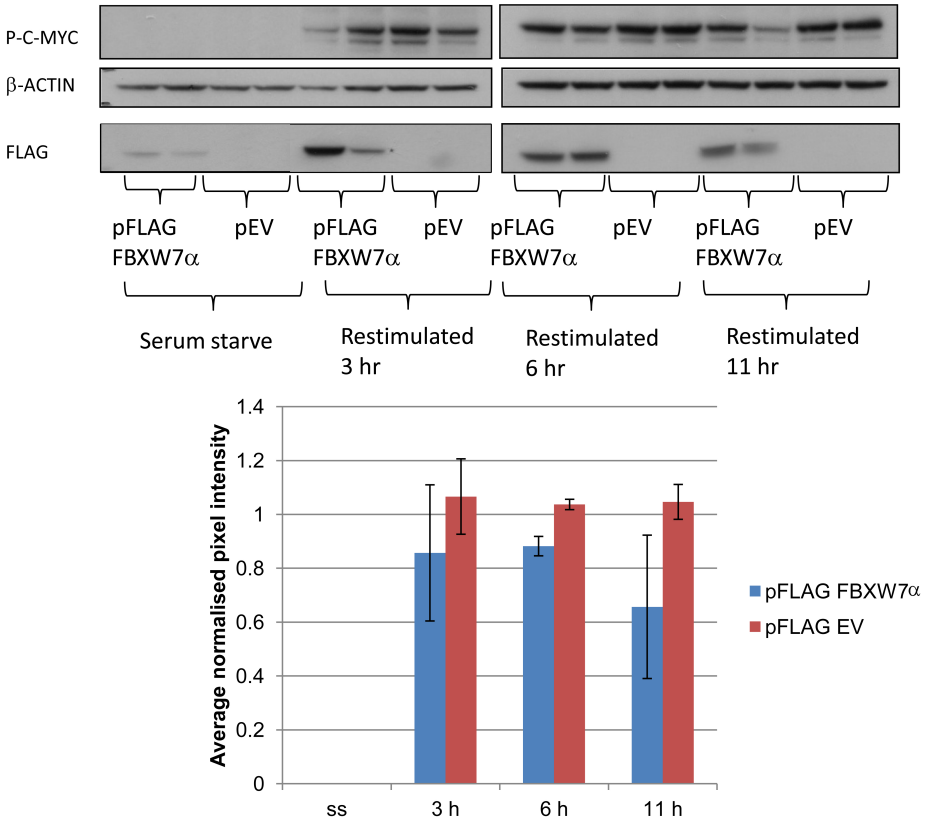


Figure 6.19: p-c-Myc protein levels remain unchanged in synchronised LOVO cells overexpressing wildtype FBXW7 (p>0.05 in all cases, Student t-tests). Cells were synchronised by 48 h serum starvation followed by serum restimulation for 3 h, 6 h or 11 h. Antibody details are shown in Table 2.6. β-actin was used as a loading control. Probing western blots with FLAG antibody was used to show transfection efficiency. Average pixel intensities normalised to β-actin are shown in the graph. Error bars represent the SEM. There were no significant differences between pFLAG FBXW7α and pEV transfected cells at all time points.

6.3.3.5 Assessment of TGIF protein levels in the nuclear fraction of propellor-tip mutant cells

Assessment of TGIF carried out in the R482Q mouse model (described in Chapters 3-5) indicated this protein was an important FBXW7 substrate.

As TGIF is a transcriptional repressor, it will be enriched in the nuclear fraction of cells. Therefore, protein lysates from cells transfected with both pFLAG FBXW7α and pEV plasmids, were fractionated into cytosolic and nuclear fractions prior to analysis (section 2.5.3.4). Figure 6.20 shows that virtually no TGIF was detected in the cytosolic fraction, whereas elevated TGIF levels were detected in the nuclear fraction of pEV transfected cells. Quantification of protein levels are shown in Figure 6.21b.

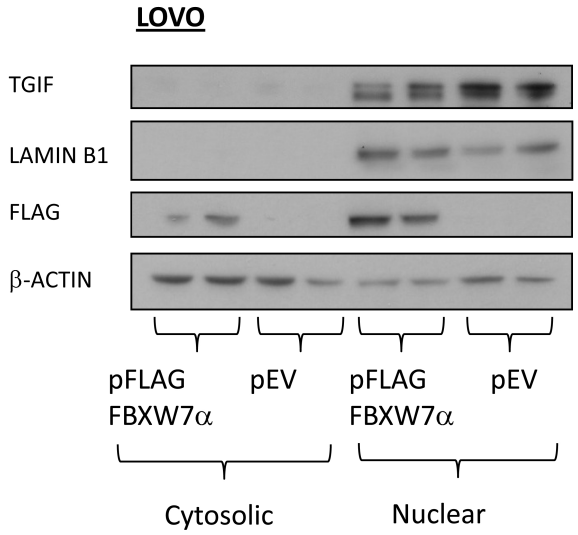


Figure 6.20: TGIF protein levels were decreased in the nuclear fraction of LOVO cells overexpressing wildtype FBXW7 (β-actin and Lamin B1 were used as loading controls for the cytosolic and nuclear fractions respectively). Assayed by western blot 72 h post-transfection with pFLAG FBXW7α and pEV plasmids. Antibody details are shown in Table 2.6.

Figure 6.21a shows the same experiment repeated on SW1463, C32 and HCT116 cells, with Figure 6.21b showing quantification of these western blots. In summary, in LOVO and SW1463 cells, there was a significant difference in the level of TGIF

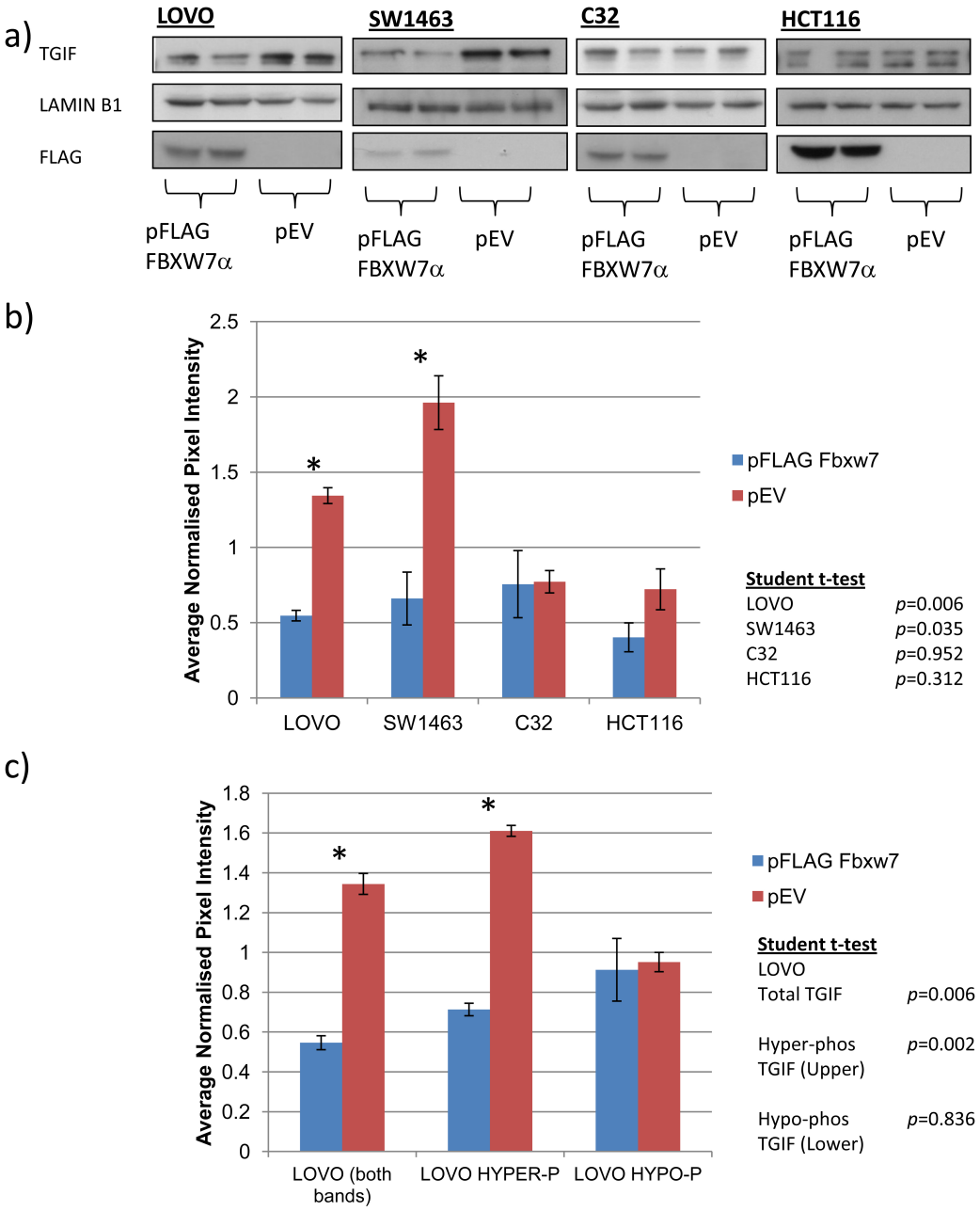


Figure 6.21: TGIF western blot on the nuclear fraction of a panel of cell lines over-expressing wildtype FBXW7. a) Western blot analysis of TGIF in nuclear fraction in a panel of cell lines. Antibody details are shown in Table 2.6. Lamin B1 was used as a loading control for nuclear fractions and probing blots with FLAG antibody was used to show transfection efficiency. Note that each experiment was repeated at least in triplicate. b) The graph shows quantification of the western blots by measuring average pixel intensities. c) Individual hyper-phosphorylated (upper) and hypo-phosphorylated (lower) bands were quantified independently in the LOVO cell line. Error bars on these graphs represent the SEM. Asterisks denote statistically significant results.

between cells transfected with pFLAG FBXW7α and pEV plasmids, whereas no significant difference in C32 and HCT116 cell lines was found.

Using the LOVO cell line, I tested if differences in TGIF protein levels could be detected both in the hyper-phosphorylated (upper) band and the hypo-phosphorylated (lower) band independently (Figure 6.21c). A significant difference was detected in the hyper-phosphorylated (upper) band but not in the hypo-phosphorylated (lower) band, consistent with the paradigm that FBXW7 substrates are phosphorylated in the CPD motif prior to ubiquitination and degradation.

Table 6.1 summarises the consequences of wildtype FBXW7 expression on tested substrates in the panel of colorectal cell lines analysed.

Substrate *FBXW7* status	**LOVO** R505C	**SW1463** R479Q	**C32** R278X	**HCT116** Wildtype
TGIF (non fractionated)	No change	No change		
TGIF (nuclear fraction)	Decrease	Decrease	No change	Decrease not significant
Cyclin E (Unsynchronised cells)	No change	Decrease		
Cyclin E (Cells at G1/S transition)	?	Decrease	No change	No change
p-c-Myc (Cells at G1/S transition)	No change			

Table 6.1: Effect of FBXW7 overexpression on the abundance of FBXW7 protein substrates in a panel of CRC cell lines. Blank entries indicate experiments not undertaken. '?' indicates cyclin E was deregulated with respect to cell cycle, as serum starvation did not result in absence of cyclin E.

6.4 Discussion

6.4.1 Interaction between Fbxw7 wildtype and R482Q proteins

I have demonstrated that Fbxw7 R482Q and Fbxw7 wildtype proteins interact. Studies have previously reported the dimerisation of Fbxw7 wildtype proteins [69; 70] and as the R482Q point mutation alters the WD40 substrate interacting domain, leaving the dimerisation domain found upstream of the F-box unaffected, successful dimerisation was expected. Dimerisation of FBXW7 may be necessary for the degradation of FBXW7 substrates that have a sub-optimal CPD's (section 1.3.4). However, perhaps more importantly, the dimerisation of mutant and wildtype FBXW7 could be a mechanism of dominant negative action of mutant FBXW7. Technical issues with transfecting plasmids into mouse cell lines hampered further investigation of the potential downstream dominant negative effect of mutant Fbxw7 R482Q on substrates of Fbxw7 in mouse cells. However, I successfully transfected a human colorectal cancer cell line and found no differences in the FBXW7 substrates assessed. Although there is 96% protein sequence homology between human and mouse Fbxw7, it is uncertain whether mouse Fbxw7 would be able to degrade endogenous human substrate proteins efficiently so I did not take this experiment further. Time constraints did not permit me to attempt these experiments in a wider selection of human cell lines.

6.4.2 shRNA *FBXW7* knockdown has no effect on FBXW7 substrates in FBXW7 propellor-tip mutant cell lines

shRNA knockdown of *FBXW7* in colorectal cancer cell lines with propellor-tip *FBXW7* mutations did not result in elevation of any of the substrates investigated.

The best knockdown of *Fbxw7* mRNA levels achieved was 70 - 80%, whilst this

is of high efficiency, it may not have been sufficient to significantly decrease protein levels, but due to the lack of a suitable antibody I could not determine the reduction in FBXW7 protein levels. Another possibility is that cells in which FBXW7 is successfully knocked down die; this is conceivable as FBXW7 is involved in regulation of a plethora of substrates, many of which are critical in cell proliferation. Additionally, as shown in Figure 4.9, an elevated level of apoptosis was observed in *Fbxw7*-null small intestinal cells, supporting the idea that *FBXW7*-null cells *in vitro* may have died. Alternatively, the propellor-tip FBXW7 mutant may have provided maximal substrate derangement in cancer cells (equivalent to that in *FBXW7*-null cells) in what we have proposed to be the 'Just-Enough' model [229] (discussed further in section 7.2.1).

6.4.3 Overexpression of wildtype FBXW7 in propellor-tip mutant cells can overcome potential dominant negative effect

When wildtype FBXW7 was overexpressed in missense propellor-tip mutant cell lines (SW1463 and LOVO), it resulted in decreased amounts of TGIF protein detected in the nuclear fraction. In contrast, in HCT116 which has wildtype FBXW7, further overexpression of wildtype FBXW7 protein did not lead to a significant increase in TGIF degradation. Also in C32 cells carrying heterozygous nonsense R278X mutation, overexpression of wildtype FBXW7 did not result in further degradation of TGIF protein levels. The R278X mutation leads to truncation of the protein before critical F-box and dimerisation domains. As neither of these domains are present in this truncated protein, it can neither recruit the ubiquitin machinery nor dimerise with wildtype protein to exert a dominant negative effect and thus is predicted to be non-functional. As the nonsense mutation is found in the heterozygous state, wildtype

FBXW7 protein is also present and therefore TGIF is already degraded to normal levels. Collectively these findings suggest that when wildtype FBXW7 is overexpressed in propellor-tip mutant cell-lines, endogenous mutant FBXW7 is overwhelmed and any potential dominant negative effects are overcome.

Post serum-starvation, when cells are re-stimulated they progress through the cell cycle from G1 to S phase and as they do so, cyclin E levels are expected to increase. In SW1463 cells (transfected with pEV) an increase in the level of cyclin E was observed, however, in contrast, when SW1463 cells in which FBXW7 wildtype was overexpressed, cyclin E was fully degraded and could not be detected. As this cell line carries a heterozygous mutation, endogenous wildtype FBXW7 will also be present, but this was not fully effective in cyclin E degradation and overexpression of wildtype FBXW7 was required to lead to degradation of all cyclin E present. Therefore, in the presence of FBXW7 mutant protein, endogenous wildtype FBXW7 cannot fully degrade cyclin E. In C32, which carries a heterozygous R278X nonsense mutation, comparable levels of cyclin E were detected in cells in which FBXW7 is overexpressed and those in which it is not.

In LOVO serum starved cells transfected with pEV, cyclin E levels did not fall to undetectable levels, suggesting that cyclin E is deregulated in this colorectal cancer cell line. Cyclin E is deregulated in many cancer cell lines [247] due to many contributing factors. For example, cyclin E is a E2F target gene and its transcription can be positively regulated by Rb pathway mutations [248].

It is important to note here that only the α isoform of FBXW7 has been overexpressed in these experiments. Although this isoform is the most abundant in most tissues [60] (section 1.3.2), it has been reported that in some cell lines, both the FBXW7α and FBXW7γ isoforms are necessary for degradation of cyclin E and c-Myc [62; 63]. Therefore, additional experiments overexpressing FBXW7γ as well as FBXW7α may be informative.

6.4.4 Further work

Overexpression of *KLF5* in a bladder cancer cell line has been shown to promote G1 to S phase transition, resulting in greater numbers of cells in S-phase following cell synchronisation and release [124]. Also *KLF5* mRNA levels were virtually undetected in serum deprived NIH3T3 cells but were significantly increased on addition of serum [210]. Similar cell synchronisation experiments to assess KLF5 protein level and cell cycle distribution in FBXW7 wildtype and propellor-tip mutant cell lines therefore may also prove fruitful.

When overexpressing wildtype FBXW7 protein in propellor-tip mutant cells, TGIF levels are reduced. Additional experiments in which mutant FBXW7 protein are over-expressed in comparison to wildtype FBXW7 will be crucial in deciphering whether propellor-tip missense mutations act in a dominant negative fashion, or rather if the level of TGIF is reduced solely due to the increased abundance of FBXW7 protein.

Chapter 7

Discussion and further work

7.1 Summary of results

There is strong evidence that *FBXW7* is a tumour suppressor gene which is mutated in a diverse range of cancer-types. The predominant mutations identified in this gene are missense mutations found at critical arginine residues at the propellor-tips, which abrogate substrate binding and hence subsequent degradation by the proteasome. Despite these data, previous mouse models to study FBXW7 function have been based on simple knockout/null alleles. With this in mind, the aim was to generate a *Fbxw7*-mutant mouse that was more representative of human cancer in order to enhance understanding of the mechanisms by which mutant FBXW7 protein promotes malignancy. This model could also be exploited to study propellor-tip mutant FBXW7 protein in a tissue-specific manner to address whether substrate deregulation varies according to tissue-type.

In order to achieve this aim, a gene-targeted approach was taken to knock-in the specific R482Q missense propellor-tip mutation and this was investigated both constitutively and by conditional mutation in the mouse intestine. Results in Chapter 3 reported that when this mutation was expressed constitutively, perinatal lethality

was observed in the heterozygous state. This phenotype was attributed to defective lung development, although incompletely penetrant developmental abnormalities including cleft palate and eyelid fusion defects were also observed. Extensive analysis of these developmental abnormalities showed that these phenotypes were different from what had previously been reported for *Fbxw7*-null mice, which developed normally in the heterzygous state showing no lung developmental abnormalities but resulted in embryonic lethality at E10.5-E11.5 in the homozygous state via disturbed vascular development, attributed to elevated Notch protein. Furthermore, analysis of the protein substrates of Fbxw7 in embryonic lung tissue from R482Q/+ mice highlighted deregulation of Klf5 and Tgif1 degradation.

As a previous study by our group indicated that *FBXW7* mutations occur at a moderate frequency in CRCs and in adenomas, the R482Q mutation was also investigated conditionally in the gut to determine if it could promote tumorigenesis. Data presented in Chapter 4 showed that heterozygous R482Q mice manifested low-multiplicity adenoma or adenocarcinoma formation after a latency period of at least 300 days compared with no tumours in wildtype mice. Normal intestinal tissue from heterozygous R482Q mice had elevated protein levels of Klf5 and Tgif1. R482Q tumours displayed signs of elevated Wnt signalling and *Ctnnb1* mutations were found in some cases. Additionally, as discussed in Chapter 5, the R482Q mutation in conjunction with tumorigenic *Apc* alleles, caused accelerated tumorigenesis, with tumour size significantly increased.

Chapter 6 reported *in vitro* work using epitope-tagged wildtype and R482Q mutant FBXW7 proteins demonstrating their interaction, thus supporting the hypothesis that mutant FBXW7 protein could potentially act via a dominant negative mechanism. Studies using FBXW7 mutant and wildtype colorectal cancer cell lines were inconclusive, perhaps due to the nature of colorectal cancer-cell lines that carry many mutations implicated in carcinogenesis.

7.2 Discussion

7.2.1 Just-Enough hypothesis

By exploring the existing genetic data and new data presented in this thesis, a 'Just Enough' model of tumour suppression [229] can be proposed and will be discussed here. This model primarily explains data for *FBXW7* but may also be more widely applicable to other tumour suppressor genes. As *FBXW7* mutations often occur in the heterozygous state, without loss of heterozygosity, *FBXW7* is not considered as a classical tumour suppressor gene.

The unusual mutation spectrum at *FBXW7* in human cancers is reminiscent of the *APC* tumour suppressor gene, in which cancer-associated mutations are selected for partial retention of protein function rather than simple loss of function. Bi-allelic null *APC* mutations are rarely found in human tumours. Instead, the two-hits are co-selected to leave a critical, yet partial, ability to down regulate β-catenin and hence lower the level of Wnt signalling. The explanation for these observations probably lies in the fact that too high a level of Wnt signalling is sub-optimal for tumorigenesis [27; 235; 249]. However, the optimal combination of mutations from both alleles produce a 'Just-Right' level of Wnt signalling [28]. The 'Just-Right' model might apply more generally in tumorigenesis, less in terms of the spectra of mutations in individual genes and more as an explanation for why specific cancer types tend to acquire mutations in specific genes, sometimes within the same signalling pathway. *APC* may be unusual in that, different mutant alleles can have optimal or sub-optimal effects, but the 'Just-Right' principle may hold more widely.

In order to explain that even partial inactivation of tumour suppressor genes can critically contribute to tumorigenesis, Berger and colleagues [250] have recently proposed a continuum model for tumour suppression. These authors reviewed cases in which tumour suppressor genes are not inactivated by the conventional 'two-hit'

mechanism [82]. Obligate haploinsufficiency (also termed a fail safe mechanism) was proposed to explain those tumour suppressor genes (including *FBXW7*) whereby two-hits are not often observed as they cause cell-lethality. However, it also may be possible in these genes, that heterozygous mutations predominate due to a requirement for an optimal level of derangement by tumour cells and could be considered as a variant of the 'Just-Right' hypothesis which we have coined the 'Just-Enough' hypothesis. Figure 7.1 shows a schematic representation of models of tumour suppression including the 'Just-Enough' model.

In *FBXW7*, arginine propellor-tip missense mutations may occur most frequently as this mutation state provides sufficient derangement of gene function to permit tumorigenesis. As shown in Figure 1.9 despite the predominance of mono-allelic missense mutations in cancers, some tumours do have two hits, although only few propellor-tip mutations have bi-allelic mutations or mono-allelic mutations and LOH. Other non propellor-tip mutations have a greater selective pressure for a second hit to provide sufficient derangement necessary for tumorigenesis. For the 'Just-Right' model, precise mutation combinations result in the optimum level of Wnt signalling with maximal Wnt signalling negatively correlated with tumorigenesis. Whereas the 'Just Enough' model of tumorigenesis for *FBXW7* proposes that a threshold of derangement is required to be surpassed for tumorigenesis to occur; for propellor-tip mutations this may only require one hit, whereas non propellor-tip mutations may require additional hits.

An example of evidence from this thesis that supports the 'Just-Enough' hypothesis is shown in Figure 4.14b; normal intestinal tissue from R482Q/+ and R482Q/R482Q mice showed a dosage dependent trend in the protein expression of Klf5 and Tgif1 compared to wildtype samples. Conversely in *Fbxw7*-null mice, an elevated level of these substrates was only observed in the homozygous (and not the heterozygous) state, suggesting that two hits (or more accurately absence of wildtype protein), were

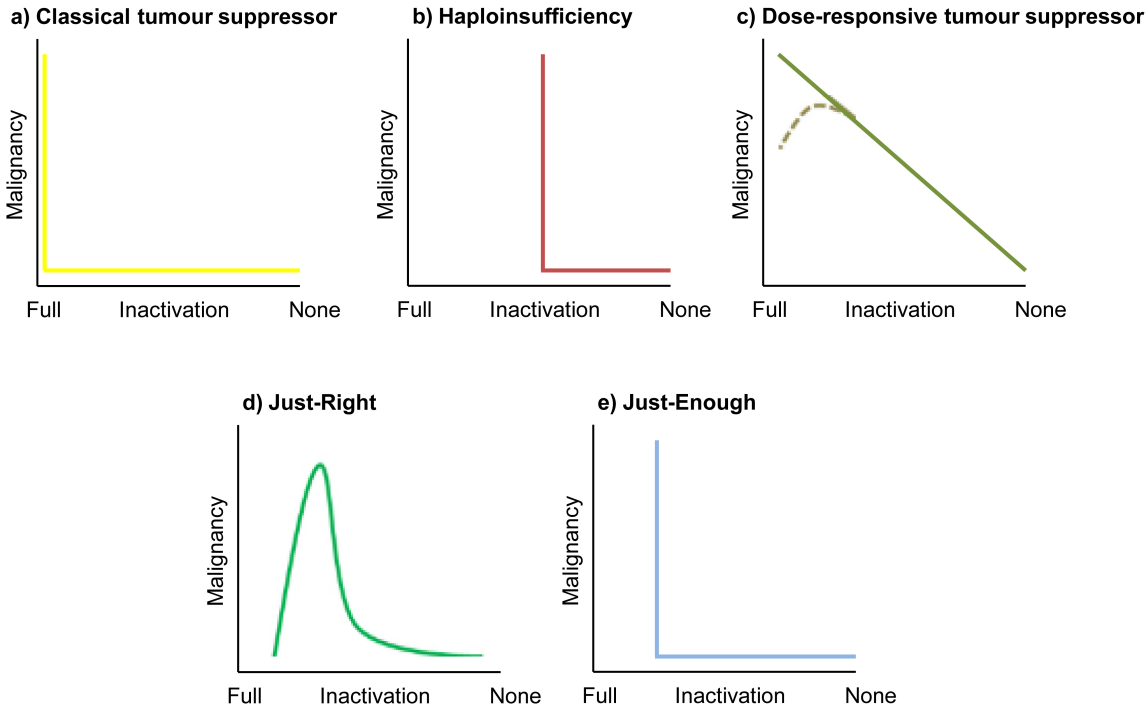


Figure 7.1: Schematic model of tumour suppression, adapted with permission from Macmillan Publishers Ltd: [Nature] (ref [250]), copyright (2001). a) Classical discrete model of tumour suppression where full gene inactivation (two-hits) is required for malignancy. b) Haploinsufficient model whereby inactivation of one allele causes malignancy. c) Dose-responsive tumour suppressor model where tumour suppression is related to a continuum of gene expression rather than discrete changes in DNA copy number. A linear relationship is depicted for schematic purposes only, the relationship need not be linear. Dotted line represents a 'fail-safe' mechanism induced by complete loss of gene expression (complete loss is negatively correlated with malignancy). d) Just-Right model where specific mutations cause optimal malignancy. e) Just-Enough model where mutations that provide sufficient derangement of gene function cause malignancy. In the case of *FBXW7*, specific mutations in critical residues within a protein-domaining domain alter substrate interactions resulting in accumulation of oncoproteins leading to malignancy. Other mutations in this gene may require two hits to exhibit sufficient protein derangement to promote tumorigenesis.

required to result in protein accumulation.

Work presented in Chapter 3 showed that constitutive R482Q/+ and $Fbxw7^{\Delta/+}$ mice exhibited different phenotypes with respect to lung development. $Fbxw7^{\Delta/\Delta}$ mice have been reported to die at an early stage of embryonic development due to vascular problems and therefore specific lung abnormalities cannot be investigated in these mice. However, it is possible to speculate that R482Q/+ mutant mice, display an 'intermediate' phenotype in terms of severity. It has been reported that conditional bi-allelic loss of Fbxw7 in the intestine in conjunction with Apc^{Min} allele [151; 188] enhanced intestinal tumorigenesis to a greater extent than mono-allelic loss of *Fbxw7* in conjunction with the Apc^{Min} allele, thus indicating that *Fbxw7* is dosage-sensitive. Comparison of R482Q/Apc mutant mice and *Fbxw7*-null/Apc mutant mice will determine if total absence of Fbxw7 protein is functionally equivalent or more tumorigenic than propellor-tip mutant Fbxw7.

As evidence suggests that gene/allelic dosage may be important for *FBXW7*, *in vitro* assays in which FBXW7 protein is overexpressed as well as *FBXW7*-null systems may be limited.

7.2.2 *FBXW7* mutations within the adenoma-carcinoma progression sequence

The precise timing of *FBXW7* mutations with respect to the adenoma-carcinoma sequence of progression of colon tumorigenesis has not been extensively researched. However, *FBXW7* mutations have been identified in early lesions (adenomas) and thus have been proposed to occur as an early event in intestinal tumorigenesis. In Chapter 4, I reported that R482Q/+ mice exhibited adenoma and adenocarcinoma development but after a long latency period, suggesting that *Fbxw7* mutations alone were insufficient to initiate tumorigenesis. Analysis of R482Q/+ tumours revealed elevated levels of Wnt signalling in these lesions and in two cases, mutations in *Ctnnb1*.

These findings highlighted that additional activation of Wnt signalling may well be necessary for tumorigenesis. Furthermore, in Chapter 5, tumours from R482Q/*Apc* mutant compound mice were significantly larger in size in comparison to *Fbxw7* wild-type/*Apc* mutant littermates, thus indicating that mutant Fbxw7 plays a critical role in enhancing tumour growth. Further work will shed light on the mechanisms of action of mutant Fbxw7 protein in tumour progression; two Fbxw7 substrates, Klf5 and Tgif1, transcriptional components that operate in several signalling pathways, may be responsible for the increased tumour growth observed.

7.2.3 Therapeutic targets

FBXW7 substrates could be exploited as targets of directed therapeutic efforts to potentially treat colorectal cancer patients with propellor-tip *FBXW7* mutations. Development of TGIF1 and KLF5 inhibitors or antagonists may prove useful therapeutic avenues to explore in the treatment of these cancer patients.

Recent work by Faresse *et al* [251] using a two-hybrid screen with TGIF1 as the bait identified a protein encoded by *IRF2BP1*, which the authors have called PCTA (PML competitor for TGIF) as an interacting partner of TGIF1. As mentioned in section 1.3.9.7, one mechanism in which TGIF1 exerts its inhibition on TGF-β signalling is mediated by sequestering cPML (cytoplasmic promyelocytic leukaemia) in the nucleus, thus preventing Smad2 phosphorylation [134]. The interaction of PCTA and TGIF1 was confirmed by co-immunoprecipitation experiments and cell-based studies have highlighted that this protein acts as a TGIF antagonist. It was highlighted that the mechanism of action of PCTA was mediated by selective competition with cPML for TGIF association, resulting in increased cytoplasmic levels of cPML, which enhanced Smad2 phosphorylation and thus TGF-β mediated signalling. Further investigations into overexpression of PCTA or synthetic analogues as well as development of small molecules inhibitors of TGIF may prove interesting.

In order to identify exisiting therapeutic agents that specifically target KLF5, Bialkowska *et al* [170] performed ultra high-throughput screening of a library of small molecule inhibitors, using a reporter cell line that stably expressed a luciferase reporter gene under the control of human *KLF5* promoter. The authors identified a selection of compounds that were KLF5 specific and were not cytotoxic to intestinal epithelia cells. Two of these molecules have been further characterised and proposed as novel therapeutic agents for validation in animal models.

7.3 Further work

Several lines of enquiry have arisen throughout the work presented in this thesis which merit further investigation. I will now address some of these future experiments.

1. **R482Q role in lung tumorigenesis:**

   In Chapter 3, constitutive knock-in of R482Q exhibited defective lung maturation in the heterozygous state. Although *FBXW7* mutations have been infrequently reported in lung adenocarcinomas [74], it would be interesting to determine if R482Q mutation alone can cause lung malignancies. To this end, the conditional R482Q knock-in model has been supplied to collaborators (Professor Catrin Pritchard, University of Leicester) to activate recombination in the lung using adenoviral-Cre inhalation. Guerra *et al* [252] generated an oncogenic $Kras^{V12}$ allele that manifests lung adenocarcimonas at 6-8 months old. The aim is to additionally breed the R482Q mouse to this strain to investigate if R482Q $Kras^{V12}$ compound mice exhibit enhanced or accelerated tumorigenesis.

2. **R482Q in other cancer types:**

   As *FBXW7* mutations are present across a broad spectrum of cancer types, it also is possible to use R482Q mice to study this mutation conditionally in other

tissues. *FBXW7* mutations have been reported at a moderate frequency in the endometrium and therefore R482Q mice could provide a tool to further study *FBXW7* mutations in this tissue type.

3. **Proteomic approach:**

   A proteomics approach to investigate differential binding abilities of FBXW7 wildtype and arginine propellor-tip mutant proteins may prove insightful. Tools to implement this strategy could include *in vitro* based tagged-wildtype and mutant proteins, or possibly MEFs derived from propellor-tip and *Fbxw7*-null mice. Crystallographic studies have identified that arginine residues at the apex of the propellors (R465, R479 and R505) directly interact with phosphodegron sequences [65; 66]. In this thesis I have regarded all arginine-propellor tip mutants to have identical function, but it would be interesting to formally test if all these mutations are indeed functionally identical.

4. **Validation of Klf5 and Tgif1 as critical substrates:**

   I have presented data that indicate Klf5 and Tgif1 to be the critical Fbxw7 substrates deregulated in R482Q/+ mice in both the embryonic lung and the intestine. Genetic rescue experiments using available Klf5 [122] and Tgif1 [131; 253] knockout models could indicate if these substrates truly are the components that induce disrupted development and enhanced tumorigenesis.

Appendix A

Nomenclature of *Fbxw7*-mutant mice

Genotype	Explanation
R482Qfl/+	Heterozygous floxed *Fbxw7* R482Q allele
R482Qfl/R482Qfl	Homozygous floxed *Fbxw7* R482Q allele
R482Q/+	Heterozygous, Cre^{+}, R482Q knock-in
R482Q/R482Q	Homozygous, Cre^{+}, R482Q knock-in
$Fbxw7^{fl/+}$	Heterozygous floxed *Fbxw7* exon 5 [151]
$Fbxw7^{fl/fl}$	Homozygous floxed *Fbxw7* exon 5 [151]
$Fbxw7^{\Delta/+}$	Heterozygous, Cre^{+}, *Fbxw7*-null allele (and wildtype allele)
$Fbxw7^{\Delta/\Delta}$	Homozygous, Cre^{+}, *Fbxw7*-null allele
R482Q/+ Apc^{Min}	Heterozygous, *Vil1*-Cre^{+}, R482Q knock-in and Apc^{Min} heterozygous
R482Q/+ Apc^{1322T}	Heterozygous, *Vil1*-Cre^{+}, R482Q knock-in and Apc^{1322T} heterozygous [235]

Table A.1: Nomenclature of *Fbxw7*-mutant mice used in this study. Note that in Chapter 3 all Cre-mediated crosses used *PGK*-Cre, a ubiquitously expressed Cre [183] and in Chapter 4 and 5 all Cre-mediated crosses used *Vil1*-Cre, a gut-specific Cre [216]. Wildtype control mice used were always littermates of the 'test' mice.

Appendix B

Primers

Gene	Sequence 5'-3'	Product Size (bp)
Fbxw7α F	CTCACCAGCTCTCCTCTCCATT	151
Fbxw7α R	GCTGAACATGGTACAAGGCCA	
Fbxw7β F	TTGTCAGAGACTGCCAAGCAG	178
Fbxw7β R	GACTTTGCATGGTTTCTTTCCC	
Fbxw7γ F	AACCATGGCTTGGTTCCTGTTG	148
Fbxw7γ R	CAGAACCATGGTCCAACTTTC	
*Fbxw7*exon5 F	TTCATTCCTGGAACCCAAAGA	72
*Fbxw7*exon5 R	TCCTCAGCCAAAATTCTCCAGTA	
Gapdh F	TGAAGCAGGCATCTGAGGG	102
Gapdh R	CGAAGGTGGAAGAGTGGGAG	
Tgif F	GCCTATCCCTCAGAGCAAGA	101
Tgif R	CTTTGCCATCCTTTCTCAGC	
Klf5 F	GCCAGTTAATTCGCCAACTC	150
Klf5 R	TGAGTCCTCAGGTGAGCTTTT	
Serpine1 (Pai-I) F	TCATCAATGACTGGGTGGAA	147
Serpine1 (Pai-I) R	TGCTGGCCTCTAAGAAAGGA	
Ctgf F	CCCACACAAGGGCCTCTTCT	102
Ctgf R	ACCGACCCACCGAAGACAC	
Cdkn1a (p21) F	TTGCACTCTGGTGTCTGAGC	112
Cdkn1a (p21) R	TCTGCGCTTGGAGTGATAGA	
Crabp2 F	CTTCAAGATCGGGGAGGAAT	102
Crabp2 R	CTCTGCTCGCACACCATTT	
Foxa1 F	CATGAGAGCAACGACTGGAA	141
Foxa1 R	GCTCGTGGTCATGGTGTTC	
Rara F	CCTCACCGACTTGGTCTTTG	142
Rara R	CAGCATGTCCACCTTGTCTG	
Stra6 F	TTTGTGCCTTTACTGCATGG	147
Stra6 R	TGGGTATCCATGGTGAGTCC	

Table B.1: SYBR-Green primer sequences

Gene	Sequence 5'-3'	Product Size (bp)
Kras E1F	TCTTGTGTGAGACATGTTCTAATTT	201
Kras E1R	GCACGCAGACTGTAGAGCAG	
Kras E2F	CCAGACTGTGTTTCTCCCTTC	239
Kras E2R	TCACATGCCAACTTTCTTATTCA	
Ctnnb1 E2F	TTCAGGTAGCATTTTCAGTTCAC	297
Ctnnb1 E2R	TAGCTTCCAAACACAAATGC	
Tp53 E5F	CCGACCTCCGTTCTCTCTC	250
Tp53 E5R	CCAGTCCTAACCCCACAGG	
Tp53 E6F	TCCCGGCTTCTGACTTATTC	172
Tp53 E6R	GACGCACAAACCAAAACAAA	
Tp53 E7F	GTAGGGAGCGACTTCACCTG	201
Tp53 E7R	CAGAAGCTGGGGAAGAAACA	
Tp53 E8F	TACTGCCTTGTGCTGGTCCT	231
Tp53 E8R	GTGACTTTGGGGTGAAGCTC	
*Apc*E151F	AGAATCAGCTGCGTCCAAGT	214
*Apc*E151R	TTAGCAGAATCTGCTTCCTGTG	
*Apc*E152F	CATCAGCTGACGATGAAATAGG	250
*Apc*E152R	TTGGAGGGAGACTTGGCTC	
*Apc*E153F	TCAACCAGGCATAATAAAGCTG	247
*Apc*E153R	GACTATCTGGAAGGTCACTGGG	
*Apc*E154F	TAGTGGAATGGTGAGTGGCA	230
*Apc*E154R	TATCCACGTCTGGAAGGACC	
*Apc*E155F	AAGCAGACTGCTGTAAATGCTG	243
*Apc*E155R	GTTTTCATTTGATTCCTCAGGC	
*Apc*AF	CCTAAGAGAGAACAATTGCCTACA	303
*Apc*AR	TTCCTAACGTGAAGGGATGG	
*Apc*BF	CTCAAGTCTGCCATCCCTTC	472
*Apc*BR	GTCGTCCTGGGAGGTATGAA	
*Apc*CF	ACTACCACTGCAGCCCAGAT	495
*Apc*CR	CTGTGAGGGACTCTGCCTTC	
*Apc*DF	GAAGGCAGAGTCCCTCACAG	416
*Apc*DR	AGGCTGATCCACATGATGTTT	
*Apc*EF	GAAGAAGAAGAGAGACCGACAAA	366
*Apc*ER	TGAACTGCACCTTGAAAAACA	
*Apc*FF	AAAGTCCCTGCTGCTGAGAA	387
*Apc*FR	TGTTGGCATGGCTGAAATAA	

Table B.2: Sequencing primers

Appendix C

FBXW7 protein alignment

```
Score = 1341 bits (3470),  Expect = 0.0, Method: Compositional matrix adjust.
 Identities = 682/710 (96%), Positives = 694/710 (97%), Gaps = 3/710 (0%)

Human  1    MNQELLSVGSKRRRTGGSLRGNPSSSQVDEEQMNRVVEEEQQQQLRQQEEEHTARNGEVV  60
            MNQELLSVGSKRRRTGGSLRGN SSSQVDE QMNRVVEE+ QQQ R QEEEHTARNGE+V
Mouse  1    MNQELLSVGSKRRRTGGSLRGNASSSQVDEGQMNRVVEEDPQQQARHQEEEHTARNGELV  60

Human  61   GVEPRPGGQNDSQQGQLEENNNRFISVDEDSSGNQEEQEEDEEHAGEQDEEDEEEEE---  117
            G  PRPG QND+QQGQ+EENNNRFISVDEDSSGNQEEQEEDEEHAGEQ+EE+EEEEE
Mouse  61   GANPRPGDQNDTQQGQVEENNNRFISVDEDSSGNQEEQEEDEEHAGEQEEEEEEEEEEE  120

Human  118  MDQESDDFDQSDDSSREDEHTHTNSVTNSSSIVDLPVHQLSSPFYTKTTKMKRKLDHGSE  177
            MDQESDDFD SDDSSREDEHTH ++VTN SS+ DLP HQLSSPFYTKTTKMKRKLDHGSE
Mouse  121  MDQESDDFDPSDDSSREDEHTHNSNVTNCSSVSDLPAHQLSSPFYTKTTKMKRKLDHGSE  180

Human  178  VRSFSLGKKPCKVSEYTSTTGLVPCSATPTTFGDLRAANGQGQQRRRITSVQPPTGLQEW  237
            VRSFSLGKKPCKVS+YTSTTGLVPCSATPTTFGDLRAANGQGQQRRRITSVQPPTGLQEW
Mouse  181  VRSFSLGKKPCKVSDYTSTTGLVPCSATPTTFGDLRAANGQGQQRRRITSVQPPTGLQEW  240

Human  238  LKMFQSWSGPEKLLALDELIDSCEPTQVKHMMQVIEPQFQRDFISLLPKELALYVLSFLE  297
            LKMFQSWSGPEKLLALDELIDSCEPTQVKHMMQVIEPQFQRDFISLLPKELALYVLSFLE
Mouse  241  LKMFQSWSGPEKLLALDELIDSCEPTQVKHMMQVIEPQFQRDFISLLPKELALYVLSFLE  300

Human  298  PKDLLQAAQTCRYWRILAEDNLLWREKCKEEGIDEPLHIKRRKVIKPGFIHSPWKSAYIR  357
            PKDLLQAAQTCRYWRILAEDNLLWREKCKEEGIDEPLHIKRRK+IKPGFIHSPWKSAYIR
Mouse  301  PKDLLQAAQTCRYWRILAEDNLLWREKCKEEGIDEPLHIKRRKIIKPGFIHSPWKSAYIR  360

Human  358  QHRIDTNWRRGELKSPKVLKGHDDHVITCLQFCGNRIVSGSDDNTLKVWSAVTGKCLRTL  417
            QHRIDTNWRRGELKSPKVLKGHDDHVITCLQFCGNRIVSGSDDNTLKVWSAVTGKCLRTL
Mouse  361  QHRIDTNWRRGELKSPKVLKGHDDHVITCLQFCGNRIVSGSDDNTLKVWSAVTGKCLRTL  420

Human  418  VGHTGGVWSSQMRDNIIISGSTDRTLKVWNAETGECIHTLYGHTSTVRCMHLHEKRVVSG  477
            VGHTGGVWSSQMRDNIIISGSTDRTLKVWNAETGECIHTLYGHTSTVRCMHLHEKRVVSG
Mouse  421  VGHTGGVWSSQMRDNIIISGSTDRTLKVWNAETGECIHTLYGHTSTVRCMHLHEKRVVSG  480

Human  478  SRDATLRVWDIETGQCLHVLMGHVAAVRCVQYDGRRVVSGAYDFMVKVWDPETETCLHTL  537
            SRDATLRVWDIETGQCLHVLMGHVAAVRCVQYDGRRVVSGAYDFMVKVWDPETETCLHTL
Mouse  481  SRDATLRVWDIETGQCLHVLMGHVAAVRCVQYDGRRVVSGAYDFMVKVWDPETETCLHTL  540

Human  538  QGHTNRVYSLQFDGIHVVSGSLDTSIRVWDVETGNCIHTLTGHQSLTSGMELKDNILVSG  597
            QGHTNRVYSLQFDGIHVVSGSLDTSIRVWDVETGNCIHTLTGHQSLTSGMELKDNILVSG
Mouse  541  QGHTNRVYSLQFDGIHVVSGSLDTSIRVWDVETGNCIHTLTGHQSLTSGMELKDNILVSG  600

Human  598  NADSTVKIWDIKTGQCLQTLQGPNKHQSAVTCLQFNKNFVITSSDDGTVKLWDLKTGEFI  657
            NADSTVKIWDIKTGQCLQTLQGP+KHQSAVTCLQFNKNFVITSSDDGTVKLWDLKTGEFI
Mouse  601  NADSTVKIWDIKTGQCLQTLQGPSKHQSAVTCLQFNKNFVITSSDDGTVKLWDLKTGEFI  660

Human  658  RNLVTLESGGSGGVVWRIRASNTKLVCAVGSRNGTEETKLLVLDFDVDMK  707
            RNLVTLESGGSGGVVWRIRASNTKLVCAVGSRNGTEETKLLVLDFDVDMK
Mouse  661  RNLVTLESGGSGGVVWRIRASNTKLVCAVGSRNGTEETKLLVLDFDVDMK  710
```

Figure C.1: Alignment of FBXW7α isoform protein sequence of human and mouse. Sequence obtained from Ensembl and aligned using BLASTP software. Highlighted in yellow are non-conserved residues, highlighted in green is the conserved arginine residue (human 479, mouse 482), critical in substrate recognition and commonly mutated in cancers.

```
Score = 1244 bits (3219),  Expect = 0.0, Method: Compositional matrix adjust.
 Identities = 614/627 (97%), Positives = 620/627 (98%), Gaps = 0/627 (0%)

Human  1    MCVPRSGLILSCICLYCGVLLPVLLPNLPFLTCLSMSTLESVTYLPEKGLYCQRLPSSRT  60
            +CVP S L+LSC+C   GVLLPV LPNLPFL CLSMSTLESVTYLPEKGLYCQRLPSSRT
Mouse  3    VCVPSSVLVLSCVCWCWGVLLPVPLPNLPFLACLSMSTLESVTYLPEKGLYCQRLPSSRT  62

Human  61   HGGTESLKGKNTENMGFYGTLKMIFYKMKRKLDHGSEVRSFSLGKKPCKVSEYTSTTGLV  120
            HGGTESLKGKNTENMGFYGTLKMIFYKMKRKLDHGSEVRSFSLGKKPCKVS+YTSTTGLV
Mouse  63   HGGTESLKGKNTENMGFYGTLKMIFYKMKRKLDHGSEVRSFSLGKKPCKVSDYTSTTGLV  122

Human  121  PCSATPTTFGDLRAANGQGQQRRRITSVQPPTGLQEWLKMFQSWSGPEKLLALDELIDSC  180
            PCSATPTTFGDLRAANGQGQQRRRITSVQPPTGLQEWLKMFQSWSGPEKLLALDELIDSC
Mouse  123  PCSATPTTFGDLRAANGQGQQRRRITSVQPPTGLQEWLKMFQSWSGPEKLLALDELIDSC  182

Human  181  EPTQVKHMMQVIEPQFQRDFISLLPKELALYVLSFLEPKDLLQAAQTCRYWRILAEDNLL  240
            EPTQVKHMMQVIEPQFQRDFISLLPKELALYVLSFLEPKDLLQAAQTCRYWRILAEDNLL
Mouse  183  EPTQVKHMMQVIEPQFQRDFISLLPKELALYVLSFLEPKDLLQAAQTCRYWRILAEDNLL  242

Human  241  WREKCKEEGIDEPLHIKRRKVIKPGFIHSPWKSAYIRQHRIDTNWRRGELKSPKVLKGHD  300
            WREKCKEEGIDEPLHIKRRK+IKPGFIHSPWKSAYIRQHRIDTNWRRGELKSPKVLKGHD
Mouse  243  WREKCKEEGIDEPLHIKRRKIIKPGFIHSPWKSAYIRQHRIDTNWRRGELKSPKVLKGHD  302

Human  301  DHVITCLQFCGNRIVSGSDDNTLKVWSAVTGKCLRTLVGHTGGVWSSQMRDNIIISGSTD  360
            DHVITCLQFCGNRIVSGSDDNTLKVWSAVTGKCLRTLVGHTGGVWSSQMRDNIIISGSTD
Mouse  303  DHVITCLQFCGNRIVSGSDDNTLKVWSAVTGKCLRTLVGHTGGVWSSQMRDNIIISGSTD  362

Human  361  RTLKVWNAETGECIHTLYGHTSTVRCMHLHEKRVVSGSRDATLRVWDIETGQCLHVLMGH  420
            RTLKVWNAETGECIHTLYGHTSTVRCMHLHEKRVVSGSRDATLRVWDIETGQCLHVLMGH
Mouse  363  RTLKVWNAETGECIHTLYGHTSTVRCMHLHEKRVVSGSRDATLRVWDIETGQCLHVLMGH  422

Human  421  VAAVRCVQYDGRRVVSGAYDFMVKVWDPETETCLHTLQGHTNRVYSLQFDGIHVVSGSLD  480
            VAAVRCVQYDGRRVVSGAYDFMVKVWDPETETCLHTLQGHTNRVYSLQFDGIHVVSGSLD
Mouse  423  VAAVRCVQYDGRRVVSGAYDFMVKVWDPETETCLHTLQGHTNRVYSLQFDGIHVVSGSLD  482

Human  481  TSIRVWDVETGNCIHTLTGHQSLTSGMELKDNILVSGNADSTVKIWDIKTGQCLQTLQGP  540
            TSIRVWDVETGNCIHTLTGHQSLTSGMELKDNILVSGNADSTVKIWDIKTGQCLQTLQGP
Mouse  483  TSIRVWDVETGNCIHTLTGHQSLTSGMELKDNILVSGNADSTVKIWDIKTGQCLQTLQGP  542

Human  541  NKHQSAVTCLQFNKNFVITSSDDGTVKLWDLKTGEFIRNLVTLESGGSGGVVWRIRASNT  600
            +KHQSAVTCLQFNKNFVITSSDDGTVKLWDLKTGEFIRNLVTLESGGSGGVVWRIRASNT
Mouse  543  SKHQSAVTCLQFNKNFVITSSDDGTVKLWDLKTGEFIRNLVTLESGGSGGVVWRIRASNT  602

Human  601  KLVCAVGSRNGTEETKLLVLDFDVDMK  627
            KLVCAVGSRNGTEETKLLVLDFDVDMK
Mouse  603  KLVCAVGSRNGTEETKLLVLDFDVDMK  629
```

Figure C.2: Alignment of FBXW7β isoform protein sequence of human and mouse. Sequence obtained from Ensembl and aligned using BLASTP software. Highlighted in yellow are non-conserved residues, highlighted in green is the conserved arginine residue (human 479, mouse 482), critical in substrate recognition and commonly mutated in cancers.

```
Score = 1206 bits (3121),  Expect = 0.0, Method: Compositional matrix adjust.
 Identities = 582/589 (98%), Positives = 587/589 (99%), Gaps = 0/589 (0%)

Human  1    MSKPGKPTLNHGLVPVDLKSAKEPLPHQTVMKIFSISIIAQGLPFCRRRMKRKLDHGSEV  60
            MSKPGK  +NHGLVPVDLKSAK+PLPHQTVMKIFSISIIAQGLPFCRRRMKRKLDHGSEV
Mouse  1    MSKPGKAPVNHGLVPVDLKSAKDPLPHQTVMKIFSISIIAQGLPFCRRRMKRKLDHGSEV  60

Human  61   RSFSLGKKPCKVSEYTSTTGLVPCSATPTTFGDLRAANGQGQQRRRITSVQPPTGLQEWL  120
            RSFSLGKKPCKVS+YTSTTGLVPCSATPTTFGDLRAANGQGQQRRRITSVQPPTGLQEWL
Mouse  61   RSFSLGKKPCKVSDYTSTTGLVPCSATPTTFGDLRAANGQGQQRRRITSVQPPTGLQEWL  120

Human  121  KMFQSWSGPEKLLALDELIDSCEPTQVKHMMQVIEPQFQRDFISLLPKELALYVLSFLEP  180
            KMFQSWSGPEKLLALDELIDSCEPTQVKHMMQVIEPQFQRDFISLLPKELALYVLSFLEP
Mouse  121  KMFQSWSGPEKLLALDELIDSCEPTQVKHMMQVIEPQFQRDFISLLPKELALYVLSFLEP  180

Human  181  KDLLQAAQTCRYWRILAEDNLLWREKCKEEGIDEPLHIKRRKVIKPGFIHSPWKSAYIRQ  240
            KDLLQAAQTCRYWRILAEDNLLWREKCKEEGIDEPLHIKRRK+IKPGFIHSPWKSAYIRQ
Mouse  181  KDLLQAAQTCRYWRILAEDNLLWREKCKEEGIDEPLHIKRRKIIKPGFIHSPWKSAYIRQ  240

Human  241  HRIDTNWRRGELKSPKVLKGHDDHVITCLQFCGNRIVSGSDDNTLKVWSAVTGKCLRTLV  300
            HRIDTNWRRGELKSPKVLKGHDDHVITCLQFCGNRIVSGSDDNTLKVWSAVTGKCLRTLV
Mouse  241  HRIDTNWRRGELKSPKVLKGHDDHVITCLQFCGNRIVSGSDDNTLKVWSAVTGKCLRTLV  300

Human  301  GHTGGVWSSQMRDNIIISGSTDRTLKVWNAETGECIHTLYGHTSTVRCMHLHEKRVVSGS  360
            GHTGGVWSSQMRDNIIISGSTDRTLKVWNAETGECIHTLYGHTSTVRCMHLHEKRVVSGS
Mouse  301  GHTGGVWSSQMRDNIIISGSTDRTLKVWNAETGECIHTLYGHTSTVRCMHLHEKRVVSGS  360

Human  361  RDATLRVWDIETGQCLHVLMGHVAAVRCVQYDGRRVVSGAYDFMVKVWDPETETCLHTLQ  420
            RDATLRVWDIETGQCLHVLMGHVAAVRCVQYDGRRVVSGAYDFMVKVWDPETETCLHTLQ
Mouse  361  RDATLRVWDIETGQCLHVLMGHVAAVRCVQYDGRRVVSGAYDFMVKVWDPETETCLHTLQ  420

Human  421  GHTNRVYSLQFDGIHVVSGSLDTSIRVWDVETGNCIHTLTGHQSLTSGMELKDNILVSGN  480
            GHTNRVYSLQFDGIHVVSGSLDTSIRVWDVETGNCIHTLTGHQSLTSGMELKDNILVSGN
Mouse  421  GHTNRVYSLQFDGIHVVSGSLDTSIRVWDVETGNCIHTLTGHQSLTSGMELKDNILVSGN  480

Human  481  ADSTVKIWDIKTGQCLQTLQGPNKHQSAVTCLQFNKNFVITSSDDGTVKLWDLKTGEFIR  540
            ADSTVKIWDIKTGQCLQTLQGP+KHQSAVTCLQFNKNFVITSSDDGTVKLWDLKTGEFIR
Mouse  481  ADSTVKIWDIKTGQCLQTLQGPSKHQSAVTCLQFNKNFVITSSDDGTVKLWDLKTGEFIR  540

Human  541  NLVTLESGGSGGVVWRIRASNTKLVCAVGSRNGTEETKLLVLDFDVDMK  589
            NLVTLESGGSGGVVWRIRASNTKLVCAVGSRNGTEETKLLVLDFDVDMK
Mouse  541  NLVTLESGGSGGVVWRIRASNTKLVCAVGSRNGTEETKLLVLDFDVDMK  589
```

Figure C.3: Alignment of FBXW7γ isoform protein sequence of human and mouse. Sequence obtained from Ensembl and aligned using BLASTP software. Highlighted in yellow are non-conserved residues, highlighted in green is the conserved arginine residue (human 479, mouse 482), critical in substrate recognition and commonly mutated in cancers.

Appendix D

Aged *Fbxw7*-mutant mice

Genotype	Mouse Number	Age	Genotype	Mouse Number	Age
R482Q/+	13	418	R482Q/+	38	442
R482Q/+	14	418	R482Q/+	39	397
R482Q/+	15	396	R482Q/+	40	396
R482Q/+	16	453	R482Q/+	41	401
R482Q/+	17	488	Wildtype	1	396
R482Q/+	18	488	Wildtype	2	453
R482Q/+	19	427	Wildtype	3	452
R482Q/+	20	488	Wildtype	4	522
R482Q/+	21	522	Wildtype	5	525
R482Q/+	22	488	Wildtype	6	452
R482Q/+	23	488	Wildtype	7	423
R482Q/+	24	453	Wildtype	8	383
R482Q/+	25	519	Wildtype	9	399
R482Q/+	26	439	Wildtype	10	400
R482Q/+	27	383	$Fbxw7^{\Delta/+}$	3	310
R482Q/+	28	383	$Fbxw7^{\Delta/+}$	4	310
R482Q/+	29	359	$Fbxw7^{\Delta/+}$	5	383
R482Q/+	30	315	$Fbxw7^{\Delta/+}$	6	383
R482Q/+	31	333	$Fbxw7^{\Delta/+}$	7	383
R482Q/+	32	315	$Fbxw7^{\Delta/+}$	8	315
R482Q/+	33	315	$Fbxw7^{\Delta/+}$	9	399
R482Q/+	34	315	$Fbxw7^{\Delta/+}$	10	400
R482Q/+	35	375	$Fbxw7^{\Delta/+}$	11	368
R482Q/+	36	365	$Fbxw7^{\Delta/+}$	12	343
R482Q/+	37	412	$Fbxw7^{\Delta/+}$	13	343

Table D.1: Ages of *Fbxw7*-mutant mice which did not display any intestinal phenotypes, age shown in days.

Appendix E

R482Q/*Vil1*-Cre/*Apc*-mutant breeding

Parents: ♀ ♂

R482Q/R482Q, Vil1-Cre (het) x Apc^{Min} (het)

Possible Offspring:

R482Q	Vil1-Cre	Apc^{Min}	Useful?
R482Q/+	Positive	Het	YES, TEST
R482Q/+	Positive	Wt	NO
R482Q/+	Negative	Het	YES, CONTROL
R482Q/+	Negative	Wt	NO

Parents: ♀ ♂

R482Q/+, Vil1-Cre (het) x R482Q/+, Apc^{Min} (het)

Possible Offspring:

R482Q	Vil1-Cre	Apc^{Min}	Useful?
R482Q/R482Q	Positive	Het	YES, TEST R482Q/R482Q
R482Q/R482Q	Positive	Wt	NO
R482Q/R482Q	Negative	Het	YES, CONTROL
R482Q/R482Q	Negative	Wt	NO
R482Q/+	Positive	Het	YES, TEST
R482Q/+	Positive	Wt	NO
R482Q/+	Negative	Het	YES, CONTROL
R482Q/+	Negative	Wt	NO

Figure E.1: Examples of breeding crosses used to generate R482Q/+ Apc^{Min} compound mice. Possible genotypes combinations of offspring are shown.

Parents: ♀ ♂

R482Q/R482Q, Vil1-Cre (het)	x	Apc^{1322T} (het)
	OR	
R482Q/R482Q	x	Apc^{1322T} (het), Vil1-Cre

Possible Offspring:

R482Q	Vil1-Cre	Apc^{1322T}	Useful?
R482Q/+	Positive	Het	YES, TEST
R482Q/+	Positive	Wt	NO
R482Q/+	Negative	Het	YES, CONTROL
R482Q/+	Negative	Wt	NO

Parents: ♀ ♂

R482Q/+, Vil1-Cre (het)	x	R482Q/+, Apc^{1322T} (het)

Possible Offspring:

R482Q	Vil1-Cre	Apc^{1322T}	Useful?
R482Q/R482Q	Positive	Het	YES, TEST R482Q/R482Q
R482Q/R482Q	Positive	Wt	NO
R482Q/R482Q	Negative	Het	YES, CONTROL
R482Q/R482Q	Negative	Wt	NO
R482Q/+	Positive	Het	YES, TEST
R482Q/+	Positive	Wt	NO
R482Q/+	Negative	Het	YES, CONTROL
R482Q/+	Negative	Wt	NO

Figure E.2: Examples of breeding crosses used to generate R482Q/+ Apc^{1322T} compound mice. Possible genotypes combinations of offspring are shown.

Appendix F

Raw intestinal polyp data from R482Q/+ *Apc*-mutant compound mice

Label	Genotype	Age	Sex	SB1 <1	SB1 1-2	SB1 2-3	SB1 3+	SB2 <1	SB2 1-2	SB2 2-3	SB2 3+	SB3 <1	SB3 1-2	SB3 2-3	SB3 3+	COL <1	COL 1-2	COL 2-3	COL 3+
A	R482Q/+ Apc^{Mn}	105	F	3	5	5	3	5	12	4	1	8	17	7	0	2	1	1	0
B	R482Q/+ Apc^{Mn}	101	F	2	11	6	2	6	11	6	1	13	26	6	0	3	2	1	1
C	R482Q/+ Apc^{Mn}	87	M	0	8	4	1	0	7	4	2	10	21	9	1	0	1	0	0
D	R482Q/+ Apc^{Mn}	98	F	0	11	5	2	5	23	6	0	6	30	8	1	2	0	1	0
E	R482Q/+ Apc^{Mn}	90	M	2	17	6	2	0	21	12	1	5	21	9	0	0	0	0	0
F	R482Q/+ Apc^{Mn}	90	M	1	11	4	1	8	25	5	0	10	20	7	0	0	0	1	0
G	R482Q/+ Apc^{Mn}	111	M	0	5	2	2	0	13	7	2	5	20	6	0	3	0	0	1
H	R482Q/+ Apc^{Mn}	98	M	0	3	4	3	4	13	2	0	2	13	5	0	0	0	0	0
I	Apc^{Mn}	99	M	2	3	0	0	7	1	0	0	15	1	0	0	2	1	0	0
J	Apc^{Mn}	99	M	1	3	1	0	6	1	0	0	9	6	0	0	3	0	0	1
K	Apc^{Mn}	105	F	0	4	0	1	5	10	0	0	13	14	0	0	2	0	0	0
L	Apc^{Mn}	101	M	1	1	1	0	12	2	0	0	13	9	0	0	0	0	0	0
M	Apc^{Mn}	101	M	1	2	0	0	1	4	0	0	8	6	0	0	0	0	0	0

Table F.1: Raw intestinal polyp data from R482Q/+ Apc^{Min} compound and Apc^{Min} mice. Polyps have been categorised according to intestinal location (SB1, SB2, SB3 and colon) and size (diameter in mm). 8 R482Q/+ Apc^{Min} and 5 Apc^{Min} mice have been analysed.

Label	Genotype	Age	Sex	SB1 <1	SB1 1-2	SB1 2-3	SB1 3+	SB2 <1	SB2 1-2	SB2 2-3	SB2 3+	SB3 <1	SB3 1-2	SB3 2-3	SB3 3+	COL <1	COL 1-2	COL 2-3	COL 3+
A	R482Q/+ Apc^{1322T}	95	F	12	13	6	5	3	18	4	2	5	6	6	1	0	0	0	0
B	R482Q/+ Apc^{1322T}	110	F	2	9	6	4	0	6	5	1	1	1	1	0	1	0	0	0
C	R482Q/+ Apc^{1322T}	80	M	6	14	8	3	12	10	2	0	3	6	1	1	0	0	0	0
D	R482Q/+ Apc^{1322T}	123	F	3	1	5	3	2	8	5	0	1	1	0	0	1	0	0	0
E	R482Q/+ Apc^{1322T}	88	F	7	10	8	3	2	12	3	1	4	2	1	0	0	0	0	0
F	R482Q/+ Apc^{1322T}	93	M	1	2	1	3	2	1	0	0	0	0	0	0	0	0	0	0
G	R482Q/+ Apc^{1322T}	108	F	1	1	3	7	0	3	1	0	2	2	0	0	0	0	0	0
H	R482Q/+ Apc^{1322T}	71	F	11	20	10	2	11	19	3	0	1	10	1	0	0	1	0	0
I	R482Q/+ Apc^{1322T}	113	M	0	2	3	5	2	4	1	3	0	0	2	0	1	0	0	0
J	R482Q/+ Apc^{1322T}	118	F	0	7	5	6	0	0	3	2	0	0	1	2	0	0	0	0
K	R482Q/+ Apc^{1322T}	118	M	0	4	4	2	3	3	2	0	0	3	0	1	0	0	0	0
L	R482Q/+ Apc^{1322T}	118	M	1	2	4	3	3	2	1	2	0	2	2	0	0	1	0	0
M	R482Q/+ Apc^{1322T}	108	F	1	1	3	7	0	3	1	0	2	2	0	0	0	0	0	0
N	Apc^{1322T}	95	F	7	2	2	0	13	2	2	0	12	4	0	0	0	0	0	0
O	Apc^{1322T}	110	F	4	5	1	0	1	2	0	0	0	1	0	0	0	0	0	0
P	Apc^{1322T}	80	F	5	3	2	0	2	0	0	0	2	0	0	0	0	0	0	0
Q	Apc^{1322T}	123	F	2	3	0	2	1	0	1	1	1	2	0	0	0	0	0	0
R	Apc^{1322T}	93	F	6	2	2	0	0	2	0	0	0	0	0	0	0	0	0	0
S	Apc^{1322T}	71	M	7	7	4	1	12	4	3	0	2	3	0	0	0	1	0	0
T	Apc^{1322T}	118	F	0	3	6	6	0	4	5	3	0	0	0	0	3	0	0	0
U	Apc^{1322T}	110	F	2	8	2	5	0	3	3	4	0	2	0	0	0	0	1	0
V	Apc^{1322T}	127	F	6	10	6	3	5	4	2	4	1	4	0	0	2	1	1	0

Table F.2: Raw intestinal polyp data from R482Q/+ Apc^{1322T} compound and Apc^{1322T} mice. Polyps have been categorised according to intestinal location (SB1, SB2, SB3 and colon) and size (diameter in mm). 13 R482Q/+ Apc^{1322T} and 9 Apc^{1322T} mice have been analysed.

References

[1] S. Akhoondi, D. Sun, N. von der Lehr, S. Apostolidou, K. Klotz, A. Maljukova, D. Cepeda, H. Fiegl, D. Dafou, C. Marth, E. Mueller-Holzner, M. Corcoran, M. Dagnell, S. Z. Nejad, B. N. Nayer, M. R. Zali, J. Hansson, S. Egyhazi, F. Petersson, P. Sangfelt, H. Nordgren, D. Grander, S. I. Reed, M. Widschwendter, O. Sangfelt, and C. Spruck, "Fbxw7/hcdc4 is a general tumor suppressor in human cancer," *Cancer Res*, vol. 67, no. 19, pp. 9006–12, 2007. 1, 12, 14, 18, 25, 72, 73, 74, 112, 114, 163, 166

[2] D. Hanahan and R. A. Weinberg, "The hallmarks of cancer," *Cell*, vol. 100, no. 1, pp. 57–70, 2000. 1

[3] D. Hanahan and R. A. Weinberg, "Hallmarks of cancer: the next generation," *Cell*, vol. 144, no. 5, pp. 646–74, 2011. 1

[4] J. Ferlay, H. R. Shin, F. Bray, D. Forman, C. Mathers, and D. M. Parkin, "Estimates of worldwide burden of cancer in 2008: Globocan 2008," *Int J Cancer*, vol. 127, no. 12, pp. 2893–917, 2010. 2

[5] D. Pinto and H. Clevers, "Wnt, stem cells and cancer in the intestine," *Biol Cell*, vol. 97, no. 3, pp. 185–96, 2005. 3

[6] N. A. Wright and M. Irwin, "The kinetics of villus cell populations in the mouse small intestine. i. normal villi: the steady state requirement," *Cell Tissue Kinet*, vol. 15, no. 6, pp. 595–609, 1982. 3

[7] T. P. Pretlow, W. Edelmann, R. Kucherlapati, T. G. Pretlow, and L. H. Augenlicht, "Spontaneous aberrant crypt foci in apc1638n mice with a mutant apc allele," *Am J Pathol*, vol. 163, no. 5, pp. 1757–63, 2003. 4

[8] J. E. Paulsen, I. L. Steffensen, E. M. Loberg, T. Husoy, E. Namork, and J. Alexander, "Qualitative and quantitative relationship between dysplastic aberrant crypt foci and tumorigenesis in the min/+ mouse colon," *Cancer Res*, vol. 61, no. 13, pp. 5010–5, 2001. 4

[9] E. Sangiorgi and M. R. Capecchi, "Bmi1 is expressed in vivo in intestinal stem cells," *Nat Genet*, vol. 40, no. 7, pp. 915–20, 2008. 4

[10] T. Kayahara, M. Sawada, S. Takaishi, H. Fukui, H. Seno, H. Fukuzawa, K. Suzuki, H. Hiai, R. Kageyama, H. Okano, and T. Chiba, "Candidate markers for stem and early progenitor cells, musashi-1 and hes1, are expressed in crypt base columnar cells of mouse small intestine," *FEBS Lett*, vol. 535, no. 1-3, pp. 131–5, 2003. 4

[11] C. S. Potten, C. Booth, G. L. Tudor, D. Booth, G. Brady, P. Hurley, G. Ashton, R. Clarke, S. Sakakibara, and H. Okano, "Identification of a putative intestinal stem cell and early lineage marker; musashi-1," *Differentiation*, vol. 71, no. 1, pp. 28–41, 2003. 4

[12] N. Barker, J. H. van Es, J. Kuipers, P. Kujala, M. van den Born, M. Cozijnsen, A. Haegebarth, J. Korving, H. Begthel, P. J. Peters, and H. Clevers, "Identification of stem cells in small intestine and colon by marker gene lgr5," *Nature*, vol. 449, no. 7165, pp. 1003–7, 2007. 4

[13] E. R. Fearon and B. Vogelstein, "A genetic model for colorectal tumorigenesis," *Cell*, vol. 61, no. 5, pp. 759–67, 1990. 5

[14] L. D. Wood, D. W. Parsons, S. Jones, J. Lin, T. Sjoblom, R. J. Leary, D. Shen, S. M. Boca, T. Barber, J. Ptak, N. Silliman, S. Szabo, Z. Dezso, V. Ustyanksky, T. Nikolskaya, Y. Nikolsky, R. Karchin, P. A. Wilson, J. S. Kaminker, Z. Zhang, R. Croshaw,

J. Willis, D. Dawson, M. Shipitsin, J. K. Willson, S. Sukumar, K. Polyak, B. H. Park, C. L. Pethiyagoda, P. V. Pant, D. G. Ballinger, A. B. Sparks, J. Hartigan, D. R. Smith, E. Suh, N. Papadopoulos, P. Buckhaults, S. D. Markowitz, G. Parmigiani, K. W. Kinzler, V. E. Velculescu, and B. Vogelstein, "The genomic landscapes of human breast and colorectal cancers," *Science*, vol. 318, no. 5853, pp. 1108–13, 2007. 5

[15] T. Sjoblom, S. Jones, L. D. Wood, D. W. Parsons, J. Lin, T. D. Barber, D. Mandelker, R. J. Leary, J. Ptak, N. Silliman, S. Szabo, P. Buckhaults, C. Farrell, P. Meeh, S. D. Markowitz, J. Willis, D. Dawson, J. K. Willson, A. F. Gazdar, J. Hartigan, L. Wu, C. Liu, G. Parmigiani, B. H. Park, K. E. Bachman, N. Papadopoulos, B. Vogelstein, K. W. Kinzler, and V. E. Velculescu, "The consensus coding sequences of human breast and colorectal cancers," *Science*, vol. 314, no. 5797, pp. 268–74, 2006. 5

[16] S. Velho, C. Oliveira, A. Ferreira, A. C. Ferreira, G. Suriano, J. Schwartz, S., A. Duval, F. Carneiro, J. C. Machado, R. Hamelin, and R. Seruca, "The prevalence of pik3ca mutations in gastric and colon cancer," *Eur J Cancer*, vol. 41, no. 11, pp. 1649–54, 2005. 5

[17] S. Velho, C. Moutinho, L. Cirnes, C. Albuquerque, R. Hamelin, F. Schmitt, F. Carneiro, C. Oliveira, and R. Seruca, "Braf, kras and pik3ca mutations in colorectal serrated polyps and cancer: primary or secondary genetic events in colorectal carcinogenesis?," *BMC Cancer*, vol. 8, p. 255, 2008. 5

[18] H. Rajagopalan, P. V. Jallepalli, C. Rago, V. E. Velculescu, K. W. Kinzler, B. Vogelstein, and C. Lengauer, "Inactivation of hcdc4 can cause chromosomal instability," *Nature*, vol. 428, no. 6978, pp. 77–81, 2004. 5, 19, 20, 74, 115, 137, 164, 166, 180

[19] Z. Kemp, A. Rowan, W. Chambers, N. Wortham, S. Halford, O. Sieber, N. Mortensen, A. von Herbay, T. Gunther, M. Ilyas, and I. Tomlinson, "Cdc4 mutations occur in a subset of colorectal cancers but are not predicted to cause loss of function and are not

associated with chromosomal instability," *Cancer Res*, vol. 65, no. 24, pp. 11361–6, 2005. 5, 19, 20, 72, 74, 115, 130, 163, 178

[20] M. Miyaki, T. Yamaguchi, T. Iijima, K. Takahashi, H. Matsumoto, and T. Mori, "Somatic mutations of the cdc4 (fbxw7) gene in hereditary colorectal tumors," *Oncology*, vol. 76, no. 6, pp. 430–4, 2009. 5, 19, 20, 115

[21] E. Sancho, E. Batlle, and H. Clevers, "Signaling pathways in intestinal development and cancer," *Annu Rev Cell Dev Biol*, vol. 20, pp. 695–723, 2004. 5

[22] J. Groden, A. Thliveris, W. Samowitz, M. Carlson, L. Gelbert, H. Albertsen, G. Joslyn, J. Stevens, L. Spirio, M. Robertson, and et al., "Identification and characterization of the familial adenomatous polyposis coli gene," *Cell*, vol. 66, no. 3, pp. 589–600, 1991. 6

[23] K. W. Kinzler, M. C. Nilbert, B. Vogelstein, T. M. Bryan, D. B. Levy, K. J. Smith, A. C. Preisinger, S. R. Hamilton, P. Hedge, A. Markham, and et al., "Identification of a gene located at chromosome 5q21 that is mutated in colorectal cancers," *Science*, vol. 251, no. 4999, pp. 1366–70, 1991. 6

[24] I. S. Nathke, "The adenomatous polyposis coli protein: the achilles heel of the gut epithelium," *Annu Rev Cell Dev Biol*, vol. 20, pp. 337–66, 2004. 6

[25] T. C. He, A. B. Sparks, C. Rago, H. Hermeking, L. Zawel, L. T. da Costa, P. J. Morin, B. Vogelstein, and K. W. Kinzler, "Identification of c-myc as a target of the apc pathway," *Science*, vol. 281, no. 5382, pp. 1509–12, 1998. 6

[26] O. Tetsu and F. McCormick, "Beta-catenin regulates expression of cyclin d1 in colon carcinoma cells," *Nature*, vol. 398, no. 6726, pp. 422–6, 1999. 6

[27] H. Lamlum, M. Ilyas, A. Rowan, S. Clark, V. Johnson, J. Bell, I. Frayling, J. Efstathiou, K. Pack, S. Payne, R. Roylance, P. Gorman, D. Sheer, K. Neale, R. Phillips, I. Talbot, W. Bodmer, and I. Tomlinson, "The type of somatic mutation at apc in familial adenomatous polyposis is determined by the site of the germline mutation:

a new facet to knudson's 'two-hit' hypothesis," *Nat Med*, vol. 5, no. 9, pp. 1071–5, 1999. 7, 143, 200

[28] C. Albuquerque, C. Breukel, R. van der Luijt, P. Fidalgo, P. Lage, F. J. Slors, C. N. Leitao, R. Fodde, and R. Smits, "The 'just-right' signaling model: Apc somatic mutations are selected based on a specific level of activation of the beta-catenin signaling cascade," *Hum Mol Genet*, vol. 11, no. 13, pp. 1549–60, 2002. 7, 143, 200

[29] R. Fodde, R. Smits, and H. Clevers, "Apc, signal transduction and genetic instability in colorectal cancer," *Nat Rev Cancer*, vol. 1, no. 1, pp. 55–67, 2001. 7

[30] M. Barbacid, "ras genes," *Annu Rev Biochem*, vol. 56, pp. 779–827, 1987. 8

[31] T. Hinoi, A. Akyol, B. K. Theisen, D. O. Ferguson, J. K. Greenson, B. O. Williams, K. R. Cho, and E. R. Fearon, "Mouse model of colonic adenoma-carcinoma progression based on somatic apc inactivation," *Cancer Res*, vol. 67, no. 20, pp. 9721–30, 2007. 8, 9

[32] H. L. Moses, J. Coffey, R. J., E. B. Leof, R. M. Lyons, and J. Keski-Oja, "Transforming growth factor beta regulation of cell proliferation," *J Cell Physiol Suppl*, vol. Suppl 5, pp. 1–7, 1987. 8, 111, 159

[33] R. J. Akhurst and R. Derynck, "Tgf-beta signaling in cancer–a double-edged sword," *Trends Cell Biol*, vol. 11, no. 11, pp. S44–51, 2001. 8, 159

[34] K. L. Woodford-Richens, A. J. Rowan, P. Gorman, S. Halford, D. C. Bicknell, H. S. Wasan, R. R. Roylance, W. F. Bodmer, and I. P. Tomlinson, "Smad4 mutations in colorectal cancer probably occur before chromosomal instability, but after divergence of the microsatellite instability pathway," *Proc Natl Acad Sci U S A*, vol. 98, no. 17, pp. 9719–23, 2001. 9

[35] R. Salovaara, S. Roth, A. Loukola, V. Launonen, P. Sistonen, E. Avizienyte, P. Kristo, H. Jarvinen, S. Souchelnytskyi, M. Sarlomo-Rikala, and L. A. Aaltonen, "Frequent

loss of smad4/dpc4 protein in colorectal cancers," *Gut*, vol. 51, no. 1, pp. 56–9, 2002. 9

[36] D. P. Lane, "Cancer. p53, guardian of the genome," *Nature*, vol. 358, no. 6381, pp. 15–6, 1992. 9

[37] B. Vogelstein, D. Lane, and A. J. Levine, "Surfing the p53 network," *Nature*, vol. 408, no. 6810, pp. 307–10, 2000. 9

[38] A. P. Arrigo, K. Tanaka, A. L. Goldberg, and W. J. Welch, "Identity of the 19s 'prosome' particle with the large multifunctional protease complex of mammalian cells (the proteasome)," *Nature*, vol. 331, no. 6152, pp. 192–4, 1988. 9

[39] A. Hershko, H. Heller, S. Elias, and A. Ciechanover, "Components of ubiquitin-protein ligase system. resolution, affinity purification, and role in protein breakdown," *J Biol Chem*, vol. 258, no. 13, pp. 8206–14, 1983. 10

[40] A. M. Burger and A. K. Seth, "The ubiquitin-mediated protein degradation pathway in cancer: therapeutic implications," *Eur J Cancer*, vol. 40, no. 15, pp. 2217–29, 2004. 11

[41] C. Bai, P. Sen, K. Hofmann, L. Ma, M. Goebl, J. W. Harper, and S. J. Elledge, "Skp1 connects cell cycle regulators to the ubiquitin proteolysis machinery through a novel motif, the f-box," *Cell*, vol. 86, no. 2, pp. 263–74, 1996. 10, 15

[42] J. Jin, T. Cardozo, R. C. Lovering, S. J. Elledge, M. Pagano, and J. W. Harper, "Systematic analysis and nomenclature of mammalian f-box proteins," *Genes Dev*, vol. 18, no. 21, pp. 2573–80, 2004. 11

[43] T. Cardozo and M. Pagano, "The scf ubiquitin ligase: insights into a molecular machine," *Nat Rev Mol Cell Biol*, vol. 5, no. 9, pp. 739–51, 2004. 11

[44] L. H. Hartwell, R. K. Mortimer, J. Culotti, and M. Culotti, "Genetic control of the cell division cycle in yeast: V. genetic analysis of cdc mutants," *Genetics*, vol. 74, no. 2, pp. 267–86, 1973. 13

[45] R. M. Feldman, C. C. Correll, K. B. Kaplan, and R. J. Deshaies, "A complex of cdc4p, skp1p, and cdc53p/cullin catalyzes ubiquitination of the phosphorylated cdk inhibitor sic1p," *Cell*, vol. 91, no. 2, pp. 221–30, 1997. 13

[46] S. Henchoz, Y. Chi, B. Catarin, I. Herskowitz, R. J. Deshaies, and M. Peter, "Phosphorylation- and ubiquitin-dependent degradation of the cyclin-dependent kinase inhibitor far1p in budding yeast," *Genes Dev*, vol. 11, no. 22, pp. 3046–60, 1997. 13

[47] E. J. Hubbard, G. Wu, J. Kitajewski, and I. Greenwald, "sel-10, a negative regulator of lin-12 activity in caenorhabditis elegans, encodes a member of the cdc4 family of proteins," *Genes Dev*, vol. 11, no. 23, pp. 3182–93, 1997. 13, 29

[48] A. C. Minella and B. E. Clurman, "Mechanisms of tumor suppression by the scf(fbw7)," *Cell Cycle*, vol. 4, no. 10, pp. 1356–9, 2005. 13

[49] Y. Tan, O. Sangfelt, and C. Spruck, "The fbxw7/hcdc4 tumor suppressor in human cancer," *Cancer Lett*, vol. 271, no. 1, pp. 1–12, 2008. 13

[50] M. Welcker and B. E. Clurman, "Fbw7 ubiquitin ligase: a tumour suppressor at the crossroads of cell division, growth and differentiation," *Nat Rev Cancer*, vol. 8, no. 2, pp. 83–93, 2008. 13, 14, 15

[51] Y. Cheng and G. Li, "Role of the ubiquitin ligase fbw7 in cancer progression," *Cancer Metastasis Rev*, 2011. 13, 33

[52] H. Strohmaier, C. H. Spruck, P. Kaiser, K. A. Won, O. Sangfelt, and S. I. Reed, "Human f-box protein hcdc4 targets cyclin e for proteolysis and is mutated in a breast cancer cell line," *Nature*, vol. 413, no. 6853, pp. 316–22, 2001. 13, 18, 25

[53] D. M. Koepp, L. K. Schaefer, X. Ye, K. Keyomarsi, C. Chu, J. W. Harper, and S. J. Elledge, "Phosphorylation-dependent ubiquitination of cyclin e by the scffbw7 ubiquitin ligase," *Science*, vol. 294, no. 5540, pp. 173–7, 2001. 13, 16, 25, 164

[54] K. H. Moberg, D. W. Bell, D. C. Wahrer, D. A. Haber, and I. K. Hariharan, "Archipelago regulates cyclin e levels in drosophila and is mutated in human cancer cell lines," *Nature*, vol. 413, no. 6853, pp. 311–6, 2001. 13, 25

[55] C. H. Spruck, H. Strohmaier, O. Sangfelt, H. M. Muller, M. Hubalek, E. Muller-Holzner, C. Marth, M. Widschwendter, and S. I. Reed, "hcdc4 gene mutations in endometrial cancer," *Cancer Res*, vol. 62, no. 16, pp. 4535–9, 2002. 13, 18

[56] M. Welcker, A. Orian, J. E. Grim, R. N. Eisenman, and B. E. Clurman, "A nucleolar isoform of the fbw7 ubiquitin ligase regulates c-myc and cell size," *Curr Biol*, vol. 14, no. 20, pp. 1852–7, 2004. 13, 28

[57] A. Matsumoto, Y. Tateishi, I. Onoyama, Y. Okita, K. Nakayama, and K. I. Nakayama, "Fbxw7beta resides in the endoplasmic reticulum membrane and protects cells from oxidative stress," *Cancer Sci*, vol. 102, no. 4, pp. 749–55, 2011. 13, 14

[58] P. Bonetti, T. Davoli, C. Sironi, B. Amati, P. G. Pelicci, and E. Colombo, "Nucleophosmin and its aml-associated mutant regulate c-myc turnover through fbw7 gamma," *J Cell Biol*, vol. 182, no. 1, pp. 19–26, 2008. 13

[59] M. Welcker, E. A. Larimore, L. Frappier, and B. E. Clurman, "Nucleolar targeting of the fbw7 ubiquitin ligase by a pseudosubstrate and glycogen synthase kinase 3," *Mol Cell Biol*, vol. 31, no. 6, pp. 1214–24, 2011. 13

[60] A. Matsumoto, I. Onoyama, and K. I. Nakayama, "Expression of mouse fbxw7 isoforms is regulated in a cell cycle- or p53-dependent manner," *Biochem Biophys Res Commun*, vol. 350, no. 1, pp. 114–9, 2006. 13, 104, 114, 196

[61] J. E. Grim, M. P. Gustafson, R. K. Hirata, A. C. Hagar, J. Swanger, M. Welcker, H. C. Hwang, J. Ericsson, D. W. Russell, and B. E. Clurman, "Isoform- and cell cycle-dependent substrate degradation by the fbw7 ubiquitin ligase," *J Cell Biol*, vol. 181, no. 6, pp. 913–20, 2008. 14

[62] F. van Drogen, O. Sangfelt, A. Malyukova, L. Matskova, E. Yeh, A. R. Means, and S. I. Reed, "Ubiquitylation of cyclin e requires the sequential function of scf complexes containing distinct hcdc4 isoforms," *Mol Cell*, vol. 23, no. 1, pp. 37–48, 2006. 14, 196

[63] O. Sangfelt, D. Cepeda, A. Malyukova, F. van Drogen, and S. I. Reed, "Both scf(cdc4alpha) and scf(cdc4gamma) are required for cyclin e turnover in cell lines that do not overexpress cyclin e," *Cell Cycle*, vol. 7, no. 8, pp. 1075–82, 2008. 14, 196

[64] T. F. Smith, C. Gaitatzes, K. Saxena, and E. J. Neer, "The wd repeat: a common architecture for diverse functions," *Trends Biochem Sci*, vol. 24, no. 5, pp. 181–5, 1999. 15

[65] S. Orlicky, X. Tang, A. Willems, M. Tyers, and F. Sicheri, "Structural basis for phosphodependent substrate selection and orientation by the scfcdc4 ubiquitin ligase," *Cell*, vol. 112, no. 2, pp. 243–56, 2003. 15, 16, 25, 206

[66] B. Hao, S. Oehlmann, M. E. Sowa, J. W. Harper, and N. P. Pavletich, "Structure of a fbw7-skp1-cyclin e complex: multisite-phosphorylated substrate recognition by scf ubiquitin ligases," *Mol Cell*, vol. 26, no. 1, pp. 131–43, 2007. 15, 17, 27, 206

[67] J. M. Galan and M. Peter, "Ubiquitin-dependent degradation of multiple f-box proteins by an autocatalytic mechanism," *Proc Natl Acad Sci U S A*, vol. 96, no. 16, pp. 9124–9, 1999. 15

[68] N. Pashkova, L. Gakhar, S. C. Winistorfer, L. Yu, S. Ramaswamy, and R. C. Piper, "Wd40 repeat propellers define a ubiquitin-binding domain that regulates turnover of f box proteins," *Mol Cell*, vol. 40, no. 3, pp. 433–43, 2010. 16, 35

[69] W. Zhang and D. M. Koepp, "Fbw7 isoform interaction contributes to cyclin e proteolysis," *Mol Cancer Res*, vol. 4, no. 12, pp. 935–43, 2006. 16, 163, 194

[70] M. Welcker and B. E. Clurman, "Fbw7/hcdc4 dimerization regulates its substrate interactions," *Cell Div*, vol. 2, p. 7, 2007. 16, 73, 74, 163, 194

[71] X. Tang, S. Orlicky, Z. Lin, A. Willems, D. Neculai, D. Ceccarelli, F. Mercurio, B. H. Shilton, F. Sicheri, and M. Tyers, "Suprafacial orientation of the scfcdc4 dimer accommodates multiple geometries for substrate ubiquitination," *Cell*, vol. 129, no. 6, pp. 1165–76, 2007. 16

[72] P. Nash, X. Tang, S. Orlicky, Q. Chen, F. B. Gertler, M. D. Mendenhall, F. Sicheri, T. Pawson, and M. Tyers, "Multisite phosphorylation of a cdk inhibitor sets a threshold for the onset of dna replication," *Nature*, vol. 414, no. 6863, pp. 514–21, 2001. 16

[73] S. Bamford, E. Dawson, S. Forbes, J. Clements, R. Pettett, A. Dogan, A. Flanagan, J. Teague, P. A. Futreal, M. R. Stratton, and R. Wooster, "The cosmic (catalogue of somatic mutations in cancer) database and website," *Br J Cancer*, vol. 91, no. 2, pp. 355–8, 2004. 18

[74] J. Woo Lee, Y. Hwa Soung, S. Young Kim, S. Woo Nam, W. Sang Park, J. Young Lee, N. Jin Yoo, and S. Hyung Lee, "Somatic mutation of hcdc4 gene is rare in lung adenocarcinomas," *Acta Oncol*, vol. 45, no. 4, pp. 487–8, 2006. 18, 205

[75] D. Nowak, M. Mossner, C. D. Baldus, O. Hopfer, E. Thiel, and W. K. Hofmann, "Mutation analysis of hcdc4 in aml cells identifies a new intronic polymorphism," *Int J Med Sci*, vol. 3, no. 4, pp. 148–51, 2006. 18

[76] E. L. Kwak, K. H. Moberg, D. C. Wahrer, J. E. Quinn, P. M. Gilmore, C. A. Graham, I. K. Hariharan, D. P. Harkin, D. A. Haber, and D. W. Bell, "Infrequent mutations of archipelago (hago, hcdc4, fbw7) in primary ovarian cancer," *Gynecol Oncol*, vol. 98, no. 1, pp. 124–8, 2005. 18

[77] T. Yan, J. S. Wunder, N. Gokgoz, K. K. Seto, R. S. Bell, and I. L. Andrulis, "hcdc4 variation in osteosarcoma," *Cancer Genet Cytogenet*, vol. 169, no. 2, pp. 138–42, 2006. 18

[78] A. P. Weng, A. A. Ferrando, W. Lee, J. P. t. Morris, L. B. Silverman, C. Sanchez-Irizarry, S. C. Blacklow, A. T. Look, and J. C. Aster, "Activating mutations of notch1 in human t cell acute lymphoblastic leukemia," *Science*, vol. 306, no. 5694, pp. 269–71, 2004. 19, 29

[79] B. J. Thompson, S. Buonamici, M. L. Sulis, T. Palomero, T. Vilimas, G. Basso, A. Ferrando, and I. Aifantis, "The scffbw7 ubiquitin ligase complex as a tumor suppressor in t cell leukemia," *J Exp Med*, vol. 204, no. 8, pp. 1825–35, 2007. 19, 29

[80] A. Malyukova, T. Dohda, N. von der Lehr, S. Akhoondi, M. Corcoran, M. Heyman, C. Spruck, D. Grander, U. Lendahl, and O. Sangfelt, "The tumor suppressor gene hcdc4 is frequently mutated in human t-cell acute lymphoblastic leukemia with functional consequences for notch signaling," *Cancer Res*, vol. 67, no. 12, pp. 5611–6, 2007. 19

[81] V. Asnafi, A. Buzyn, S. Le Noir, F. Baleydier, A. Simon, K. Beldjord, O. Reman, F. Witz, T. Fagot, E. Tavernier, P. Turlure, T. Leguay, F. Huguet, J. P. Vernant, F. Daniel, M. C. Bene, N. Ifrah, X. Thomas, H. Dombret, and E. Macintyre, "Notch1/fbxw7 mutation identifies a large subgroup with favorable outcome in adult t-cell acute lymphoblastic leukemia (t-all): a group for research on adult acute lymphoblastic leukemia (graall) study," *Blood*, vol. 113, no. 17, pp. 3918–24, 2009. 19

[82] A. G. Knudson, "Hereditary cancer: two hits revisited," *J Cancer Res Clin Oncol*, vol. 122, no. 3, pp. 135–40, 1996. 19, 74, 163, 201

[83] S. Knuutila, Y. Aalto, K. Autio, A. M. Bjorkqvist, W. El-Rifai, S. Hemmer, T. Huhta, E. Kettunen, S. Kiuru-Kuhlefelt, M. L. Larramendy, T. Lushnikova, O. Monni, H. Pere, J. Tapper, M. Tarkkanen, A. Varis, V. M. Wasenius, M. Wolf, and Y. Zhu, "Dna copy number losses in human neoplasms," *Am J Pathol*, vol. 155, no. 3, pp. 683–94, 1999. 22

[84] A. Sterian, T. Kan, A. T. Berki, Y. Mori, A. Olaru, K. Schulmann, F. Sato, S. Wang, B. Paun, K. Cai, J. P. Hamilton, J. M. Abraham, and S. J. Meltzer, "Mutational and loh analyses of the chromosome 4q region in esophageal adenocarcinoma," *Oncology*, vol. 70, no. 3, pp. 168–72, 2006. 22

[85] R. P. Kuiper, L. Vreede, R. Venkatachalam, C. Ricketts, E. Kamping, E. Verwiel, L. Govaerts, M. Debiec-Rychter, E. Lerut, F. van Erp, N. Hoogerbrugge, L. van Kempen, E. F. Schoenmakers, A. Bonne, E. R. Maher, and A. Geurts van Kessel, "The tumor suppressor gene fbxw7 is disrupted by a constitutional t(3;4)(q21;q31) in a patient with renal cell cancer," *Cancer Genet Cytogenet*, vol. 195, no. 2, pp. 105–11, 2009. 22

[86] M. Hagedorn, M. Delugin, I. Abraldes, N. Allain, M. A. Belaud-Rotureau, M. Turmo, C. Prigent, H. Loiseau, A. Bikfalvi, and S. Javerzat, "Fbxw7/hcdc4 controls glioma cell proliferation in vitro and is a prognostic marker for survival in glioblastoma patients," *Cell Div*, vol. 2, p. 9, 2007. 24

[87] T. Yokobori, K. Mimori, M. Iwatsuki, H. Ishii, I. Onoyama, T. Fukagawa, H. Kuwano, K. I. Nakayama, and M. Mori, "p53-altered fbxw7 expression determines poor prognosis in gastric cancer cases," *Cancer Res*, vol. 69, no. 9, pp. 3788–94, 2009. 24

[88] M. Esteller, "Cpg island hypermethylation and tumor suppressor genes: a booming present, a brighter future," *Oncogene*, vol. 21, no. 35, pp. 5427–40, 2002. 24

[89] S. Akhoondi, L. Lindstrom, M. Widschwendter, M. Corcoran, J. Bergh, C. Spruck, D. Grander, and O. Sangfelt, "Inactivation of fbxw7/hcdc4-beta expression by promoter hypermethylation is associated with favorable prognosis in primary breast cancer," *Breast Cancer Res*, vol. 12, no. 6, p. R105, 2010. 24

[90] Z. Gu, K. Inomata, H. Mitsui, and A. Horii, "Promoter hypermethylation is not the major mechanism for inactivation of the fbxw7 beta-form in human gliomas," *Genes Genet Syst*, vol. 83, no. 4, pp. 347–52, 2008. 24

[91] J. H. Mao, J. Perez-Losada, D. Wu, R. Delrosario, R. Tsunematsu, K. I. Nakayama, K. Brown, S. Bryson, and A. Balmain, "Fbxw7/cdc4 is a p53-dependent, haploinsufficient tumour suppressor gene," *Nature*, vol. 432, no. 7018, pp. 775–9, 2004. 24, 30, 33, 34, 72, 112, 114, 137

[92] X. Ye, G. Nalepa, M. Welcker, B. M. Kessler, E. Spooner, J. Qin, S. J. Elledge, B. E. Clurman, and J. W. Harper, "Recognition of phosphodegron motifs in human cyclin e by the scf(fbw7) ubiquitin ligase," *J Biol Chem*, vol. 279, no. 48, pp. 50110–9, 2004. 25, 26

[93] A. Koff, A. Giordano, D. Desai, K. Yamashita, J. W. Harper, S. Elledge, T. Nishimoto, D. O. Morgan, B. R. Franza, and J. M. Roberts, "Formation and activation of a cyclin e-cdk2 complex during the g1 phase of the human cell cycle," *Science*, vol. 257, no. 5077, pp. 1689–94, 1992. 26, 186

[94] J. D. Singer, M. Gurian-West, B. Clurman, and J. M. Roberts, "Cullin-3 targets cyclin e for ubiquitination and controls s phase in mammalian cells," *Genes Dev*, vol. 13, no. 18, pp. 2375–87, 1999. 26

[95] K. Keyomarsi, S. L. Tucker, T. A. Buchholz, M. Callister, Y. Ding, G. N. Hortobagyi, I. Bedrosian, C. Knickerbocker, W. Toyofuku, M. Lowe, T. W. Herliczek, and S. S. Bacus, "Cyclin e and survival in patients with breast cancer," *N Engl J Med*, vol. 347, no. 20, pp. 1566–75, 2002. 26

[96] C. H. Spruck, K. A. Won, and S. I. Reed, "Deregulated cyclin e induces chromosome instability," *Nature*, vol. 401, no. 6750, pp. 297–300, 1999. 26

[97] S. Ekholm-Reed, C. H. Spruck, O. Sangfelt, F. van Drogen, E. Mueller-Holzner, M. Widschwendter, A. Zetterberg, and S. I. Reed, "Mutation of hcdc4 leads to cell cycle deregulation of cyclin e in cancer," *Cancer Res*, vol. 64, no. 3, pp. 795–800, 2004. 26, 164, 187

[98] K. R. Loeb, H. Kostner, E. Firpo, T. Norwood, D. T. K, B. E. Clurman, and J. M.

Roberts, "A mouse model for cyclin e-dependent genetic instability and tumorigenesis," *Cancer Cell*, vol. 8, no. 1, pp. 35–47, 2005. 26

[99] A. C. Minella, K. R. Loeb, A. Knecht, M. Welcker, B. J. Varnum-Finney, I. D. Bernstein, J. M. Roberts, and B. E. Clurman, "Cyclin e phosphorylation regulates cell proliferation in hematopoietic and epithelial lineages in vivo," *Genes Dev*, vol. 22, no. 12, pp. 1677–89, 2008. 27

[100] S. R. Hann and R. N. Eisenman, "Proteins encoded by the human c-myc oncogene: differential expression in neoplastic cells," *Mol Cell Biol*, vol. 4, no. 11, pp. 2486–97, 1984. 27

[101] Q. M. Guo, R. L. Malek, S. Kim, C. Chiao, M. He, M. Ruffy, K. Sanka, N. H. Lee, C. V. Dang, and E. T. Liu, "Identification of c-myc responsive genes using rat cdna microarray," *Cancer Res*, vol. 60, no. 21, pp. 5922–8, 2000. 27

[102] S. Pelengaris, M. Khan, and G. Evan, "c-myc: more than just a matter of life and death," *Nat Rev Cancer*, vol. 2, no. 10, pp. 764–76, 2002. 27, 189

[103] F. Bahram, N. von der Lehr, C. Cetinkaya, and L. G. Larsson, "c-myc hot spot mutations in lymphomas result in inefficient ubiquitination and decreased proteasome-mediated turnover," *Blood*, vol. 95, no. 6, pp. 2104–10, 2000. 27

[104] M. Yada, S. Hatakeyama, T. Kamura, M. Nishiyama, R. Tsunematsu, H. Imaki, N. Ishida, F. Okumura, K. Nakayama, and K. I. Nakayama, "Phosphorylation-dependent degradation of c-myc is mediated by the f-box protein fbw7," *EMBO J*, vol. 23, no. 10, pp. 2116–25, 2004. 27

[105] R. Sears, F. Nuckolls, E. Haura, Y. Taya, K. Tamai, and J. R. Nevins, "Multiple ras-dependent phosphorylation pathways regulate myc protein stability," *Genes Dev*, vol. 14, no. 19, pp. 2501–14, 2000. 28

[106] S. Y. Kim, A. Herbst, K. A. Tworkowski, S. E. Salghetti, and W. P. Tansey, "Skp2

regulates myc protein stability and activity," *Mol Cell*, vol. 11, no. 5, pp. 1177–88, 2003. 28, 110

[107] N. Popov, M. Wanzel, M. Madiredjo, D. Zhang, R. Beijersbergen, R. Bernards, R. Moll, S. J. Elledge, and M. Eilers, "The ubiquitin-specific protease usp28 is required for myc stability," *Nat Cell Biol*, vol. 9, no. 7, pp. 765–74, 2007. 28, 36, 110

[108] L. Chang and M. Karin, "Mammalian map kinase signalling cascades," *Nature*, vol. 410, no. 6824, pp. 37–40, 2001. 28

[109] E. Shaulian and M. Karin, "Ap-1 as a regulator of cell life and death," *Nat Cell Biol*, vol. 4, no. 5, pp. E131–6, 2002. 28

[110] A. S. Nateri, L. Riera-Sans, C. Da Costa, and A. Behrens, "The ubiquitin ligase scffbw7 antagonizes apoptotic jnk signaling," *Science*, vol. 303, no. 5662, pp. 1374–8, 2004. 28

[111] W. Wei, J. Jin, S. Schlisio, J. W. Harper, and J. Kaelin, W. G., "The v-jun point mutation allows c-jun to escape gsk3-dependent recognition and destruction by the fbw7 ubiquitin ligase," *Cancer Cell*, vol. 8, no. 1, pp. 25–33, 2005. 28

[112] D. Fang, C. Elly, B. Gao, N. Fang, Y. Altman, C. Joazeiro, T. Hunter, N. Copeland, N. Jenkins, and Y. C. Liu, "Dysregulation of t lymphocyte function in itchy mice: a role for itch in th2 differentiation," *Nat Immunol*, vol. 3, no. 3, pp. 281–7, 2002. 28

[113] S. Artavanis-Tsakonas, M. D. Rand, and R. J. Lake, "Notch signaling: cell fate control and signal integration in development," *Science*, vol. 284, no. 5415, pp. 770–6, 1999. 29

[114] T. Iso, L. Kedes, and Y. Hamamori, "Hes and herp families: multiple effectors of the notch signaling pathway," *J Cell Physiol*, vol. 194, no. 3, pp. 237–55, 2003. 29

[115] J. Sjolund, C. Manetopoulos, M. T. Stockhausen, and H. Axelson, "The notch pathway in cancer: differentiation gone awry," *Eur J Cancer*, vol. 41, no. 17, pp. 2620–9, 2005. 29

[116] N. Gupta-Rossi, O. Le Bail, H. Gonen, C. Brou, F. Logeat, E. Six, A. Ciechanover, and A. Israel, "Functional interaction between sel-10, an f-box protein, and the nuclear form of activated notch1 receptor," *J Biol Chem*, vol. 276, no. 37, pp. 34371–8, 2001. 29

[117] C. Oberg, J. Li, A. Pauley, E. Wolf, M. Gurney, and U. Lendahl, "The notch intracellular domain is ubiquitinated and negatively regulated by the mammalian sel-10 homolog," *J Biol Chem*, vol. 276, no. 38, pp. 35847–53, 2001. 29

[118] L. Qiu, C. Joazeiro, N. Fang, H. Y. Wang, C. Elly, Y. Altman, D. Fang, T. Hunter, and Y. C. Liu, "Recognition and ubiquitination of notch by itch, a hect-type e3 ubiquitin ligase," *J Biol Chem*, vol. 275, no. 46, pp. 35734–7, 2000. 29, 110

[119] T. Marumoto, D. Zhang, and H. Saya, "Aurora-a - a guardian of poles," *Nat Rev Cancer*, vol. 5, no. 1, pp. 42–50, 2005. 30

[120] Y. Fujii, M. Yada, M. Nishiyama, T. Kamura, H. Takahashi, R. Tsunematsu, E. Susaki, T. Nakagawa, A. Matsumoto, and K. I. Nakayama, "Fbxw7 contributes to tumor suppression by targeting multiple proteins for ubiquitin-dependent degradation," *Cancer Sci*, vol. 97, no. 8, pp. 729–36, 2006. 30, 165

[121] S. Finkin, Y. Aylon, S. Anzi, M. Oren, and E. Shaulian, "Fbw7 regulates the activity of endoreduplication mediators and the p53 pathway to prevent drug-induced polyploidy," *Oncogene*, vol. 27, no. 32, pp. 4411–21, 2008. 30

[122] T. Shindo, I. Manabe, Y. Fukushima, K. Tobe, K. Aizawa, S. Miyamoto, K. Kawai-Kowase, N. Moriyama, Y. Imai, H. Kawakami, H. Nishimatsu, T. Ishikawa, T. Suzuki, H. Morita, K. Maemura, M. Sata, Y. Hirata, M. Komukai, H. Kagechika, T. Kadowaki, M. Kurabayashi, and R. Nagai, "Kruppel-like zinc-finger transcription factor

klf5/bteb2 is a target for angiotensin ii signaling and an essential regulator of cardiovascular remodeling," *Nat Med*, vol. 8, no. 8, pp. 856–63, 2002. 30, 108, 159, 206

[123] J. T. Dong and C. Chen, "Essential role of klf5 transcription factor in cell proliferation and differentiation and its implications for human diseases," *Cell Mol Life Sci*, vol. 66, no. 16, pp. 2691–706, 2009. 30, 111, 140

[124] C. Chen, M. S. Benjamin, X. Sun, K. B. Otto, P. Guo, X. Y. Dong, Y. Bao, Z. Zhou, X. Cheng, J. W. Simons, and J. T. Dong, "Klf5 promotes cell proliferation and tumorigenesis through gene regulation and the tsu-pr1 human bladder cancer cell line," *Int J Cancer*, vol. 118, no. 6, pp. 1346–55, 2006. 30, 111, 141, 159, 197

[125] H. Wan, F. Luo, S. E. Wert, L. Zhang, Y. Xu, M. Ikegami, Y. Maeda, S. M. Bell, and J. A. Whitsett, "Kruppel-like factor 5 is required for perinatal lung morphogenesis and function," *Development*, vol. 135, no. 15, pp. 2563–72, 2008. 30, 106, 107, 111

[126] N. Yagi, I. Manabe, T. Tottori, A. Ishihara, F. Ogata, J. H. Kim, S. Nishimura, K. Fujiu, Y. Oishi, K. Itaka, Y. Kato, M. Yamauchi, and R. Nagai, "A nanoparticle system specifically designed to deliver short interfering rna inhibits tumor growth in vivo," *Cancer Res*, vol. 69, no. 16, pp. 6531–8, 2009. 30

[127] D. Zhao, H. Q. Zheng, Z. Zhou, and C. Chen, "The fbw7 tumor suppressor targets klf5 for ubiquitin-mediated degradation and suppresses breast cell proliferation," *Cancer Res*, vol. 70, no. 11, pp. 4728–38, 2010. 30, 91

[128] N. Liu, H. Li, S. Li, M. Shen, N. Xiao, Y. Chen, Y. Wang, W. Wang, R. Wang, Q. Wang, J. Sun, and P. Wang, "The fbw7/human cdc4 tumor suppressor targets proproliferative factor klf5 for ubiquitination and degradation through multiple phosphodegron motifs," *J Biol Chem*, vol. 285, no. 24, pp. 18858–67, 2010. 30, 91

[129] C. Chen, X. Sun, Q. Ran, K. D. Wilkinson, T. J. Murphy, J. W. Simons, and J. T.

Dong, "Ubiquitin-proteasome degradation of klf5 transcription factor in cancer and untransformed epithelial cells," *Oncogene*, vol. 24, no. 20, pp. 3319–27, 2005. 30

[130] C. Chen, Z. Zhou, P. Guo, and J. T. Dong, "Proteasomal degradation of the klf5 transcription factor through a ubiquitin-independent pathway," *FEBS Lett*, vol. 581, no. 6, pp. 1124–30, 2007. 30

[131] L. Bartholin, S. E. Powers, T. A. Melhuish, S. Lasse, M. Weinstein, and D. Wotton, "Tgif inhibits retinoid signaling," *Mol Cell Biol*, vol. 26, no. 3, pp. 990–1001, 2006. 31, 111, 206

[132] D. Wotton, R. S. Lo, L. A. Swaby, and J. Massague, "Multiple modes of repression by the smad transcriptional corepressor tgif," *J Biol Chem*, vol. 274, no. 52, pp. 37105–10, 1999. 31

[133] D. Wotton, P. S. Knoepfler, C. D. Laherty, R. N. Eisenman, and J. Massague, "The smad transcriptional corepressor tgif recruits msin3," *Cell Growth Differ*, vol. 12, no. 9, pp. 457–63, 2001. 31

[134] S. R. Seo, N. Ferrand, N. Faresse, C. Prunier, L. Abecassis, M. Pessah, M. F. Bourgeade, and A. Atfi, "Nuclear retention of the tumor suppressor cpml by the homeodomain protein tgif restricts tgf-beta signaling," *Mol Cell*, vol. 23, no. 4, pp. 547–59, 2006. 31, 204

[135] M. T. Bengoechea-Alonso and J. Ericsson, "Tumor suppressor fbxw7 regulates tgfbeta signaling by targeting tgif1 for degradation," *Oncogene*, vol. 29, no. 38, pp. 5322–8, 2010. 31, 91

[136] B. L. Olson, M. B. Hock, S. Ekholm-Reed, J. A. Wohlschlegel, K. K. Dev, A. Kralli, and S. I. Reed, "Scfcdc4 acts antagonistically to the pgc-1alpha transcriptional coactivator by targeting it for ubiquitin-mediated proteolysis," *Genes Dev*, vol. 22, no. 2, pp. 252–64, 2008. 32

[137] G. Wu, E. J. Hubbard, J. K. Kitajewski, and I. Greenwald, "Evidence for functional and physical association between caenorhabditis elegans sel-10, a cdc4p-related protein, and sel-12 presenilin," *Proc Natl Acad Sci U S A*, vol. 95, no. 26, pp. 15787–91, 1998. 32

[138] J. Li, A. M. Pauley, R. L. Myers, R. Shuang, J. R. Brashler, R. Yan, A. E. Buhl, C. Ruble, and M. E. Gurney, "Sel-10 interacts with presenilin 1, facilitates its ubiquitination, and alters a-beta peptide production," *J Neurochem*, vol. 82, no. 6, pp. 1540–8, 2002. 32

[139] J. H. Mao, I. J. Kim, D. Wu, J. Climent, H. C. Kang, R. DelRosario, and A. Balmain, "Fbxw7 targets mtor for degradation and cooperates with pten in tumor suppression," *Science*, vol. 321, no. 5895, pp. 1499–502, 2008. 32, 37

[140] C. Kanei-Ishii, T. Nomura, T. Takagi, N. Watanabe, K. I. Nakayama, and S. Ishii, "Fbxw7 acts as an e3 ubiquitin ligase that targets c-myb for nemo-like kinase (nlk)-induced degradation," *J Biol Chem*, vol. 283, no. 45, pp. 30540–8, 2008. 32

[141] K. Kitagawa, Y. Hiramatsu, C. Uchida, T. Isobe, T. Hattori, T. Oda, K. Shibata, S. Nakamura, A. Kikuchi, and M. Kitagawa, "Fbw7 promotes ubiquitin-dependent degradation of c-myb: involvement of gsk3-mediated phosphorylation of thr-572 in mouse c-myb," *Oncogene*, vol. 28, no. 25, pp. 2393–405, 2009. 32

[142] R. C. Wu, Q. Feng, D. M. Lonard, and B. W. O'Malley, "Src-3 coactivator functional lifetime is regulated by a phospho-dependent ubiquitin time clock," *Cell*, vol. 129, no. 6, pp. 1125–40, 2007. 32

[143] A. Sundqvist, M. T. Bengoechea-Alonso, X. Ye, V. Lukiyanchuk, J. Jin, J. W. Harper, and J. Ericsson, "Control of lipid metabolism by phosphorylation-dependent degradation of the srebp family of transcription factors by scf(fbw7)," *Cell Metab*, vol. 1, no. 6, pp. 379–91, 2005. 32

[144] M. T. Bengoechea-Alonso and J. Ericsson, "A phosphorylation cascade controls the degradation of active srebp1," *J Biol Chem*, vol. 284, no. 9, pp. 5885–95, 2009. 32

[145] M. T. Bengoechea-Alonso and J. Ericsson, "The ubiquitin ligase fbxw7 controls adipocyte differentiation by targeting c/ebpalpha for degradation," *Proc Natl Acad Sci U S A*, vol. 107, no. 26, pp. 11817–22, 2010. 32

[146] H. Inuzuka, S. Shaik, I. Onoyama, D. Gao, A. Tseng, R. S. Maser, B. Zhai, L. Wan, A. Gutierrez, A. W. Lau, Y. Xiao, A. L. Christie, J. Aster, J. Settleman, S. P. Gygi, A. L. Kung, T. Look, K. I. Nakayama, R. A. DePinho, and W. Wei, "Scf(fbw7) regulates cellular apoptosis by targeting mcl1 for ubiquitylation and destruction," *Nature*, vol. 471, no. 7336, pp. 104–9, 2011. 32

[147] I. E. Wertz, S. Kusam, C. Lam, T. Okamoto, W. Sandoval, D. J. Anderson, E. Helgason, J. A. Ernst, M. Eby, J. Liu, L. D. Belmont, J. S. Kaminker, K. M. O'Rourke, K. Pujara, P. B. Kohli, A. R. Johnson, M. L. Chiu, J. R. Lill, P. K. Jackson, W. J. Fairbrother, S. Seshagiri, M. J. Ludlam, K. G. Leong, E. C. Dueber, H. Maecker, D. C. Huang, and V. M. Dixit, "Sensitivity to antitubulin chemotherapeutics is regulated by mcl1 and fbw7," *Nature*, vol. 471, no. 7336, pp. 110–4, 2011. 32

[148] M. Biswas, D. Phan, M. Watanabe, and J. Y. Chan, "The fbw7 tumor suppressor regulates nuclear factor e2-related factor 1 transcription factor turnover through proteasome-mediated proteolysis," *J Biol Chem*, vol. 286, no. 45, pp. 39282–9, 2011. 32

[149] J. D. Hoeck, A. Jandke, S. M. Blake, E. Nye, B. Spencer-Dene, S. Brandner, and A. Behrens, "Fbw7 controls neural stem cell differentiation and progenitor apoptosis via notch and c-jun," *Nat Neurosci*, vol. 13, no. 11, pp. 1365–72, 2010. 33, 85, 115

[150] A. Jandke, C. Da Costa, R. Sancho, E. Nye, B. Spencer-Dene, and A. Behrens, "The f-box protein fbw7 is required for cerebellar development," *Dev Biol*, vol. 358, no. 1, pp. 201–12, 2011. 33, 115

[151] R. Sancho, A. Jandke, H. Davis, M. E. Diefenbacher, I. Tomlinson, and A. Behrens, "F-box and wd repeat domain-containing 7 regulates intestinal cell lineage commitment and is a haploinsufficient tumor suppressor," *Gastroenterology*, vol. 139, no. 3, pp. 929–41, 2010. 33, 37, 73, 102, 103, 104, 112, 116, 122, 138, 139, 160, 203, 207

[152] I. Onoyama, A. Suzuki, A. Matsumoto, K. Tomita, H. Katagiri, Y. Oike, K. Nakayama, and K. I. Nakayama, "Fbxw7 regulates lipid metabolism and cell fate decisions in the mouse liver," *J Clin Invest*, vol. 121, no. 1, pp. 342–54, 2011. 33, 73, 110, 115

[153] I. Onoyama, R. Tsunematsu, A. Matsumoto, T. Kimura, I. M. de Alboran, K. Nakayama, and K. I. Nakayama, "Conditional inactivation of fbxw7 impairs cell-cycle exit during t cell differentiation and results in lymphomatogenesis," *J Exp Med*, vol. 204, no. 12, pp. 2875–88, 2007. 33, 37, 73, 110, 115

[154] Y. Ishikawa, I. Onoyama, K. I. Nakayama, and K. Nakayama, "Notch-dependent cell cycle arrest and apoptosis in mouse embryonic fibroblasts lacking fbxw7," *Oncogene*, vol. 27, no. 47, pp. 6164–74, 2008. 33, 73, 114

[155] B. J. Thompson, V. Jankovic, J. Gao, S. Buonamici, A. Vest, J. M. Lee, J. Zavadil, S. D. Nimer, and I. Aifantis, "Control of hematopoietic stem cell quiescence by the e3 ubiquitin ligase fbw7," *J Exp Med*, vol. 205, no. 6, pp. 1395–408, 2008. 33, 37, 73, 114, 115

[156] K. Balamurugan, J. M. Wang, H. H. Tsai, S. Sharan, M. Anver, R. Leighty, and E. Sterneck, "The tumour suppressor c/ebpdelta inhibits fbxw7 expression and promotes mammary tumour metastasis," *EMBO J*, vol. 29, no. 24, pp. 4106–17, 2010. 34

[157] T. Kimura, M. Gotoh, Y. Nakamura, and H. Arakawa, "hcdc4b, a regulator of cyclin e, as a direct transcriptional target of p53," *Cancer Sci*, vol. 94, no. 5, pp. 431–6, 2003. 34

[158] Y. Xu, T. Sengupta, L. Kukreja, and A. C. Minella, "Microrna-223 regulates cyclin e activity by modulating expression of f-box and wd-40 domain protein 7," *J Biol Chem*, vol. 285, no. 45, pp. 34439–46, 2010. 34, 181

[159] J. Kurashige, M. Watanabe, M. Iwatsuki, K. Kinoshita, S. Saito, Y. Hiyoshi, H. Kamohara, Y. Baba, K. Mimori, and H. Baba, "Overexpression of microrna-223 regulates the ubiquitin ligase fbxw7 in oesophageal squamous cell carcinoma," *Br J Cancer*, vol. 106, no. 1, pp. 182–8, 2012. 34

[160] M. Lerner, J. Lundgren, S. Akhoondi, A. Jahn, H. F. Ng, F. A. Moqadam, J. A. Oude Vrielink, R. Agami, M. L. Den Boer, D. Grander, and O. Sangfelt, "Mirna-27a controls fbw7/hcdc4-dependent cyclin e degradation and cell cycle progression," *Cell Cycle*, vol. 10, no. 13, pp. 2172–83, 2011. 34, 181

[161] P. Cohen and S. Frame, "The renaissance of gsk3," *Nat Rev Mol Cell Biol*, vol. 2, no. 10, pp. 769–76, 2001. 35

[162] J. Durgan and P. J. Parker, "Regulation of the tumour suppressor fbw7alpha by pkc-dependent phosphorylation and cancer-associated mutations," *Biochem J*, vol. 432, no. 1, pp. 77–87, 2010. 35

[163] J. S. Mo, E. J. Ann, J. H. Yoon, J. Jung, Y. H. Choi, H. Y. Kim, J. S. Ahn, S. M. Kim, M. Y. Kim, J. A. Hong, M. S. Seo, F. Lang, E. J. Choi, and H. S. Park, "Serum- and glucocorticoid-inducible kinase 1 (sgk1) controls notch1 signaling by downregulation of protein stability through fbw7 ubiquitin ligase," *J Cell Sci*, vol. 124, no. Pt 1, pp. 100–12, 2011. 35

[164] C. Schulein, M. Eilers, and N. Popov, "Pi3k-dependent phosphorylation of fbw7 modulates substrate degradation and activity," *FEBS Lett*, vol. 585, no. 14, pp. 2151–7, 2011. 35

[165] N. Popov, S. Herold, M. Llamazares, C. Schulein, and M. Eilers, "Fbw7 and usp28

regulate myc protein stability in response to dna damage," *Cell Cycle*, vol. 6, no. 19, pp. 2327–31, 2007. 36

[166] M. Schwickart, X. Huang, J. R. Lill, J. Liu, R. Ferrando, D. M. French, H. Maecker, K. O'Rourke, F. Bazan, J. Eastham-Anderson, P. Yue, D. Dornan, D. C. Huang, and V. M. Dixit, "Deubiquitinase usp9x stabilizes mcl1 and promotes tumour cell survival," *Nature*, vol. 463, no. 7277, pp. 103–7, 2010. 36

[167] S. Orlicky, X. Tang, V. Neduva, N. Elowe, E. D. Brown, F. Sicheri, and M. Tyers, "An allosteric inhibitor of substrate recognition by the scf(cdc4) ubiquitin ligase," *Nat Biotechnol*, vol. 28, no. 7, pp. 733–7, 2010. 37

[168] H. H. Xia, H. He, J. De Wang, Q. Gu, M. C. Lin, B. Zou, L. F. Yu, Y. W. Sun, A. O. Chan, H. F. Kung, and B. C. Wong, "Induction of apoptosis and cell cycle arrest by a specific c-jun nh2-terminal kinase (jnk) inhibitor, sp-600125, in gastrointestinal cancers," *Cancer Lett*, vol. 241, no. 2, pp. 268–74, 2006. 37

[169] M. Shih Ie and T. L. Wang, "Notch signaling, gamma-secretase inhibitors, and cancer therapy," *Cancer Res*, vol. 67, no. 5, pp. 1879–82, 2007. 37

[170] A. B. Bialkowska, M. Crisp, T. Bannister, Y. He, S. Chowdhury, S. Schurer, P. Chase, T. Spicer, F. Madoux, C. Tian, P. Hodder, D. Zaharevitz, and V. W. Yang, "Identification of small-molecule inhibitors of the colorectal cancer oncogene kruppel-like factor 5 expression by ultrahigh-throughput screening," *Mol Cancer Ther*, vol. 10, no. 11, pp. 2043–51, 2011. 37, 205

[171] M. T. Tetzlaff, W. Yu, M. Li, P. Zhang, M. Finegold, K. Mahon, J. W. Harper, R. J. Schwartz, and S. J. Elledge, "Defective cardiovascular development and elevated cyclin e and notch proteins in mice lacking the fbw7 f-box protein," *Proc Natl Acad Sci U S A*, vol. 101, no. 10, pp. 3338–45, 2004. 37, 73, 100, 104, 115

[172] R. Tsunematsu, K. Nakayama, Y. Oike, M. Nishiyama, N. Ishida, S. Hatakeyama, Y. Bessho, R. Kageyama, T. Suda, and K. I. Nakayama, "Mouse fbw7/sel-10/cdc4 is

required for notch degradation during vascular development," *J Biol Chem*, vol. 279, no. 10, pp. 9417–23, 2004. 37, 73, 100, 104, 115

[173] S. Matsuoka, Y. Oike, I. Onoyama, A. Iwama, F. Arai, K. Takubo, Y. Mashimo, H. Oguro, E. Nitta, K. Ito, K. Miyamoto, H. Yoshiwara, K. Hosokawa, Y. Nakamura, Y. Gomei, H. Iwasaki, Y. Hayashi, Y. Matsuzaki, K. Nakayama, Y. Ikeda, A. Hata, S. Chiba, K. I. Nakayama, and T. Suda, "Fbxw7 acts as a critical fail-safe against premature loss of hematopoietic stem cells and development of t-all," *Genes Dev*, vol. 22, no. 8, pp. 986–91, 2008. 37, 73, 115

[174] R. Rudling, A. B. Hassan, J. Kitau, N. Mandir, and R. A. Goodlad, "A simple device to rapidly prepare whole mounts of murine intestine," *Cell Prolif*, vol. 39, no. 5, pp. 415–20, 2006. 41

[175] G. E. Truett, P. Heeger, R. L. Mynatt, A. A. Truett, J. A. Walker, and M. L. Warman, "Preparation of pcr-quality mouse genomic dna with hot sodium hydroxide and tris (hotshot)," *Biotechniques*, vol. 29, no. 1, pp. 52, 54, 2000. 44

[176] A. P. Feinberg and B. Vogelstein, "A technique for radiolabeling dna restriction endonuclease fragments to high specific activity," *Anal Biochem*, vol. 132, no. 1, pp. 6–13, 1983. 50

[177] G. M. Church and W. Gilbert, "Genomic sequencing," *Proc Natl Acad Sci U S A*, vol. 81, no. 7, pp. 1991–5, 1984. 50

[178] R. Poulsom, J. M. Longcroft, R. E. Jeffery, L. A. Rogers, and J. H. Steel, "A robust method for isotopic riboprobe in situ hybridisation to localise mrnas in routine pathology specimens," *Eur J Histochem*, vol. 42, no. 2, pp. 121–32, 1998. 52

[179] K. J. Livak and T. D. Schmittgen, "Analysis of relative gene expression data using real-time quantitative pcr and the 2(-delta delta c(t)) method," *Methods*, vol. 25, no. 4, pp. 402–8, 2001. 52

[180] E. L. Jackson, N. Willis, K. Mercer, R. T. Bronson, D. Crowley, R. Montoya, T. Jacks, and D. A. Tuveson, "Analysis of lung tumor initiation and progression using conditional expression of oncogenic k-ras," *Genes Dev*, vol. 15, no. 24, pp. 3243–8, 2001. 65

[181] C. Berthet-Colominas, S. Monaco, A. Novelli, G. Sibai, F. Mallet, and S. Cusack, "Head-to-tail dimers and interdomain flexibility revealed by the crystal structure of hiv-1 capsid protein (p24) complexed with a monoclonal antibody fab," *EMBO J*, vol. 18, no. 5, pp. 1124–36, 1999. 68

[182] H. Davis, A. Lewis, B. Spencer-Dene, H. Tateossian, G. Stamp, A. Behrens, and I. Tomlinson, "Fbxw7 mutations typically found in human cancers are distinct from null alleles and disrupt lung development," *J Pathol*, vol. 224, no. 2, pp. 180–9, 2011. 77

[183] Y. Lallemand, V. Luria, R. Haffner-Krausz, and P. Lonai, "Maternally expressed pgk-cre transgene as a tool for early and uniform activation of the cre site-specific recombinase," *Transgenic Res*, vol. 7, no. 2, pp. 105–12, 1998. 80, 207

[184] G. Singh, J. Singh, S. L. Katyal, W. E. Brown, J. A. Kramps, I. L. Paradis, J. H. Dauber, T. A. Macpherson, and N. Squeglia, "Identification, cellular localization, isolation, and characterization of human clara cell-specific 10 kd protein," *J Histochem Cytochem*, vol. 36, no. 1, pp. 73–80, 1988. 88

[185] S. Ohnishi, F. Laub, N. Matsumoto, M. Asaka, F. Ramirez, T. Yoshida, and M. Terada, "Developmental expression of the mouse gene coding for the kruppel-like transcription factor klf5," *Dev Dyn*, vol. 217, no. 4, pp. 421–9, 2000. 95

[186] D. M. Simon and T. J. Mariani, "Role of ppars and retinoid x receptors in the regulation of lung maturation and development," *PPAR Res*, vol. 2007, p. 91240, 2007. 102, 109

[187] J. E. Balmer and R. Blomhoff, "Gene expression regulation by retinoic acid," *J Lipid Res*, vol. 43, no. 11, pp. 1773–808, 2002. 102

[188] R. Babaei-Jadidi, N. Li, A. Saadeddin, B. Spencer-Dene, A. Jandke, B. Muhammad, E. E. Ibrahim, R. Muraleedharan, M. Abuzinadah, H. Davis, A. Lewis, S. Watson, A. Behrens, I. Tomlinson, and A. S. Nateri, "Fbxw7 influences murine intestinal homeostasis and cancer, targeting notch, jun, and dek for degradation," *J Exp Med*, vol. 208, no. 2, pp. 295–312, 2011. 103, 116, 138, 139, 160, 203

[189] X. Montagutelli, "Effect of the genetic background on the phenotype of mouse mutations," *J Am Soc Nephrol*, vol. 11 Suppl 16, pp. S101–5, 2000. 105

[190] A. A. Ten Have-Opbroek, "Lung development in the mouse embryo," *Exp Lung Res*, vol. 17, no. 2, pp. 111–30, 1991. 105

[191] K. J. Liu, J. R. Arron, K. Stankunas, G. R. Crabtree, and M. T. Longaker, "Chemical rescue of cleft palate and midline defects in conditional gsk-3beta mice," *Nature*, vol. 446, no. 7131, pp. 79–82, 2007. 106, 107, 109

[192] H. Tateossian, R. E. Hardisty-Hughes, S. Morse, M. R. Romero, H. Hilton, C. Dean, and S. D. Brown, "Regulation of tgf-beta signalling by fbxo11, the gene mutated in the jeff otitis media mouse mutant," *Pathogenetics*, vol. 2, no. 1, p. 5, 2009. 106, 107

[193] R. E. Hardisty-Hughes, H. Tateossian, S. A. Morse, M. R. Romero, A. Middleton, Z. Tymowska-Lalanne, A. J. Hunter, M. Cheeseman, and S. D. Brown, "A mutation in the f-box gene, fbxo11, causes otitis media in the jeff mouse," *Hum Mol Genet*, vol. 15, no. 22, pp. 3273–9, 2006. 106, 107

[194] D. S. Basseres, E. Levantini, H. Ji, S. Monti, S. Elf, T. Dayaram, M. Fenyus, O. Kocher, T. Golub, K. K. Wong, B. Halmos, and D. G. Tenen, "Respiratory failure due to differentiation arrest and expansion of alveolar cells following lung-specific loss of the transcription factor c/ebpalpha in mice," *Mol Cell Biol*, vol. 26, no. 3, pp. 1109–23, 2006. 106, 107

[195] P. C. Martis, J. A. Whitsett, Y. Xu, A. K. Perl, H. Wan, and M. Ikegami, "C/ebpalpha is required for lung maturation at birth," *Development*, vol. 133, no. 6, pp. 1155–64, 2006. 106, 107

[196] H. Wan, Y. Xu, M. Ikegami, M. T. Stahlman, K. H. Kaestner, S. L. Ang, and J. A. Whitsett, "Foxa2 is required for transition to air breathing at birth," *Proc Natl Acad Sci U S A*, vol. 101, no. 40, pp. 14449–54, 2004. 107

[197] A. Grunder, T. T. Ebel, M. Mallo, G. Schwarzkopf, T. Shimizu, A. E. Sippel, and H. Schrewe, "Nuclear factor i-b (nfib) deficient mice have severe lung hypoplasia," *Mech Dev*, vol. 112, no. 1-2, pp. 69–77, 2002. 106, 107

[198] I. Sur, B. Rozell, V. Jaks, A. Bergstrom, and R. Toftgard, "Epidermal and craniofacial defects in mice overexpressing klf5 in the basal layer of the epidermis," *J Cell Sci*, vol. 119, no. Pt 17, pp. 3593–601, 2006. 107, 111

[199] G. Li, C. Gustafson-Brown, S. K. Hanks, K. Nason, J. M. Arbeit, K. Pogliano, R. M. Wisdom, and R. S. Johnson, "c-jun is essential for organization of the epidermal leading edge," *Dev Cell*, vol. 4, no. 6, pp. 865–77, 2003. 107, 109

[200] R. Zenz, H. Scheuch, P. Martin, C. Frank, R. Eferl, L. Kenner, M. Sibilia, and E. F. Wagner, "c-jun regulates eyelid closure and skin tumor development through egfr signaling," *Dev Cell*, vol. 4, no. 6, pp. 879–89, 2003. 107, 109

[201] V. Kaartinen, J. W. Voncken, C. Shuler, D. Warburton, D. Bu, N. Heisterkamp, and J. Groffen, "Abnormal lung development and cleft palate in mice lacking tgf-beta 3 indicates defects of epithelial-mesenchymal interaction," *Nat Genet*, vol. 11, no. 4, pp. 415–21, 1995. 107

[202] S. H. Koo, M. C. Cunningham, B. Arabshahi, J. S. Gruss, and r. Grant, J. H., "The transforming growth factor-beta 3 knock-out mouse: an animal model for cleft palate," *Plast Reconstr Surg*, vol. 108, no. 4, pp. 938–48; discussion 949–51, 2001. 107

[203] R. Balling, G. Mutter, P. Gruss, and M. Kessel, "Craniofacial abnormalities induced by ectopic expression of the homeobox gene hox-1.1 in transgenic mice," *Cell*, vol. 58, no. 2, pp. 337–47, 1989. 107

[204] J. M. Snyder, M. Jenkins-Moore, S. K. Jackson, K. L. Goss, H. H. Dai, P. J. Bangsund, V. Giguere, and S. E. McGowan, "Alveolarization in retinoic acid receptor-beta-deficient mice," *Pediatr Res*, vol. 57, no. 3, pp. 384–91, 2005. 107

[205] B. J. Collins, W. Kleeberger, and D. W. Ball, "Notch in lung development and lung cancer," *Semin Cancer Biol*, vol. 14, no. 5, pp. 357–64, 2004. 108

[206] E. Bertolino, B. Reimund, D. Wildt-Perinic, and R. G. Clerc, "A novel homeobox protein which recognizes a tgt core and functionally interferes with a retinoid-responsive motif," *J Biol Chem*, vol. 270, no. 52, pp. 31178–88, 1995. 108, 111, 160

[207] D. M. Simon, M. C. Arikan, S. Srisuma, S. Bhattacharya, L. W. Tsai, E. P. Ingenito, F. Gonzalez, S. D. Shapiro, and T. J. Mariani, "Epithelial cell ppar[gamma] contributes to normal lung maturation," *FASEB J*, vol. 20, no. 9, pp. 1507–9, 2006. 109

[208] R. D. Williams, R. Al-Saadi, T. Chagtai, S. Popov, B. Messahel, N. Sebire, M. Gessler, J. Wegert, N. Graf, I. Leuschner, M. Hubank, C. Jones, G. Vujanic, and K. Pritchard-Jones, "Subtype-specific fbxw7 mutation and mycn copy number gain in wilms' tumor," *Clin Cancer Res*, vol. 16, no. 7, pp. 2036–45, 2010. 110

[209] R. Hamid and S. J. Brandt, "Transforming growth-interacting factor (tgif) regulates proliferation and differentiation of human myeloid leukemia cells," *Mol Oncol*, vol. 3, no. 5-6, pp. 451–63, 2009. 110

[210] R. Sun, X. Chen, and V. W. Yang, "Intestinal-enriched kruppel-like factor (kruppel-like factor 5) is a positive regulator of cellular proliferation," *J Biol Chem*, vol. 276, no. 10, pp. 6897–900, 2001. 111, 140, 141, 197

[211] H. Q. Zheng, Z. Zhou, J. Huang, L. Chaudhury, J. T. Dong, and C. Chen, "Kruppel-like factor 5 promotes breast cell proliferation partially through upregulating the transcription of fibroblast growth factor binding protein 1," *Oncogene*, vol. 28, no. 42, pp. 3702–13, 2009. 111

[212] M. Iwatsuki, K. Mimori, H. Ishii, T. Yokobori, Y. Takatsuno, T. Sato, H. Toh, I. Onoyama, K. I. Nakayama, H. Baba, and M. Mori, "Loss of fbxw7, a cell cycle regulating gene, in colorectal cancer: clinical significance," *Int J Cancer*, vol. 126, no. 8, pp. 1828–37, 2010. 116, 165

[213] C. T. Pham, D. M. MacIvor, B. A. Hug, J. W. Heusel, and T. J. Ley, "Long-range disruption of gene expression by a selectable marker cassette," *Proc Natl Acad Sci U S A*, vol. 93, no. 23, pp. 13090–5, 1996. 117

[214] J. R. Saam and J. I. Gordon, "Inducible gene knockouts in the small intestinal and colonic epithelium," *J Biol Chem*, vol. 274, no. 53, pp. 38071–82, 1999. 120

[215] B. B. Madison, L. Dunbar, X. T. Qiao, K. Braunstein, E. Braunstein, and D. L. Gumucio, "Cis elements of the villin gene control expression in restricted domains of the vertical (crypt) and horizontal (duodenum, cecum) axes of the intestine," *J Biol Chem*, vol. 277, no. 36, pp. 33275–83, 2002. 120

[216] F. el Marjou, K. P. Janssen, B. H. Chang, M. Li, V. Hindie, L. Chan, D. Louvard, P. Chambon, D. Metzger, and S. Robine, "Tissue-specific and inducible cre-mediated recombination in the gut epithelium," *Genesis*, vol. 39, no. 3, pp. 186–93, 2004. 120, 207

[217] H. Ireland, R. Kemp, C. Houghton, L. Howard, A. R. Clarke, O. J. Sansom, and D. J. Winton, "Inducible cre-mediated control of gene expression in the murine gastrointestinal tract: effect of loss of beta-catenin," *Gastroenterology*, vol. 126, no. 5, pp. 1236–46, 2004. 120

[218] D. Pinto, S. Robine, F. Jaisser, F. E. El Marjou, and D. Louvard, "Regulatory sequences of the mouse villin gene that efficiently drive transgenic expression in immature and differentiated epithelial cells of small and large intestines," *J Biol Chem*, vol. 274, no. 10, pp. 6476–82, 1999. 120

[219] C. Beroud and T. Soussi, "Apc gene: database of germline and somatic mutations in human tumors and cell lines," *Nucleic Acids Res*, vol. 24, no. 1, pp. 121–4, 1996. 131

[220] M. Hollstein, K. Rice, M. S. Greenblatt, T. Soussi, R. Fuchs, T. Sorlie, E. Hovig, B. Smith-Sorensen, R. Montesano, and C. C. Harris, "Database of p53 gene somatic mutations in human tumors and cell lines," *Nucleic Acids Res*, vol. 22, no. 17, pp. 3551–5, 1994. 134

[221] A. Walther, E. Johnstone, C. Swanton, R. Midgley, I. Tomlinson, and D. Kerr, "Genetic prognostic and predictive markers in colorectal cancer," *Nat Rev Cancer*, vol. 9, no. 7, pp. 489–99, 2009. 137

[222] K. M. Crusio, B. King, L. B. Reavie, and I. Aifantis, "The ubiquitous nature of cancer: the role of the scf(fbw7) complex in development and transformation," *Oncogene*, vol. 29, no. 35, pp. 4865–73, 2010. 138

[223] V. Marsh, D. J. Winton, G. T. Williams, N. Dubois, A. Trumpp, O. J. Sansom, and A. R. Clarke, "Epithelial pten is dispensable for intestinal homeostasis but suppresses adenoma development and progression after apc mutation," *Nat Genet*, vol. 40, no. 12, pp. 1436–44, 2008. 139

[224] R. B. Halberg, J. Waggoner, K. Rasmussen, A. White, L. Clipson, A. J. Prunuske, J. W. Bacher, R. Sullivan, M. K. Washington, H. C. Pitot, J. H. Petrini, D. G. Albertson, and W. F. Dove, "Long-lived min mice develop advanced intestinal cancers through a genetically conservative pathway," *Cancer Res*, vol. 69, no. 14, pp. 5768–75, 2009. 139

[225] A. Velcich, W. Yang, J. Heyer, A. Fragale, C. Nicholas, S. Viani, R. Kucherlapati,

M. Lipkin, K. Yang, and L. Augenlicht, "Colorectal cancer in mice genetically deficient in the mucin muc2," *Science*, vol. 295, no. 5560, pp. 1726–9, 2002. 139

[226] K. P. Janssen, P. Alberici, H. Fsihi, C. Gaspar, C. Breukel, P. Franken, C. Rosty, M. Abal, F. El Marjou, R. Smits, D. Louvard, R. Fodde, and S. Robine, "Apc and oncogenic kras are synergistic in enhancing wnt signaling in intestinal tumor formation and progression," *Gastroenterology*, vol. 131, no. 4, pp. 1096–109, 2006. 139

[227] R. B. Halberg, D. S. Katzung, P. D. Hoff, A. R. Moser, C. E. Cole, R. A. Lubet, L. A. Donehower, R. F. Jacoby, and W. F. Dove, "Tumorigenesis in the multiple intestinal neoplasia mouse: redundancy of negative regulators and specificity of modifiers," *Proc Natl Acad Sci U S A*, vol. 97, no. 7, pp. 3461–6, 2000. 139

[228] Y. Zhu, J. A. Richardson, L. F. Parada, and J. M. Graff, "Smad3 mutant mice develop metastatic colorectal cancer," *Cell*, vol. 94, no. 6, pp. 703–14, 1998. 139

[229] H. Davis and I. Tomlinson, "Cdc4/fbxw7 and the 'just enough' model of tumorigenesis," *Journal of Pathology*, vol. Accepted manuscript, in press, 2012. 140, 195, 200

[230] N. W. Bateman, D. Tan, R. G. Pestell, J. D. Black, and A. R. Black, "Intestinal tumor progression is associated with altered function of klf5," *J Biol Chem*, vol. 279, no. 13, pp. 12093–101, 2004. 141

[231] R. S. Lo, D. Wotton, and J. Massague, "Epidermal growth factor signaling via ras controls the smad transcriptional co-repressor tgif," *EMBO J*, vol. 20, no. 1-2, pp. 128–36, 2001. 141

[232] B. B. McConnell and V. W. Yang, "Mammalian kruppel-like factors in health and diseases," *Physiol Rev*, vol. 90, no. 4, pp. 1337–81, 2010. 142

[233] A. R. Moser, H. C. Pitot, and W. F. Dove, "A dominant mutation that predisposes to multiple intestinal neoplasia in the mouse," *Science*, vol. 247, no. 4940, pp. 322–4, 1990. 144

[234] L. K. Su, K. W. Kinzler, B. Vogelstein, A. C. Preisinger, A. R. Moser, C. Luongo, K. A. Gould, and W. F. Dove, "Multiple intestinal neoplasia caused by a mutation in the murine homolog of the apc gene," *Science*, vol. 256, no. 5057, pp. 668–70, 1992. 144, 146

[235] P. Pollard, M. Deheragoda, S. Segditsas, A. Lewis, A. Rowan, K. Howarth, L. Willis, E. Nye, A. McCart, N. Mandir, A. Silver, R. Goodlad, G. Stamp, M. Cockman, P. East, B. Spencer-Dene, R. Poulsom, N. Wright, and I. Tomlinson, "The apc 1322t mouse develops severe polyposis associated with submaximal nuclear beta-catenin expression," *Gastroenterology*, vol. 136, no. 7, pp. 2204–2213 e1–13, 2009. 145, 146, 157, 200, 207

[236] C. Luongo, A. R. Moser, S. Gledhill, and W. F. Dove, "Loss of apc+ in intestinal adenomas from min mice," *Cancer Res*, vol. 54, no. 22, pp. 5947–52, 1994. 145

[237] A. Lewis, S. Segditsas, M. Deheragoda, P. Pollard, R. Jeffery, E. Nye, H. Lockstone, H. Davis, S. Clark, G. Stamp, R. Poulsom, N. Wright, and I. Tomlinson, "Severe polyposis in apc(1322t) mice is associated with submaximal wnt signalling and increased expression of the stem cell marker lgr5," *Gut*, vol. 59, no. 12, pp. 1680–6, 2010. 145, 157, 158

[238] S. J. Leedham, A. T. Thliveris, R. B. Halberg, M. A. Newton, and N. A. Wright, "Gastrointestinal stem cells and cancer: bridging the molecular gap," *Stem Cell Rev*, vol. 1, no. 3, pp. 233–41, 2005. 158

[239] M. O. Nandan, A. M. Ghaleb, B. B. McConnell, N. V. Patel, S. Robine, and V. W. Yang, "Kruppel-like factor 5 is a crucial mediator of intestinal tumorigenesis in mice harboring combined apcmin and krasv12 mutations," *Mol Cancer*, vol. 9, p. 63, 2010. 158, 159

[240] K. M. Haigis, P. D. Hoff, A. White, A. R. Shoemaker, R. B. Halberg, and W. F. Dove, "Tumor regionality in the mouse intestine reflects the mechanism of loss of apc function," *Proc Natl Acad Sci U S A*, vol. 101, no. 26, pp. 9769–73, 2004. 158

[241] B. B. McConnell, A. B. Bialkowska, M. O. Nandan, A. M. Ghaleb, F. J. Gordon, and V. W. Yang, "Haploinsufficiency of kruppel-like factor 5 rescues the tumor-initiating effect of the apc(min) mutation in the intestine," *Cancer Res*, vol. 69, no. 10, pp. 4125–33, 2009. 159

[242] S. J. Freemantle, M. J. Spinella, and E. Dmitrovsky, "Retinoids in cancer therapy and chemoprevention: promise meets resistance," *Oncogene*, vol. 22, no. 47, pp. 7305–15, 2003. 160

[243] A. C. Dillard and M. A. Lane, "Retinol decreases beta-catenin protein levels in retinoic acid-resistant colon cancer cell lines," *Mol Carcinog*, vol. 46, no. 4, pp. 315–29, 2007. 160

[244] A. J. Lee, D. Endesfelder, A. J. Rowan, A. Walther, N. J. Birkbak, P. A. Futreal, J. Downward, Z. Szallasi, I. P. Tomlinson, M. Howell, M. Kschischo, and C. Swanton, "Chromosomal instability confers intrinsic multidrug resistance," *Cancer Res*, vol. 71, no. 5, pp. 1858–70, 2011. 178

[245] M. Welcker, A. Orian, J. Jin, J. E. Grim, J. W. Harper, R. N. Eisenman, and B. E. Clurman, "The fbw7 tumor suppressor regulates glycogen synthase kinase 3 phosphorylation-dependent c-myc protein degradation," *Proc Natl Acad Sci U S A*, vol. 101, no. 24, pp. 9085–90, 2004. 184

[246] S. I. Reed, "Ratchets and clocks: the cell cycle, ubiquitylation and protein turnover," *Nat Rev Mol Cell Biol*, vol. 4, no. 11, pp. 855–64, 2003. 186

[247] F. S. Leach, S. J. Elledge, C. J. Sherr, J. K. Willson, S. Markowitz, K. W. Kinzler, and B. Vogelstein, "Amplification of cyclin genes in colorectal carcinomas," *Cancer Res*, vol. 53, no. 9, pp. 1986–9, 1993. 187, 196

[248] Y. Geng, E. N. Eaton, M. Picon, J. M. Roberts, A. S. Lundberg, A. Gifford, C. Sardet, and R. A. Weinberg, "Regulation of cyclin e transcription by e2fs and retinoblastoma protein," *Oncogene*, vol. 12, no. 6, pp. 1173–80, 1996. 196

[249] R. Smits, N. Hofland, W. Edelmann, M. Geugien, S. Jagmohan-Changur, C. Albuquerque, C. Breukel, R. Kucherlapati, M. F. Kielman, and R. Fodde, "Somatic apc mutations are selected upon their capacity to inactivate the beta-catenin downregulating activity," *Genes Chromosomes Cancer*, vol. 29, no. 3, pp. 229–39, 2000. 200

[250] A. H. Berger, A. G. Knudson, and P. P. Pandolfi, "A continuum model for tumour suppression," *Nature*, vol. 476, no. 7359, pp. 163–9, 2011. 200, 202

[251] N. Faresse, F. Colland, N. Ferrand, C. Prunier, M. F. Bourgeade, and A. Atfi, "Identification of pcta, a tgif antagonist that promotes pml function in tgf-beta signalling," *EMBO J*, vol. 27, no. 13, pp. 1804–15, 2008. 204

[252] C. Guerra, N. Mijimolle, A. Dhawahir, P. Dubus, M. Barradas, M. Serrano, V. Campuzano, and M. Barbacid, "Tumor induction by an endogenous k-ras oncogene is highly dependent on cellular context," *Cancer Cell*, vol. 4, no. 2, pp. 111–20, 2003. 205

[253] J. Shen and C. A. Walsh, "Targeted disruption of tgif, the mouse ortholog of a human holoprosencephaly gene, does not result in holoprosencephaly in mice," *Mol Cell Biol*, vol. 25, no. 9, pp. 3639–47, 2005. 206